Structures and Stabilities of H_2 Adlayers on Ionic Crystal Surfaces

Jamal N. Dawoud

A Thesis

in

The Department

of

Chemistry and Biochemistry

Presented in Partial Fulfilment of the Requirements
For the Degree of Doctor of Philosophy at
Concordia University
Montreal, Quebec, Canada

February 2006

Your file Votre référence
ISBN: 978-0-494-16265-1
Our file Notre référence
ISBN: 978-0-494-16265-1

To my Father, Mother, Wife and Daughter

ABSTRACT

Structures and Stabilities of H_2 Adlayers on Ionic Crystal Surfaces: H_2/MgO(001), H_2/LiF(001) and H_2/NaCl(001).

Jamal Dawoud, Ph.D.
Concordia University, 2006.

Our Monte Carlo (MC) simulations investigate the possible formation of a series of structures, $p(2\times2)\rightarrow p(8\times2) \rightarrow p(4\times2) \rightarrow p(6\times2)$ with coverages Θ=0.5, 0.625, 0.75 and 0.83 respectively, by H_2 molecules on the MgO(001) and LiF(001) surfaces. On H_2/MgO(001) the sequence $p(2\times2) \rightarrow p(4\times2) \rightarrow p(6\times2)$ is possible and is stable up to 9 K, while on H_2/LiF(001) the progression $p(2\times2)\rightarrow p(8\times2) \rightarrow p(4\times2)$ is found. These structures are consistent with recent Helium Atom Scattering (HAS) results in terms of coverage and thermal stability, but disagree in terms of symmetry. The HAS work found "*c*" type structures whereas the MC simulations (without quantum considerations) yield a "*p*" type structures. The $p(2\times2)$ structures contains two H_2 molecules per unit cell, with each molecule lying parallel to the plane of the surface (θ = 90°) directly above every other cationic site. The molecules adopt a "T" configuration with respect to their nearest neighbours. For the $p(8\times2)$, $p(4\times2)$ and $p(6\times2)$ structures, there are two kinds of adsorption sites: a parallel site, as in the case of $p(2\times2)$ structure, and a tilted site, where the H_2 molecules sit between cationic and anionic sites with the molecular axis directed towards the anionic site, with $\theta \sim 60°$. To reconcile the results of the simulations and experiments, the quantum mechanical rotational

motion of the adsorbed H_2 molecules was studied using perturbation theory. These calculations show that the adsorbed hydrogen molecules are azimuthally delocalized and hence these structures are indeed *c*-type.

For the H_2/NaCl(001) system, the MC simulations of the bi-layer system show that the formation of a second layer is possible, in which the molecules lie tilted ($\theta = 45^{o}$) at the top of the Cl^{-} sites in a unit cell of $p(2\times1)$ symmetry. It also found the molecules in the bottom layer lie flat over the Na^{+} sites and arranged in a unit cell of $p(2\times1)$ symmetry, where the molecules adopt a tee configuration along diagonals, and have the same orientation along the rows. In terms of thermal stability, the bottom layer is stable up to 12 K whereas the upper layer is orientationally disordered at T > 5 K and molecules desorb at T > 8 K. These predicted structures are in agreement with the experimental findings in terms of coverage and thermal stability but disagree in terms of symmetry since the PIRS-ATR and HAS experimental findings show a (1×1) structure. To solve this problem, the rotational motion of H_2 molecules has been studied using perturbation theory and it is found that quantum effects will azimuthally delocalize the orientation of the molecular axis of H_2. Thus, those predicted structures become a (1×1) structure.

ACKNOWLEDGEMENTS

I would like to express my deepest gratitude and sincere appreciation to Prof. David B. Jack for his fruitful supervision, support, suggestions, guidance and encouragement throughout the course of this work.

Special thanks to Prof. Raymond Le Van Mao and Prof. Gilles H. Peslherbe for being members of my committee. I am greatly thankful for their time and valuable comments.

I would like to thank Dr. A. K. Sallabi for his valuable suggestions, comments, useful discussions and helping me in solving computer technical problems.

My great thanks are extended to my wife, brothers, sisters and friends for their support, and encouraging me throughout my Ph.D. studies.

TABLE OF CONTENTS

List of Figures

List of Tables

List of Abbreviations and Symbols

Symbol	Abbreviation
LiF(001)	Lithium fluoride. "001" refers to the plane of cleavage of Lithium fluoride.
NaCl(001)	Sodium chloride. "001" refers to the plane of cleavage of Sodium chloride.
MgO(001)	Magnesium oxide. "001" refers to the plane of cleavage of Magnesium oxide.
EMT	Effective medium theory.
FTIR	Fourier transfer infrared.
HAS	Helium atom scattering.
MC	Monte Carlo.
PIRS	Polarized infrared spectroscopy
PT	Perturbation theory.
SCF	Self-consistent Field
c(2×2)	Epitaxial structure of the adsorbed layer: centered two by two structure.
c(4×2)	Epitaxial structure of the adsorbed layer: centered four by two structure.
c(6×2)	Epitaxial structure of the adsorbed layer: centered six by two structure.
c(8×2)	Epitaxial structure of the adsorbed layer: centered eight by two structure.
p(2×2)	Epitaxial structure of the adsorbed layer: primitive two by two structure.
p(2×1)	Epitaxial structure of the adsorbed layer: primitive two by one structure.
p(4×2)	Epitaxial structure of the adsorbed layer: primitive four by two structure.
p(6×2)	Epitaxial structure of the adsorbed layer: primitive six by two

	structure.
$p(8\times2)$	Epitaxial structure of the adsorbed layer: primitive eight by two structure.
θ	Polar angle is the angle between the molecular axis and the surface normal.
φ	Azimuthal angle is the angle restricted between the projection of the molecular axis and the x-axis of the surface plane
NVT	Number of molecules, volume and temperature.
ζ	Random number.
k_B	Boltzmann constant.
$\vec{r}$	Position vector.
δE	Energy difference.
Θ	Quadrupole moment.
μ	Dipole moment.
$V_{el.}$	Electrostatic potential.
$V_{ind.}$	Induction energy.
$V_{coul.}$	Coulombic potential.
$\vec{E}$	Surface electric field.
$\Phi(\vec{r})$	Surface electric potential.
α	Polarizability.
$\alpha_{\perp}, \alpha_{\parallel}$	Polarizabilities in the perpendicular and parallel directions with respect to the molecular axis respectively.
a_o	Lattice constant.

A_{ij} , β_{ij}	Born-Mayer parameters.
$f_{2n}(r_{ij})$	Tang-Toennies damping function.
A_i, B_i	Softness parameters.
C_6^{ij}, C_8^{ij}, & C_{10}^{ij}	Dispersion coefficients.
ψ_n	Rotational wave function
$\hat{\mathrm{H}}$	Hamiltonian operator.
$Y(\theta,\varphi)$	Spherical harmonics function.
$\Psi_{Jm}(\theta,\varphi)$	Rotational wave function.
$V(\theta,\varphi)$	Rotational potential.
E_{Jm}	Rotational energy level.
J	Rotational quantum number.
m	Rotational magnetic quantum number.
q_{st}	Isosteric heat of adsorption.
$\hbar$	Planck constant.

CHAPTER 1: INTRODUCTION

The study of the molecules adsorbed on solid surfaces has been of interest for well over a century, often because of industrial applications [1]. Historically, Michael Faraday did the first work on adsorption in 1834 [2] and show that gas molecules accumulate over a surface as a result of attractive forces exerted on these molecules by the solid substrate. Afterwards, considerable experimental attention was focused on the adsorption of atoms and molecules on surfaces once huge improvements in experimental techniques became available. This provided a wealth of information on adsorbate and surface structures at low temperatures [3, 4, and 5], isotopic separation [6], and two dimensional phase transitions [7, 8]. In particular, the study of the adsorption of molecules at ionic crystal surfaces can help one understand some of the basic ideas and issues of surface science. At the molecular level, experimental results cannot provide a complete understanding of all the details regarding molecule-surface interactions and structures. An increase in computing power has made the theoretical investigation of these systems possible so that a complete picture of adsorbate and adsorbent structures may be obtained. This provides a powerful tool for the understanding of elementary processes of interest in surface science, such as adsorption, desorption, structural and dynamical properties of adsorbed layers and thin films. Work of this kind has been successfully performed on "classical" type systems, such as CO/NaCl(001) [9] and CO/MgO(001) [10], where quantum effects may be ignored. Simple systems where quantum effects might be important are also of interest, but have only recently been examined.

The adsorption of H_2 molecules at ionic crystal surfaces is an interesting system for the study of surface structures, molecule-surface interactions and has recently attracted experimental attention [11, 25, and 29]. These differ from other adsorbate-substrate systems in that quantum effects may be important because of the light mass of the adsorbate, just as they are important in understanding condensed H_2, which is a quantum solid [12]. One of the advantages of using H_2 molecules is the availability of finding them in different rotational manifolds (*para* and *ortho* forms), which allows one to compare systems that are identical in all properties except their rotational states. Other motivations for studying these systems are the possibility of finding 2D super-fluid behavior at low temperatures [13] and the importance in astrophysics of understanding the role of hydrogen adsorbed on dust grains in outer space [14]. Experimental and theoretical studies on the interaction of hydrogen molecules with ionic crystal surfaces started in the 1930s when Stern and co-workers [15] studied the scattering of H_2 on LiF surface in order to verify the wave nature of matter and subsequently discovered the phenomenon of selective adsorption [16]. This attracted other experimentalists, as well as theoreticians, to do further work on surface characterization, adlayers structures and 2D phase transitions.

Theoretical / computational investigations of the physical adsorption of H_2 molecules on ionic crystal surfaces might answer some of the following important questions: 1) what kind of structures form on the ionic surfaces; 2) what is the effect of the substrate surface on the quantum states of the adsorbed H_2

molecules; 3) how strong is the coupling between the rotational quantum states of adsorbed H_2 molecules; 4) are there any implications for information storage or quantum computing? These studies will increase our knowledge of the behaviour of H_2 and its properties in the adsorbed phase, which may be of interest in areas of practical application such as hydrogen storage, fuel cell technology, and heterogeneous catalysis.

Recently, the physical adsorption of H_2 molecules on ionic crystal surfaces has been extensively studied experimentally by using helium atom scattering, and polarization infrared techniques. A variety of monolayer structures have been observed such as:

1) H_2/MgO(001): $c(2\times2)\rightarrow c(4\times2)\rightarrow c(6\times2)$;
2) H_2/NaCl(001): (1×1); and
3) H_2/LiF(001): $c(2\times2)\rightarrow c(8\times2)$;

but the details of these structures are unknown.

Before the discussion of the adsorption of hydrogen molecules on ionic crystal surfaces, it is worthwhile reviewing some of the general ideas in surface science as will be discussed in the next section.

1.1. Review of some basic concepts

1.1.1. Adsorption and types

When a gas molecule strikes a solid surface, it may rebound from the surface elastically with no energy transferred between them, scatter inelastically, undergo a reaction, or stick to the surface (adsorb). If it is adsorbed it may diffuse on the surface, remain fixed, or dissolve in the bulk phase (*absorption*). The solid surface, sometimes called *the adsorbent* or *substrate*, can be defined as a boundary that separates two phases, namely the bulk solid phase of the substrate and the gas phase of adsorbing molecules, and is the region where the adsorbing molecules (adsorbate) aggregate. The solid surface usually has a strong affinity for gas molecules, ions or particles and has the ability to bind them through interactions that are either chemical or physical in nature. Therefore, adsorption is a process in which a particle sticks to a surface as a result of attraction forces that exists at the surface. These forces at the surface are only extensions of the forces within the bulk. The atom in the surface layer is clearly in an unusual position because it does not have its full complement of neighbours [its coordination number is smaller than for atoms within the bulk], and hence there is an imbalance of forces at the surface, so that a surface atom suffers a net force acting inwards for atoms and molecules in its environment. This results in the adsorption of atoms or molecules at the surface.

The adsorption of a molecule on a solid surface is always an exothermic process. This may be shown from general thermodynamic arguments. For the adsorption of gas particle onto a solid surface to be a spontaneous process, the change in Gibbs Free Energy $\Delta G = \Delta H - T\Delta S$ must be negative. But for adsorption ΔS must be negative because the adsorbed phase is a more ordered system, with fewer degrees of freedom, than the gas phase. So the only way to make ΔG negative is to have ΔH more negative than $T\Delta S$. With ΔH always negative, the adsorption process must be exothermic [1], and heat is always liberated on adsorption.

Generally, there are two types of adsorption, depending on the nature of the forces involved. In chemical adsorption (*chemisorption*) where a single layer of molecules, atoms, or ions is attached to the adsorbent surface by covalent bonds where electron sharing occurred between them, whereas in physical adsorption (*physisorption*), the adsorbed molecules are held by the weaker van der Waals forces. Chemisorption and physisorption are usually distinguishable from each other without any great difficulty. These differences can be summarized in the following points:

1. The binding energy of physical adsorption is typically less than 10 kcal/mol, for example, the binding energy of CO molecule adsorbed on NaCl(100) [17, 18] is -4.4 kcal/mol, which falls into the physisorption

category, whereas the values of the binding energy of chemisorption are typically from 25 to 120 kcal/mol.

2. Physical adsorption achieves equilibrium more rapidly than chemisorption since it activation energy is only a tenth to a third of that of chemisorption process.

3. Physical adsorption is a reversible process where the physisorbed layer can be removed by lowering the pressure of the gas or increasing the temperature of the surface, whereas the removal of chemisorbed layer is more complicated process. Sometimes the original species may not desorb, for example, heating a graphite surface after adsorbing atomic oxygen results in desorption of carbon monoxide.

4. A further point of distinction between the two types of adsorption concerns the number of layers adsorbed. Chemisorption leads at most to monolayer coverage of the available surface. With physical adsorption, several adsorbed layers may be formed, especially near the normal boiling point of the adsorbing substances.

Usually chemisorption processes involve physical adsorption as a precursor step. This is always favourable over a process with no physical adsorption

present, because of the resultant lowering in activation energy required for chemisorption.

In this thesis we are concerned solely with the physical adsorption of H_2 molecules on ionic crystal surfaces [MgO, NaCl and LiF] at low temperatures where the binding energies in all cases less than 1 kcal/mol.

1.1.2. Adsorption energy

When a quantity of gas molecules are admitted to the solid surface, part of the gas molecules are adsorbed on the surface and part remains unadsorbed. The adsorbed molecules are bound to the surface by relatively weak van der Waals interactions. This binding energy can be defined as the energy removed in the transfer of a molecule from the gaseous state to the adsorbed state under conditions of constant pressure *P* and temperature *T*, *i.e.* the change in enthalpy *H* upon adsorption. The enthalpy of a gas particle is $H_g = U_g + PV$ where the internal energy is given by $U_g = \frac{1}{2} \cdot nk_B T$, where k_B is Boltzmann's constant and n is the particle's number of degrees of freedom; n = 3 for a monatomic gas and n = 5 for a diatomic molecule. Assuming the ideal gas law, the enthalpy per particle may be written as

$$H_g = U_g + k_B T = \left(\frac{n+2}{2}\right) \cdot k_B T \qquad (1.1)$$

If the particle adsorbs onto localized adsorption sites the enthalpy per particle on the surface is

$$H_s = U_0 + \sum_{\alpha=1}^{n} \frac{\hbar \cdot \omega_\alpha}{2} \cdot \coth \frac{\hbar \cdot \omega_\alpha}{2 \cdot k_B T} \quad , \tag{1.2}$$

where ω_α is the vibrational frequency of the α^{th} degree of freedom, and U_0 is the potential energy minimum of the particle at the surface ($U_0 < 0$). The isosteric heat of adsorption, q_{st}, is given by the change in enthalpy upon adsorption $H_s - H_g$ at constant coverage or

$$q_{st} = U_0 + \sum_{\alpha=1}^{n} \frac{\hbar \cdot \omega_\alpha}{2} \cdot \coth \frac{\hbar \cdot \omega_\alpha}{2 \cdot k_B T} - \left(\frac{n+2}{2} \right) \cdot k_B T \tag{1.3}$$

.

At high temperatures, the value of $\frac{\hbar \cdot \omega_\alpha}{2 \cdot k_B T}$ becomes << 1, and the approximation $\coth\left(\frac{\hbar \cdot \omega_\alpha}{2 \cdot k_B T} \right) = \frac{2 \cdot k_B T}{\hbar \cdot \omega_\alpha}$ is valid. Therefore, Eqn. (1.3) can be written in a simpler form as below,

$$q_{st} = U_0 + \left(\frac{n-2}{2} \right) \cdot k_B T \tag{1.4}$$

At low temperatures, $\frac{\hbar \cdot \omega_\alpha}{2 \cdot k_B T}$ is very large and $\coth \frac{\hbar \cdot \omega_\alpha}{2 \cdot k_B T}$ is approximately unity so that

$$q_{st} = U_0 + \sum_{\alpha=1}^{n} \frac{\hbar \cdot \omega_\alpha}{2} - \left(\frac{n+2}{2} \right) \cdot k_B T \tag{1.5}$$

1.1.3. Surface structures

1.1.3.1. Substrate Structure

A crystalline solid can be described as a solid phase where the particles pack together to form a regular repeating pattern in three dimensions. The smallest repeating unit of the pattern, which shows the full symmetry of the solid structure, is called the primitive unit cell [20]. The surface unit cell (2D) can be used to describe the repetitive arrangement patterns of the entire surface. This unit cell can conventionally be defined by two vectors $\mathbf{a}_1$ and $\mathbf{a}_2$ along two sides of the unit cell with a common origin as shown in Fig. 1.1.

The ionic crystalline solids considered in this thesis are held together by the strong coulomb attractions of the oppositively charged ions, which occupy the lattice points in a fcc crystal. The (001) surface of these cubic crystal has 4-fold rotational symmetry and its primitive unit cell is a square, $|\mathbf{a}_1| = |\mathbf{a}_2|$.

1.1.3.2. Overlayer Structure

The ordered layers formed by the adsorption of molecules or atoms on a solid surface have specific structures, which can be defined with respect to the substrate structure. These structures are controlled by the competition between the lateral molecule-molecule interaction and molecule-surface interaction. Based upon both factors, the structure of an adsorbed layer may be commensurate [dependent on substrate structure in which the ratio of the adlayer and substarte lattice constants is integer] or incommensurate [the intermolecular separations within the adlayer is controlled by the lateral admolecules interaction forces where the ratio of the adlayer and lattice constants is irrational] [21, 22].

Arrangements of the ordered layers atoms or molecules can be described by two vectors $\mathbf{b_1}$ and $\mathbf{b_2}$, which define the unit cell of the adsorbent layer as shown in Fig. 1.1. The nomenclature for overlayer structures involves a comparison of the basis vectors ($\mathbf{b_1}$, and $\mathbf{b_2}$) of the overlayer lattice with the corresponding substrate lattice vectors ($\mathbf{a_1}$, and $\mathbf{a_2}$).

The substrate lattice is defined as that plane parallel to the surface below which the three dimensional (bulk) periodicity is found. The relation between the overlayer lattice and the substrate lattice is expressed by the ratios of the lengths of the basis vectors $|b_1|/|a_1|$ and $|b_2|/|a_2|$ and the angle of rotation between two lattices. The nomenclature for several possible structures of adsorbates overlayer is illustrated in Fig. 1.1.

It is worthwhile to mention here a brief explanation about the difference between the *p*-type and *c*-type structures. The nomenclature of the surface layers comes from the unit cell, which is a reflection of the arrangements and orientations of the particles in the surface layer. For a centered square or rectangular unit cell (*c*-type structure), an atom, ion, or molecule should exist at the center of the unit cell where it has the same symmetry (orientation) and environment as those at the corners, plus have a plane of symmetry making right (upper) and left (bottom) halves mirror images; otherwise we have a *p*-type structure as shown in Fig. 1.2.

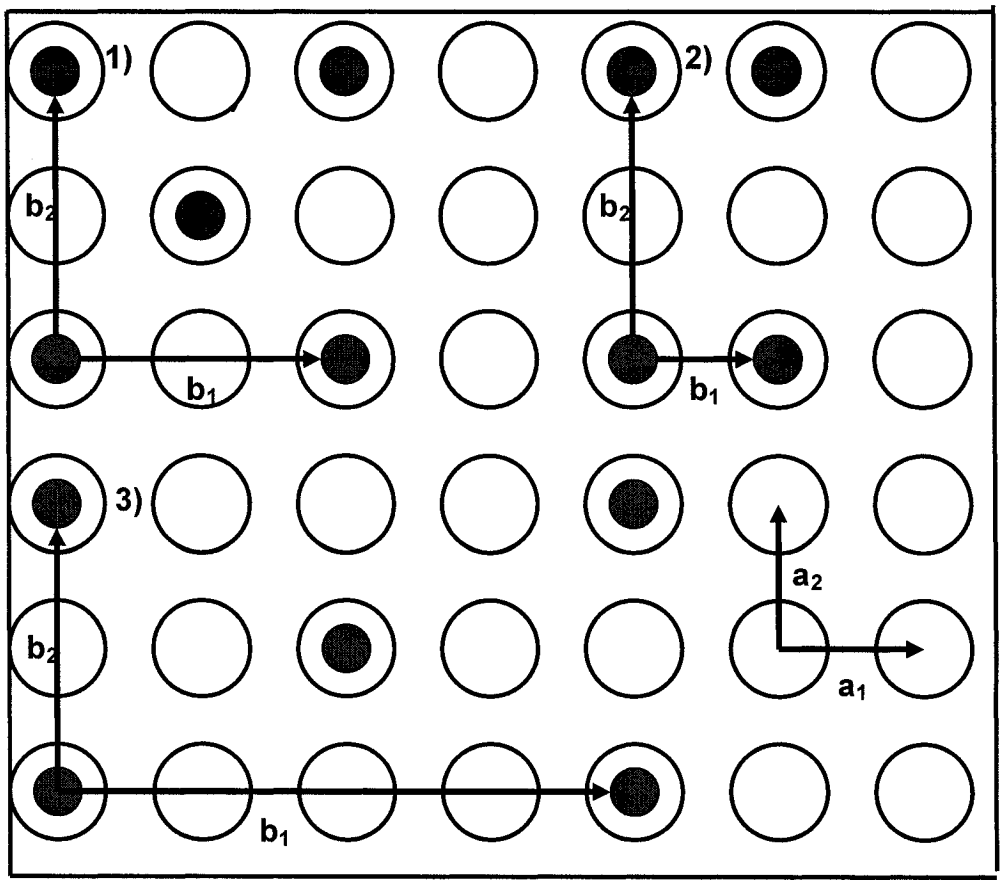

FIG. 1.1: Examples for over-layer structures: 1) $c(2\times2)$, 2) $p(1\times2)$, 3) $c(4\times2)$. As shown above, the unit cell of the substrate is described by two vectors $\mathbf{a}_1$ and $\mathbf{a}_2$, whereas the adsorbate unit cell is defined by two vectors $\mathbf{b}_1$, and $\mathbf{b}_2$.

$c(2\times2)$ unit cell structure; $p(2\times2)$ unit cell structure

FIG. 1.2: A schematic diagram of $c(2\times2)$; and $p(2\times2)$ unit cell structures.

1.1.4. Rotational states of H_2 molecule

Molecular hydrogen is a homonuclear diatomic molecule with nuclear spin I_N = ½ on each proton. Because the protons are indistinguishable fermions, the total molecular wave function, involving the product of the nuclear spin and rotational states, must be anti-symmetric with respect to particle permutation. The symmetry of the rotational states is determined by the rotational quantum number J; if J is even then the state is symmetric whereas if J is odd then the state is antisymmetric. The nuclear spin states are denoted as *ortho* or *para* states if they are symmetric or antisymmetric respectively. Because the overall wave function must be antisymmetric, molecular hydrogen in the *para* state can only have even values of J, whereas the *ortho* state must have odd values of J. It should be noted that the "ground-state" (J=0) of the *para* species is spherical whereas all other states are anisotropic in their charge distribution [23].

It is necessary to give a brief note about the orientations of the different adsorbed H_2 species on ionic crystal surface. Generally, helicoptering (J, $m = \pm J$) state involves that H_2 molecule migrates with its molecular axis parallel the surface plane, *i.e.* its axis of rotation perpendicular to the surface plane, whereas in the cartwheeling (J, $m = 0$) state, the H_2 migrates on the surface vertically, its molecular axis parallels the surface normal, *i.e.* its axis of rotation parallels the surface plane. For H_2 in its ground state (J=0, m=0), the molecule does not rotate [24]. These three cases have been illustrated in Fig. 1.3.

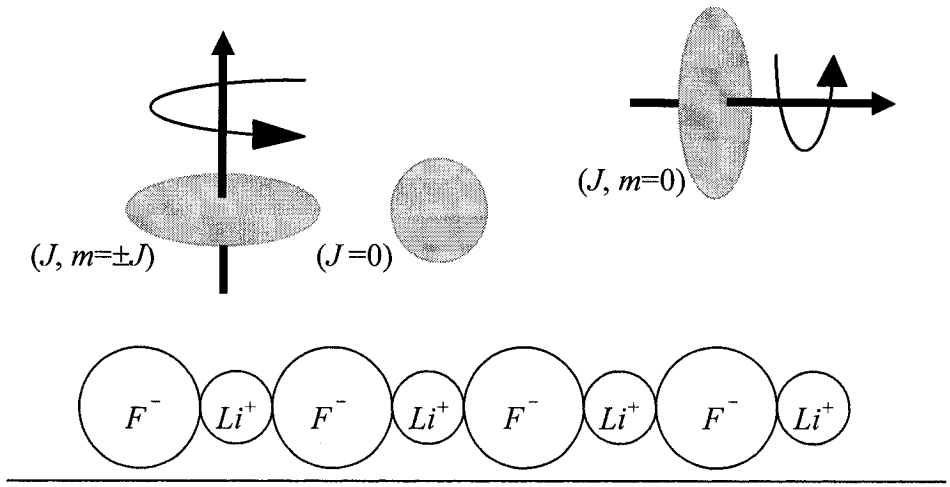

FIG. 1.3: A schematic diagram illustrating the molecular axis of different H_2 species and their axes of rotations in adsorbed phase over the LiF surface.

1.2. Survey of previous work

1.2.1. H_2/MgO(001)

The study of the adsorption of hydrogen molecules on MgO surface started relatively recently in 1988. These experimental works mainly focused on finding a hydrogen super-fluid at low temperatures [25] and any new kinds of phase transitions. Vilches' group first reported the adsorption-isotherm and heat capacity measurements on the monolayers and multilayers of the H_2 molecules adsorbed on MgO surface. They speculated on the existence of structural phase transitions accompanying changes in coverage. They determined the binding energy of an H_2 molecule with the substrate to be –0.606 kcal/mol [26, 27] but

found no evidence regarding the super-fluidity of H_2 in the adsorbed phase for temperatures below 10 K.

Recently, the behaviour and properties of molecular hydrogen adsorbate layers on MgO(001) surface have been investigated using helium atom scattering (HAS) technique [28, 29] in the range of 7–12 K. These experiments show the existence of an interesting series of commensurate structures: $c(2\times2) \rightarrow c(4\times2) \rightarrow c(6\times2)$ at surface coverages of: 0.5, 0.75 and 0.83 respectively. After the formation of the third structure, further accumulation of H_2 molecules leads to the formation of a second layer. Studies at low coverage showed that H_2 molecules bind to the surface with an energy in the range of -0.46 to -0.58 kcal/mol [28]. They also argued that hydrogen molecules prefer to locate on top of Mg^{2+} sites.

Some interest has been paid to creating a reasonable theoretical model for the interaction potential of the H_2 — MgO(001) system. In 1991, Vidali and his co-workers [30, 31] constructed a model in which the repulsion potential is calculated using the effective medium theory (EMT). This model was applied to the calculation of the external vibration of the adsorbed H_2 molecule in the direction of the surface normal [30, 31] and the specular intensity for the scattering of H_2 from MgO(001) surface [32]. This model yielded a potential well depth D considerable smaller than the value estimated from experiment. To obtain more realistic results, the C_6 coefficient of H_2 was adjusted to reproduce the assumed potential well depth (D), and the experimental binding energy. Their

calculations showed a well depth of –0.76 kcal/mol and zero point energy of 0.156 kcal/mol so that the H_2 molecule binding energy is –0.604 kcal/mol.

Recently, the dynamics of H_2 molecules in the $c(4\times2)$, $c(6\times2)$ adlayers and in the second layer were studied theoretically [33] and the different types of external vibrations were calculated as a function of molecule height and surface corrugation variations. These calculations were unable to give a reasonable explanation of the presence of the two different Einstein modes, even though the possibility of using two different heights for H_2 molecules in the unit cell was applied.

It is obvious that the experimental findings of the H_2 monolayers on MgO(001) have not been adequately explained by theoretical calculations with respect to binding energies, structural details, and vibrational modes. Therefore additional theoretical calculations and computer simulations are required to verify these points. To study and examine the adlayer structures of H_2 on MgO(001) system, it is required to have a reasonable interaction potential model of molecule-molecule/surface to obtain good results and explore this system in detail. Unfortunately the interaction potential of H_2 molecules with the MgO(001) surface have not yet been completely determined [32] and hence, one of our goals in this work is to construct a reasonable molecule-surface potential model based on the available data reported in the literature regarding H_2 and MgO(001) surface.

Previous theoretical calculations are concerned mainly with studying the lattice dynamics or vibrations of H_2 molecules on MgO(001) surface with no explanations of the details of monolayer structures in terms of adsorption sites, molecular orientations, thermal stabilities, and rotational states of H_2 species in adsorbed phase. In order to investigate these structures, Monte Carlo simulations are performed to find reasonable answers, especially as no such work has been conducted previously.

1.2.2. H_2/NaCl(001)

One of the first systems studied to investigate the nature of the adsorbent-substrate interaction is H_2 on a NaCl surface. It has been widely studied using infrared (IR) spectroscopy and recently helium atom scattering (HAS) techniques. The first infrared spectrum of H_2 and its isotopes on a NaCl film had observed by Folman and Kozirovski [34]. They found that the isosteric heat of adsorption of H_2 is around –1.29 kcal/mol. Using semi-empirical potentials, the physical adsorption of the hydrogen molecule on the ideal and distorted lattice of NaCl(001) surface have also been examined by Folman *et al.* [35]. These calculations show that the H_2 molecule prefers to reside in a parallel orientation to the surface plane at the top of Na^+ site with a binding energy of –1.14 and –1.35 kcal/mol for ideal and distorted lattice of NaCl(001) respectively. This difference in binding energy was mainly attributed to the equilibrium distance of the adsorbed molecule from the Na^+ site, which is farther in the ideal case:

2.50Å as compared to 2.23 Å in the distorted case. These are classical calculations where no distinction between *ortho* and *para* states is made. Vidali *et al.* [30] has constructed a model for the interaction potential of H_2 with NaCl surface using the EMT method. This potential was used to calculate the external vibration of H_2 molecule in the direction of the surface normal. It was also used to calculate a binding energy of –0.68 kcal/mol, which is in good agreement with experimental findings [36].

Ewing's group used polarization Fourier transform infrared attenuated total internal reflection spectroscopy (PIRS-ATR) to study the monolayer structures and dynamics of H_2 on NaCl(001) [37]. They observed a commensurate (1×1) structure at a temperature of 5.2 K, and interpreted the results in terms of two kinds of neighbouring adsorption sites. The proposed structure is described as a combination of *para*-H_2 ($J = 0$) molecules located on the top of the cationic sites (Na^+) and aligned parallel to the surface while, *ortho*-H_2 ($J = 1$) covers the anionic sites (Cl^-) and aligned perpendicular to the surface. Taking into account the height difference of the molecules above the anionic and cationic sites, due to the different ionic radii, they concluded that the occupation of these adjacent sites is sterically possible. The binding energy of H_2 above the cationic site was found to be around –0.813 ± 0.18 kcal/mole [37].

Afterwards, Heidberg *et al.* [38] studied the adsorption-desorption properties of the H_2 molecules physisorbed on NaCl(001) surface using Fourier transfer

infrared spectroscopy (FTIR) together with interaction potential calculations. They found that *para*-H_2 and helicoptering *ortho*-H_2 ($J = 1$, $m = \pm 1$) prefer to locate over the cationic Na^+ sites whereas the cartwheeling *ortho*-H_2 ($J = 1$, $m = 0$) prefers to locate at the anionic Cl^- sites. According to these calculations, they found that above the Na^+ site, the binding energy of a single hydrogen molecule in the helicoptering *ortho*- state is -0.812 kcal/mol and decreases to –0.65 kcal/mol for the *para*-state whereas, above the Cl^- anionic site the cartwheeling *ortho*-state was slightly bound to the surface with a binding energy of –0.42 kcal/mol. One year later, Heidberg's *et al* [39] also studied the monolayer structure and dynamics of adsorbed hydrogen molecules on NaCl(001) surface at T=11±1 K using the PIRS-ATR technique. They found that the H_2 molecules adopt a (1×1) geometry and proposed that the molecule's centers of mass is located on average above the Na^+ sites. From quantum calculations they found that the most likely molecules to adsorb are helicoptering *ortho*-H_2 or *para*-H_2 species [38]. The cartwheeling molecules in the state ($J = 1$, $m = 0$) are very weakly bound and do not adsorb at the experimental temperatures of 10 -12 K. Their quantum calculations of the molecular rotational motion of molecules in the adsorbed phase showed strong hindering of rotations when the rotational axis is parallel to the surface (θ motion), but allows free rotation in the plane parallel to the surface (φ motion).

More recently, the structure and vibrations of monolayers of *normal-* and *para*-H_2 molecules adsorbed on a single crystal of NaCl(001) surface have been studied using helium atom scattering (HAS) technique at T= 8 K [40]. These results were found to be consistent with a well-ordered (1×1) monolayer structure, as proposed in the literature [38, 39], where the hydrogen molecules occupy cationic sites. At low coverage, they found that *normal*-H_2 and *para*-H_2 bind to the surface with energies of –0.922 ± 0.12 and –0.853 ± 0.12 kcal/mol respectively. This difference in adsorption energies is consistent with Heidberg's *et al.* finding that helicoptering *ortho*-H_2, found in the *normal*-H_2 mixture, has a stronger binding compared with *para*-H_2. At T > 18 K, Traeger and Toennies [40] found that the hydrogen molecules desorb from the surface. The HAS results show there was no phase transition even when the temperature was increased to 12 K, as also observed in the experimental work of Heidberg's *et al.* [38, 39]. The external vibrations of H_2 and its isotopes were also measured using HAS. In particular, the surface perpendicular zero-point energy of H_2 molecules was found to be around 0.3 kcal/mol, which is consistent with the calculations of Briquez *et al.* [38].

Regarding the results and information as presented above for H_2/NaCl(001) system, it is obvious that Heidberg *et al* [38, 39] and Ewing's group [37] have each proposed slightly different results and models of the structure of the saturated H_2 monolayer. It is probable that some or all of these discrepancies are related to the different experimental circumstances, especially in light of the weak

physical adsorption of hydrogen molecules making the structure of the adsorbed layer highly sensitive to the surface temperature and H_2 gas pressure. The HAS experiment of Traeger and Toennies was found to be most consistent with Heidberg's results.

The theoretical calculations reported above are limited to a single molecule and hence the molecule-molecule interaction in the adsorbed phase was not included. It was thought that the spacing between molecules on NaCl was sufficiently distant that neighbouring molecules have little effect on molecular orientations and rotational states in adsorbed phase. In order to verify and investigate these ambiguous issues, and resolve the discrepancy between the Ewing and Heidberg groups, Monte Carlo simulations are proposed to verify all of these points as suggested by Ewing [37].

1.2.3. H_2/LiF(001)

The interaction potential of a hydrogen molecule with the (001) face of LiF surface has been extensively studied using scattering experiments. The pioneering work of Stern *et al.* in 1933 [15, 16] revealed the phenomenon of selective adsorption and probed the variation of the molecule-surface interaction potential along the surface. It also served to demonstrate the wave nature of atomic and molecular motion. These experimental achievements strongly stimulated a large number of theoretical and experimental studies and, without

doubt, greatly contributed to the development of techniques that could measure the variations in the electric field on solid surfaces [41].

In 1970, O'Keefe's group [42] first reported the reflection and diffraction of thermal energy beams of H_2, and D_2 from the (001) surface of LiF. They found that an H_2 molecule is weakly bound to the surface with a binding energy of –0.701 kcal/mol. The diffraction pattern of the scattering of H_2 gas by a crystal LiF surface has also been theoretically studied and the binding energy of H_2 with the surface was calculated to be –0.4 kcal/mol [43].

Recently Kroes *et al.* [44, 45] proposed a new model potential to describe the interaction of different H_2 species with LiF(001) surface and explain the differences in the diffraction of cold beams of *para*-H_2 and *normal*-H_2 species. In this model, H_2 is considered as a rigid rotor with a point electric quadrupole interacting with a stationary (001) LiF lattice. These calculations show that H_2 prefers to sit on top of the Li^+ site at an equilibrium height of 2.7 Å with the molecular axis parallel to the surface and a binding energy of –0.715 kcal/mol. Above the F^- site, they found that H_2 prefers to orient its molecular axis perpendicular to the surface at an equilibrium height of 2.97 Å and with a binding energy of –0.61 kcal/mol. This orientation dependence of the H_2 molecular axis over the surface ions was attributed to the variation in the electrostatic interaction as the molecule migrates over the surface. The strongest variation is observed

as the molecule moves from cationic site to anionic site, especially in case of the *ortho*-H_2 species.

Recently, Toennies' group has studied the structures and dynamics of the H_2 monolayers on LiF(001) surface using HAS technique at T=8 K. They found that H_2 molecules form two commensurate structures: $c(2\times2)\rightarrow c(8\times2)$ with surface coverages of 0.5, and 0.625 respectively [46]. At low coverage the H_2 are likely to locate over the cationic Li^+ site, which is in good agreement with the results published in the literature [44]. The proposed structure for $c(2\times2)$ adlayer was consisting of all the hydrogen molecules occupied every other Li^+ sites on the surface, whereas in the case of $c(8\times2)$, the proposed structure contains two kinds of adsorption sites; molecules located on top of Li^+ sites and other molecules sitting between the cationic and anionic sites. Up to now there are no theoretical studies that provide the details of these structures.

1.3. Our Research and its Objectives

It is clear that the monolayer structures and dynamics of H_2 molecules physisorbed on ionic crystal surfaces have been experimentally examined for the last decades and a half. These pictures constructed from the experimental results are still incomplete and in some cases inconsistent. In particular, one would like to know the details of the adlayer structure and their thermal stabilities.

To determine these details one must have, or develop, a good understanding of the basic substrate-adsorbate interactions.

The current models of the adlayer structure of the H_2/MgO(001) system are not able to reproduce the vibrational modes of the layer that are observed experimentally. In particular, using the molecular positions proposed by Skofronick *et al.* [29], Bruch [33] was unable to explain the presence of two different Einstein modes in the $c(4\times2)$ and $c(6\times2)$ structures, even when the possibility of H_2 molecules having two different heights above the surface was invoked. Therefore, accurate details of the molecular positions are needed to complete our understanding of these structures and provide a basis for a complete interpretation of the phonon modes. It will also set the stage for a discussion of quantum effects, namely, the role of molecular rotational states (*ortho* and *para*) in the adsorbed phase.

For the H_2/NaCl(001), the primary issue to be considered is the discrepancies in the experimental findings and proposals of the Heidberg–Toennies groups *vs.* the Ewing group. In particular, they do not agree on whether the hydrogen molecules adsorb on only the cationic sites (H-T groups) or on both cationic and anionic sites (Ewing). They also diverge on which rotational states adsorb on which site; helicoptering *ortho* and *para* states on cationic sites with cartwheeling *ortho* on anionic sites (H-T groups) or *para* above cationic sites and *ortho* above the anionic sites (Ewing). Since these experiments were not done

under identical conditions there is a possibility that they may be reconciled if temperature is taken into account. Monte Carlo simulations hold out the possibility of comparing these structures at different temperatures. Furthermore, they can also be used to examine multilayers and answer the question of whether the anionic sites are occupied and under what conditions occupation is possible.

To round out a study of hydrogen adsorption on ionic crystals, an examination of the H_2/LiF(001) system is also in order. Preliminary experimental results for this system exist and will provide a test of whether the methods and molecule-surface interaction potentials used in this thesis are applicable more generally.

As implied above, Metropolis Monte Carlo simulations may be used to determine the structures and symmetries of the H_2 monolayers, surface coverage and their thermal stabilities. These details might eventually be used (by others) to calculate vibrational frequencies of the adsorbed layers. This would be a significant advance over other theoretical work that examined only single particle adsorption and thus were not able to determine the structural details desired.

In this work, the Metropolis MC simulation was applied mainly to determine the structures of the H_2 monolayers, hydrogen surface coverage and their thermal stabilities. In order to run the simulations, classical interaction potentials were constructed for use in the energy calculations. From the structures obtained

and using the interaction potential developed, quantum mechanical calculations using perturbation theory were performed to determine the nature of the adsorption states of the H_2 molecules on the surface, their effect on the structural symmetry of the monolayers, and yield a clearer picture of the behaviour of adsorbed H_2 molecules in its different rotational (*ortho vs. para*) states. The result of these simulations and calculations match the experimental work well and are presented in the next chapters.

CHAPTER 2: THE METROPOLIS MONTE CARLO METHOD

2.1. Introduction to Computer Simulation Methods

As computers become more powerful, accessible, and as chemists develop better algorithms and software, a larger variety of problems in chemistry can be tackled by computational methods. Computational chemistry can be defined as a branch of chemistry using numerical techniques inserted within a computer program, and governed by the fundamental laws of physics. It can be used as a research tool to predict and simulate the chemical properties, structures, or any processes of chemical relevance. Computational methods can be used for a variety of purposes: to calculate properties at equilibrium by Metropolis Monte Carlo methods, to study molecular conformations by minimizing empirical potential energy function, to predict the properties of non-existent molecules that look like interesting candidates for synthesis, to search and analyze huge databases of known molecular structures and properties [47], etc...

Computer simulations methods are generally divided into two main types: Molecular Dynamics and Monte Carlo methods. The performance of these techniques depends on three parts: choosing a model to interpret and describe all interactions between the particles or molecules in the system, then mathematical formulas to calculate the energy of the system as a function of the molecular coordinates and finally the data of simulations are analyzed in order to calculate the required properties [48]. The type of the problem that one is looking to examine and the objectives of the research, determine which kind of simulation method should be used. One of the best methods for determining the

structures of H_2 adlayers on the ionic crystal surfaces, MgO(001), NaCl(001) and LiF(001), at finite temperatures and their properties at equilibrium is the Metropolis Monte Carlo method. A brief picture of this method will be presented in the following section.

2.1.1. The Metropolis Monte Carlo method

Monte Carlo methods can be described as statistical simulation methods, and defined in terms of any method that utilizes sequences of random numbers to perform the simulation. Monte Carlo methods have been used for centuries, but only in the past several decades has the technique gained the status of a full-fledged numerical method capable of addressing the most complex applications. In 1953, Nicholas Metropolis and coworkers [49] proposed a new sampling procedure, which incorporates the temperature of the system. This is done so that the Boltzmann average of a property of the system can be easily calculated. Therefore it is easy to control temperature through the simulations and get the results quickly. The Metropolis MC method can be used with a large number of particles and will generate many configurations and examine them in a relatively short time.

In our research work, simulations have been performed using the Metropolis Monte Carlo method in the canonical ensemble[1] [32, 50, 51], where a system of

[1] In a canonical ensemble, Q(N,V,T), the number of molecules as well as the volume and the temperature of the system are kept constant [52].

adsorbate molecules are placed in the ionic crystal surface potential over the top of a patch of surface. Periodic boundary conditions in the lateral directions were imposed, as well as a cutoff radius of 13.5 Å for H_2—H_2 interactions. In the course of the Monte Carlo simulations, the number of molecules in the system was determined by the assumed initial structure and coverage of the adlayer. These molecules stayed near the surface with no restriction on the motion in the direction of the surface normal. For each Monte Carlo cycle, a randomly chosen molecule is subjected to a random translation or rotation in 3D in order to generate a new configuration. The energy of the new configuration is calculated and the difference in energy with the old one, $\delta \mathbf{E}$ is evaluated. Acceptance of the new configuration is determined by the Metropolis sampling algorithm as follows: If $\delta \mathbf{E}$ is negative, the configuration is immediately accepted; otherwise its Boltzmann probability is calculated and compared to a randomly generated number between 0 and 1. If the Boltzmann factor, $\exp(-\delta \mathbf{E} / k_B T)$, is greater than the random number, then the new configuration is accepted, otherwise the molecule is returned to its initial state. When all molecules in the layer are subjected to this procedure, one cycle is finished. This process is repeated for many cycles until the system approaches its thermodynamic equilibrium, where there is no further change in the average energy of the system. After the system reaches its thermodynamic equilibrium, thousands of MC cycles are needed before the simulations are stopped and then the accumulated data can be analyzed. Application of this procedure (see Fig. 2.1) yields configurations, which are weighted according to the Boltzmann probability and hence are suitable for

studying average structures, energies, and other properties. One of the advantages of using the Metropolis procedure is the possibility of accepting configurations with higher energies than the current configuration thus allowing MC methods to energetically climb uphill and escape from a local minimum.

The quality of the simulation results is affected mainly by two factors: the size of the particle displacements in each Monte Carlo step and the number of Monte Carlo steps attempted. If the displacement size of a given Monte Carlo step is too large, the change in the energy between old state and new state may become very large and virtually all of the attempts will be probabilistically rejected. This causes the simulation to get "stuck" at a particular configuration. Conversely, if the Monte Carlo step size is too small, always, the system will return to its starting configuration, which usually a local minimum. In either case, the total number of attempts may have to become exceedingly large. In our MC simulation, the molecular translations and rotations are constructed by multiplying the fixed amplitude by a randomly generated number to create a new move. These amplitudes are constant during a simulation but are chosen to maintain a satisfactory ratio of acceptance of around 50% (the hit:miss ratio), so as to optimize the convergence and efficiency of the simulation.

To maintain an efficient run of the MC simulation, periodic boundary conditions and an interaction cut-off radius have been applied. By implementing periodic boundary conditions, the MC simulation has the ability to calculate the

macroscopic properties of the system from the results of relatively small number of molecules or particles while eliminating boundary effects. Consequently, an infinite system is created from a small finite number of particles [50]. As shown in Fig. 2.2, the molecules are located on a solid surface and distributed within a two dimensional square box, which is replicated in both of the lateral surface directions to produce a periodic array. During the simulation, the molecules can move on the surface in which one of these molecules could cross the boundary and one of its images, from its replicates, moves in through the opposite face (see Fig. 2.2). It should be noted here that the range of the interaction forces between molecules determines the maximum interaction distance as well as the size of the central box (see Fig. 2.2). In our model, the surface of the ionic crystal was built as an infinite array of the cations and anions using the periodic boundary condition. In the direction of the surface normal, there was no any restriction imposed on the molecular motions and periodic boundary conditions were not employed. Nonetheless, the surface potential effectively confined the molecules to the immediate vicinity of the solid surface.

The importance of applying the cut-off radius in the MC simulation is to truncate the calculation of the interaction potential between molecules in the layer at relatively large separation, where the intermolecular distances are greater than the effective range of potential. At large intermolecular separations, the van der Waals potential contributions become negligible and hence a considerable saving in computational time can be achieved when those terms

are excluded in the calculations. Here in the Metropolis MC simulation, a cut-off radius $\mathbf{r_c}$ around the molecule "***i***" has been applied in which $\mathbf{r_{ij}}$ describe the separation between a neighbouring molecule "***j***" and the molecule in question ***i***. In the case of H_2 molecules adsorbed on MgO(001), the cut-off radius was set at 13.5 Å and the size of the central square box was 35.64 Å (12 surface square lattices). If $\mathbf{r_{ij} \leq r_c}$ then the interaction potential is fully calculated between those interacting molecules. It is also worthwhile to mention that the cut-off radius distance should not be greater than half the length of the box, since otherwise the molecule could be interacted with its own image or interacted with more than one image of other molecules as a result of using periodic boundary condition.

The sequences of configurations that are generated eventually become independent of sufficiently distant previous configurations. For the simulations presented here it was found that configurations separated by 100 cycles were statistically independent. Thus by sampling and recording the various quantities of interest, *e.g.* energy, orientation angles, *etc.*, one can construct average values and distributions of these quantities. For example, the total average energy of the system, $\overline{E}$, can be calculated from the values of the total energy of the system at each sampling cycle, E_i, using the following formula [52],

$$\overline{E} = \langle E \rangle = \frac{1}{n} \sum_{i=1}^{n} E_i \qquad (2.1)$$

where n is the total number of cycles sampled throughout the simulation. This

formula is readily generalized to most quantities that are generated within the simulation such as angles of orientation, atomic positions, *etc.*

So, by running the simulation for sufficiently long numbers of cycles a large set of statistically independent data points may be constructed and used to calculate properties of interest. The larger the constructed data sets are, the more precise the values of the properties will be.

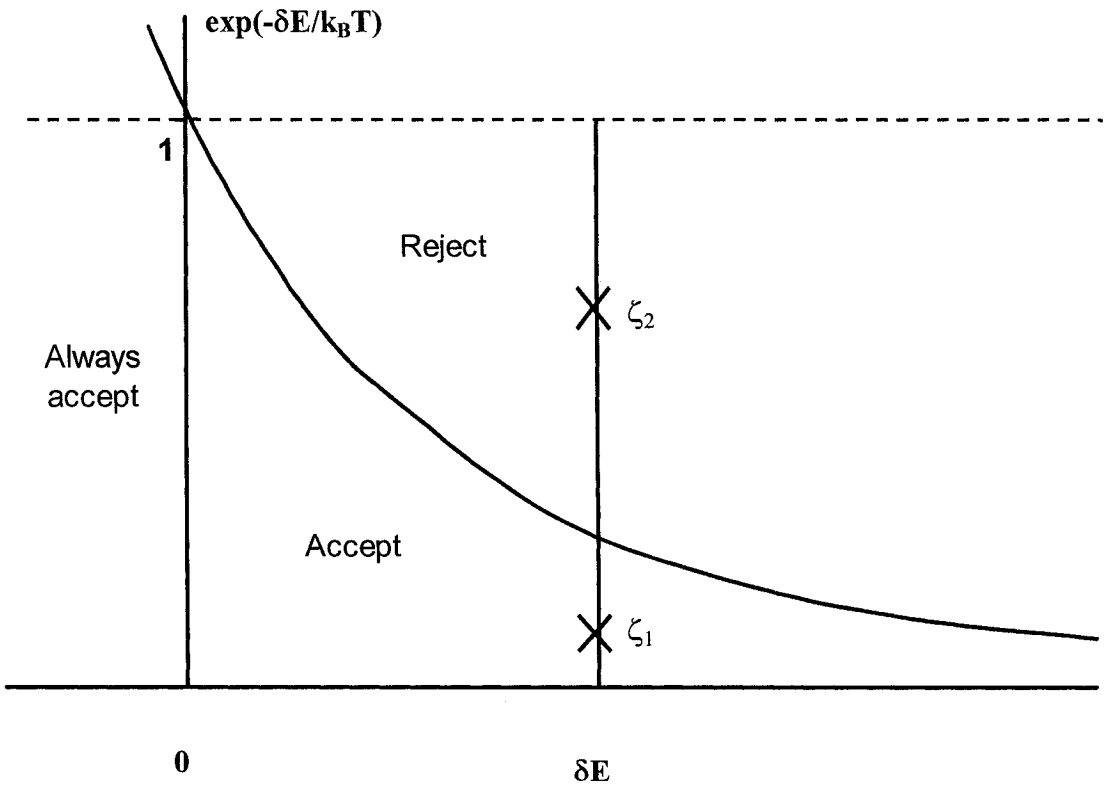

FIG. 2.1: A schematic diagram of the acceptance criteria in the Monte Carlo method as taken from ref. [49].

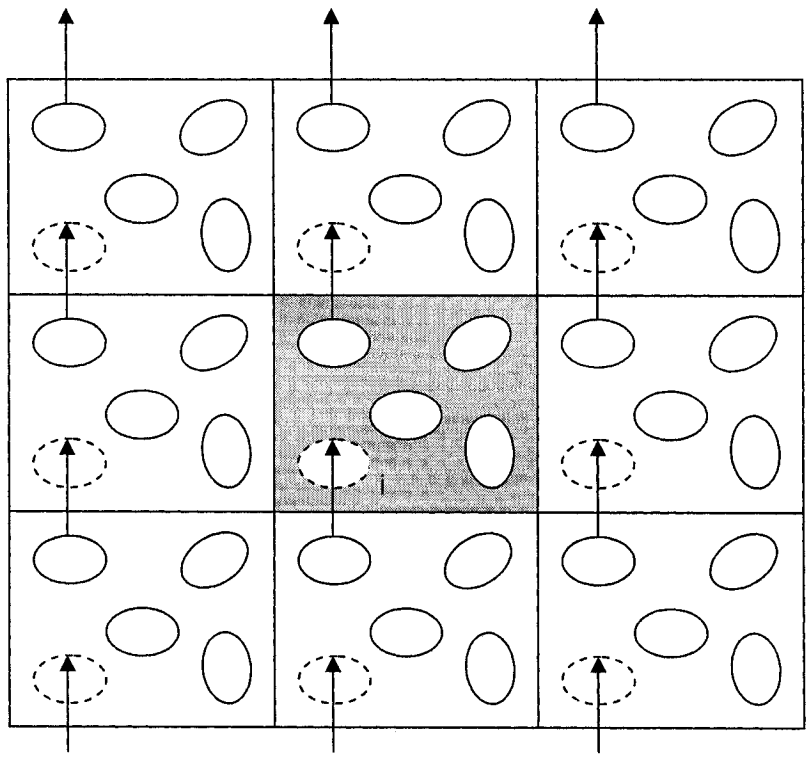

FIG. 2.2: The effect in two dimensional box. The gray square represents the central box, whereas the white ones represent the replicated boxes of the central square gray box. The doted ellipsoids are the periodic images of the ellipsoid I, whereas the arrows describe the moves.

CHAPTER 3: PERTURBATION THEORY

3.1. Perturbation Theory

Quantum mechanical systems may be exposed to perturbations including external fields, magnetic fields, or electromagnetic radiation. Due to such perturbations, the quantum system considered is stimulated and, as a consequence, changes its state. This change of state may include changes in the shape of wave functions, state energies, and occupation probability of states. Perturbation theory is one of the most important methods for obtaining approximate solutions to Schrödinger's equation.

As mentioned in the Introduction, the behavior of a H_2 molecule in the adsorbed phase may be similar to that of H_2 in the condensed phase (quantum solid). Consequently the adsorption of hydrogen molecules on ionic crystal surfaces represents a reasonable quantum model for studying. Taking into account that the Metropolis Monte Carlo simulations depend on classical statistics and the energy states of the particles are regarded as continuous (even for bound states), since our simulations do not consider the quantum properties of the H_2 molecule in the adsorbed phase. The Metropolis Monte Carlo simulations thus form a first approximation of what the adlayer structure should look like. It is suspected that discrepancies between the simulations and the experiments may be quantum mechanical in origin. Therefore, it is necessary to find a reasonable quantum method that is able and suitable to help us resolve any problems might appear in our simulations as well as explore some of the issues of quantum species adsorbed on ionic crystal surfaces.

Due to the weak physisorptive nature of the interaction of a H_2 molecule with the ionic crystal surfaces, the rotational states of the H_2 molecule are expected to be slightly perturbed by the surface electric field from the gas phase states. In this case, perturbation theory (PT) is a useful mathematical technique when the difference in rotational state between the new system (H_2 in adsorbed phase) and the old (H_2 in gas phase) can be regarded as a small correction. Therefore, time independent perturbation theory was applied to calculate the rotational energies as well as the wave functions of H_2 molecule in the adsorbed phase. The PT has been explained in great detail in many references [53]. In our theoretical calculations, the H_2 molecule is considered to be a rigid rotor rotating in the electric field of the (001) face of the solid ionic crystal lattice. The rotational potential was calculated as either a function of azimuthal angle (φ) or as a function of both the polar (θ) and azimuthal angles (φ) (see Fig. 3.1). This rotational potential was constructed and considered as a perturbing Hamiltonian ($\hat{H}'$) and added to the gas phase rotational Hamiltonian ($\hat{H}^o$) to form the rotational Hamiltonian operator of the H_2 molecule in adsorbed phase. This Hamiltonian operator was used to approximately solve the Schrödinger equation and get the rotational energies as well as wave functions. This procedure will be described in detail in the following sections.

3.1.1. H_2 molecule rotates in a surface electric field

Our PT treatment for a hydrogen molecule rotating above the ionic surface is considered for two cases: the case where the molecule is restricted to the

plane of the surface and the case where the molecule is allowed to rotate in three dimensions.

3.1.1.1. Rotation restricted to a plane: one dimension

The rotational potential is generated by rotating an H_2 molecule, sitting flat over the surface (polar angle fixed at θ = 90°), around its center of mass. The azimuthal (φ) orientation of the H—H bond with respect to the x-axis was allowed to vary in the xy-plane, *i.e.* the molecule remains parallel to the surface. Generally, this potential was represented exactly by the following function,

$$V(\varphi) = A_o + A_1 \cdot \cos(4 \cdot \varphi) \tag{3.1}$$

The Hamiltonian operator for a rigid, diatomic molecule rotating in the presence of the electric field of the surface has the form

$$\hat{\mathrm{H}} = \frac{-\hbar^2}{2 \cdot I} \cdot \frac{\partial^2}{\partial \varphi^2} + V(\varphi) \tag{3.2}$$

where, I is the moment of inertia of H_2 molecule and is given by $\mu \cdot r^2$ (μ is the reduced mass of the H_2 molecule, and r is its bond length).

The first and second terms in Eq. (3.2) represent the unperturbed Hamiltonian of an H_2 molecule rotating freely, and the perturbing Hamiltonian operator respectively. The Schrödinger equation describing this system can be written as:

$$\left(\frac{-\hbar^2}{2\cdot I}\cdot\frac{\partial^2}{\partial\varphi^2}+V(\varphi)\right)\cdot\psi_n = E_n\cdot\psi_n \tag{3.3}$$

where, ψ_n is the rotational wave function. If the perturbation term is set to zero the wave function is given by: $\psi_n = \frac{1}{\sqrt{2\pi}}\exp(in\varphi)$ and characterized by a quantum number n= 0, ±1, ±2, ... whose sign designates the direction of rotation. E_n: is the rotational energy of the H_2 molecule in level n.

Through applying PT technique (second order correction level) by pre-multiplying Eq. (3.3) from the left side with ψ_n^* and integrating over φ, we obtain the following:

$$E_n = \langle\psi_n|\hat{H}^o|\psi_n\rangle + \langle\psi_n|\hat{H}'|\psi_n\rangle + \sum_{l\neq n}\frac{\left|\langle\psi_n|\hat{H}'|\psi_l\rangle\right|^2}{E_n^o - E_l^o} \tag{3.4}$$

The different terms in Eq. (3.4) were calculated and found to be:

$$\langle \psi_n | \hat{H}^o | \psi_n \rangle = \frac{n^2 \cdot \hbar^2}{2 \cdot I}$$

$$\langle \psi_n | \hat{H}' | \psi_n \rangle = A_o$$

$$\sum_{l \neq n} \frac{\left| \langle \psi_n | \hat{H}' | \psi_l \rangle \right|^2}{E_n^{(o)} - E_l^{(o)}} = \frac{-I \cdot A_1^2}{16 \cdot \hbar^2} \cdot \frac{1}{n+2}$$

After substituting these integrals in Eq. (3.4). The rotational energy of the adsorbed hydrogen molecule can be calculated by using the following simple formula:

$$E_{n \geq 0} = \frac{n^2 \cdot \hbar^2}{2 \cdot I} + A_o - \frac{I \cdot A_1^2}{16 \cdot \hbar^2} \cdot \frac{1}{n+2} \tag{3.5}$$

The probability density ψ_o^2 was calculated by determining the corrected ground rotational wave function of the adsorbed H_2 molecule through applying PT technique (second order correction) and orthonormal condition as follows:

The ground wave function using just the first and second order wave function corrections [53] can be written as:

$$\psi_{n=0} \approx \psi_{n=0}^{(o)} + \psi_{n=0}^{(1)} + \psi_{n=0}^{(2)} \tag{3.6}$$

where,

$$\psi_{n=0}^{(o)} = \frac{1}{\sqrt{2\pi}} \cdot \exp(in\varphi) = \frac{1}{\sqrt{2\pi}}$$

$$\psi_{n=0}^{(1)} = \sum_{m \neq n} \frac{\left\langle \psi_m^{(o)} \middle| \hat{H}' \middle| \psi_n^{(o)} \right\rangle}{E_n^{(o)} - E_m^{(o)}} \cdot \psi_m^{(o)} = \frac{-1}{\sqrt{2\pi}} \cdot \frac{I \cdot A_1 \pi^2}{2 \cdot h^2} \cdot \cos(4 \cdot \varphi)$$

$$\psi_{n=0}^{(2)} = \sum_{k \neq n} \left[\sum_{m \neq n} \frac{\left\langle \psi_k^{(o)} \middle| \hat{H}' \middle| \psi_n^{(o)} \right\rangle \cdot \left\langle \psi_m^{(o)} \middle| \hat{H}' \middle| \psi_n^{(o)} \right\rangle}{(E_n^{(o)} - E_k^{(o)}) \cdot (E_n^{(o)} - E_m^{(o)})} - \frac{\left\langle \psi_n^{(o)} \middle| \hat{H}' \middle| \psi_n^{(o)} \right\rangle \cdot \delta_{mk} \cdot \left\langle \psi_k^{(o)} \middle| \hat{H}' \middle| \psi_n^{(o)} \right\rangle}{(E_n^{(o)} - E_m^{(o)}) \cdot (E_n^{(o)} - E_k^{(o)})} \right] \cdot \psi_k^{(o)}$$

$$- \frac{1}{2} \cdot \sum_{m \neq n} \frac{\left\langle \psi_m^{(o)} \middle| \hat{H}' \middle| \psi_n^{(o)} \right\rangle \cdot \left\langle \psi_n^{(o)} \middle| \hat{H}' \middle| \psi_m^{(o)} \right\rangle}{(E_n^{(o)} - E_m^{(o)})^2} \cdot \psi_m^{(o)}$$

$$= \frac{1}{\sqrt{2\pi}} \left[\frac{A_1^2 \cdot I^2 \cdot \pi^4}{32 \cdot h^4} \cdot \cos(8 \cdot \varphi) - \frac{(4 \cdot A_o \cdot A_1 + A_1^2) \cdot I^2 \cdot \pi^4}{64 \cdot h^4} \cdot \cos(4 \cdot \varphi) \right]$$

Then, after substitute these wave functions in Eq. (3.6), the ground state rotational wave function has the form:

$$\psi_{n=0} \approx \frac{1}{\sqrt{2\pi}} \left[1 - \left(\frac{I\pi^2}{64 \cdot h^4} \right) \cdot (32 \cdot A_1 h^2 + I \cdot \pi^2 \cdot (4 \cdot A_o A_1 + A_1^2)) \cdot \cos(4 \cdot \varphi) + \frac{A_1^2 I^2 \pi^4}{32 \cdot h^4} \cdot \cos(8 \cdot \varphi) \right] \tag{3.7}$$

By applying a similar procedure, the first excited state (n=1) rotational wave function can be calculated using the following formula:

$$\psi_{n=1} \approx \frac{e^{i\varphi}}{\sqrt{2\pi}} \left[\begin{array}{l} 1 - \frac{I\pi^2}{72 \cdot h^4} \left(12 \cdot A_1 \cdot h^2 + I\pi^2 (4 \cdot A_o A_1 + A_1^2) \right) \cdot e^{4i\cdot\varphi} \\ - \frac{I\pi^2}{8 \cdot h^4} \left(4 \cdot A_1 h^2 + I\pi^2 (4 \cdot A_o A_1 + A_1^2) \right) \cdot e^{-4i\cdot\varphi} + \frac{A_1^2 I^2 \pi^4}{24 \cdot h^4} \left(\frac{e^{8i\cdot\varphi}}{5} + e^{-8i\cdot\varphi} \right) \end{array} \right] \quad (3.8)$$

3.1.1.2. H_2 molecule rotating in three dimensions

The rotational potential of an adsorbed H_2 molecule with its center of mass fixed on the top of cationic/anionic site, was constructed by varying the orientation of the H—H bond with respect to its polar (θ) and azimuthal (φ) angles (See Fig. 3.1). In general, it is found that this rotational potential, can be described by the following function:

$$\begin{aligned} V(\theta,\varphi) = A_o + A_1 \cdot \cos(4 \cdot \varphi) + A_2 \cdot \cos^2\theta + A_3 \cdot \cos^2(2 \cdot \theta) \\ + A_4 \cdot \cos^2\theta \cdot \cos(4 \cdot \varphi) + A_5 \cdot \cos^4\theta \cdot \cos(4 \cdot \varphi) \end{aligned} \quad . \quad (3.9)$$

In order to obtain the energy levels for the adsorbed hydrogen molecule, it is necessary to solve the Schrödinger equation for the Hamiltonian:

$$\hat{H} = \frac{-\hbar^2}{2 \cdot I} \left[\frac{1}{\sin\theta} \frac{\partial}{\partial\theta} \left(\sin\theta \frac{\partial}{\partial\theta} \right) + \frac{1}{\sin^2\theta} \frac{\partial^2}{\partial\varphi^2} \right] + V(\theta,\varphi) \quad (3.10)$$

The orientation of a H_2 molecule, considered as a rigid rotor, is completely specified by two angles θ and φ so that the nuclear portion of the wave function of the hydrogen molecule can be written in terms of spherical harmonics ($Y(\theta,\varphi)$). The spherical harmonics are solutions of the Schrödinger equation of a hydrogen molecule with no external potential (V=0) can be written as,

$$\hat{H}^{o} \cdot Y_{Jm}(\theta,\varphi) = E_J \cdot Y_{Jm}(\theta,\varphi) \tag{3.11}$$

where,

J is the rotational quantum number,

m is the rotational magnetic quantum number,

E_J is the energy of H_2 molecule in the rotational level J.

If the rotational potential is included the Schrödinger equation becomes

$$\hat{H} \cdot \Psi_{Jm}(\theta,\varphi) = E_J \cdot \Psi_{Jm}(\theta,\varphi) \tag{3.12}$$

where the wave function may be expressed as

$$\Psi_{Jm}(\theta,\varphi) = Y_{Jm}(\theta,\varphi) + \sum_{\substack{k\neq J \\ n\neq m}} A_{Jk,mn} \cdot Y_{kn}(\theta,\varphi) \tag{3.13}$$

The rotational energy levels of an adsorbed H_2 molecule were calculated using a time independent perturbation theory (second order level of correction) in

which the rotational potential, $V(\theta,\varphi)$, represents the perturbed Hamiltonian, $\hat{\mathrm{H}}'$.

By pre-multiplying Eq. (3.12) with $\Psi^{*}_{Jm}(\theta,\varphi)$, and integrating over the angular coordinates, the rotational energy levels can be obtained using the following:

$$E_{Jm} = \langle Y_{Jm} | \hat{\mathrm{H}}^{o} | Y_{Jm} \rangle + \langle Y_{Jm} | \hat{\mathrm{H}}' | Y_{Jm} \rangle + \sum_{\substack{n \neq J \\ m'=+n}}^{-n} \frac{\left| \langle Y_{Jm} | \hat{\mathrm{H}}' | Y_{nm'} \rangle \right|^{2}}{E_{J}^{(o)} - E_{n}^{(o)}} \tag{3.14}$$

where,

$$\langle Y_{Jm} | \hat{\mathrm{H}}^{o} | Y_{Jm} \rangle = \frac{J(J+1)\cdot \hbar^{2}}{2 \cdot I}$$

To solve the remaining two other terms in Eq. (3.14), we use the method of separation of variables, and thus, the spherical harmonic functions are written in the following form,

$$Y_{Jm}(\theta,\varphi) = \Theta_{J}^{m}(\theta) \cdot \Phi_{m}(\varphi) \tag{3.15}$$

where,

$$\Theta_{J}^{m}(\theta) = \left[\frac{(2 \cdot J+1) \cdot (J-|m|)!}{2 \cdot (J+|m|)!} \right]^{1/2} \cdot p_{J}^{|m|}(\cos\theta), \; and \;\; \Phi_{m}(\varphi) = \frac{1}{\sqrt{2 \cdot \pi}} \cdot \exp(im\varphi).$$

Therefore, the integrals in the second and third terms of Eq. (3.14) can be determined as:

$$1.\ \langle Y_{Jm}|\hat{H}'|Y_{Jm}\rangle = \left\langle \Theta_J^m(\theta)\cdot\Phi_m(\varphi)\middle|\hat{H}'\middle|\Theta_J^m(\theta)\cdot\Phi_m(\varphi)\right\rangle$$

$$= A_o\cdot\left\langle \Theta_J^m\cdot\Phi_m\middle|\Theta_J^m\cdot\Phi_m\right\rangle + A_1\cdot\langle\Phi_m|\cos(4\cdot\varphi)|\Phi_m\rangle\cdot\left\langle\Theta_J^m\middle|\Theta_J^m\right\rangle$$

$$+ A_2\cdot\langle\Phi_m|\Phi_m\rangle\cdot\left\langle\Theta_J^m\middle|\cos^2\theta\middle|\Theta_J^m\right\rangle + A_3\cdot\langle\Phi_m|\Phi_m\rangle\cdot\left\langle\Theta_J^m\middle|\cos^2(2\cdot\theta)\middle|\Theta_J^m\right\rangle$$

$$+ A_4\cdot\langle\Phi_m|\cos(4\cdot\varphi)|\Phi_m\rangle\cdot\left\langle\Theta_J^m\middle|\cos^2\theta\middle|\Theta_J^m\right\rangle$$

$$+ A_5\cdot\langle\Phi_m|\cos(4\cdot\varphi)|\Phi_m\rangle\cdot\left\langle\Theta_J^m\middle|\cos^4\theta\middle|\Theta_J^m\right\rangle$$

which simplifies using the orthonormal conditions[2] to,

$$\langle Y_{Jm}|\hat{H}'|Y_{Jm}\rangle = A_o + A_2\cdot\left\langle\Theta_J^m\middle|\cos^2\theta\middle|\Theta_J^m\right\rangle + A_3\cdot\left\langle\Theta_J^m\middle|\cos^2(2\cdot\theta)\middle|\Theta_J^m\right\rangle\ ;$$

and

$2.\ \langle Y_{Jm}|\hat{H}'|Y_{nm'}\rangle$, which must be dealt with as two cases:

a. If $m \neq m'$, then:

$\langle Y_{Jm}|\hat{H}'|Y_{nm'}\rangle$ This integral has been calculated as follows,

i) For *para*-H_2; $J = 0$, $m = 0$,

$$\langle Y_{00}|\hat{H}'|Y_{nm'\neq 0}\rangle = \langle Y_{00}|\hat{H}'|Y_{4\pm 4}\rangle$$

---

[2] The orthonormal conditions are: $\langle\Phi_m|\Phi_n\rangle = \delta_{mn}$, and $\left\langle\Theta_J^m\middle|\Theta_n^m\right\rangle = \frac{2}{(2\cdot J+1)}\cdot\frac{(J+|m|)!}{(J-|m|)!}\cdot\delta_{Jn}$

where $\delta_{ij} = \begin{cases}1 & i = j\\ 0 & i \neq j\end{cases}$.

ii) For helicoptering *ortho*-H_2; $J = 1$, $m = \pm 1$,

In the case of $J = 1$, $m = 1$,

$$\langle Y_{11} | \hat{H}' | Y_{nm'\neq 1} \rangle = \langle Y_{11} | \hat{H}' | Y_{3-3} \rangle + \langle Y_{11} | \hat{H}' | Y_{5-3} \rangle + \langle Y_{11} | \hat{H}' | Y_{55} \rangle$$

whereas, for cartwheeling *ortho*-H_2; $J = 1$, $m = 0$,

$$\langle Y_{10} | \hat{H}' | Y_{nm'\neq 0} \rangle = \langle Y_{10} | \hat{H}' | Y_{5\pm 4} \rangle$$

On average, the contribution of these integrals, $\langle Y_{Jm} | \hat{\mathrm{H}}' | Y_{nm'} \rangle$, to the rotational energies was found to be negligible, and was not included in our calculations.

b. If $m = m'$, then:

$$\langle Y_{Jm} | \hat{\mathrm{H}}' | Y_{nm} \rangle = A_o \cdot \langle \Phi_m | \Phi_m \rangle \cdot \langle \Theta_J^m | \Theta_n^m \rangle + A_1 \cdot \langle \Phi_m | \cos(4 \cdot \varphi) | \Phi_m \rangle \cdot \langle \Theta_J^m | \Theta_n^m \rangle$$

$$+ A_2 \cdot \langle \Phi_m | \Phi_m \rangle \cdot \langle \Theta_J^m | \cos^2 \theta | \Theta_n^m \rangle$$

$$+ A_3 \cdot \langle \Phi_m | \Phi_m \rangle \cdot \langle \Theta_J^m | \cos^2 (2 \cdot \theta) | \Theta_n^m \rangle$$

$$+ A_4 \cdot \langle \Phi_m | \cos(4 \cdot \varphi) | \Phi_m \rangle \cdot \langle \Theta_J^m | \cos^2 \theta | \Theta_n^m \rangle$$

$$+ A_5 \cdot \langle \Phi_m | \cos(4 \cdot \varphi) | \Phi_m \rangle \cdot \langle \Theta_J^m | \cos^4 \theta | \Theta_n^m \rangle$$

$$= A_2 \cdot \langle \Theta_J^m | \cos^2 \theta | \Theta_n^m \rangle + A_3 \cdot \langle \Theta_J^m | \cos^2 (2 \cdot \theta) | \Theta_n^m \rangle$$

The integral $\langle Y_{Jm} | \hat{\mathrm{H}}' | Y_{nm} \rangle \neq 0$ only when $n = J + 2$, therefore, the rotational energy can be calculated by using the following formula:

$$E_{Jm} = \frac{J \cdot (J+1) \cdot \hbar^2}{2 \cdot I} + A_o + A_2 \cdot \left\langle \Theta_J^m \middle| \cos^2 \theta \middle| \Theta_J^m \right\rangle + A_3 \cdot \left\langle \Theta_J^m \middle| \cos^2 (2 \cdot \theta) \middle| \Theta_J^m \right\rangle - \frac{I \cdot \left| A_2 \cdot \left\langle \Theta_J^m \middle| \cos^2 \theta \middle| \Theta_{J+2}^m \right\rangle + A_3 \cdot \left\langle \Theta_J^m \middle| \cos^2 (2 \cdot \theta) \middle| \Theta_{J+2}^m \right\rangle \right|^2}{\hbar^2 \cdot (2 \cdot J + 3)} \quad (3.16)$$

The wave function of the H_2 species in adsorbed phase may be determined using just the first order wave function correction:

$$\Psi_{Jm}^{ads.} \approx Y_{Jm}^{(0)} + \sum_{k \neq J} \frac{\left\langle Y_{Jm}^{(0)} \middle| \hat{\mathrm{H}}' \middle| Y_{km}^{(0)} \right\rangle}{E_{Jm}^{(0)} - E_{km}^{(0)}} \cdot Y_{km}^{(0)} \quad (3.17)$$

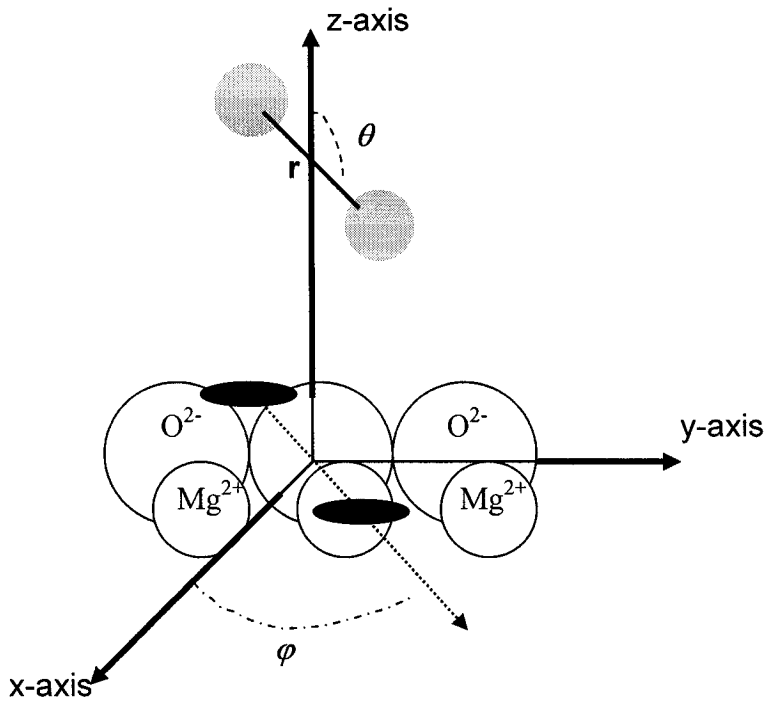

FIG. 3.1: Schematic diagram of a H_2 molecule located over MgO surface, where the mass center of H_2 (H atoms represent by gray solid circle) is on the top of O^{2-} site. The molecular orientation with respect to the surface normal is given by θ, the bond length is given by **r**, and the azimuthal orientation of the H—H bond with respect to the x-axis is given by φ.

CHAPTER 4: INTERACTION POTENTIAL MODEL

4.1. Model of the adsorption of H_2 on ionic crystal surfaces

The effectiveness of the methods of simulations to solve chemical problems depends mainly on the potential model that is used to represent and describe the interaction forces involved among particles, atoms or ions in the system under investigation. Therefore considerable attention has been given, relatively recently (since 1970) [54], to constructing accurate and realistic atom (molecule)-surface interaction potentials. The reliability of these interaction potentials are of great importance for extracting information such as surface structures, thermal stability, as well as thermodynamic quantities such as heat of adsorption, specific heat, ...*etc* and comparing them with experimental findings [55,56].

Various methods have been developed to study the interaction of atoms and neutral molecules with solid surfaces such as SCF calculations [57], and other *ab initio* studies [58]. However, these methods are computationally expensive and are best suited to simple isolated molecules in specific adsorption sites and orientations. To perform simulations that allow freedom of movement and to include molecule-molecule interactions most of the theoretical efforts were dedicated to the construction of semi-empirical interaction potentials, which would fit the experimental data [59, 60]. For the hydrogen on ionic crystal systems the construction of semi-empirical or empirical potentials is possible but not trivial.

For molecules adsorbed on an ionic solid, the interaction potential can be written easily as a summation of molecule-molecule and molecule-surface interactions. To a good approximation, the potentials may be represented as a sum of pair-wise potentials between the various atom-atom and atom-ion interactions [61]. Therefore, the total potential consists of two parts: the inter-atomic potential, and the atom-surface potential. In this work, these potentials are constructed by the same technique used by Polanyi's group [62, 63]. The atom-atom and atom-ion potentials, within two-body approximation, have been employed to describe the repulsion and dispersion interactions; while the electrostatic interactions have been represented using distributed atomic multipoles. By summing over all of the interactions the total potential energy is constructed.

In general the interaction potential between two particles can be separated into two main types: 'long-range' interaction where the potential energy is inversely proportional to the distance between the interacting particles, this kind of interaction usually divided into three contributions, electrostatic, induction and dispersion, and 'short-range' interaction where the potential energy decreases exponentially with distance as is typical of exchange and repulsion interactions. In the next two sections we will give a brief description for all of these types of interactions in the potential model of the H_2 molecules adsorbed over the ionic crystal surfaces [MgO(001), LiF(001) and NaCl(001)].

4.1.1. Molecule-molecule interaction potential

The interaction potential between two hydrogen molecules mainly comes from classical electrostatic interactions, which may be calculated by using distributed point dipoles. The repulsion-dispersion interactions are estimated using the Buckingham potential formula. In this work, these interactions are simplified by using 'site-site' or 'atom-atom' approximation, where the H_2 molecules are represented as two H atoms that interact individually with H atoms of other H_2 molecules. Consequently, the molecule-molecule interaction potential can be calculated as a sum of atom-atom potentials.

4.1.1.1. Electrostatic model

The hydrogen molecule has only a permanent quadrupole moment. As a result, a two dipole model is used where point dipoles (μ) are placed on each H atom to represent the molecular quadrupole moment of H_2. According to the "2 point dipoles" model, the dipoles have the same magnitude but are oriented along opposite directions of the H_2 bond axis (see Fig. 4.1). Using the definitions of the molecular multipole moments for linear molecules, it was found that atomic point dipoles can be calculated from the value of the quadrupole moment of the hydrogen molecule as shown below,

$$\Theta = 2 \cdot \sum_{i=1}^{2} p_i \cdot x_i + \sum_{i=1}^{2} q_i \cdot x_i^2 \tag{4.1}$$

$$= 2 \cdot \left(p_1 \cdot x_1 + p_2 \cdot x_2 \right) \tag{4.2}$$

As shown in Fig. 4.1, Eq. (4.2) can be rewritten in the following form,

$$= 2 \cdot \left(\mu \cdot \frac{r_o}{2} + (-\mu) \cdot (-\frac{r_o}{2}) \right) = 2 \cdot \mu \cdot r_o \tag{4.3}$$

So the atomic point dipole (μ_H) can be calculated from the molecular quadrupole moment (Θ_{H_2}) using the following formula,

$$\mu = \frac{\Theta}{2 \cdot r_o} \tag{4.4}$$

where Θ is the quadrupole moment of H_2, which has an experimental value of +0.6177 D.Å [64], and r_o is the length of the H_2 bond, and has a value of 0.74 Å [65]. According to Eq. 4.4, the point dipole on each of the H atoms is ± 0.4174 D.

For H_2 molecules the induction energy has been neglected because it contributes only around 1% of the amount of the total interaction energy. Leaving this term out saves time in doing these calculations. Consequently, the electrostatic potential can be visualized as the interaction between the distributed point dipoles $\bar{\mu}$ on the atoms of one H_2 molecule with those of other H_2 molecules, and can be calculated as a sum of dipole-dipole interactions using the following formula:

$$V^{dd} = \sum_{nn'} \frac{R^2(\mu_i^n \cdot \mu_j^{n'}) - 3 \cdot (\mu_i^n \cdot R)(\mu_j^{n'} \cdot R)}{4 \cdot \pi\varepsilon_o R^5} \tag{4.5}$$

where,

μ_i^n : is the point dipole of the ith atom of the nth H_2 molecule.

$\mu_j^{n'}$: is the point dipole of the jth atom of the n'th H_2 molecule.

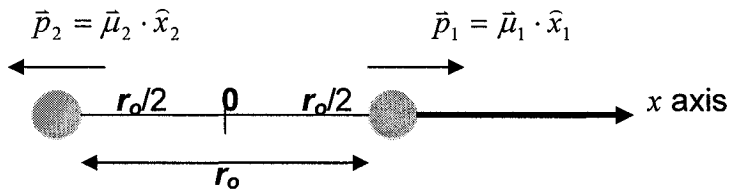

FIG. 4.1: The electrostatic model of the H_2 molecule, where r_o is its bond lenght, p_i is the atomic quadrupole moment. Note that $|\mu_1| = |\mu_2| = \mu$, and $|\hat{x}_1| = |\hat{x}_2| = r_o/2$.

4.1.1.2. Dispersion and repulsion interactions

At intermediate and short distances, the dispersion-repulsion energy forms a significant contribution to the total interaction energy. Therefore, it is mandatory to take into account these contributions to get a realistic and logical description of the interaction potential between two molecules. At infinite distance, the dispersion interaction, which is due to electron correlation, is negligible ($E_{disp.}$=0). As the inter-molecular separation gets smaller, the dispersion energy becomes stronger. But as the intermolecular separation becomes less than their

dimensions the two molecules start to repel each other and the energy rises rapidly. In general the dispersion interaction leads to an increase in the electron density between the interacting atoms or molecules whereas the repulsion leads to a decrease in the electron density between them, therefore at very short separation the reduction in the electron density appears as an increase in the repulsion potential with a reduction in the dispersion energy.

In our model, the repulsion and dispersion interactions between molecules are modeled using the Buckingham potential formula,

$$V_{atom}^{gg}(r_{ij}^{nn'}) = A_{ij} \cdot \mathrm{e}^{-\beta_{ij} \cdot r_{ij}^{nn'}} - \frac{C_6^{ij}}{(r_{ij}^{nn'})^6} \tag{4.6}$$

where, $r_{ij}^{nn'}$ is the distance between the *i*th atom on the nth molecule and *j*th atom on the n'th molecule; A_{ij} and β_{ij} are the strength and the decay constants that characterize the repulsive potential range at various atomic sites respectively. The C_6 is the London dispersion coefficient denoting the strength of the mutually induced dipole-dipole interaction.

The values of the repulsion and dispersion parameters used to generate atom-atom interactions have been derived from the *ab initio* studies of H_2 dimers [66, 67], and the procedure that applied to obtain these parameters are described in detail as in the following two sections.

4.1.1.2.1. Repulsion parameters

The Born-Mayer A_{ij} and β_{ij} parameters of H—H atoms interaction that used to describe 'site-site' repulsion potential have been derived from the repulsion parameters of H_2—H_2 molecules interaction that was estimated by Toennies' group [66]. These parameters ($A_{ij}=A_H$, $\beta_{ij}=\beta_H$) are derived as follows:

a) For the softness parameter, we supposed that both are the same [44], *i.e.*: $\beta_{H_2} = \beta_H$.

b) The repulsion potential parameter of H_2 molecule are derived based on the Born-Mayer formula of the repulsion potential ($V_{rep.} = A_{H_2} \cdot \exp(-\beta_{H_2} \cdot r)$), so according to Fig. 4.2:

$$V_{rep.}(r) = A_{H_2} \cdot \exp(-\beta_{H_2} \cdot r') = A_{H_2} \cdot \exp(-\beta_{H_2} \cdot (r + r_o))$$

$$= A_{H_2} \cdot \exp(-\beta_H \cdot r_o) \cdot \exp(-\beta_H \cdot r)$$

$$V_{rep.}(site - site) = A_H \cdot \exp(-\beta_H \cdot r)$$

where,

$$A_H = A_{H_2} \cdot \exp(-\beta_H \cdot r_o)$$

A list of the values of the site-site repulsion parameters constructed by the above procedure can be found in Table 4.1.

The repulsion radii and softness parameters of the hydrogen atomic site may be derived from the Born-Mayer parameters listed in Table 4.1 using Eq. (4.19).

Table 4.1: The repulsion potential parameters of molecule-molecule and site-site interactions. The A_i values are in kcal/mol, while β_i values are in Å^{-1}.

	$H_2 - H_2{}^a$	$H - H^b$
A_{H_2}	10568.523	
β_{H_2}	3.2124	
A_H		980.889
β_H		3.2124

a) Taken from ref. [66], b) This work.

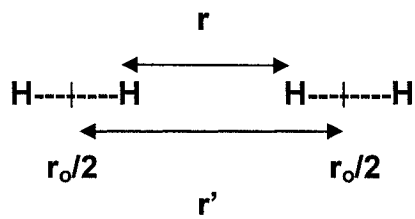

FIG.4.2: Schematic diagram of H_2—H_2 interaction model.

4.1.1.2.2. Dispersion parameters

The dispersion coefficients $C_6^{ij}, C_8^{ij}, and\ C_{10}^{ij}$ for atom-atom long-range interactions can be estimated in a number of ways. One of these methods is to generate these parameters from van der Waals coefficients $Pl_6H, Pl_8H, and\ Pl_{10}H$, atomic dispersion parameters, which can be derived from the long-range dispersion interaction coefficients of the H_2 dimer, {C_6=12.3 a.u, C_8=217.8 a.u, and C_{10}=4976 a.u [67]}. The coefficients of the atom—atom dispersion interactions were calculated as follows:

$$C_6^{H_2-H_2} = (Pl_6H_2)^2 = (2 \cdot Pl_6H)^2 \Rightarrow Pl_6H = \frac{\sqrt{C_6^{H_2-H_2}}}{2} \Rightarrow C_6^{H-H} = (Pl_6H)^2$$

By the same procedure,

$$Pl_8H = \frac{\sqrt{C_8^{H_2-H_2}}}{2} \Rightarrow C_8^{H-H} = (Pl_8H)^2$$

and

$$Pl_{10}H = \frac{\sqrt{C_{10}^{H_2-H_2}}}{2} \Rightarrow C_{10}^{H-H} = (Pl_{10}H)^2$$

These parameters for H—H long-range interactions are shown in Table 4.2. Note that the values of C_6, C_8, and C_{10} for H---H interaction have been used to

generate the dispersion coefficients of H atom with ions of the surface as will be seen in section 4.1.2.2.

Table 4.2: Estimated values of $C_6, C_8, and\ C_{10}$ for H---H dispersion interaction.

Parameter	C_6 (Å^6·kcal/mol)	C_8 (Å^8·kcal/mol)	C_{10} (Å^{10}·kcal/mol)
H—H	42.38	210.163	1344.689

4.1.2. Molecule-surface (gas-solid) interaction potential

The surfaces of dielectric substrates with square symmetry, like LiF, NaCl, and MgO (001) faces, are good experimental and theoretical candidates for molecular physisorption studies, where there is no significant surface reconstruction. For the MgO(001) surface, where the coordination number of the oxygen changes from six in the bulk to five on surface, the asymmetry between bulk and vacuum results in the polarization of the solid and the creation of a surface electric field [68, 69]. The creation of the surface electric field raises the possibility of surface reconstruction.

There are a number of experimental and theoretical studies that examine the stability of MgO substrates with (001), (011) or (111) surfaces. One of these studies using MD simulations at T=300 K shows that the (011) and (111) faces are highly distorted with surface reconstruction in order to lower their surface

energies. This reconstruction occurred as a result of oxygen anions migrating from the bulk toward the surface to create small (001) faces [70, 71]. These studies also indicate that the (001) face enjoys high stability, where the ions are arranged in a square unit cell, and consist of one MgO pair with length $\mathbf{a_o}$= 2.97Å as shown in Fig. 4.3. The length of the surface unit cell is smaller than that of the face of the bulk unit cell [72] because the cubic symmetry needs to be repeated in only two dimensions as opposed to three for the bulk.

Although the clean (001) surface does not reconstruct, there is a possibility that the adsorption of molecules will induce reconstruction. Because the physical adsorption of H_2 molecule on the substrate is very weak, (it's binding energy is around –0.7 kcal/mol), the substrate surface structure does not perturb and hence the distance between ions is the same as in the bulk structure. In our model, the MgO(001) clean surface was constructed as an array of closed-shell ions that is periodic in *xy* plane, regular in *z* direction, and has the same characteristics (spacing, symmetry, and composition) as the bulk solid. To simplify our calculations, the thermal motions of the surface ions are not included, since our simulations a re performed at very cold temperature region (T=1-13 K).

Similar assumptions have been applied in the case of the physical adsorption of H_2 molecules on NaCl(001) and LiF(001) surfaces, where the formal charge on the atoms of these ionic solid are ±1. For NaCl(001), the lattice

constant are greater than that of MgO(001) and hence more space is available for hydrogen molecules to adsorb. The LiF(001) surface has a lattice constant that is smaller than that of the MgO(001) surface (see Table 4.3), although it's ions are arranged in a square unit cell just as in the case of the MgO(001) surface. Throughout this work, we assume that the NaCl and LiF surfaces are rigid and un-deformable as in the case of MgO.

As mentioned earlier, the H_2 molecule is considered as two atoms interacting individually with the ions of the surface and hence the interaction potential between the single adsorbed molecule and the surface may be determined as a pair-wise sum of the interaction potential between the constituent atoms of the admolecule and the ions of the solid substrate. The total interaction potential can be described by the following equation:

$$V^{gs}(\vec{r}_{i'}) = \sum_i V^{gs}_{atom}(\vec{r}_{i'} - \vec{R}_i) = \sum_i V^{gs}_{atom}(\vec{r}_{ii'}) \tag{4.7}$$

where,

$\vec{R}_i$ is the solid lattice vector

$V^{gs}_{atom}(\vec{r}_{ii'})$ is the interaction potential between the gas atom(i') and the ith ion in the solid separated by a distance $\vec{r}_{ii'}$ as shown in Fig. 4.4. The coordinate z represents the perpendicular distance of the gas atom from the substrate,

In a similar approach to the calculation of molecule-molecule interaction potential, the total interaction potential between a H_2 molecule and the substrate [MgO, NaCl, or LiF] has been calculated as a sum of pair-wise atom-ion interactions consisting of three contributions: electrostatic, repulsion and dispersion. In the next section, we will discuss these contributions in detail.

Table 4.3: The lattice constant, $\mathbf{a_o}$, of the square unit cell of the (001) face and their bulk solid lattice constant, **c**, of the MgO, NaCl and LiF surfaces.

	MgO	NaCl	LiF
$\mathbf{a_o}$ (Å)	2.97	3.99	2.85
c (Å)	4.2	5.64	4.03

4.1.2.1. Electrostatic interaction

In our potential model, the electrostatic interaction between a hydrogen molecule and the surface [MgO(001), NaCl(001), or LiF(001)] is divided into two contributions: the Coulomb potential and the induction energy. The Coulomb potential describes the interaction between the electric field $\vec{E}(r)$ of the surface with the point dipoles ($\vec{\mu}$) located on the two atomic sites of H_2 molecule.

Therefore, the Coulomb interaction potential of a single H_2 molecule, for example, on the MgO(001) may be calculated using the following formula;

$$V_{coul.}^{gs} = \sum_{i=1}^{2} \vec{\mu}(\vec{r}_i) \cdot \vec{E}(\vec{r}_i) \tag{4.8}$$

The electric field $\vec{E}(\vec{r}_i)$ at the (001) face of the ionic crystal surface can be determined from the electrostatic potential $\Phi(\vec{r})$ of the surface [62, 63, and 74] as follows:

$$\vec{E}(\vec{r}) = -\nabla\Phi(\vec{r});$$

Where,

$$\Phi(\vec{r}) = -\frac{4e}{a}\left[\frac{\exp\left(-\frac{2\cdot\pi\cdot z}{a}\right)}{1+\exp(-\sqrt{2}\cdot\pi)}\right]\left[\cos\left(\frac{2\cdot\pi\cdot x}{a}\right)+\cos\left(\frac{2\cdot\pi\cdot y}{a}\right)\right] \tag{4.9}$$

where, a is a constant related to the lattice constant c of the crystal through using the following relation: $c = \sqrt{2}\cdot a$ and e is the magnitude of the electronic charge on an individual ion.

The coordinate system of the position $\vec{r} = (x, y, z)$ has its origin at the anionic site for MgO, LiF and NaCl surfaces, for example, MgO(001), at an O^{2-} site. The z-axis is perpendicular to the surface plane, while the x and y-axes

are in the surface plane pointing toward adjacent O^{2-} sites along $\langle 110 \rangle$ and $\langle 111 \rangle$ directions of the MgO unit cell.

In the adsorbed phase, the H_2 molecule resides close to the surface where the electric field is strong enough to distort the charge distribution of the H_2 molecule and induce a dipole moment. The strength of the induced dipole is proportional to the strength of the electric field

$$\vec{\mu}_{ind.} = \vec{\alpha} \cdot \vec{E} \tag{4.10}$$

where, $\vec{\alpha}$ is the matrix of the H_2 molecular polarizability. In our model, the molecular polarizability was represented by atomic polarizabilities perpendicular $(\alpha_i^{\perp})$ and parallel $(\alpha_i^{//})$ to the molecular axis, therefore the induction energy due to the interaction between the induced dipole and the surface electric field may be calculated using the following relation;

$$V_{ind.}^{gs} = -\sum_{i=1}^{2} \int_0^E \vec{\mu}_{ind.} \cdot d\vec{E} = \frac{-1}{2} \sum_{i=1}^{2} \alpha_i \cdot E^2(r_i) \tag{4.11}$$

$$= -\frac{1}{2} \sum_{i=1}^{2} \left(\alpha_i^{\perp} \vec{E}_{\perp}^2(r_i) + \alpha_i^{//} \vec{E}_{//}^2(r_i) \right)$$

where the sum is over the two atomic sites of H_2 molecule. The required parameters that need to generate H_2 point dipoles and their atomic polarizabilities are listed in Table 4.4.

The total electrostatic potential of a single H_2 molecule on the (001) face of the ionic crystal surfaces may be written as

$$V_{el}^{gs} = V_{coul.}^{gs} + V_{ind.}^{gs} \tag{4.12}$$

It is worth mentioning here that the potential functions used in the electrostatic calculations are similar to those applied by Polyani's group in their study of the HBr/LiF(001) system [62].

4.1.2.2. Dispersion and repulsion interactions

Part of the potential interaction between the hydrogen admolecule and the substrate ions is due to short-range repulsion and long-range dispersion interactions. In this work, they are treated as being pair-wise additive where the potential is written as a summation of two body interactions between each constituent atom of the admolecule and the individual ions of the substrate. For a gas atom and an ion separated by a distance r_{ij}, the repulsion-dispersion interaction may be calculated using Tang-Toennies formula [75]:

$$V_{atom}^{gs}(r_{ij}) = A_{ij} \cdot \exp(-\beta_{ij} \cdot r_{ij}) - \sum_{n=3}^{5} \left(f_{2n}(r_{ij}) \frac{C_{2n}^{ij}}{(r_{ij})^{2n}} \right) \tag{4.13}$$

where, β_{ij} (decay constant) and A_{ij} (characterize the strength and range of the repulsion potential) are the Born-Mayer parameters, the coefficients

C_6^{ij}, C_8^{ij}, *and* C_{10}^{ij} are dispersion constants denoting the strength of the mutually induced dipole-dipole, dipole-quadrupole and quadrupole-quadrupole interactions respectively. The Tang-Toennies damping function $f_{2n}(r_{ij})$ may be written as below,

$$f_{2n}(r) = 1 - \left[\sum_{k=0}^{2n} \frac{(\beta \cdot r)}{k!}\right] \cdot \exp(-\beta \cdot r) \tag{4.14}$$

As seen from Eq. (4.14), the damping function is characterized by the decay constant (β) of the repulsion term and is used to remove the singularities at very short distance between the gas atom and the ions of the surface.

Now, we can determine the total potential for a single adsorbed atom interacting with the substrate by summing all the pair potentials over all the lattice ions. However, this process will be inefficient, as the surface potential must be recalculated for each new position and orientation of the molecule. Instead of this, we use the periodicity of MgO or NaCl or LiF lattice and replace the direct summation by a two-dimensional Fourier series of the periodic potential $V_{atom}^{gs}(r_{ij})$, as on the following equation [62, 63],

$$V^{gs}(x,y,z) = \sum_{n,m}^{\infty} V_{atom}^{n,m}(z) \cdot \cos\left(\frac{2\pi \cdot n}{a} \cdot x\right) \cdot \cos\left(\frac{2\pi \cdot n}{a} \cdot y\right) \tag{4.15}$$

where, n, m = 0,1,2,3, ... defines an infinite series. Usually equation (4.15) is truncated at $n+m$ = 2 level.

As shown in Eq. (4.13), the molecule-surface interaction potential depends on a number of atom-ion parameters, which constructed from the lateral interaction parameters of the like atom-atom or ion-ion values with the application of suitable combining rules. A brief description of the procedure of the combining rules that was used to generate the parameters of mixed or dislike atom-ion pairs for each type of interactions will be presented in the next section.

Table 4.4: Summary of the parameters for the electrostatic model of the hydrogen molecule. The positions of the H atoms are given with respect to the molecular center of mass. The two point dipoles are directed along the H_2 bond axis away from the center of mass as shown in Fig. 4.1.

	H_a atom	H_b atom
position (Å)	0.37	-0.37
point dipole (D)	0.4174	-0.4174
polarizability $\perp$(Å^3)	0.3504	0.3504
polarizability $\parallel$(Å^3)	0.5018	0.5018

4.1.2.2.1. Repulsion parameters

The repulsion potential term as presented in Eq. (4.13) can be written in an alternative formulation, where the Born-Mayer parameters become dependent on the size and softness of the interacting atoms or ions, with a mathematical expression as below

$$V_{rep.}(r_{ij}) = (B_i + B_j) \cdot \exp\left(\frac{A_i + A_j - r_{ij}}{B_i + B_j}\right) \tag{4.16}$$

where A_i, A_j are repulsion radii, and B_i, B_j are softness parameters. Therefore, the repulsion term in Eq. (4.13) and the above formula (Eq. (4.16)) are connected by the following equations:

1. The decay constant (β_{ij}) of the repulsion potential may be written as a function of the softness parameters as follows;

$$\beta_{ij} = \frac{1}{B_i + B_j} \tag{4.17}$$

2. The strength of the repulsion potential written as a function of the repulsion radii as below;

$$A_{ij} = (B_i + B_j) \cdot \exp\left(\frac{A_i + A_j}{B_i + B_j}\right) \tag{4.18}$$

It is necessary to mention here that the above formulas are used to calculate the values of the Born-Mayer parameters of the two identical atoms or ions (i.e. $i = j$), and hence we can write them as follows,

$$\beta_{jj} = \frac{1}{2 \cdot B_j} \; ; \; A_{jj} = 2 \cdot B_j \cdot \exp\left(\frac{A_j}{B_j}\right) = \frac{1}{\beta_{jj}} \cdot \exp\left(\frac{A_j}{B_j}\right) \tag{4.19}$$

In the case where we have a mixed system consisting of two non-identical atoms, or ions, combining rules proposed by Smith and Gilbert [76, 77] were used to construct the Born-Mayer repulsion parameters of unlike atoms/ions from the parameters of the like-like atom or ion system using the following relations:

1. The decay constant (β_{ij}) of the repulsion potential may be calculated using the following formula;

$$\beta_{ij} = \frac{2 \cdot \beta_{ii} \cdot \beta_{jj}}{\beta_{ii} + \beta_{jj}} \tag{4.20}$$

2. The strength of the repulsion potential (A_{ij}) may be calculated using the following relation:

$$A_{ij} = \frac{(A_{ii} \cdot \beta_{ii})^c \cdot (A_{jj} \cdot \beta_{jj})^d}{\beta_{ij}} \tag{4.21}$$

where,

$$c = \frac{\beta_{jj}}{\beta_{ii} + \beta_{jj}} \quad , \quad d = \frac{\beta_{ii}}{\beta_{ii} + \beta_{jj}}$$

Usually in our calculations of the repulsion parameters of atom-ion system, the subscripts i stand for the atoms of the molecule (namely H) and j for the surface ions, i.e. Mg^{2+}, O^{2-} or Na^{+}, Cl^{-} or Li^{+}, F^{-}.

To calculate the Born-Mayer parameters of the two identical atoms or ions, the repulsion radii (A_j) and softness (B_j) parameters for the ions Mg^{2+}, O^{2-}; Na^{+}, Cl^{-}; and Li^{+}, F^{-} are taken from the literature, whereas for the H atoms the values were estimated from the data obtained from *ab-initio* studies of H_2 dimers and are listed in Table 4.1. For the MgO surface, the parameters of its ions are taken from references [76], and [78], whereas the parameters for the LiF and NaCl surfaces are obtained from references [77] and [79] respectively. By using Eq. (4.19), the Born-Mayer (A_{jj}, β_{jj}) parameters are calculated and the results are listed in Table 4.5.

The repulsion parameters listed in Table 4.5 were inserted in Eqs. (4.20), and (4.21) to estimate the Born-Mayer parameters of atom-ion system, i.e. H—G, where G is: Mg^{2+}, O^{2-} Na^{+}, Cl^{-}; and Li^{+}, F^{-}, and are presented in Table 4.8.

Table 4.5: The two identical ion-ion repulsion parameters of the ionic crystal surfaces, MgO, NaCl and LiF.

Parameter	A_{ii} (kcal/mol)	β_{ii} (Å^{-1})
$Mg^{2+} - Mg^{2+}$	3.019×10^{7}	9.615
$O^{2-} - O^{2-}$	675.095	2.00
$Na^{+} - Na^{+}$	4.674×10^{5}	5.857
$Cl^{-} - Cl^{-}$	1.958×10^{4}	2.491
$Li^{+} - Li^{+}$	5.661×10^{4}	6.688
$F^{-} - F^{-}$	1.207×10^{4}	3.174

4.1.2.2.2. Dispersion coefficients

There are many different ways that may be used to estimate the dispersion coefficients C_6^{ij}, C_8^{ij}, and C_{10}^{ij} of unlike atoms/ions. The method used for our potential model employs combining rules derived from the Casimir-Polder theory of dispersion coefficients [80]. This method was examined before and yielded a good representation for the diatomic molecules interactions with rare gas atoms [81]. A detailed description of the combining rules of the Casimir-Polder theory with the procedure of the calculations of the values of C_6^{ij}, C_8^{ij}, and C_{10}^{ij} for the $H-G$ interactions, where $G: Mg^{2+}, O^{2-}, Na^{+}, Cl^{-}$ and Li^{+}, F^{-}, is presented as follows,

1. The C_6^{ij} coefficients of the H_2 molecule with the ions of the surface were estimated using the following relation:

$$C_6^{ij} = \frac{2 \cdot C_6^{ii} \cdot C_6^{jj} \cdot \alpha_i \cdot \alpha_j}{C_6^{ii} (\alpha_j)^2 + C_6^{jj} (\alpha_i)^2} \tag{4.22}$$

where, i refers to H_2 molecule, j refers to the ions of the ionic crystal surface , and α is the dipole polarizability.

2. The C_8^{ij} coefficients of the unlike molecule-ion (H_2-G) were calculated using the following combination rule [80]:

$$C_8^{ij} = \frac{15}{4} \cdot \sum_{k=1}^{2} \left(\frac{\alpha_k^i \cdot \alpha_{2/k}^j \cdot \Omega_k^i \cdot \Omega_{2/k}^j}{\Omega_k^i + \Omega_{2/k}^j} \right) \tag{4.23}$$

where, α_1 is the dipole polarizability, α_2 is the quadrupolar polarizability, and

$$\Omega_1^m = \frac{4}{3} \cdot \frac{C_6^{mm}}{\left(\alpha_1^m\right)^2} \quad ; m = i, j$$

$$\Omega_2^m = \frac{2 \cdot C_8^{mm} \cdot \Omega_1^m}{15 \cdot \alpha_1^m \cdot \alpha_2^m - 2 \cdot C_8^{mm}} \quad ; \; m = i, j$$

3. The values of C_{10}^{ij} for the interaction of hydrogen molecule with the ions of the adsorbent have been estimated using the following relation [82]:

$$C_{10}^{ij} \approx \frac{49 \cdot (C_8^{ij})^2}{40 \cdot (C_6^{ij})} \tag{4.24}$$

All the required information that is required to estimate the dispersion coefficients using the above formulas is listed in Table 4.6.

The dispersion coefficients of the H_2 molecule with the ions of the surface were calculated using Eqs. (4.22), (4.23), and (4.24). These results are listed in Table 4.7.

At this stage, the dispersion interactions are estimated using the dispersion coefficients of the molecule-ion pairs. However, the potential requires that the dispersion parameters be calculated in terms of the atom-ion pairs. So that the atom-ion dispersion parameters are obtained from the molecule-ion dispersion parameters through multiplying them by a scaling factor based on their atomic polarizabilities. Taking into account that there is no exact procedure for the breakdown of the molecular polarizability into its constituent atomic polarizabilities, the estimation of the atom-ion polarizabilities can be made from the examination of the van der W aals coefficients PL_6H and PL_6H_2 which are proportional to the atomic and molecular polarizabilities, i.e. $PL_6H \propto \alpha_H$, and

$PL_6H_2 \propto \alpha_{H_2}$. This procedure of calculating the scaling factor was adopted in this work as follows;

As shown earlier in section 4.1.1.2.2., the van der Waals coefficient PL_6H_2 can be written in terms of PL_6H as follows,

$$C_6^{H_2-H_2} = (Pl_6H_2)^2 = (2 \cdot Pl_6H)^2$$

$$\therefore PL_6H_2 = 2 \cdot PL_6H$$

Therefore, the ratios of $\frac{\alpha_H}{\alpha_{H_2}}$ can be calculated using the relation,

$$\frac{\alpha_H}{\alpha_{H_2}} = \frac{PL_6H}{PL_6H_2} \tag{4.25}$$

Consequently the dispersion coefficients C_6 of the atom-ion pairs ($H-Mg^{2+}$, $H-O^{2-}$, $H-Na^{+}$, $H-Cl^{-}$, and $H-Li^{+}$, $H-F^{-}$) were calculated by multiplying the corresponding values of the C_6 molecule-ion pairs by a scaling factor of 0.5 using the following relation;

$$C_6^{atom-ion} = \frac{\alpha_H}{\alpha_{H_2}} \cdot C_6^{molecule-ion} \tag{4.26}$$

$$= \frac{1}{2} \cdot C_6^{molecule-ion}$$

In case of, for example, H_2-MgO(001),

$$C_6^{H-Mg^{2+}} = \frac{1}{2} \cdot C_6^{H_2-Mg^{2+}}, \quad C_6^{H-O^{2-}} = \frac{1}{2} \cdot C_6^{H_2-O^{2-}}.$$

Using Eq. (4.26), the C_6 coefficient values of the atom-ion pairs of hydrogen atoms with the ions of MgO, NaCl, and LiF surfaces are calculated and the results are presented in Table 4.8.

To estimate the C_8 and C_{10} coefficients of the atom-ion pairs, it was assumed that the C_8/C_6 and C_{10}/C_6 ratios of the atom-ion pairs are the same as the corresponding molecule-ion ratios, *i.e.*, $\left(\frac{C_8}{C_6}\right)^{atom-ion} \approx \left(\frac{C_8}{C_6}\right)^{molecule-ion}$ and $\left(\frac{C_{10}}{C_6}\right)^{atom-ion} \approx \left(\frac{C_{10}}{C_6}\right)^{molecule-ion}$. Through multiplying these ratios by the value of C_6 of the atom-ion pairs, which were obtained using Eq. (4.26), the values of C_8 and C_{10} of the atom-ion pairs were calculated and listed in Table 4.8. It is worth noting here that in the case of H atoms interacting with the ions of the surface, the procedure employed to calculate the C_8 and C_{10} coefficients of the atom-ion pairs is equivalent to the results obtained by using the following relation;

$$C_{2n}^{H-ion} = \frac{\alpha_H}{\alpha_{H_2}} \cdot C_{2n}^{H_2-ion} \tag{4.27}$$

$$= \frac{1}{2} \cdot C_{2n}^{H_2-ion}; \quad n = 3,4,5$$

With the formulas and parameters specified in this chapter, the molecule-molecule and molecule-surface interaction potentials are fully specified.

Table 4.6: The polarizability and dispersion coefficients values of in-solid crystal $Mg^{2+}, O^{2-}, Na^{+}, Cl^{-}, Li^{+}$, F^{-} and H_2 molecule.

	C_6 $Å^6\ kcal/mol$	C_8 $Å^8\ kcal/mol$	Dipole polarizability $\alpha_1(Å^3)$	Quadrupolar polarizability $\alpha_2(Å^5)$
Mg^+	7.385[a]	11.687[b]	0.0724[c]	0.0107[d]
O^{2-}	833.515[e]	5813.66[e]	1.681[f]	1.081[g]
Na^+	21.886[a]	49.894[h]	0.15[i]	0.0316[j]
Cl^-	2485.012[a]	23606.063[h]	3.135[j]	2.697[k]
Li^+	1.0751[l]	0.9688[l]	0.028455[l]	0.002316[u]
F^-	319.3491[a]	1361.783[l]	0.89[l]	0.4091[j]
H_2	169.53[m]	840.68[m]	0.80949[m]	0.71098[m]

a) Taken from ref. [83].
b) Taken from ref. [84].
c) Taken from ref. [85].
d) Taken from ref. [86].
e) Taken from ref. [87].
f) Taken from ref. [88].
g) Taken from ref. [89].
h) Taken from ref. [90].
i) Taken from ref. [91].
j) Taken from ref. [92].
k) Taken from ref. [92].
l) Taken from ref. [93].
m) Taken from ref. [67].

Table 4.7: Calculated dispersion parameters for the molecule-ion pairs of H_2 with MgO, NaCl, and LiF interactions.

Interaction	C_6 $Å^6\ kcal/mol$	C_8 $Å^8\ kcal/mol$	C_{10} $Å^{10}\ kcal/mol$
H_2-Mg^{2+}	25.62	81.083	314.347
H_2-O^{2-}	375.099	2153.096	15139.676
H_2-Na^+	49.629	200.562	992.89
H_2-Cl^-	649.02	4735.946	42334.225
H_2-Li^+	9.975	30.103	111.29
H_2-F^-	227.069	1770.696	16914.767

Table 4.8: Calculated repulsion and dispersion parameters of the atom-ion pairs of the H_2 with MgO, NaCl, and LiF interactions.

Interaction	A $(kcal/mol)$	β $(Å^{-1})$	C_6 $Å^6\ kcal/mol$	C_8 $Å^8\ kcal/mol$	C_{10} $Å^{10}\ kcal/mol$
H(atom)-Mg^{2+}	11455.04	4.816	12.81	40.542	157.174
H(atom)-O^{2-}	758.168	2.465	187.55	1076.548	7569.838
H(atom)-Na^+	8345.968	4.149	24.814	100.281	496.445
H(atom)-Cl^-	5253.496	2.806	324.51	2367.973	21167.113
H(atom)-Li^+	3433.794	4.34	4.987	15.052	55.645
H(atom)-F^-	3467.13	3.193	113.535	885.348	8457.383

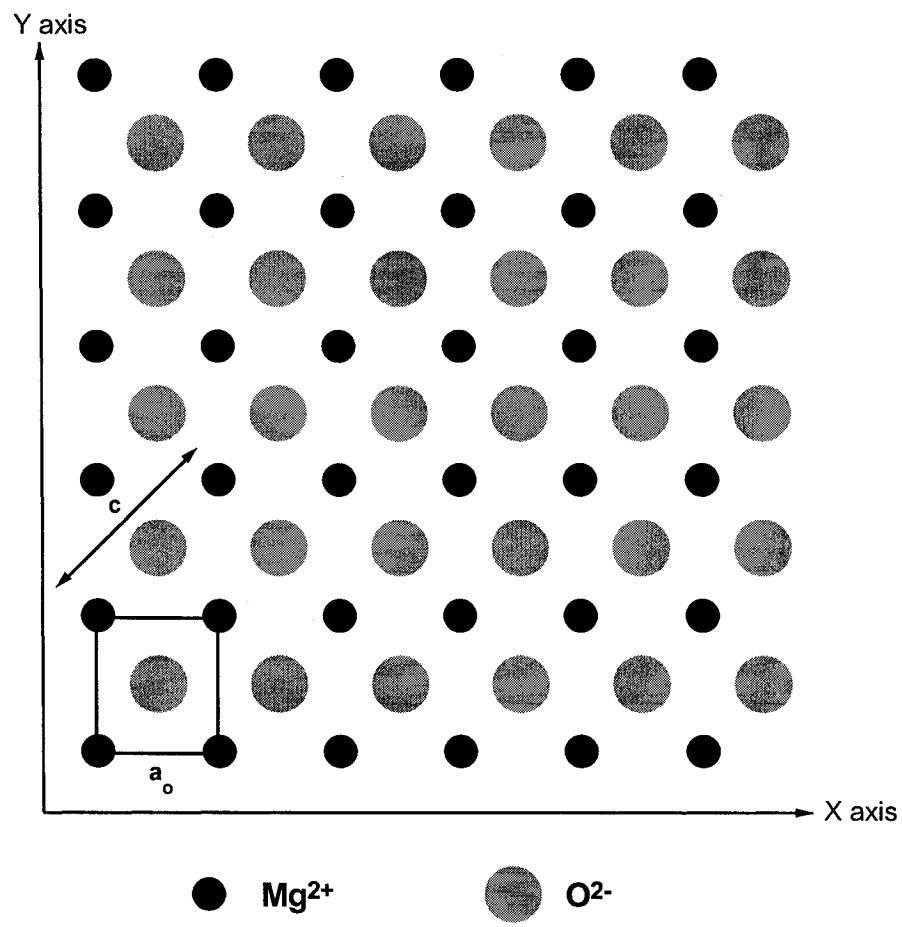

FIG.4.3: The schematic diagram of the (001) face of MgO surface, where the black circles represent the Mg^{2+} ions, and the gray ones represent the O^{2-} ions. $\mathbf{a_o}$ is the lattice constant of the XY plane of the (001) surface. **c** is the bulk solid lattice constant.

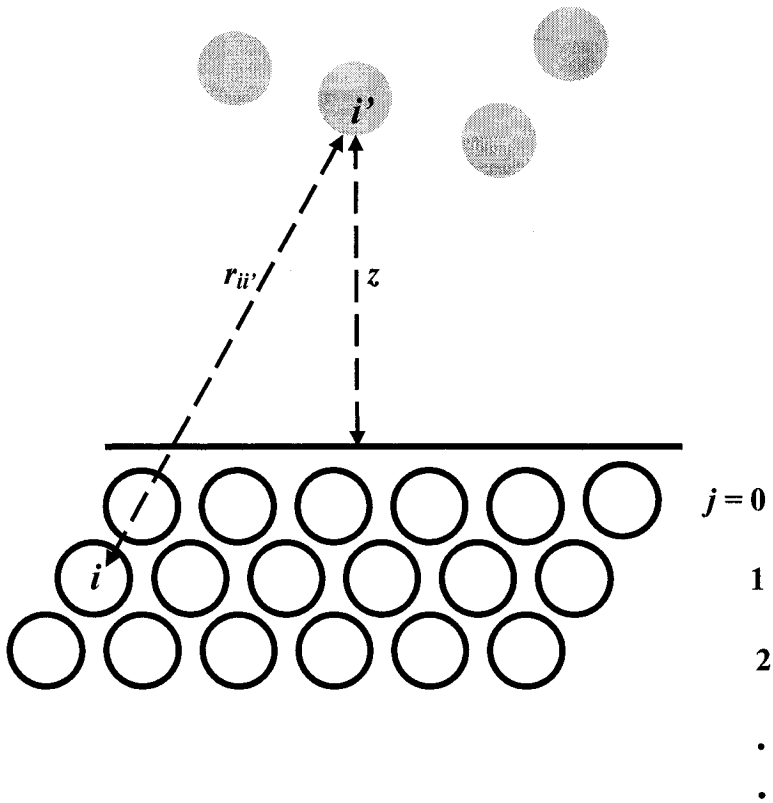

FIG.4.4: Schematic diagram of the coordination system of the gas-surface interaction potential as taken from reference [73].

CHAPTER 5: RESULTS FOR H_2 MONOLAYERS ON MgO(001)

To examine the structures of layers of H_2 molecules adsorbed on the (001) face of a MgO surface, Monte Carlo (MC) simulations in the canonical ensemble, were performed using a detailed interaction potential and classical statistics. Once the structures were obtained, a detailed calculation was applied using the time-independent perturbation theory (PT) to estimate the quantum mechanical delocalization of the H_2 molecular axis in different rotational levels in the adsorbed phase. In the following sections, a Monte Carlo study of the H_2/MgO system along with the results of the calculations of the rotational states of the adsorbed H_2 molecules is reported.

5.1. Simulation Results: H_2/MgO(001)

5.1.1. Single molecule adsorbed on MgO(001) surface

In order to test the suitability of the parameters presented in chapter 4, the adsorption of a single H_2 molecule was examined at temperatures (1-9 K) by using MC simulations. These simulations were run for 20 kcycles, at each cycle the molecule was allowed to change its position and orientation randomly. Molecular hydrogen was found to lie flat (the tilt angle θ is 90°) above the surface at a height of 2.75 Å *i.e.* the distance from the mass center of the H_2 molecule to the Mg^{2+} ion directly below. The molecule was found to bind to the surface with an energy of -0.602 kcal/mol (T=1 K). This binding energy is in excellent agreement with the experimental value (-0.606 kcal/mol) obtained from

isothermal measurements [26] at T=8.8 K and is at the upper end of the values estimated by Toennies (-0.461 to -0.577 kcal/mol) [28]. Gaussian-like distributions were obtained for both the polar and azimuthal angles and are centered at $\theta = 90^{\circ}$ and $\varphi = 45^{\circ}$ respectively. Thus, on average, the molecule lies in the plane parallel to the surface ($\theta = 90^{\circ}$) and is oriented toward the neighboring O^{2-} ions ($\varphi = 45^{\circ}$). Our finding that the H_2 molecules prefer to adsorb on the Mg^{2+} ionic sites is consistent with proposals based on recent HAS experiments [28] and neutron scattering experiments [94]. Consequently, our model yields a reasonable description of the adsorption potential of a H_2 molecule over a MgO surface.

Out of necessity, the multiparticle Monte Carlo simulations reported below neglect quantization effects, but for a single particle they can be estimated where pertinent. For adsorbed hydrogen the motion perpendicular to the surface is expected to be quantized and there may be an appreciable zero point energy due to the relatively light mass of the molecule. This will lead to a discrepancy between the potential well depth and the experimentally measured binding energy. Fitting the surface potential used above to a harmonic oscillator model with anharmonic corrections, the zero point energy was estimated to be 0.074 kcal/mol (3.2 meV) so that the binding energy becomes -0.528 kcal/mol, which falls within the range estimated by Toennies (-0.461 to -0.577 kcal/mol) [28]. Thus the potential model yields reasonable binding energies regardless of the inclusion or not of quantum effects.

5.1.2. H_2 adlayers: *p*(2×2) structure

Both neutron scattering [94] and HAS [28] experiments found that a *c*(2×2) structure was formed at a coverage of 0.5 monolayer. It was proposed that every other Mg^{2+} site is occupied and the H_2 molecules all have the same average orientation. This structure has been examined using the Metropolis Monte Carlo method using a patch of surface with 144 Mg^{2+} sites and 72 H_2 molecules to yield the correct coverage. These simulations were run for 50 kcycles at T=1 K with a variety of different initial structures consistent with the required *c*(2×2) symmetry. In all cases we obtained the same final configuration as shown in Fig. 5.1. The unit cell of the final configuration (outlined in Fig. 5.1) has *p*(2×2) symmetry and contains two H_2 molecules. The molecules are on average aligned perpendicular to each other ("T" configuration) with one molecule aligned along the intermolecular axis. This is to be expected for molecules lying in the plane of the surface since this orientation maximizes quadrupole-quadrupole interactions between molecules.

The θ distributions (see Fig. 5.2) are bell-shaped with peaks at 90° for temperatures up to 12 K. The φ distribution, as shown in Fig. 5.3, indicates that at 1 K there are two sharp peaks at φ =45° and 135°. These peaks still exist at 12 K although they have been thermally broadened. Together these distributions indicate that the *p*(2×2) structure persists up to 12 K.

The average molecular binding energy of a H_2 molecule in this structure at 1 K was found to be -0.688 kcal/mol with an average center of mass height of 2.79Å from the top of a Mg^{2+} ion, as shown in Fig. 5.4. It is worthwhile to mention that the molecular binding energy in the $p(2\times2)$ layer consists of two contributions. For example, at T=1 K the binding energy consists of a molecule-surface contribution of –0.598 kcal/mol plus a small contribution from the molecule-molecule interaction of –0.09 kcal/mol. Therefore, the binding energy of the layer is greater than that of a single molecule on the surface owing to the net attraction between molecules. The molecules in the $p(2\times2)$ layer sit slightly higher above the surface than the position of the energy minimum of a single molecule, but these values are within the error bounds (±0.05 Å) of the thermal distribution. An increase in temperature causes the peak in the height distribution to shift upwards to 3.0 Å at 12 K. When the temperature was increased beyond 12 K the molecules were no longer localized at the cation sites and start to desorb from the surface causing disorder in the surface layer. Thus, the $p(2\times2)$ layer is stable only up to 12 K. The onset of disorder in the adlayer above 12 K has also been observed in HAS experiments [28].

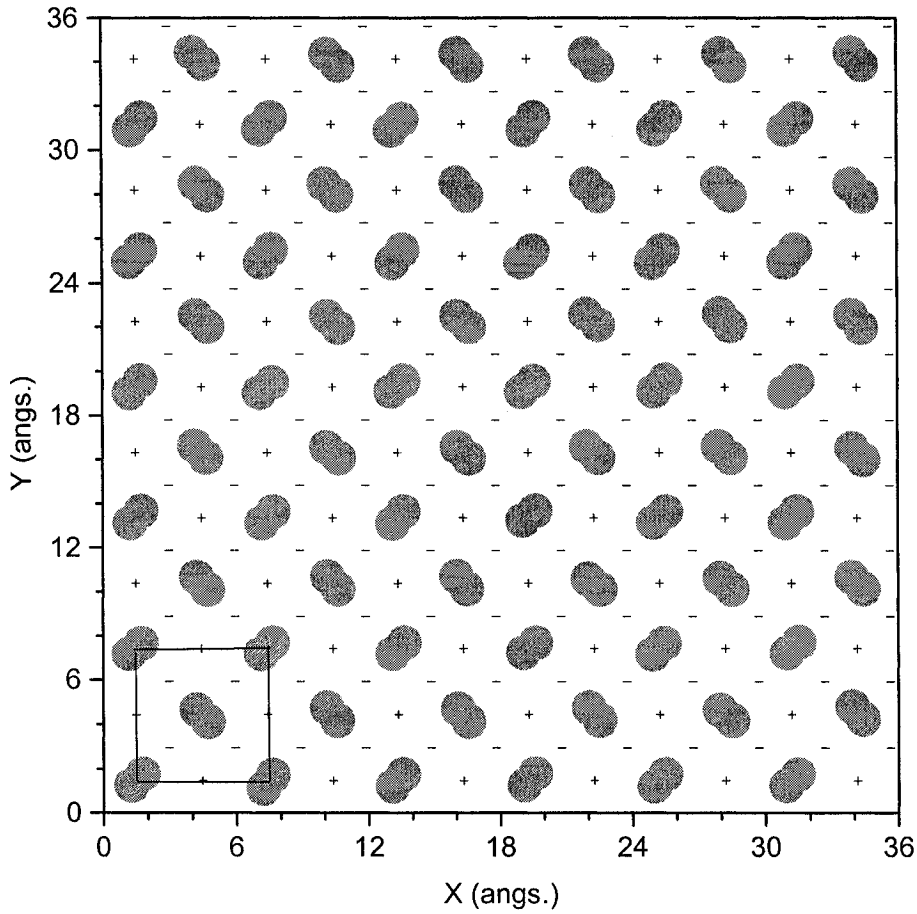

FIG. 5.1: The MgO(001) surface covered with 72 H_2 molecules at 1 K. The hydrogen atoms are shown as gray circles. The (+) symbol represents a Mg^{2+} ion and the (-) symbol represents an O^{2-} ion. The $p(2\times2)$ unit cell is also shown in solid lines.

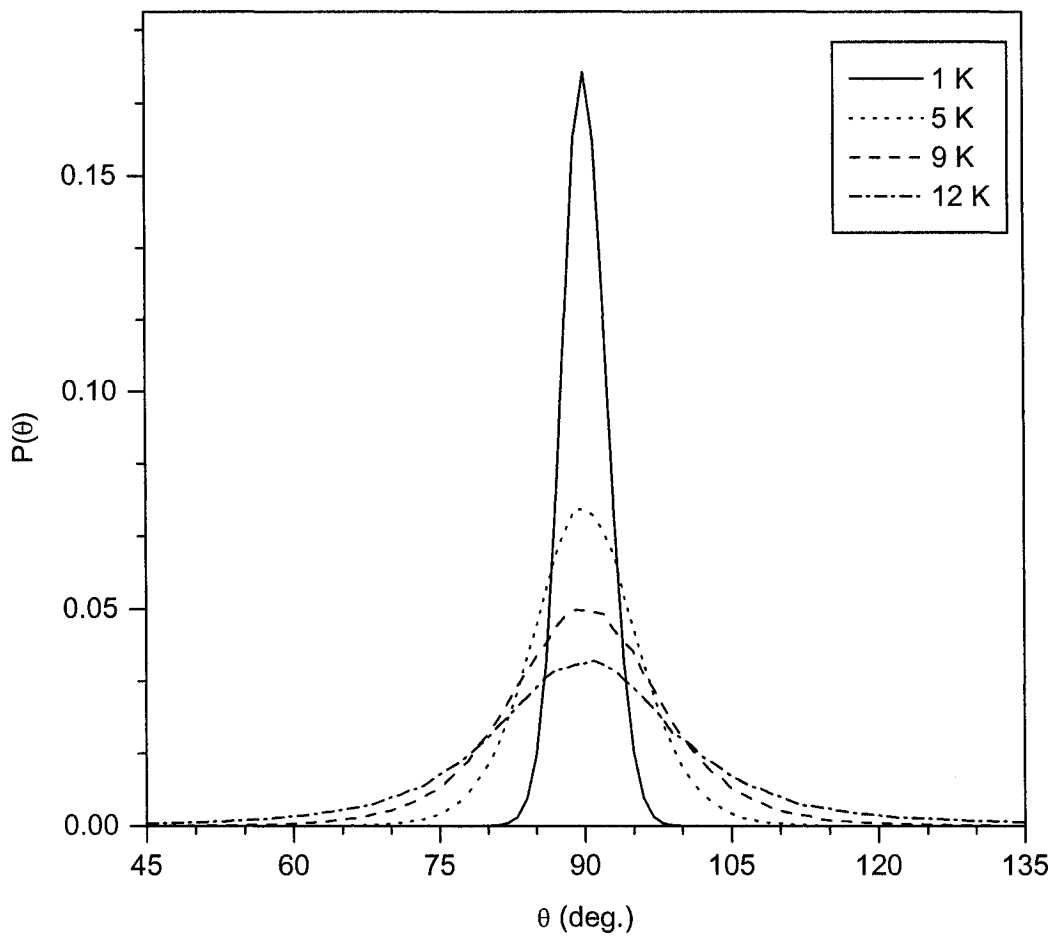

FIG. 5.2: The polar angle distribution of the *p*(2×2) layer is plotted for temperatures T=1, 5, 9, and 12 K.

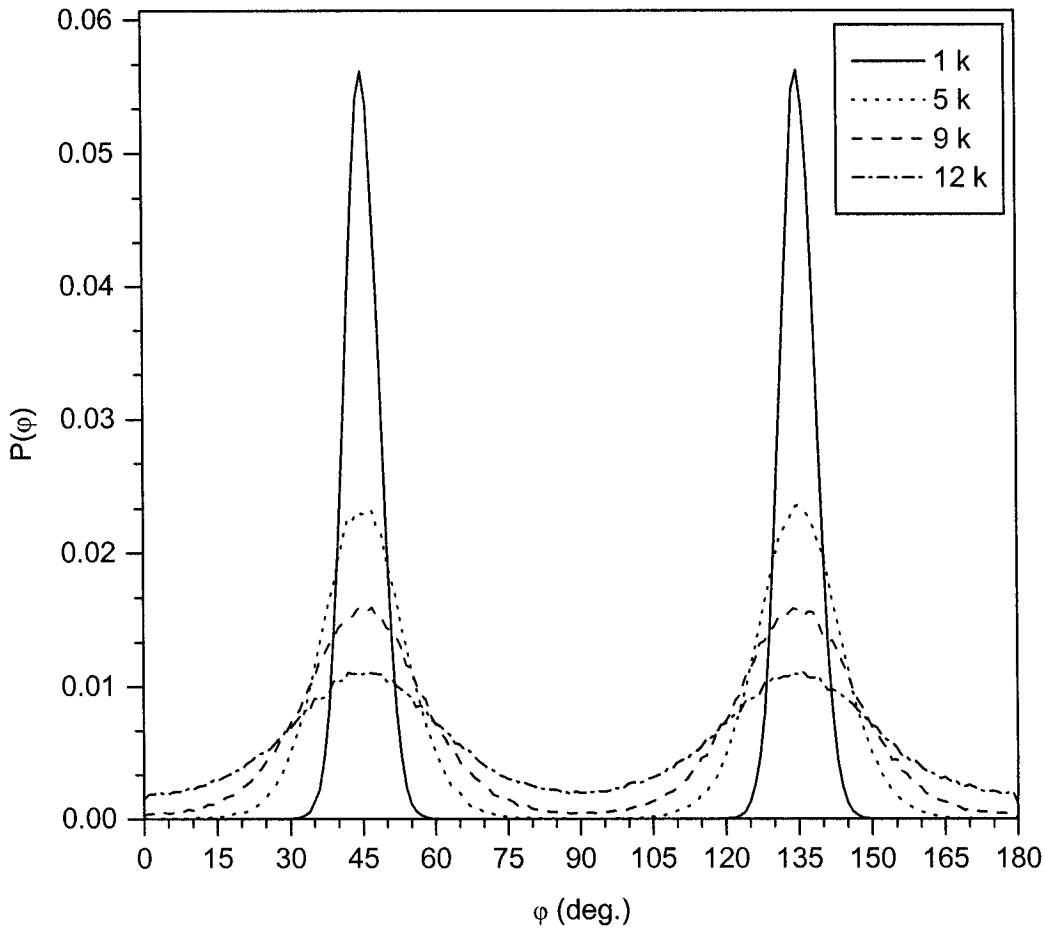

FIG. 5.3: The azimuthal angle (φ) distributions of the $p(2\times2)$ mono-layer plotted for temperatures T=1, 5, 9, and 12 K.

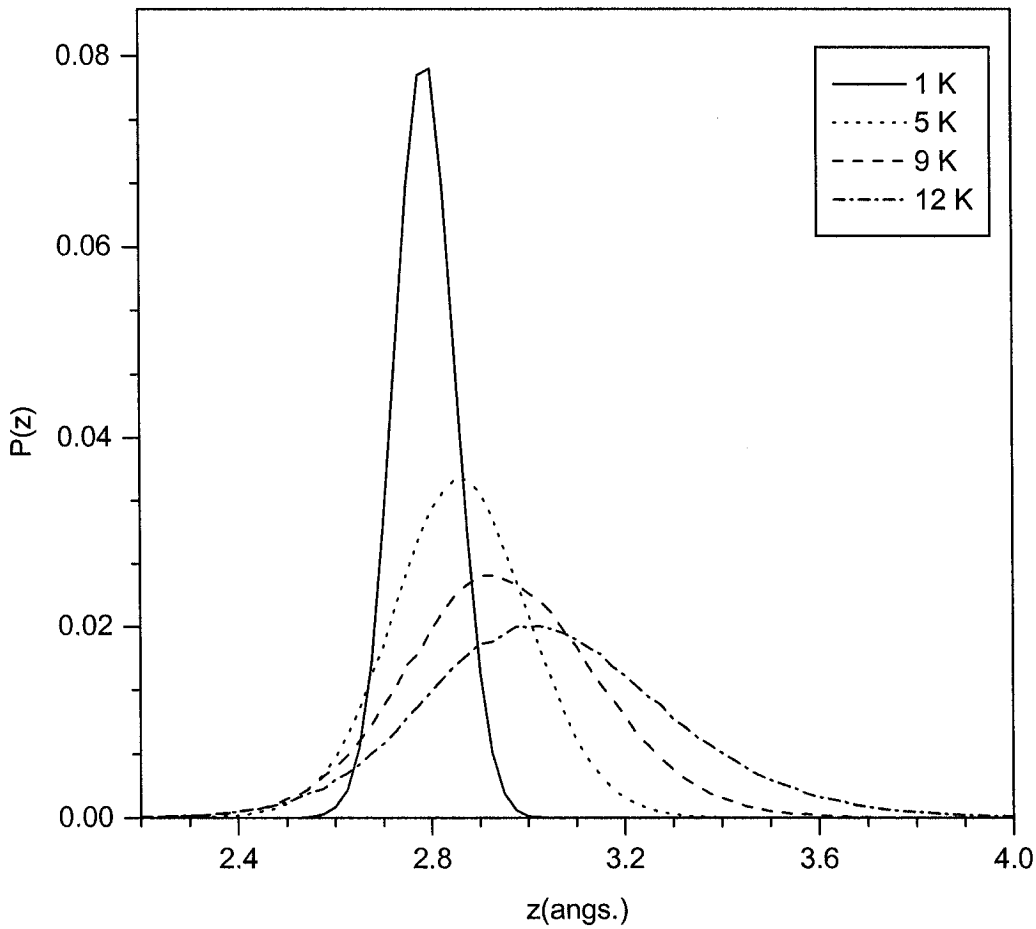

FIG. 5.4: The height (z) distribution of the H_2 molecules center of mass for the *p*(2×2) layer plotted for temperatures T=1, 5, 9 and 12 K.

5.1.3. H_2 adlayers: *p*(4×2) structure

At densities above 0.5 monolayers, two other phases have been observed experimentally. The *c*(4×2) phase has an estimated coverage of 0.75 and it was proposed that the molecules are equally spaced along the cationic channels of the surface. The unit cell then contains two types of adsorption sites: those where the molecules are adsorbed directly over the Mg^{2+} ions while the remaining molecules are displaced from the Mg^{2+} ionic sites along the cationic channels [28]. This proposed configuration was examined by using the Metropolis Monte Carlo method, with 108 molecules over a (12×12) patch of surface (in order to have a coverage of 0.75). Many configurations with different initial orientations were examined in simulations that were run for 50 kcycles at 1 K. Regardless of the initial structure chosen, the simulations all evolved to a single final configuration. This structure was found to be a *p*(4×2) structure with six molecules per unit cell (see Fig. 5.5). In this configuration it was found that there are two kinds of adsorption sites: a parallel site where H_2 molecules lay flat on the surface (atoms shown as solid gray at the corner and the center of the unit cell in Fig. 5.5), and a tilted site where the molecules (consisting of black and light gray atoms in Fig. 5.5) adsorb between the cationic and anionic sites. The parallel sites are similar to sites found in the *p*(2×2) structure where the molecules are adsorbed directly above the Mg^{2+} ions. The tilted sites, however, are offset from both the cationic and anionic sites. Typically, the absolute value of the displacement of the center of mass of the tilted H_2 molecule from the underlying Mg^{2+} site in the x and y directions are 0.73 Å and 0.38 Å respectively,

where the long axis of the unit cell is along the x direction. The molecular axes of the tilted molecules point toward nearby O^{2-} ions so that the lower H atoms, shown as black in Fig. 5.5, are closer to the anions than the cations. Within a unit cell two molecules occupy parallel sites and four molecules occupy tilted sites.

The θ distribution, as shown in Fig. 5.7, has two peaks for all temperatures tested (1, 5 and 9 K) and clearly shows the existence of two types of adsorption sites. The peak at 90° is associated with molecules on the parallel sites while the peak at 58° corresponds to the tilted molecules. The φ distribution shown in Fig. 5.8 also indicates that there are two modes of adsorption. The two sharp peaks at φ = 45° and 135° are due to molecules on the parallel sites while the larger peaks at φ = 55° and 125° are attributed to the tilted molecules. The difference in peak height is due to the presence of twice as many tilted molecules as flat molecules. An increase in temperature to 5 K causes the peaks to merge into two broad peaks at φ = 50° and 130°. Both angular distributions are still exist up to 9 K, indicating that the $p(4\times2)$ structure is stable up to this point, where the structure is shown also in Fig. 5.6.

The height distribution also shows the presence of two adsorption sites, especially at T = 1 K (see Fig. 5.9). The peak at 3.28 Å is attributed to tilted molecules and is approximately twice as large as the peak at 2.75 Å that corresponds to molecules in parallel sites. The relative peak sizes are consistent with there being twice as many molecules that occupy tilted sites as occupy

parallel sites. If viewed as separate layers, the tilted molecules sit 0.5 Å higher than the flat molecules and cause some degree of compression of the flat molecules by forcing them to sit slightly lower than in the $p(2\times2)$ structure. An increase in temperature causes both peaks in Fig. 5.9 to broaden and shift to higher values. At 11 K, the molecules start to migrate from their adsorption site and causing disorder within the adlayer. Some molecules also desorbs from surface.

At T=1 K the average binding energy of a molecule in the $p(4\times2)$ layer is –0.667 kcal/mol (a molecule-surface contribution of -0.53 kcal/mol plus a molecule-molecule contribution of -0.137 kcal/mol) while the average binding energy of the tilted molecules and flat molecules are –0.657 kcal/mole and –0.687 kcal/mole respectively. The binding energy of a flat molecule in the $p(4\times2)$ structure is less than that of the $p(2\times2)$ structure because the interaction of a molecule with its six neighboring tilted molecules is less attractive than that of a molecule with its four neighboring flat molecules in the $p(2\times2)$ case. By accepting a less favorable interaction between molecules the surface density of molecules in the $p(4\times2)$ structure can be increased above that of the $p(2\times2)$ case. One can view the $p(4\times2)$ structure as consisting of alternating rows of tilted and flat molecules.

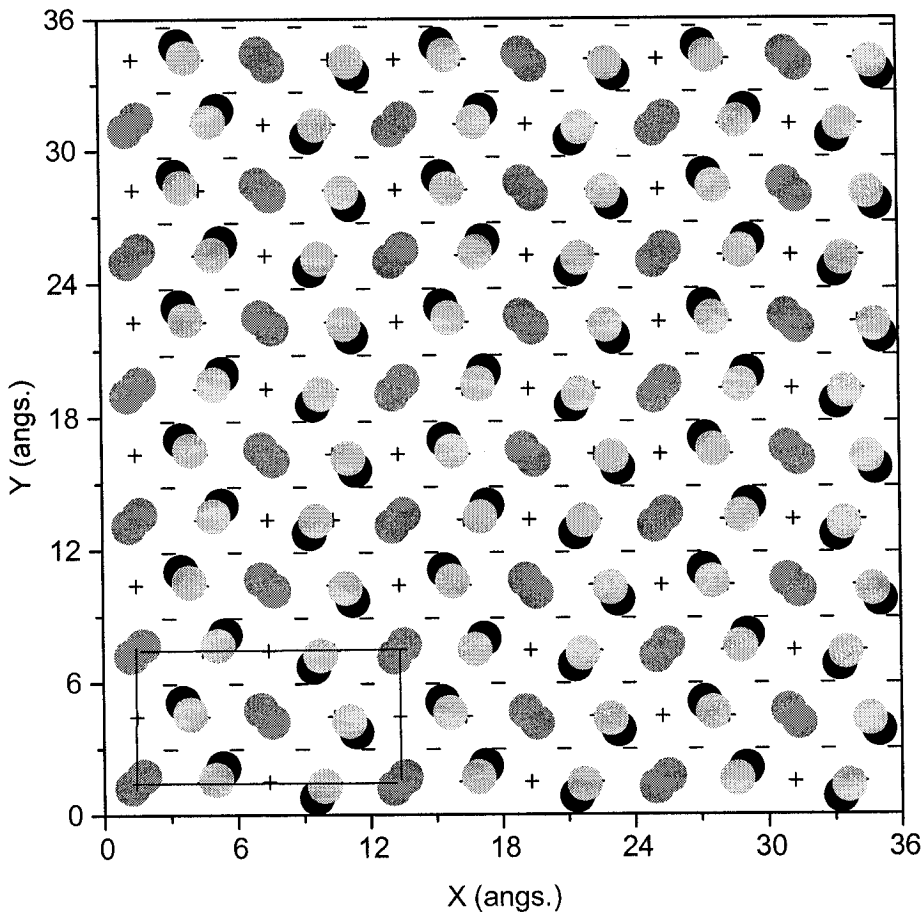

FIG. 5.5: MgO(001) surface covered with 108 H_2 molecules at 1 K. The (+) symbol represents a Mg^{2+} ion and the (-) symbol represents a O^{2-} ion. The hydrogen atoms of molecules that lie flat over Mg^{2+} sites are shown as gray circles; while for tilted H_2 molecules the lower H atoms are represented by solid black circles and the upper H atoms are represented by light gray circles. The $p(4\times2)$ unit cell is shown in solid lines.

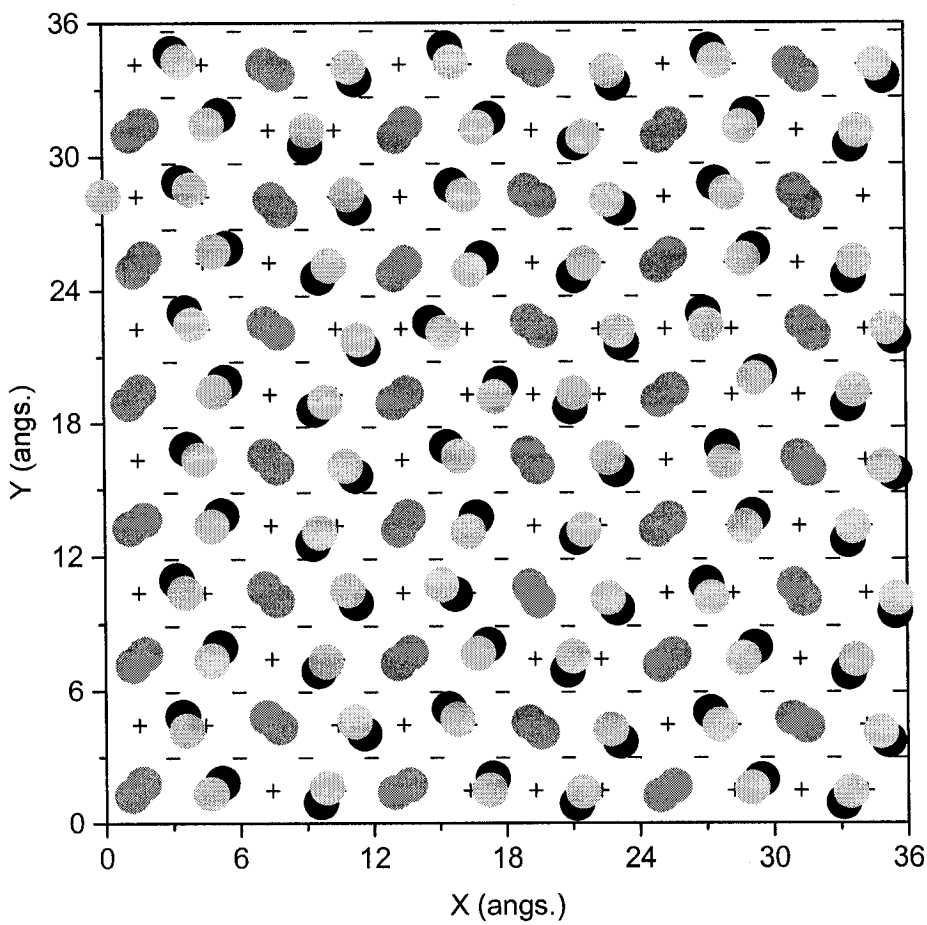

FIG. 5.6: MgO(001) surface covered with 108 H_2 molecules at 9 K. The (+) symbol represents a Mg^{2+} ion and the (-) symbol represents a O^{2-} ion. The hydrogen atoms of molecules that lie flat over Mg^{2+} sites are shown as gray circles; while for tilted H_2 molecules the lower H atoms are represented by solid black circles and the upper H atoms are represented by light gray circles.

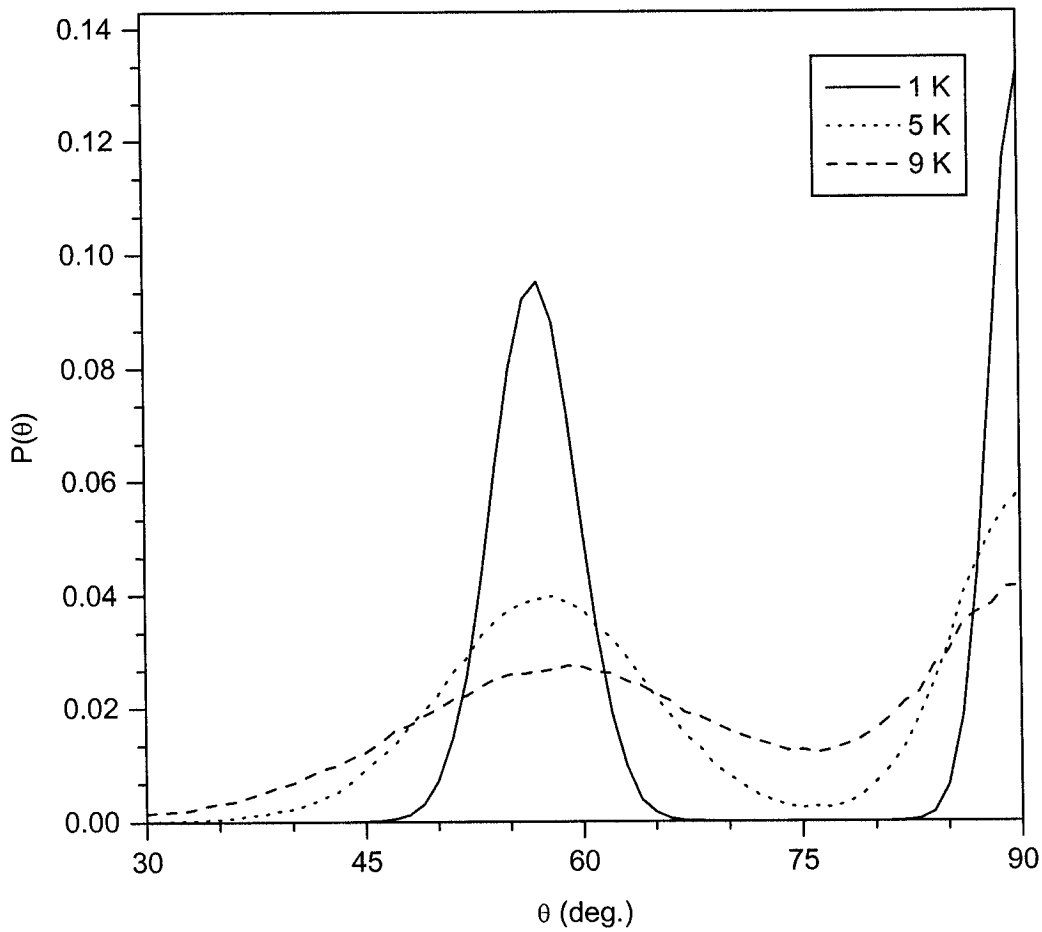

FIG. 5.7: The polar angle distribution of the $p(4\times2)$ layer plotted for temperatures T=1, 5, and 9 K. At 1 K, the distributions are symmetric and centered on $\theta \sim 58^{\circ}$, 90°.

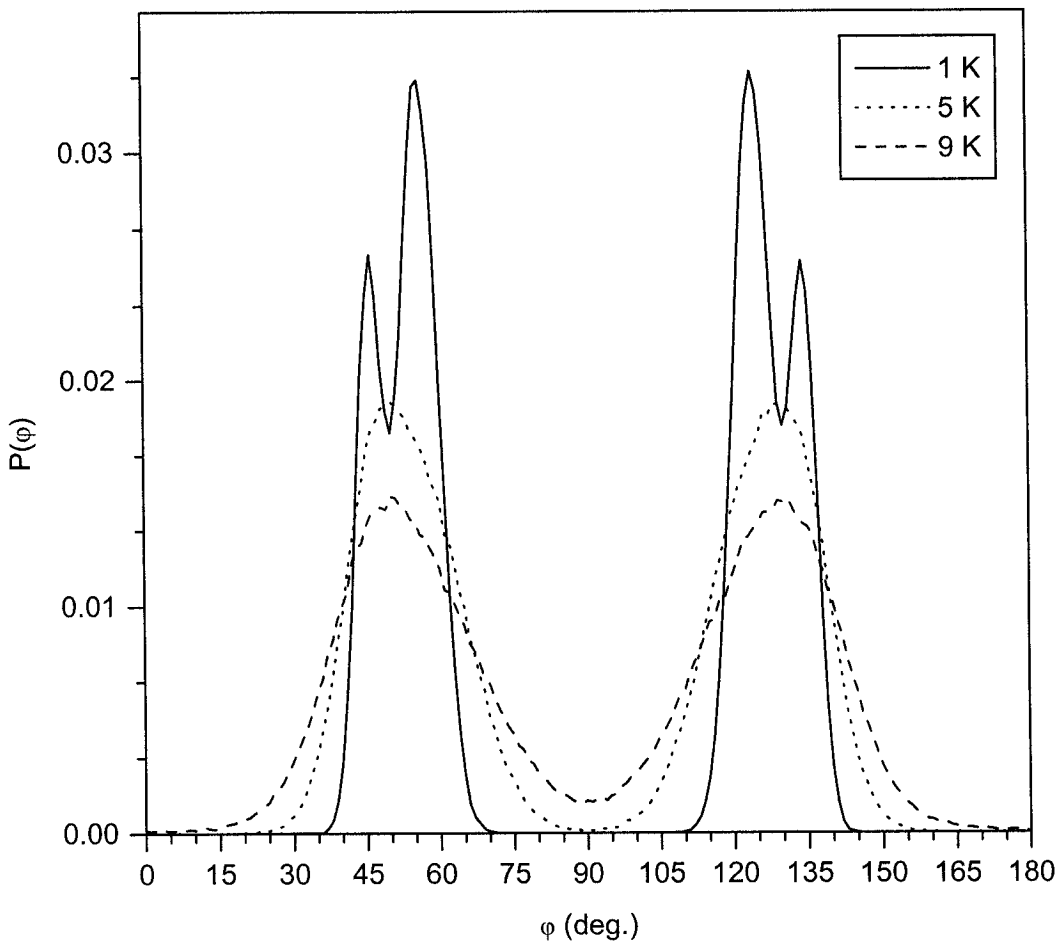

FIG. 5.8: The azimuthal angle (φ) distribution of the $p(4\times2)$ phase is plotted for temperatures T=1, 5, and 9 K. at T=1 K, the two sharp peaks at $\varphi = 45^{\circ}$ and 135° are due to flat molecules, while the larger peaks at $\varphi = 55^{\circ}$ and 125° are attributed to the tilted molecules. As the temperature increases, the peaks merge into two broad peaks at $\varphi = 50^{\circ}$ and 130°.

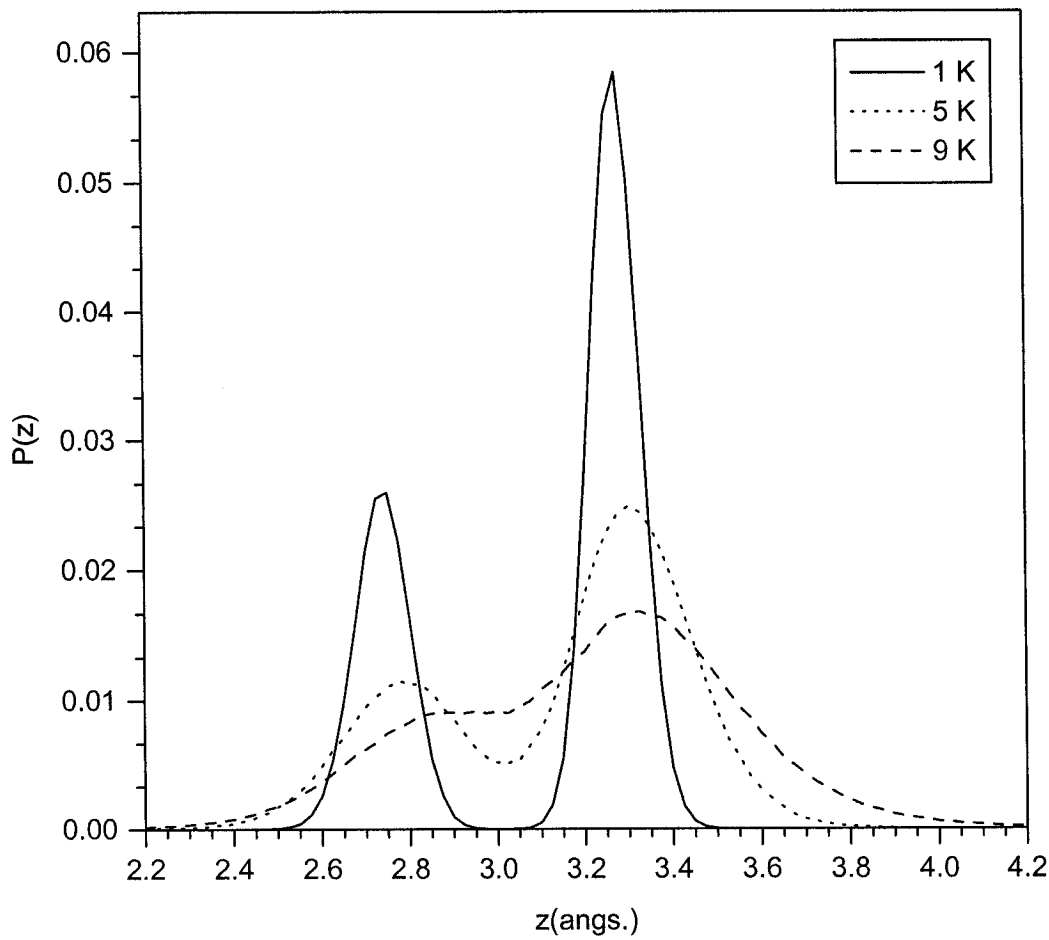

FIG. 5.9: The height (z) distribution of the H_2 molecules center of mass for the *p*(4×2) layer plotted for temperatures T=1, 5, and 9 K. At T=1 K, the peak at 2.75 Å is due to flat molecules adsorbed directly over the Mg^{2+} sites, while the peak at 3.28 Å is due to tilted H_2 molecules.

5.1.4. H_2 adlayers: *p*(6×2) structure

Recent HAS experiments [28] have shown that a third structure of H_2 molecules was formed at a coverage of 0.83. The observation of a *c*(6×2) structure matched previous results obtained by neutron scattering experiments [94]. The proposed structure [28, 94] contains two kinds of adsorption sites, similar to that found in case of *c*(4×2). To test this structure, the number of H_2 molecules in our simulations was increased to 120 in order to match the experimentally observed coverage. Several different initial structures were examined using the Monte Carlo method and were all found to form a unique final configuration with a *p*(6×2) structure as shown in Fig. 5.10 at T=1 K. Our simulations indicate that, as with the *p*(4×2) structure, there are two kinds of adsorption sites: parallel and tilted. In Fig. 5.10, molecules occupying parallel sites are shown as solid gray while the tilted molecules are shown as composites of black and light gray atoms. As before, the center of mass of hydrogen molecules occupying parallel sites sit directly above the Mg^{2+} sites while the tilted molecules are displaced from the Mg^{2+} site by 0.5 Å and 0.44 Å in x and y-directions respectively, where the long axis of the unit cell is along the x direction. Within a unit cell there are eight tilted molecules and two flat molecules for a total of ten molecules. Overall one may view the structure as consisting of rows of flat molecules separated by double rows of tilted molecules.

The polar angle distribution (see Fig. 5.12) shows that at 1 K three peaks are present. Once again the peak at 90° corresponds to the flat molecules on top

of the Mg^{2+} sites. The two additional peaks that occur at 50° and 60°, labelled A, and B respectively, are due to the tilted molecules. The difference in polar angle arises from the different local environments that the molecules experience as illustrated by the molecules labels A and B in Fig. 5.10. Molecules labelled A have only one neighbouring flat molecule while those labelled B have two neighbouring flat molecules. An increase in temperature of only a few degrees eliminates this angular distinction and the peaks labelled A and B in Fig. 5.12 coalesce into a single broad peak around 58° that persists up to a temperature of 9 K and corresponding to the structure shown in Fig. 5.11. The azimuthal distribution,(see Fig. 5.13) shows evidence of overlapping contributions from three different sites (a flat and two tilted) that span a range of angles from 45°-60° and 120°-135° for temperatures up to 9 K.

At T = 1 K, the center of mass height distribution (see Fig. 5.14) also shows the presence of three adsorption sites. The peaks labelled A, and B are due to tilted molecules whose heights are 3.2 Å and 3.35 Å respectively. Again, a temperature increase of only a few degrees causes these peaks to combine into a single peak at 3.3 Å. The remaining peak at 2.63 Å corresponds to molecules in parallel sites. An increase in temperature causes this peak to shift upward to 2.75 Å at T = 9 K. The flat molecules appear to be under more compression than in the $p(4\times2)$ structure, and are pressed closer to the surface. The increase in temperature to 9 K relieves this compression and the flat molecules relax to the

same height as in the $p(4\times2)$ case. At 11 K molecules begin to desorb from the surface and the adlayer becomes disordered.

At T=1 K the average binding energy of a molecule in the $p(6\times2)$ layer is –0.659 kcal/mol which comes from a summation of molecule-surface contribution of –0.515 kcal/mol plus a molecule-molecule contribution of –0.144 kcal/mol. There is little difference between the binding energies of the tilted molecules (–0.659 kcal/mole) and flat molecules (–0.661 kcal/mole).

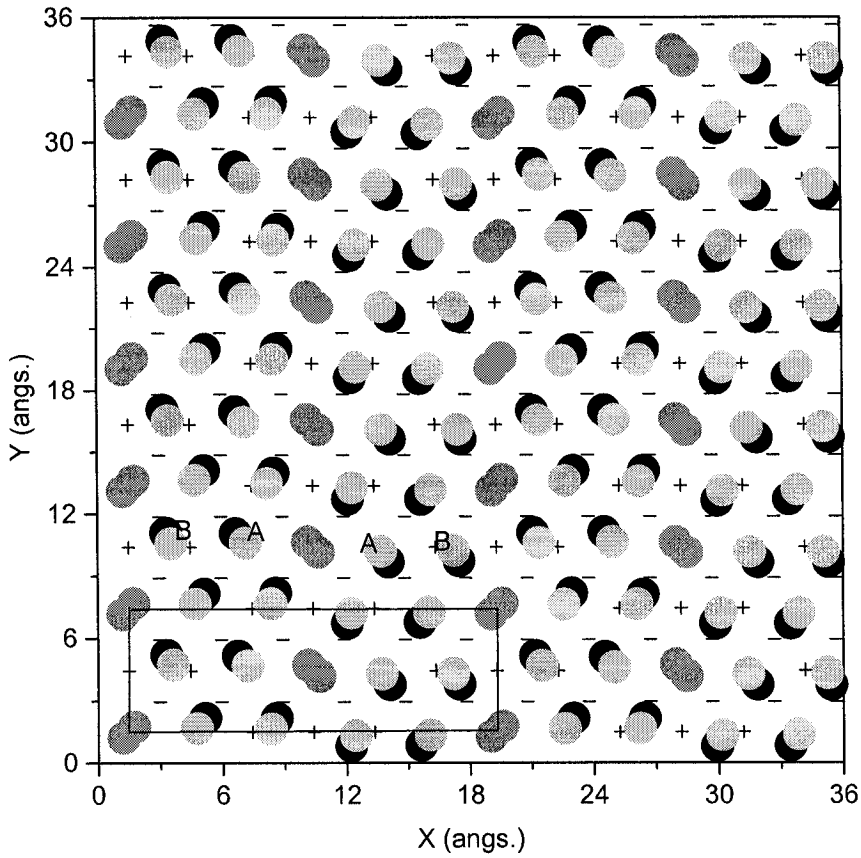

FIG. 5.10: MgO(001) surface covered with 120 H_2 molecules at 1 K. The (+) symbol represents Mg^{2+} ion and (-) sign represents a O^{2-} ion. The hydrogen atoms of flat molecules located directly over Mg^{2+} site are shown as gray circles, while for tilted molecules the lower atoms are represented by solid black circles and the upper atoms are represented by light gray circles. There are two kinds of environments for the tilted molecules; the molecule labeled A is surrounded with five tilted molecules and one flat molecule whereas the molecule labeled B is surrounded by two flat molecules and four tilted molecules. The $p(6\times2)$ unit cell is shown in solid lines.

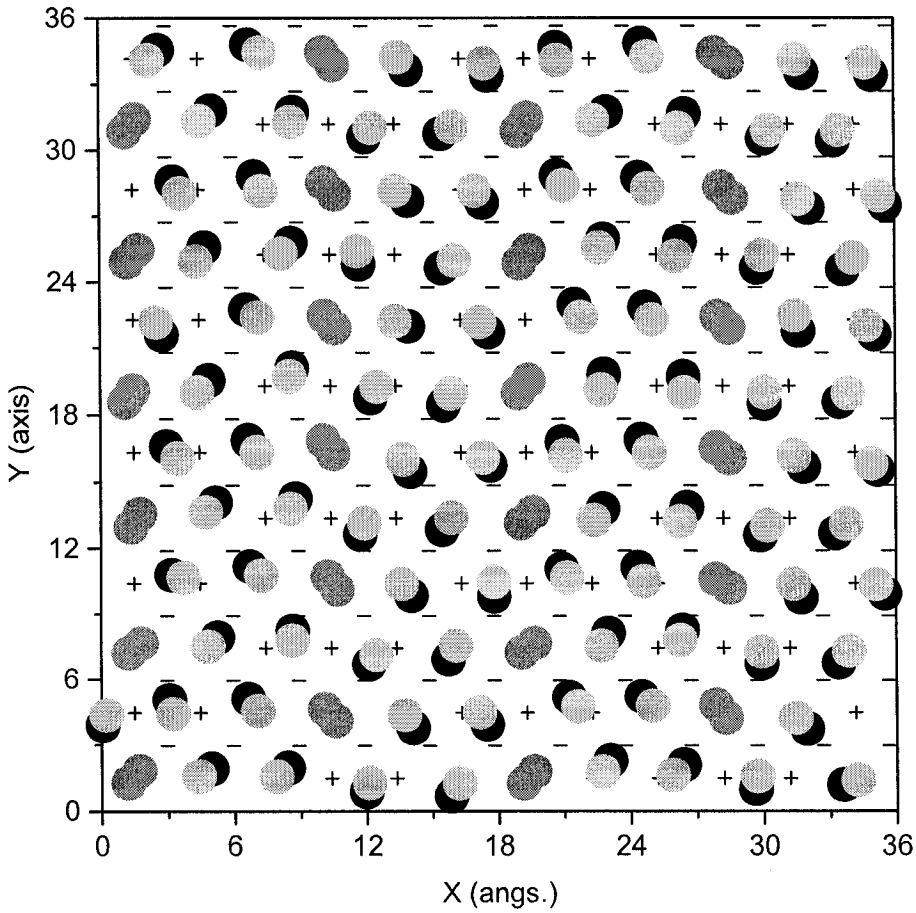

FIG. 5.11: MgO(001) surface covered with 120 H_2 molecules at 9 K. The (+) symbol represents Mg^{2+} ion and (-) sign represents a O^{2-} ion. The hydrogen atoms of flat molecules located directly over Mg^{2+} site are shown as gray circles, while for tilted molecules the lower atoms are represented by solid black circles and the upper atoms are represented by light gray circles.

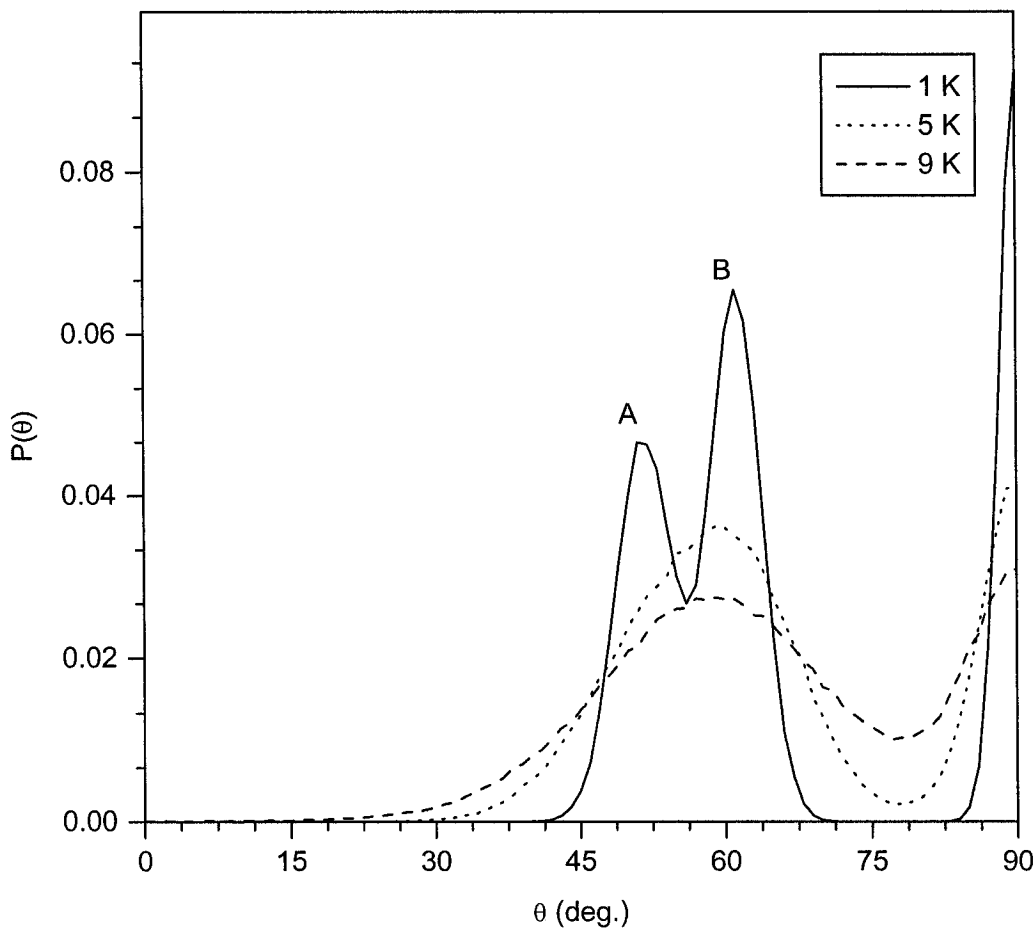

FIG. 5.12: The polar angle distributions of the $p(6\times2)$ phase plotted for temperatures T=1, 5, and 9 K. At T=1 K, the distributions show three peaks, two of them are for tilted molecules labeled A and B and centered at $\theta \sim 53^{\circ}$, 63°, while the remaining peak is for flat molecules and is centered at $\theta \sim 90^{\circ}$. By increasing the temperature, the two peaks labeled A and B are combined into one peak centered around $\theta \sim 60^{\circ}$.

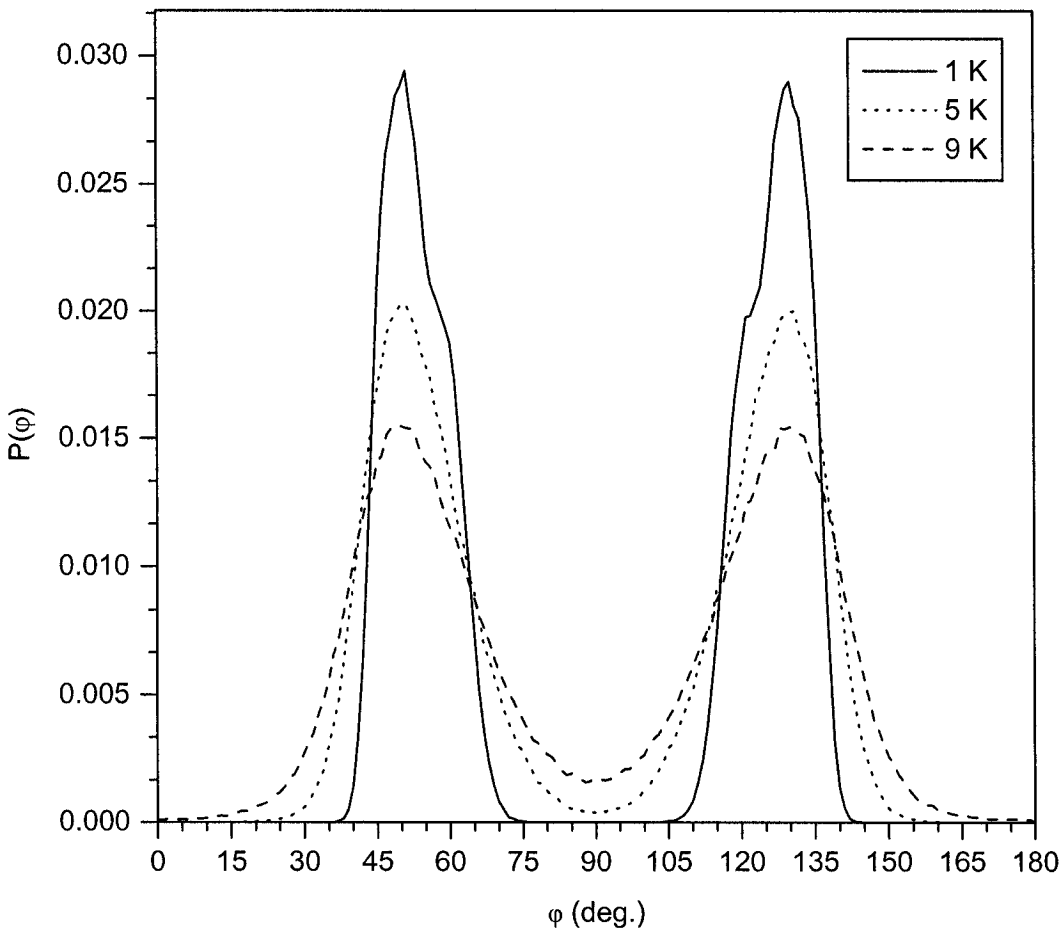

FIG. 5.13: The azimuthal angle (φ) distributions of the $p(6\times2)$ phase plotted for temperatures T=1, 5, and 9 K. There are overlapping contributions from the three different sites (a flat and two tilted) that span a range of angles from 45°-60° and 120°-135° for temperatures up to 9 K.

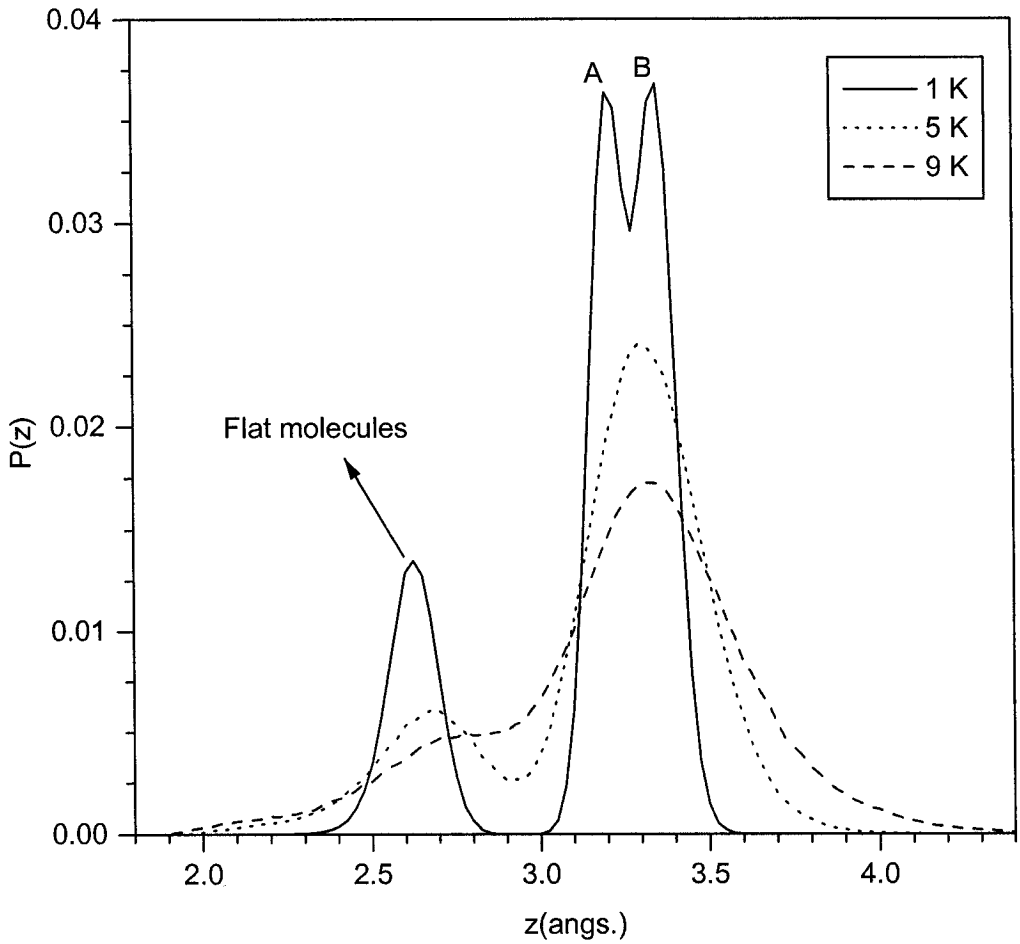

FIG. 5.14: The height (z) distribution of the H_2 molecule center of mass for the *p*(6×2) layer plotted for temperatures T=1, 5, and 9 K. At T=1 K, the peak at 2.63 Å is due to the flat molecules adsorbed over the Mg^{2+} sites, while the two peaks labeled A and B are due to tilted molecules whose heights are 3.2 Å and 3.35 Å respectively.

5.1.5. H_2 adlayers: *c*(8×2) structure

The stability of a *c*(8×2) structure, with a coverage of 0.875, was also studied. In this simulation, the (001) face of MgO contains 256 Mg^{2+} sites (16×16), and the number of H_2 molecules was set at 224 in order to have the correct coverage. Many configurations with different molecular orientations were examined in simulations that were run for 50 kcycles at T=1 K. In all cases it was found that these configurations were unstable. Molecules would desorb from the surface leaving the remaining molecules disordered. We therefore conclude that a *c*(8×2) structure is not possible, which confirms the experimental finding [28].

5.1.6. Summary and discussion of simulations

The results obtained by using the Metropolis Monte Carlo method match the experimental results in terms of coverage and stability but disagree in terms of structure. In particular, *p*-type structures are observed rather than *c*-type due to the localization of the molecular axes along either the φ = 45° or φ = 135° azimuths. A *c*-type structure would occur if the azimuthal distribution of the molecular axis showed four-fold symmetry around the $\varphi = \pm 45°, \pm 135°$ axes, or if azimuthal delocalization occurred. Four-fold symmetry and delocalization do occur, but only at temperatures above 12 K. At this temperature the molecules are not only free to rotate but are also mobile enough to desorb from the surface. Thus our simulations, which use classical statistics, are unable to yield stable *c*-type structures.

Due to its light mass, the rotational motion of the hydrogen molecule is subject to quantum effects. In particular, tunnelling of the molecular axis through the rotational barrier at the surface and azimuthal delocalization may be possible. This is explored in the next section.

5.2. Rotational State Calculations

Quantum mechanical delocalization of the hydrogen molecules' axes will change the symmetry of the adlayer structure from *p*(n×2) to *c*(n×2). Therefore, the nature of the rotational state of an adsorbed hydrogen molecule was investigated to see if delocalisation would occur. To obtain a complete understanding of the rotational states and determine which H_2 species (*ortho* and *para*) are preferentially adsorbed over the cationic and anionic sites, the full 3-dimensional rotation must be examined.

In our calculations of the energies and wave functions of H_2 species in its different rotational levels, we use a perturbation theory, applied to the time independent Schrödinger equation for a rigid rotor. The procedure of these calculations was described in all details in chapter 3, and will be used in the next sections.

5.2.1. The rotational potential

As mentioned before in chapter 3, the rotational potential of a H_2 molecule sits directly over the cationic and anionic sites of the surface has the following form

$$V(\theta,\varphi) = A_o + A_1 \cdot \cos(4\cdot\varphi) + A_2 \cdot \cos^2\theta + A_3 \cdot \cos^2(2\cdot\theta) + A_4 \cdot \cos^2\theta \cdot \cos(4\cdot\varphi) + A_5 \cdot \cos^4\theta \cdot \cos(4\cdot\varphi) \quad (3.8a)$$

In terms of spherical harmonics function, $Y_{lm}(\theta,\varphi)$, the above formula can be written as follows:

$$V(\theta,\varphi) = A_o^{'} \cdot Y_{00} + A_1^{'} \cdot Y_{20} + A_2^{'} \cdot Y_{40} + A_3^{'} \cdot (Y_{44} + Y_{4-4}) \ , \quad (3.8b)$$

which reflects the four-fold azimuthal symmetry of the surface and the rotational symmetry of the homo-nuclear hydrogen molecule. The values of the coefficients may be determined by fitting the above function to the potential energy of a molecule at the surface. The potential energy was calculated by fixing the molecular center of mass at the equilibrium heights of 2.75 Å and 3.05 Å directly above Mg^{2+} and O^{2-} sites respectively, and rotating the molecule by increments of 5° through all possible values of the polar angle θ and azimuthal angle φ. Using a least squares fit program from MAPLE V.7 (Waterloo, Maple Inc., Maple Handbook (Maple V, release 4, 1996)), the coefficients were determined and are listed in Tables 5.1 and 5.2.

The rotational potential above the Mg^{2+} and O^{2-} sites are shown in Fig. 5.15 and Fig. 5.16 respectively. From Fig. 5.15, it is apparent that a molecule above a Mg^{2+} site has the lowest energy when it lies flat on the surface plane ($\theta = 90°$). An azimuthal rotation reveals the four-fold symmetry of the surface potential with minima of –0.602 kcal/mol at $\varphi = 45$, 135, 225, and 315°. When the molecule lies flat the rotational barrier has a height of only 0.04 kcal/mol, making tunnelling a likely event. Regardless of the azimuthal orientation, the energy barrier to rotating the molecule to upright position ($\theta = 0°$) is a prohibitive 1.25 kcal/mol. Above the O^{2-} site the situation is reversed; the lowest energy occurs when the molecule is upright and the highest when the molecule lies flat (Note the reversal of the θ axes in Figs. 5.15 and 5.16). The energy barrier for rotation in the θ direction is 0.8 kcal/mol. This value is less than that above the Mg^{2+} site owing to the increased distance (3.05 Å *vs.* 2.75 Å) from the surface. Evidence of the four-fold symmetry of the surface potential appears on the top of the potential ridge where $\theta = 90°$ but is not present when the molecule sits perpendicular to the surface ($\theta = 0°$).

Table 5.1: Rotational potential fitting parameters in units of kcal/mol.

Parameter	A_o	A_1	A_2	A_3	A_4	A_5
Above Mg^{2+}	-0.5056	0.0181	1.2703	-0.0655	-0.0421	0.0245
Above O^{2-}	0.2404	-0.0085	-0.8588	0.1466	0.0192	-0.0109

Table 5.2: Rotational potential fitting parameters in units of kcal/mol.

Parameter	A_o'	A_1'	A_2'	A_3'
Above Mg^{2+}	-1.0969	1.3824	-0.0708	0.0196
Above O^{2-}	0.0799	-0.9964	0.1585	-0.0093

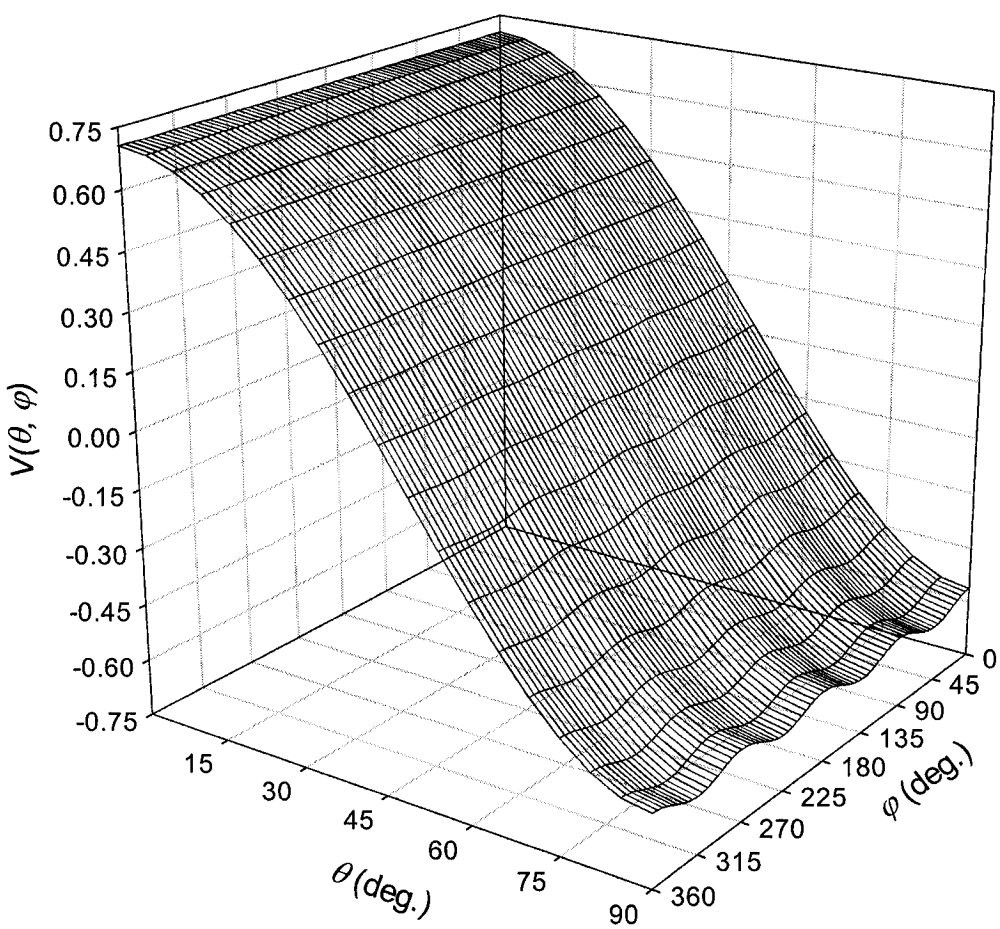

FIG. 5.15: The rotational potential $V(\theta, \varphi)$ (kcal/mol) for a H_2 molecule whose center of mass sits at a height of 2.75 Å above the Mg^{2+} site.

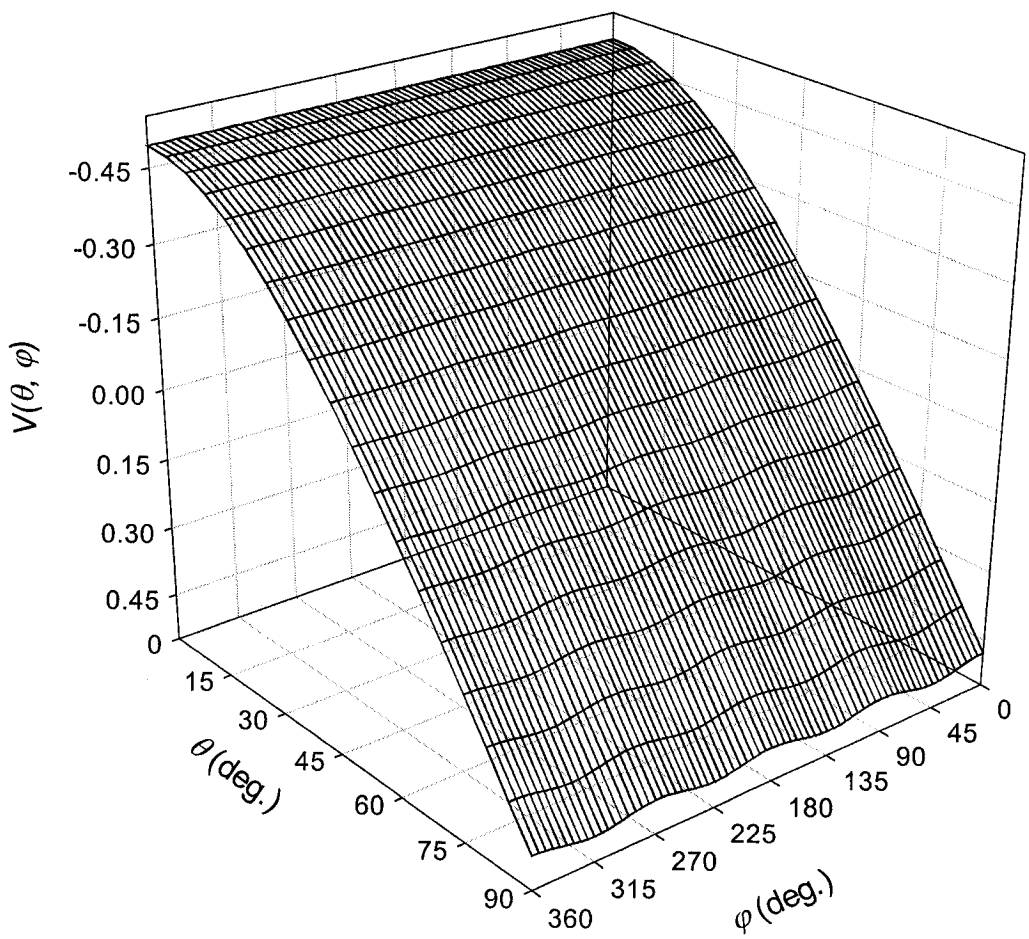

FIG. 5.16: The rotational potential $V(\theta,\varphi)$ (kcal/mol) for a H_2 molecule whose center of mass sits at height of 3.05 Å above the O^{2-} site.

5.2.2. The wave functions

Using perturbation theory, to the first order correction, the rotational wave functions of adsorbed H_2, as described before in chapter 3, may be determined using the following formula

$$\Psi_{Jm} \approx Y_{Jm} + \sum_{k \neq J} \frac{\langle Y_{Jm} | \hat{H}' | Y_{km} \rangle}{E_J - E_k} \cdot Y_{km} \tag{3.17}$$

where $\hat{H}' = V(\theta,\varphi)$ is the rotational potential given in Eq. (3.8).

Insertion of the rotational potential above the Mg^{2+} site in the Eq. (3.17), yields the following rotational wave functions for the lowest order *para* and *ortho* states.

1. For *para*-H_2 ($J = 0$, $m = 0$);

$$\Psi_{00}^{ads.} = Y_{00} - 0.372 \cdot Y_{20} + 5.725 \times 10^{-3} \cdot Y_{40} - 1.584 \times 10^{-3} \cdot (Y_{44} + Y_{4-4})$$

2. For *ortho*-H_2 (J =1, m = ±1);

$$\Psi_{11}^{ads.} = Y_{11} - 0.166 \cdot Y_{31} - 3.662 \times 10^{-3} \cdot Y_{3-3} + 2.754 \times 10^{-3} \cdot Y_{51} + 1.97 \times 10^{-4} \cdot Y_{5-3} - 1.321 \times 10^{-3} \cdot Y_{55}$$

3. For *ortho*-H_2 (J =1, m = 0);

$$\Psi_{10}^{ads.} = Y_{10} - 0.186 \cdot Y_{30} + 3.555 \times 10^{-3} \cdot Y_{50} - 5.909 \times 10^{-4} \cdot (Y_{54} + Y_{5-4})$$

The angular distribution of *para*-H_2 in its ground state ($\Psi_{00}^{ads.*} \cdot \Psi_{00}^{ads.}$) is shown in Fig. 5.17 (a) as a function of θ and φ. The distribution shows that the rotational ground state of a *para*-H_2 molecule is squashed on the surface with the distribution maximum occurring at $\theta = 90^{\circ}$, *i.e.* the molecular axis spends most of the time parallel to the surface. This is in sharp contrast with the unperturbed ground state rotational wave function, which is constant and has no dependence on either θ or φ. In Fig. 5.17 (b), the azimuthal dependence of the distribution with the polar angle fixed at $\theta = 90^{\circ}$ is shown. The distribution is almost uniform with a small ripple that reflects the four-fold symmetry of the surface. In other words, the orientation of the molecular axis is largely delocalized with a residual preference for orientations in the $\varphi = \pm 45^{\circ}, \pm 135^{\circ}$ directions.

Remarkably similar behaviour is observed for the helicoptering *ortho*-H_2, (J=1, m=±1) as may be seen in Figs. 5.18 (a) and 5.18 (b), although in this case the distributions resemble their gas phase counterparts. A comparison of Figs. 5.17 and 5.18 suggests that the adsorption of a ground state *para* molecule forces its rotational state to resemble that of a helicoptering *ortho* molecule. The similarity of the angular distributions of the *para* and helicoptering *ortho* states may assist in the inter-conversion between *para*-H_2 and *ortho*-H_2 [95] by improving the overlap of their rotational wave functions. We also note that the angular distributions of the ground state *para*-H_2 and helicoptering *ortho*-H_2 are compatible with our MC simulations that show the H_2 molecules prefer to lie flat over the Mg^{2+} sites.

The rotational state of adsorbed cartwheeling *ortho*-H_2 (J =1, m =0) retains much of the character of its gas phase state but nonetheless suffers deformation due the presence of the surface. This is illustrated in Fig. 5.19 where the orientation distribution of the molecular axis no longer has a maximum value at θ = *0°* but is peaked around θ = *35°* instead. As discussed in the next section, the cartwheeling states above the cationic sites are energetically unfavourable.

PT calculations for a hydrogen molecule located over O^{2-} site using Eq. (3.17) yields the following rotational wave functions for the lowest order *para* and *ortho* states.

1. For *para*-H_2 (J = 0, m = 0);

$$\Psi_{00}^{ads.} = Y_{00} + 0.268 \cdot Y_{20} - 4.469 \times 10^{-3} \cdot Y_{40} + 2.621 \times 10^{-4} \cdot (Y_{44} + Y_{4-4})$$

2. For *ortho*-H_2 (J =1, m = ±1);

$$\Psi_{11}^{ads.} = Y_{11} + 0.129 \cdot Y_{31} + 1.733 \times 10^{-3} \cdot Y_{3-3} - 6.161 \times 10^{-3} \cdot Y_{51} - 9.328 \times 10^{-5} \cdot Y_{5-3} + 6.258 \times 10^{-4} \cdot Y_{55}$$

3. For *ortho*-H_2 (J =1, m = 0);

$$\Psi_{10}^{ads.} = Y_{10} + 0.119 \cdot Y_{30} - 7.954 \times 10^{-3} \cdot Y_{50} + 2.799 \times 10^{-4} \cdot (Y_{54} + Y_{5-4})$$

As shown in Fig. 5.20, the angular distribution of the ground state *para*-H_2 molecule is plotted as a function of θ, φ. The distribution has a minimum value

when the molecule lies flat over the surface (θ =90°), and a maximum value when its molecular axis sits perpendicular to the surface (θ =0°). Compared to the results obtained above the Mg^{2+} site, the angular distribution of the ground state *para*-H_2 is completely reversed and at the same time is in sharp contrast to its spherical distribution in gas phase. Our findings also show that the *para*-H_2 distribution is elongated in the vertical direction over the O^{2-} site and resembles the distribution of the cartwheeling mode (see below). In terms of azimuthal angle, the angular distribution seems to be uniform with a small ripple that reflects the four-fold symmetry of the surface, and appears particularly at θ =90°. This uniform distribution represents an ideal condition to have quantum azimuthal delocalization.

In the case of helicoptering *ortho*-H_2 (J =1, m = ±1), the angular distribution also resembles its gas phase counterpart but still suffers slight deformation due to surface electric field as may be seen in Fig. 5.21. The distribution is peaked around θ =65° instead of θ = 90° as in gas phase. As we will see from the rotational energy calculations, placing a helicoptering *ortho*-H_2 over an anion site is an energetically unfavourable situation.

As shown in Fig. 5.22, the angular distribution of the cartwheeling *ortho*-H_2 (J=1, m=0) state is similar to the distribution of its gas phase counterpart as well as the adsorbed *para*-H_2 distribution. As with the adsorbed *para*-H_2, the angular distribution maximum occurs when the molecular axis sits parallel to the surface

normal (θ =0°), and the lowest value when the molecule lies flat over O^{2-} site. Consequently, an inter-conversion between *para*- and cartwheeling *ortho*- states might be possible via overlap of their rotational wave functions.

a)

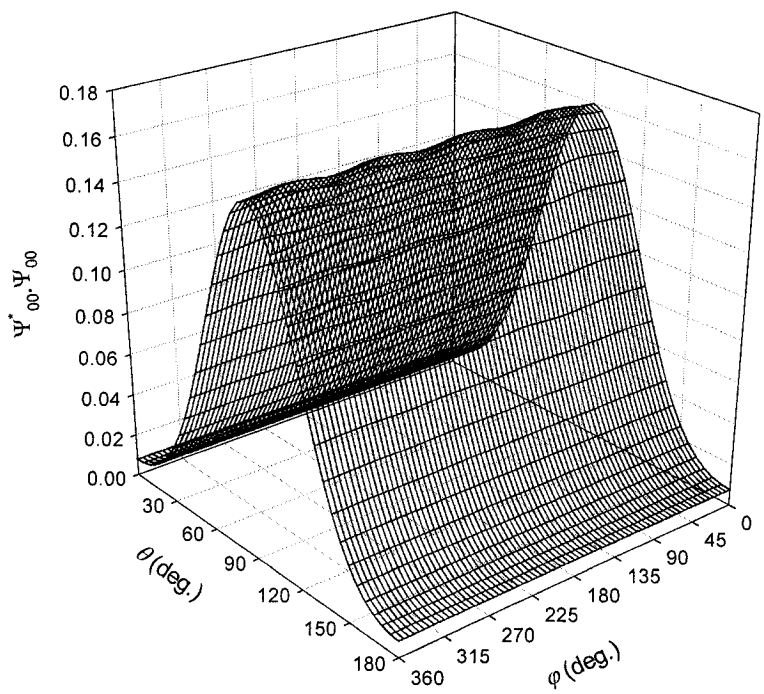

b)

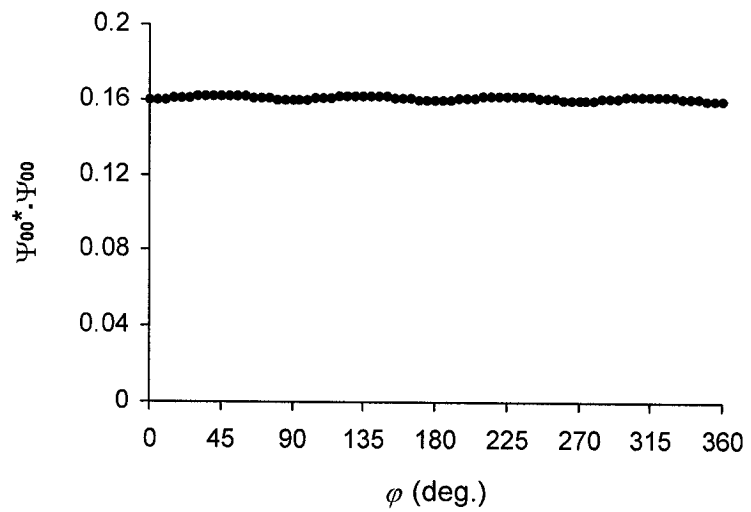

FIG. 5.17: (a) The angular distribution of a *para*-H_2 molecule above a Mg^{2+} site. (b) The azimuthal distribution for θ =90° (the most probable polar orientation).

a)

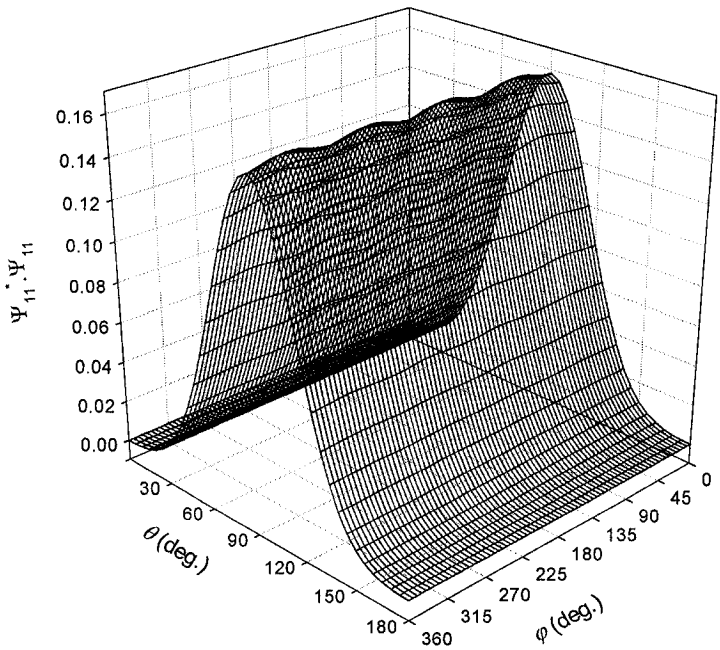

b)

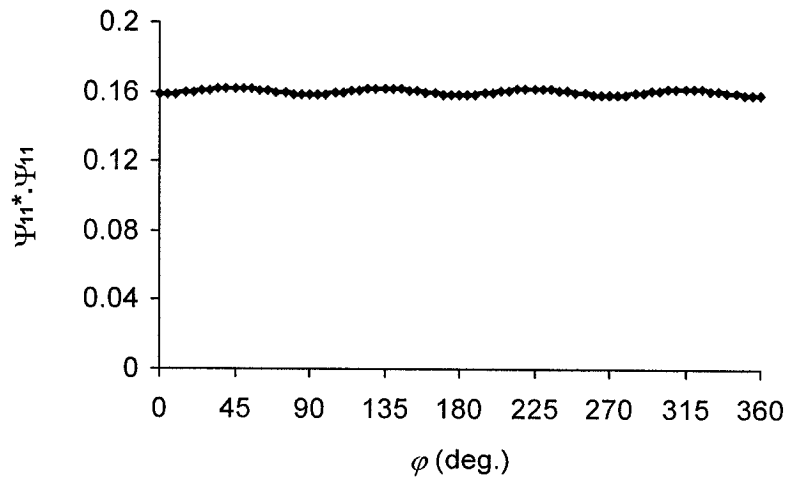

FIG. 5.18: (a) The angular distribution of a helicoptering *ortho*-H_2 molecule above a Mg^{2+} site. (b) The azimuthal distribution for θ =90° (the most probable polar orientation).

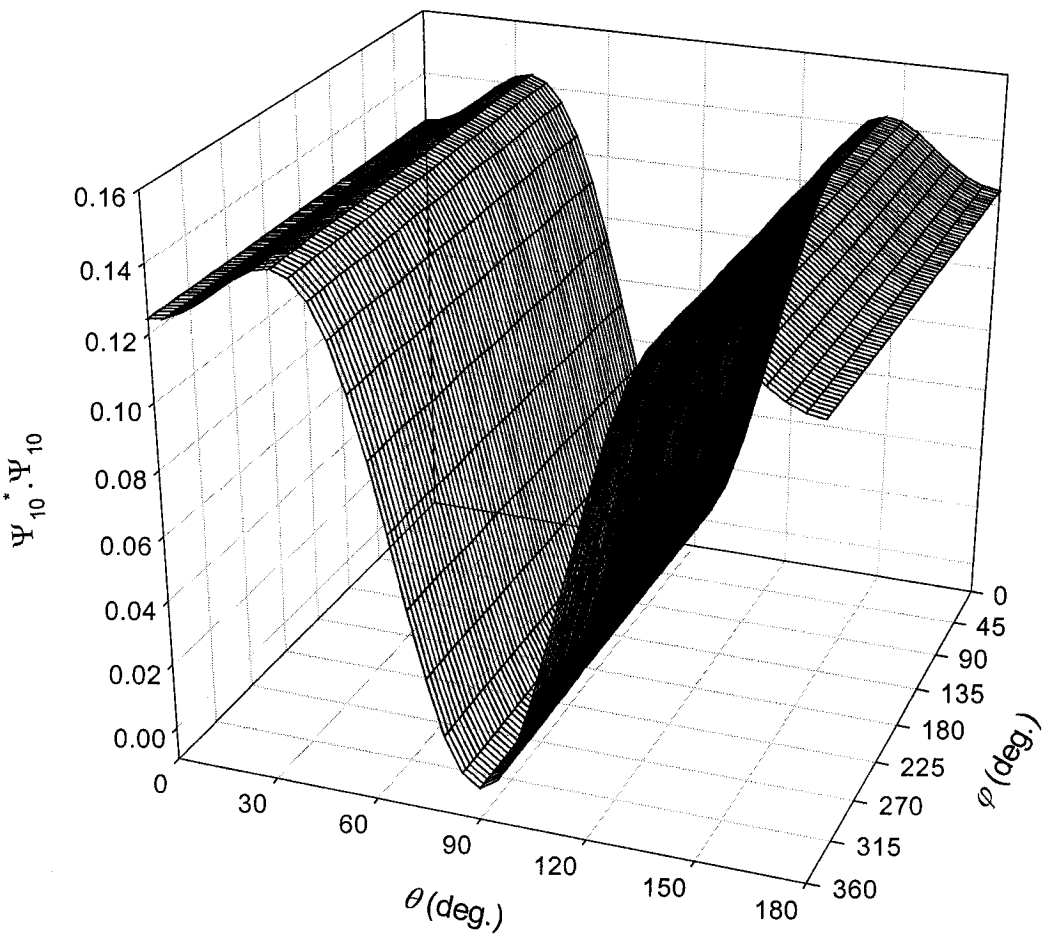

FIG. 5.19: The angular distribution of a cartwheeling *ortho*-H_2 molecule above a Mg^{2+} site at an equilibrium height of 2.75 Å.

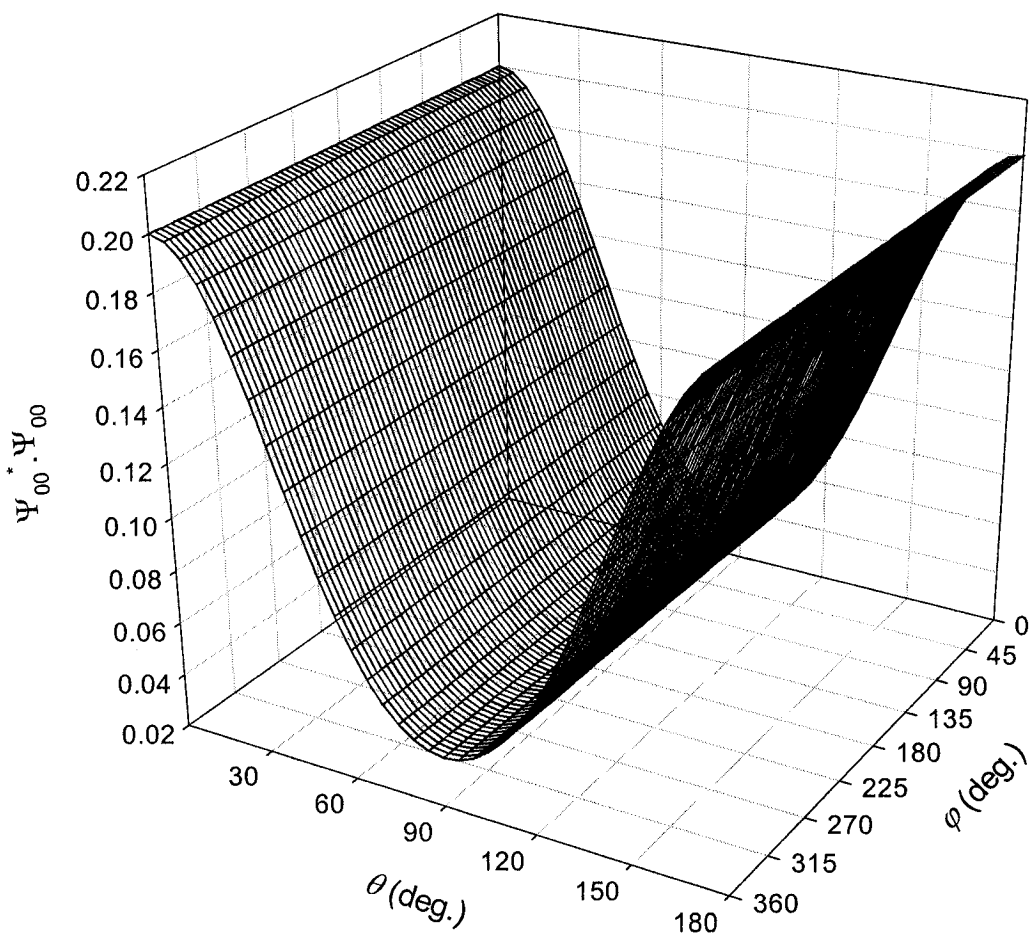

FIG. 5.20: The angular distribution of *para*-H_2 molecule above an O^{2-} site at an equilibrium height of 3.05 Å.

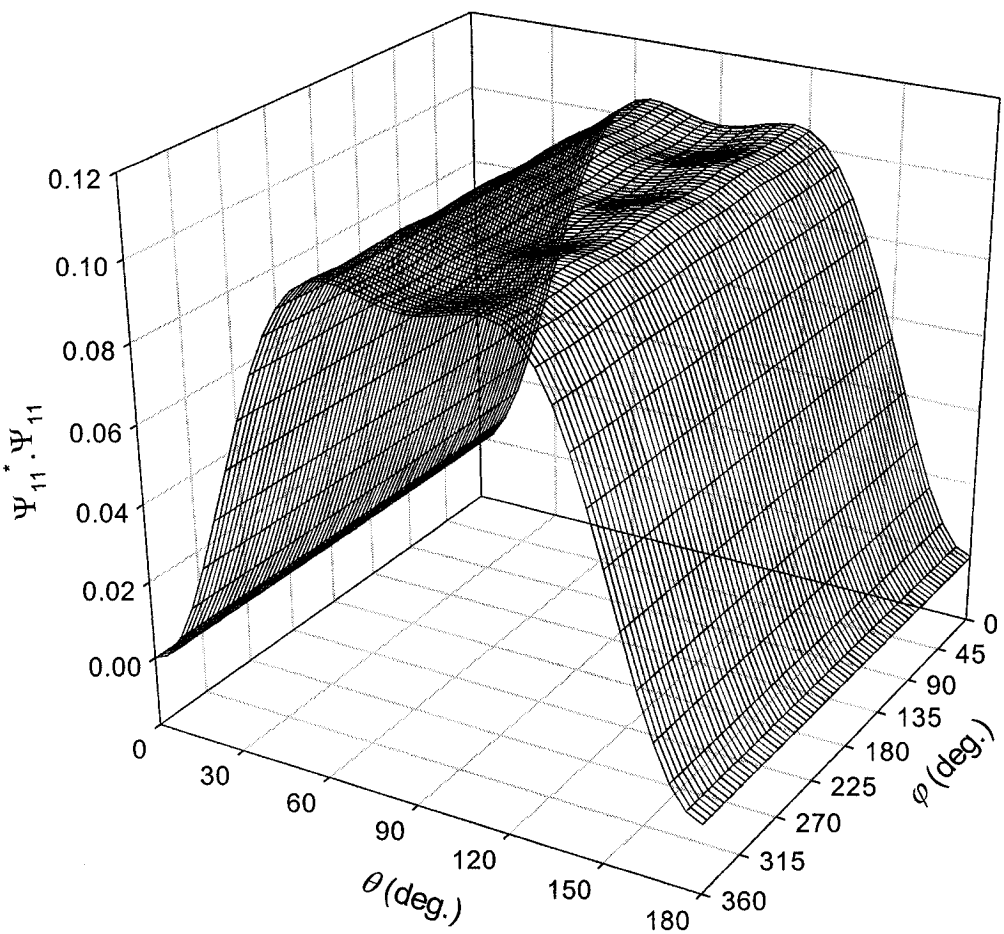

FIG. 5.21: The angular distribution of a helicoptering *ortho*-H_2 molecule above an O^{2-} site at an equilibrium height of 3.05 Å.

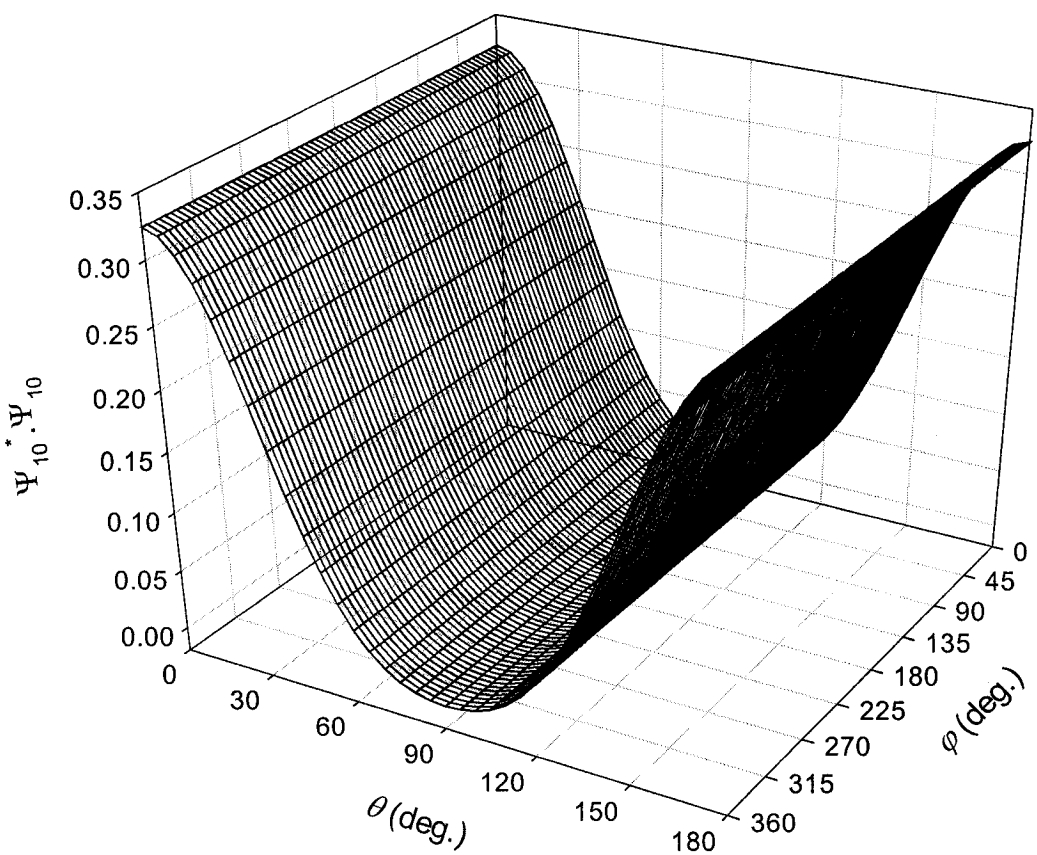

FIG. 5.22: The angular distribution of a cartwheeling *ortho*-H_2 molecule above an O^{2-} site at an equilibrium height of 3.05 Å.

5.2.3. The rotational energies

As derived in chapter 3, Perturbation theory also yields the rotational energy levels, namely

$$E_{Jm} = \frac{J\cdot(J+1)\cdot\hbar^2}{2\cdot I} + A_o + A_2\cdot\left\langle\Theta_J^m\middle|\cos^2\theta\middle|\Theta_J^m\right\rangle + A_3\cdot\left\langle\Theta_J^m\middle|\cos^2(2\cdot\theta)\middle|\Theta_J^m\right\rangle - \frac{I\cdot\left|A_2\cdot\left\langle\Theta_J^m\middle|\cos^2\theta\middle|\Theta_{J+2}^m\right\rangle + A_3\cdot\left\langle\Theta_J^m\middle|\cos^2(2\cdot\theta)\middle|\Theta_{J+2}^m\right\rangle\right|^2}{\hbar^2\cdot(2\cdot J+3)} \qquad (3.16)$$

where the spherical harmonics have been replaced by the usual separable functions as $Y_{Jm}(\theta,\varphi) = \Theta_J^m(\theta)\cdot\Phi_m(\varphi)$.

The above formula is used to calculate, for any given values of the quantum number J and m, the rotational energy levels above either a cation or anion. The relative ordering of these energy states above an Mg^{2+} site is illustrated in Fig. 5.23. In general, the adsorption onto the surface removes the degeneracy present for a given rotational state J. Each energy level is split into an ordered sequence of levels. Within a set of splittings, the $|m| = J$ states always have an energy lower than the corresponding gas phase value as well as the lowest energy in the set, while the $m = 0$ state always has the highest energy and when $J \neq 0$, these states have energies higher than the gas phase. These observations indicate that the $|m| = J$ states (as well as the *para* $J = 0$ state) are allowed to adsorb above the Mg^{2+} site whereas the $m = 0$ states cannot adsorb.

The energy states of a H_2 molecule adsorbed above an O^{2-} site are presented in Fig. 5.24. Again it is found that each rotational energy level J splits into an ordered sequence of levels. For a given set of splittings, the adsorbed m = 0 states have a lower energy than the corresponding gas phase value, while the $|m| = J$ states have the highest energy in the set, and always have energies higher than the gas phase. Consequently, the m = 0 states are allowed to adsorb over the anionic site whereas the $|m| = J$ states are not.

The binding energy of a given rotational state may be estimated by subtracting the energy in the gas phase from the energy in the adsorbed phase. These results are summarized in Table 5.3. They are useful for examining trends but are not expected to match the experimental value of the binding energy because of the significant contribution from the zero point energy in the rotational potential; the interaction potential used was originally constructed to yield the correct binding energy at the rotational potential minimum. Nonetheless, the table illustrates that the binding energy depends on the rotational state of the molecule. Above the Mg^{2+} site the helicoptering *ortho*-H_2 molecules have the strongest binding energy, with *para*-H_2 having a similar but weaker energy. The cartwheeling *ortho*-H_2 molecules have a positive energy and thus do not adsorb. The situation is reversed above the O^{2-} site where cartwheeling *ortho*-H_2 has the strongest binding energy and helicoptering *ortho*-H_2 cannot adsorb by virtue of its positive energy. The *para*-H_2 can still adsorb but the binding energy is considerable less negative than above the cation site. The change in sign of the

binding energies of the *ortho* states indicates that the helicoptering and cartwheeling states preferentially adsorb on cationic and anionic sites respectively. The change in ordering is due to the change in sign of the electrostatic potential and field above the different ionic sites as shown in Figs. 5.25, 5.26 and also reflects the fact that the potential energy is minimized when the molecule lies flat above the Mg^{2+} site or when it sits perpendicular to the surface above the O^{2-} site. This trend is consistent with other theoretical calculations of an H_2 molecule on NaCl(001) and LiF(001) surfaces [38, 44]. The adsorbed *ortho* molecules are probably localized around the ionic sites but can migrate from site to site by passing through the saddle point, which lies midway between neighbouring cation pairs and anion pairs.

Table 5.3: The estimated binding energy of the H_2 species adsorbed on MgO(001).

Adsorption site	Binding energy (kcal/mol)		
	para-H_2 ($J=0, m=0$)	*ortho*-H_2 ($J=1, m=\pm1$)	*ortho*-H_2 ($J=1, m=0$)
Mg^{2+}	-0.2578	-0.3353	+0.1757
O^{2-}	-0.0528	+0.1192	-0.2493

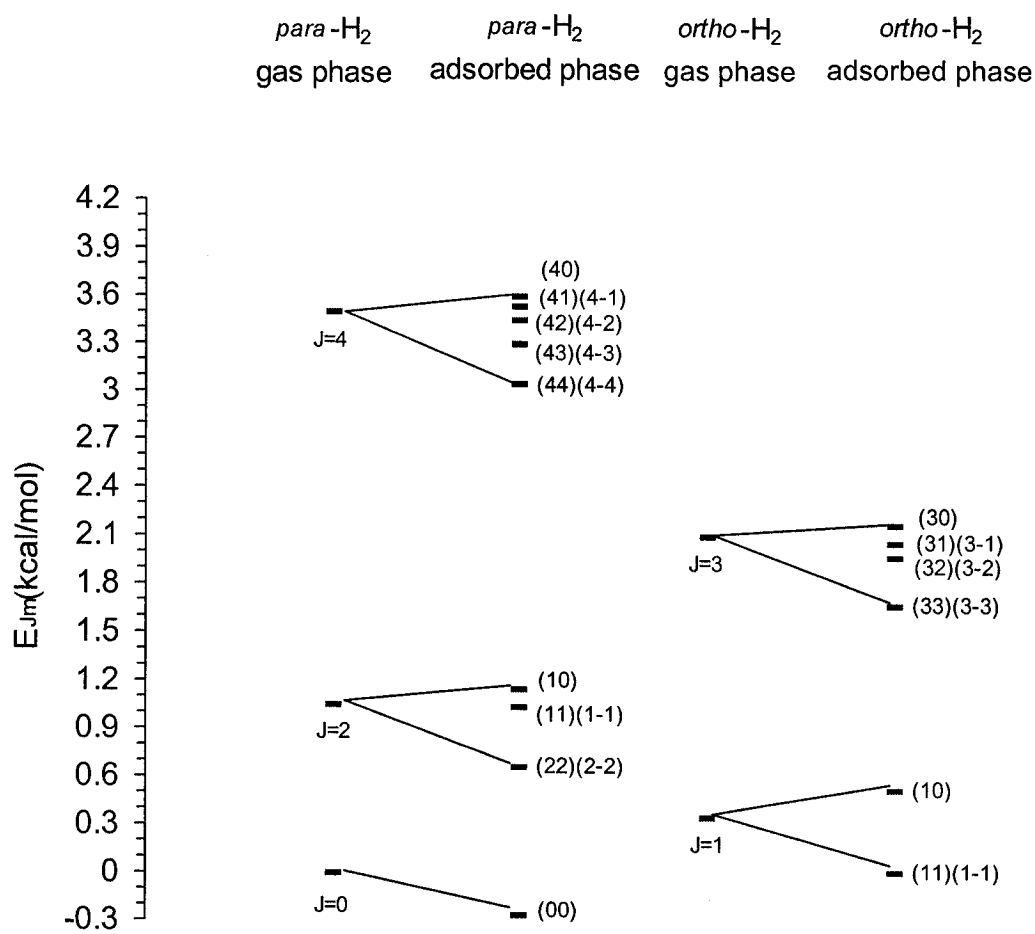

FIG. 5.23: The rotational energy levels of an H_2 molecule in the gas phase and in the adsorbed phase above a Mg^{2+} site at an equilibrium height of 2.75 Å.

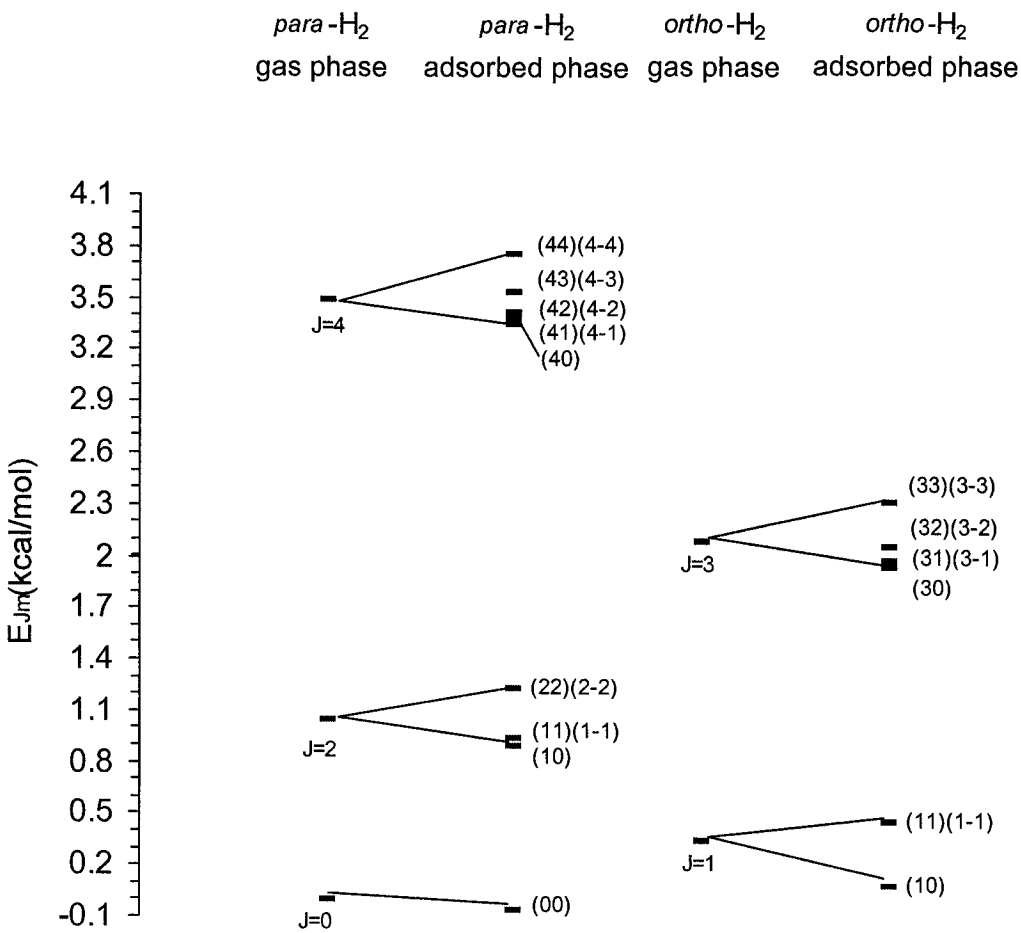

FIG. 5.24: The rotational energy levels of H_2 molecules in the gas phase and in the adsorbed phase above O^{2-} site at an equilibrium height of 3.05 Å.

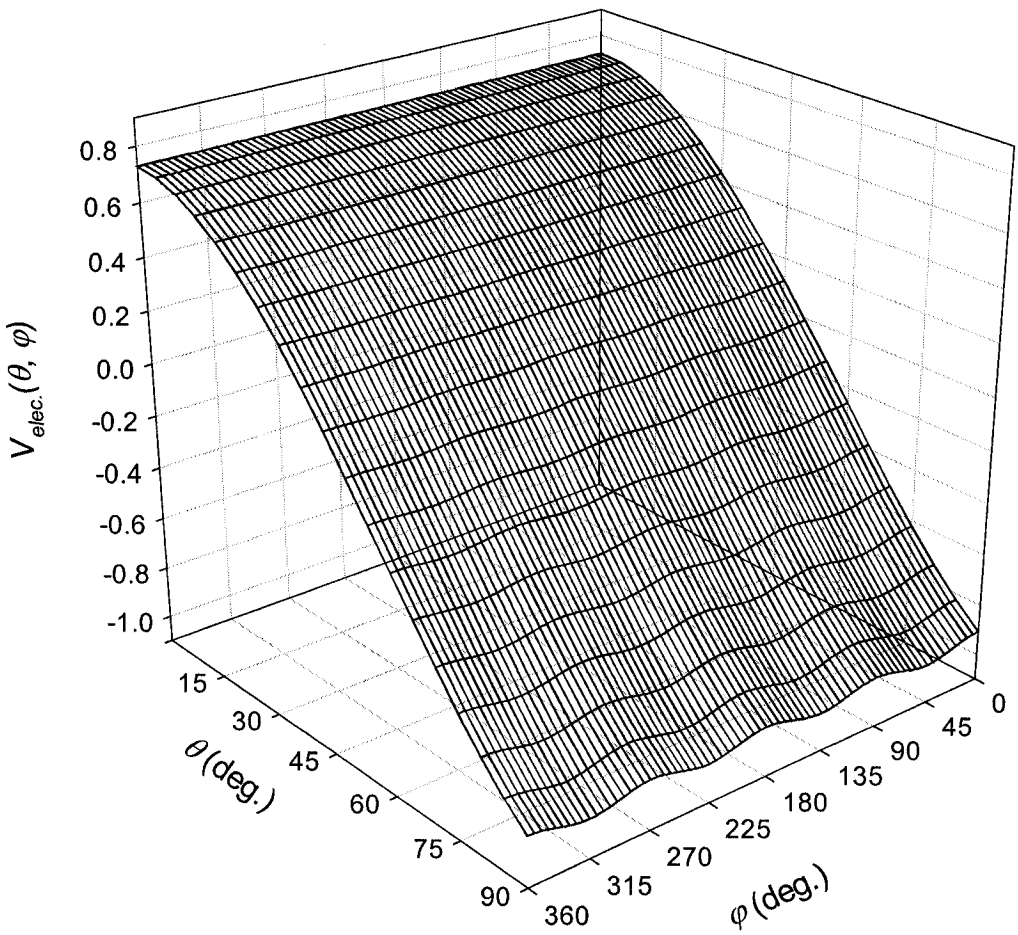

FIG. 5.25: The electrostatic potential $V_{elec.}(\theta,\varphi)$ for a H_2 molecule whose center of mass sits at a height of 2.75 Å above the Mg^{2+} site.

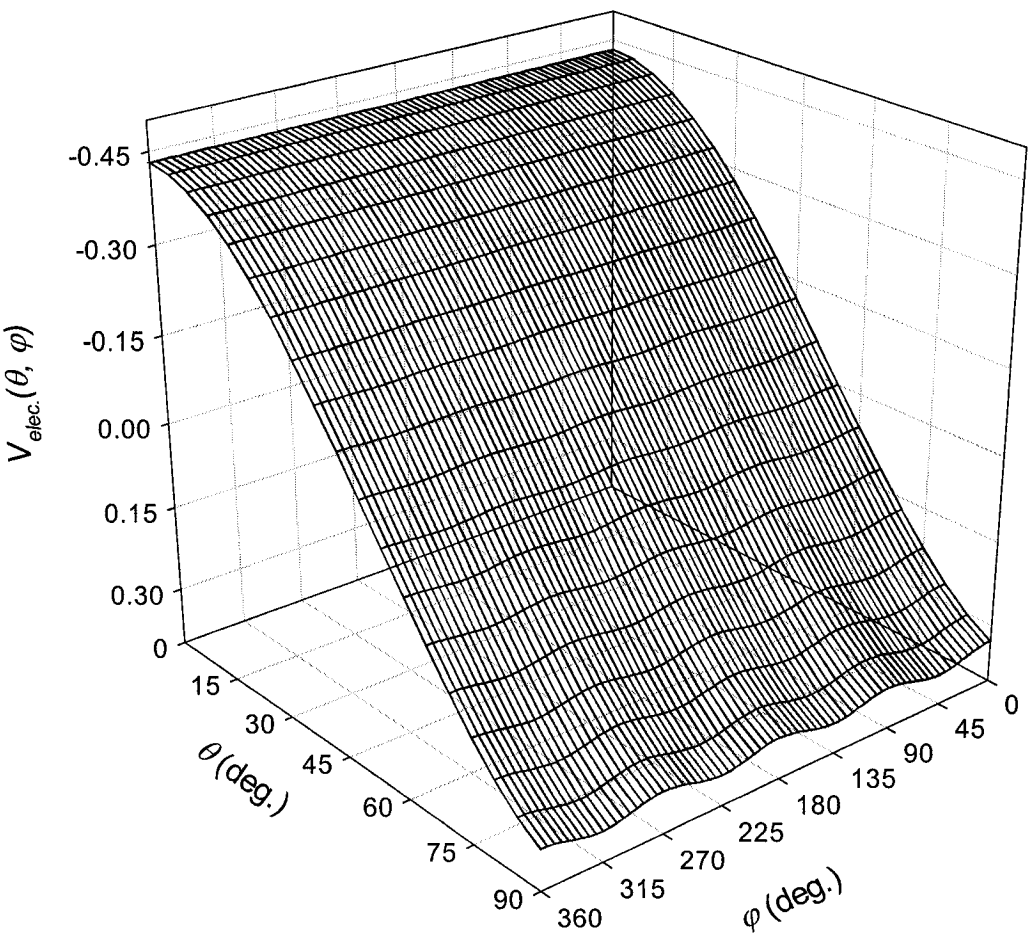

FIG. 5.26: The rotational potential $V_{elec.}(\theta,\varphi)$ for a H_2 molecule whose center of mass sits at height of 3.05 Å above the O^{2-} site.

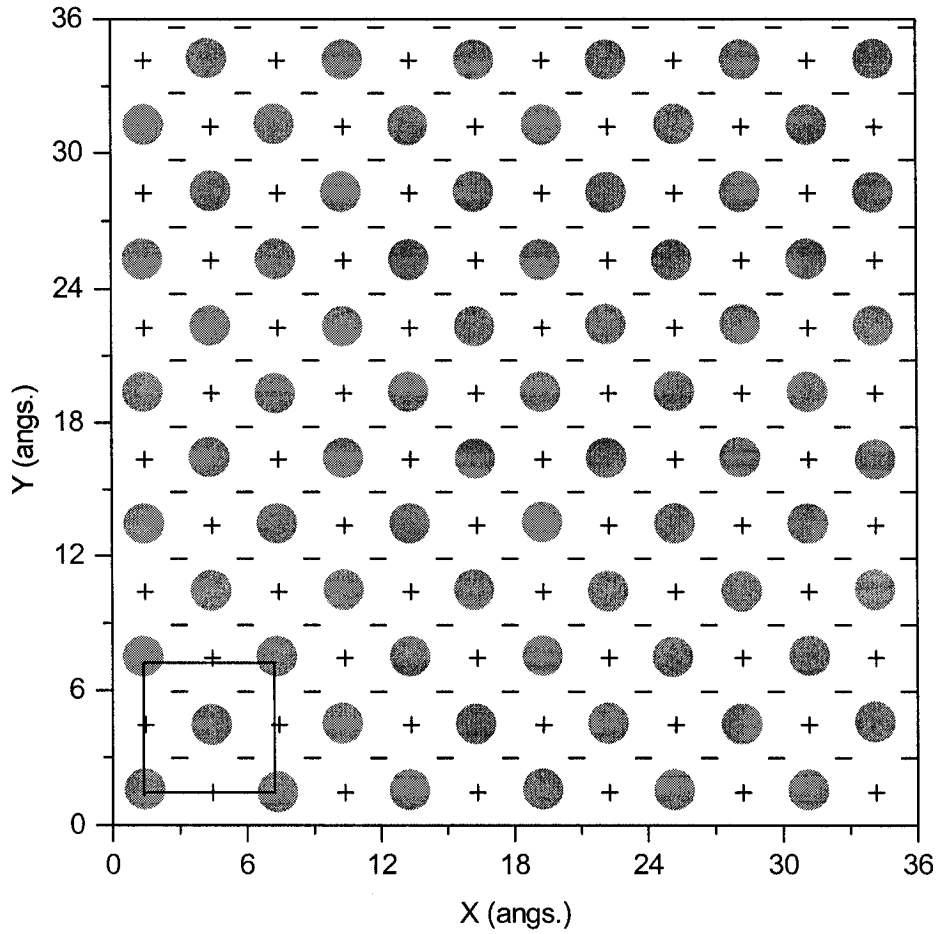

FIG. 5.27: The MgO(001) surface covered with 72 H_2 molecules at 1 K. The hydrogen molecule represents as a single circle. The (+) symbol represents a Mg^{2+} ion and the (-) symbol represents an O^{2-} ion. The $c(2\times2)$ unit cell is also shown in solid lines.

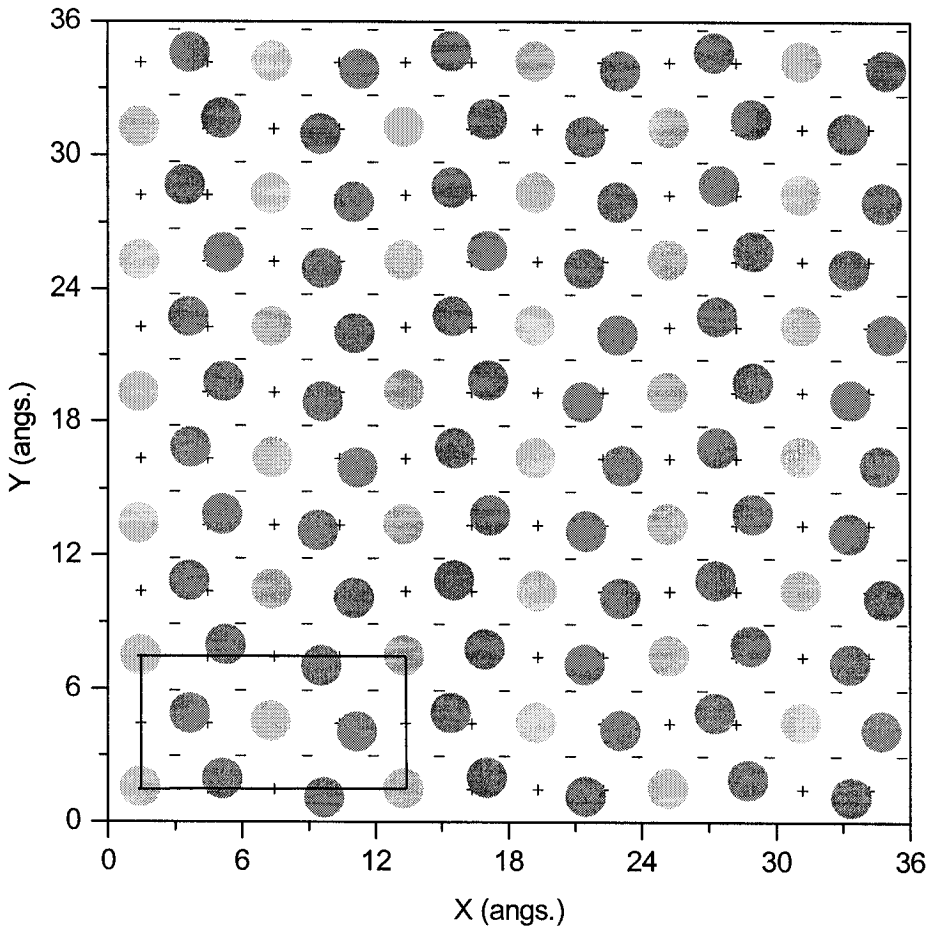

FIG. 5.28: The MgO(001) surface covered with 108 H_2 molecules at 1 K. The (+) symbol represents a Mg^{2+} ion and the (-) symbol represents a O^{2-} ion. The hydrogen molecules that lie over Mg^{2+} sites are shown as light gray circles; while for H_2 molecules whose center of mass lies between the cationic Mg^{2+} and the anionic O^{2-} sites represent as gray circles. The *c*(4×2) unit cell is shown in solid lines.

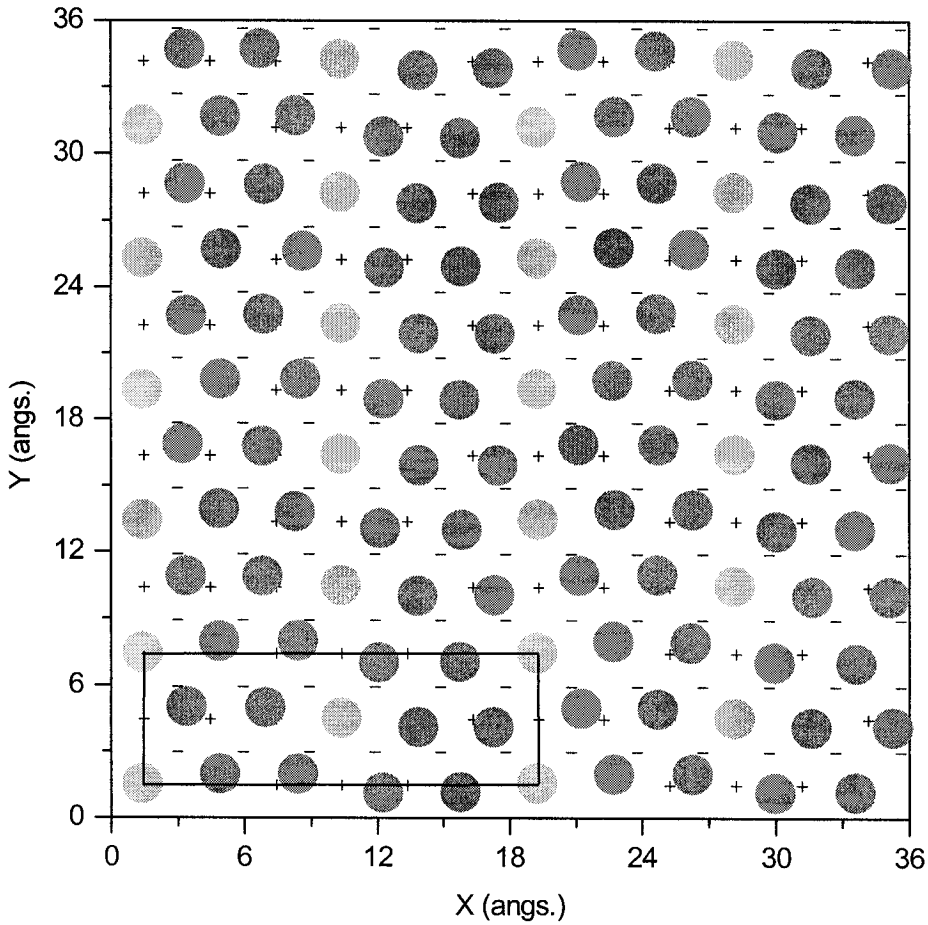

FIG. 5.29: The MgO(001) surface covered with 120 H_2 molecules at 1 K. The (+) symbol represents a Mg^{2+} ion and the (-) symbol represents a O^{2-} ion. The hydrogen molecules that lie over Mg^{2+} sites are shown as light gray circles; while for H_2 molecules whose center of mass lies between the cationic Mg^{2+} and the anionic O^{2-} sites represent as gray circles. The *c*(6×2) unit cell is shown in solid lines.

5.3. Relation between Simulations and Calculations

Using perturbation theory it has been shown that no matter what the rotational state of the H_2 molecules adsorbed directly over ionic sites is, the molecular axis will be delocalised with a residual amount of anisotropy that reflects the four-fold symmetry of the underlying surface potential. Hence, molecules that lie in the plane of the surface with preferred but unequal azimuthal orientations, as determined from the Monte Carlo simulations, will be orientationally delocalised and hence orientationally indistinguishable from site to site. Specifically, these are the molecules that lie at the vertices and center of the *p*-type unit cells. Thus the *p*-type structures are converted to *c*-type structures and the Mont Carlo simulations are thus consistent with the experimental observation of a sequence of *c*-type structures.

Our PT calculations do not include the influence of neighbouring molecules due to the relative weakness of the interaction and the complexity of the calculations. In the $c(2\times2)$ case the position of neighbouring molecules will simply yield an additional four-fold symmetric anisotropy that leaves the molecules orientationally indistinguishable. In the (4×2) and (6×2) structures the molecules at the vertices and center of the unit cell will see the same kind of hexagonal local environment, once orientational delocalisation of the neighbours is taken into account, and again be orientationally indistinguishable. Thus, the inclusion of molecular interactions will not destroy the symmetry required by the *c*-type structures.

In the $p(4\times2)$ and $p(6\times2)$ structures shown in Figs. 5.5 and 5.10 many molecules are offset from the anionic sites and are tilted with respect to the surface normal. In terms of rotational states this may interpreted as either a skewed *para*-state or a mixture of helicoptering and cartwheeling *ortho*-states. As molecules move around on the surface the degree of mixing between the *ortho*-states will change; the closer the molecule is to a Mg^{2+} ion the greater the helicoptering character whereas proximity to the O^{2-} will mix in more of the cartwheeling state.

The previous plots of the adlayer configurations implicitly showed the orientation of the hydrogen molecules axes by representing the molecule as two circles centered on each of the hydrogen atoms. The quantum calculations show that the axes are azimuthally delocalized and so the molecule could alternatively be represented by a single circle centered on the molecular centre of mass. The resulting $c(2\times2)$, $c(4\times2)$, and $c(6\times2)$ structures are shown in Figs. 5.27, 5.28, and 5.29 respectively. In all cases, the unit cells are obviously *c*-type and wave-like features are apparent along the rows.

CHAPTER 6: RESULTS FOR H_2 MONOLAYERS ON LiF(001)

The structures of mono-layers of H_2 molecules on LiF(001) have been studied using the Metropolis Monte Carlo simulation methods within the canonical ensemble. The simulations employ a potential energy model that includes detailed molecule-molecule and molecule-surface interactions. As well as calculations of the energy contributions in of the H_2/LiF(001) system, the simulations also allows one to determine the detailed structure of the H_2 adlayers and their thermal stabilities. The quantum behaviour of the H_2 molecules in the adsorbed phase was not included in our MC simulations. To estimate quantum effects, time-independent perturbation theory was applied to study the rotational motion of hydrogen molecules adsorbed on the LiF(001) surface. This was done to reconcile the simulations results with the experimental findings. The results of these simulations and calculations are presented in the following sections.

6.1. Simulation results: H_2/LiF(001)

6.1.1. Single molecule adsorbed on a LiF(001) surface

The potential model of the interaction of H_2 molecules with the (001) face of a LiF surface has been tested, via Monte Carlo (MC) simulations at low temperatures (1—11 K), to determine the quality of the interaction parameters presented in chapter 4. In these simulations, the H_2 molecule can move freely on the surface in three dimensions as well as change the orientation of its molecular axis randomly. On average, it is found that a H_2 molecule prefers to adsorb on the top of a Li^+ site at a height of 2.82 Å (the distance from the center of mass of

the H_2 molecule to the Li^+ ion directly below), and lies flat (θ = 90°) over the surface with its molecular axis oriented toward the neighbouring F^- sites ($\varphi = \pm 45°$). The binding energy was calculated and found to be –0.711 kcal/mol, very close to the isosteric heat of adsorption value -0.701 kcal/mol [42]. Our finding that H_2 prefers to locate over a Li^+ site is consistent with proposals based on the HAS results [46] and a recent theoretical study of the H_2/LiF(001) potential [44]. Consequently, our potential model seems to be a reasonable one for the study of the structures of H_2 adlayers on a LiF surface.

6.1.2. H_2 adlayers: *p*(2×2) structure

The HAS results [46] show that at a coverage of 0.5 an ordered commensurate structure with *c*(2×2) symmetry appears. Toennies' group proposed a unit cell structure with hydrogen molecules over every other Li^+ cationic site arrayed in a checkerboard fashion. All sites are equivalent in keeping with the observed *c*-type structure. This structure and others were examined using the Metropolis Monte Carlo simulations at T=1 K. In our MC simulations, the coverage of 0.5 has been replicated by placing 72 H_2 molecules, with random initial orientations, above a (12×12) patch of surface that contains 144 Li^+ adsorption sites. These simulations were run for 50 kcycles with the result of the first 10 kcycles discarded. In all cases, the MC simulations yield a single configuration with a *p*(2×2) unit cell symmetry as illustrated in Fig. 6.1. This

unit cell contains two molecules that adopt a "tee" configuration with respect to each other in the plane of the adsorbed layer, that is, their molecular axes are oriented toward the center of the closest neighbouring H_2 molecules.

The polar angle distribution (θ) for temperatures up to 14 K is shown in Fig. 6.2. It has a peak centered at $\theta = 90^{\circ}$ that indicates molecules lie flat, parallel to the plane of the surface. An increase in temperature to 14 K causes the distribution to broaden but the peak still persists. The distribution of the azimuthal angle φ is shown in Fig. 6.3 and has two peaks centered at $\varphi \approx 45^{\circ}$, and 135°. These peaks have equal height as a result of molecules adopting these orientations with equal likelihood because of the "tee" configuration adopted by neighbouring molecules in the $p(2\times2)$ structure. These peaks thermally broaden but still exist up to 14 K.

As presented in Fig. 6.4, the height distributions show that the center of mass of H_2 molecules sit over the surface with an equilibrium height of 2.82 Å at 1 K and shift upwards to 2.9 Å at 14 K. The molecules remain within a narrow range of the equilibrium heights indicating that the surface layer remains well defined and with only one kind of adsorption site in a $p(2\times2)$ ad-layer. When the temperature was increased beyond 14 K, molecules migrated from the Li^{+} cationic sites and started to desorb from the surface causing disorder in the surface layer. Thus, the $p(2\times2)$ structure is not stable beyond 14 K.

The average binding energy of H_2 molecules in a $p(2\times2)$ layer is –0.824 kcal/mol at T= 1 K. This value is slightly greater than the value for isolated particles, even though the molecules adopt the same orientation with respect to the surface. The additional binding energy comes from the attractive interaction between molecules within the layer.

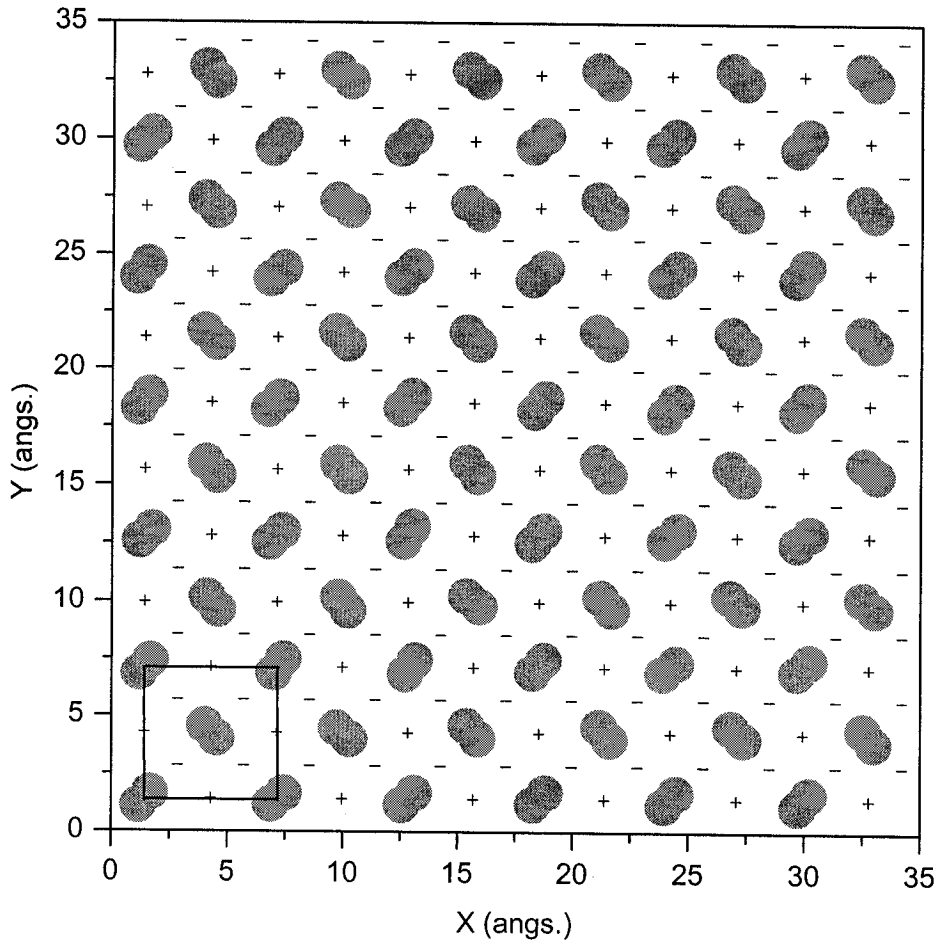

FIG. 6.1: The LiF(001) surface covered with 72 H_2 molecules at 1 K. The hydrogen atoms are shown as grey circles. The (+) symbol represents Li^+ ion and (-) symbol represents a F^- ion. The *p*(2×2) unit cell is shown in solid lines.

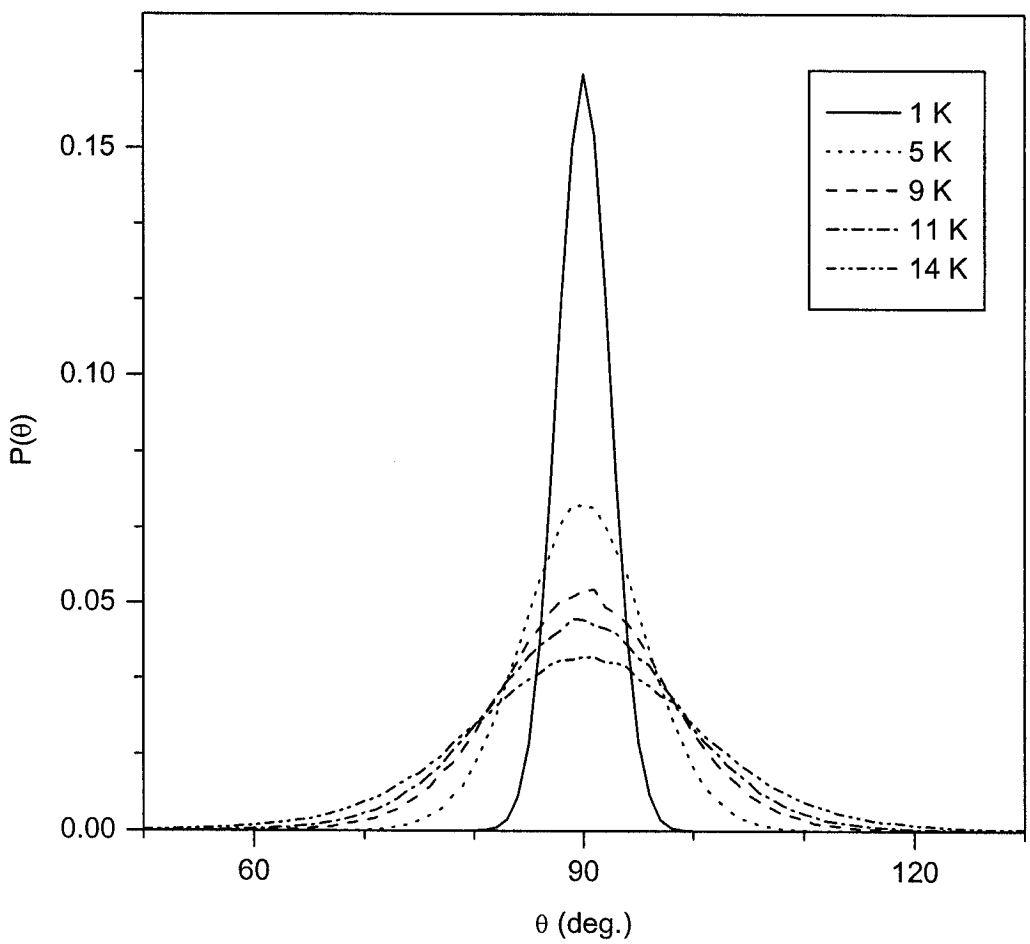

FIG. 6.2: The polar angle distribution of the $p(2\times2)$ layer is plotted for temperatures T=1, 5, 9, 11 and 14 K, the distributions are symmetric and centred on $\theta \sim 90^{\circ}$. By increasing the temperature, the peaks decrease in height and broaden in width.

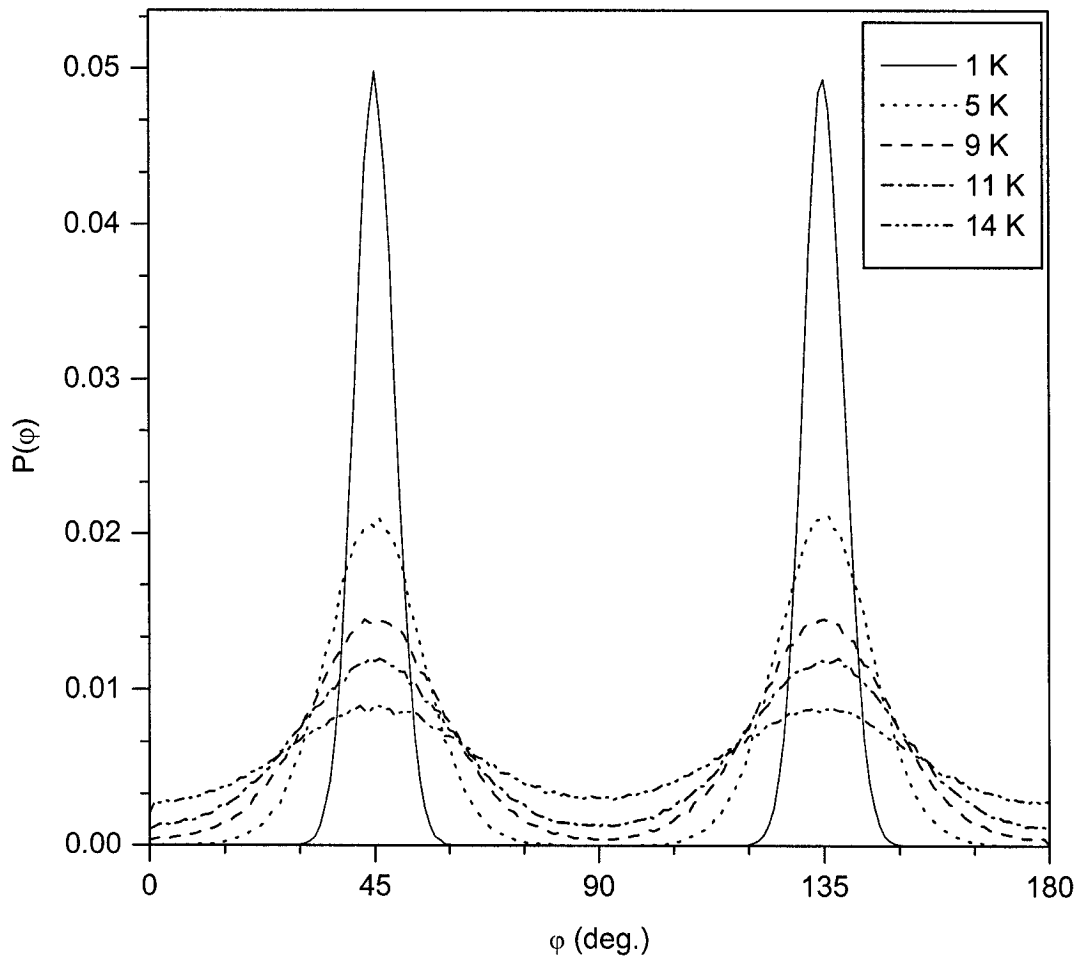

FIG. 6.3: The azimuthal angle (φ) distributions of the $p(2\times2)$ phase is plotted for temperatures T=1, 5, 9, 11 and 14 K. Note that the peaks are symmetric and centred on the $\varphi \sim 45^{\circ}$, and 135° directions. As the temperature increases the peak heights decrease and the widths broaden.

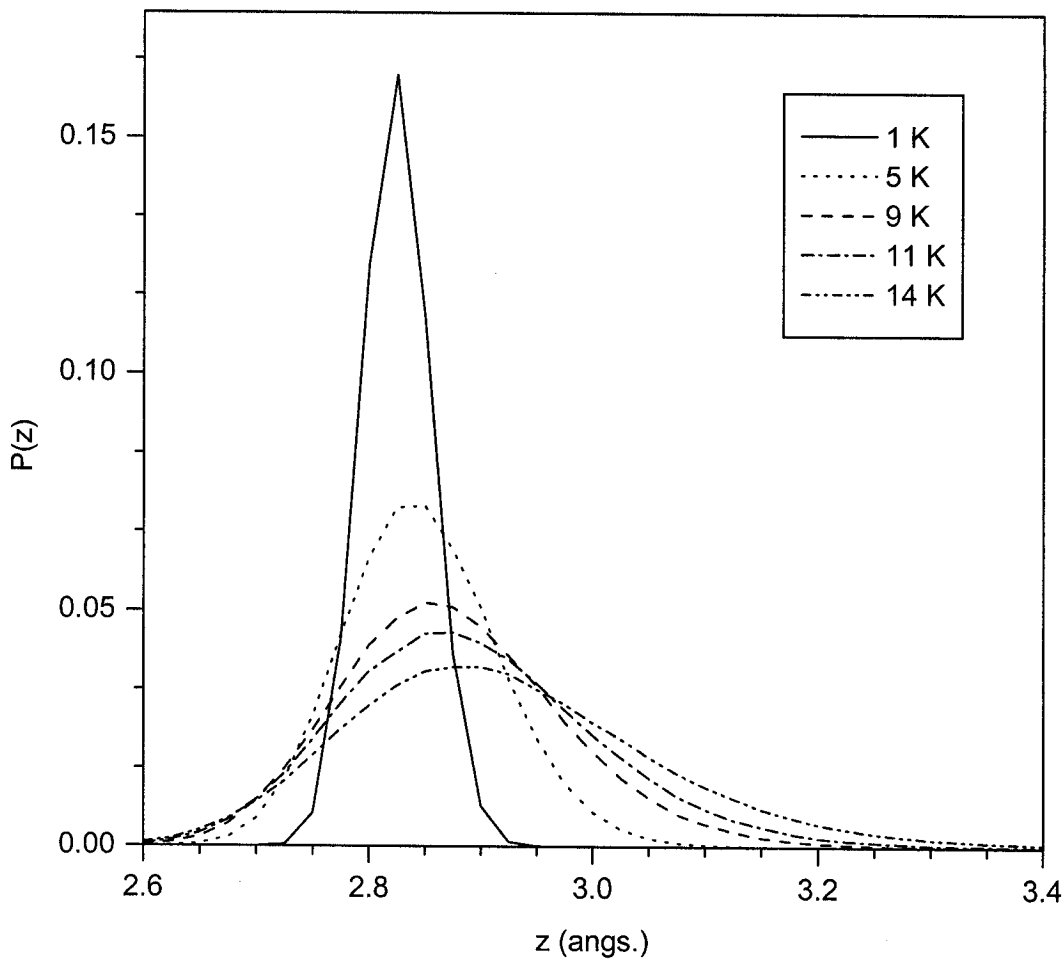

FIG. 6.4: The height (z) distribution of the H_2 molecules centre of mass for the $p(2\times2)$ layer plotted for temperatures T=1, 5, 9, 11 and 14 K.

6.1.3. H_2 adlayers: *p*(8×2) structure

The HAS work of Toennies' group [46] indicates that at a coverage of 0.625, a stable structure with *c*(8×2) symmetry arises. It was proposed that the unit cell consists of molecules that sit directly over the cationic sites while others are distributed around the anionic sites. This proposed structure, as well as others, were examined using the Metropolis MC simulations. In these simulations, 160 H_2 molecules were placed on a (16×16) patch of surface to match the experimentally observed coverage. Regardless of the initial configurations chosen, the MC simulations yielded a single unique final configuration with *p*(8×2) symmetry as shown in Fig. 6.5. The unit cell consists of two kinds of adsorption sites: a parallel site, where the H_2 molecules lie flat (θ = 90°) on the surface, with its center of mass directly over the top of Li^+ sites; and a tilted site, where the H_2 molecules lie between the cation and anion sites with their molecular axes oriented towards the nearest F^- sites (the polar angle θ = 63°). In Fig. 6.5, the parallel molecules are shown as solid gray atoms while the tilted molecules are shown as a combination of black and light gray atoms with the lower H atoms shown as black circles. The lower atoms are closer to the anionic sites than the cationic sites and the molecular center of mass is shifted away from the underlying Li^+ sites by 0.88 Å and 0.15 Å in the x and y directions respectively, where the long axis of the unit cell lies along the x axis.

The thermal stability of the $p(8\times2)$ layer was monitored through an examination of the temperature dependence of the polar (θ) and azimuthal (φ) angle distributions. As shown in Fig. 6.6, the distributions have two sharp peaks at 1 K. The peak at $\theta = 63^{\circ}$ represents the tilted molecules whereas the peak at 90° represents molecules that lie flat on the surface (parallel site). Upon raising the temperature a few degrees Kelvin, the two peaks broaden in width, and decrease in height, but still maintain their preferred orientations. Obviously the polar angle distributions show the presence of two kinds of adsorption sites. The φ distributions shown in Fig. 6.7 also indicate the presence of two kinds of adsorption sites. The two peaks centered at $\varphi = 55^{\circ}$ and 125° are associated with the tilted molecules whereas the two peaks centered at $\varphi = 45^{\circ}$ and 135° are associated with the flat molecules over Li^{+} cationic sites. At T=5 K, these peaks merge to form two equivalent peaks centered at $\varphi = 50^{\circ}$ and 130°. Beyond 5 K, the tilted molecules become positionally and orientationally disordered, while the parallel molecules remain localized above the cationic sites with preferred polar and azimuthal orientations. Indications of this are signalled by the disappearance of the polar angle peak at $\theta = 63^{\circ}$ (attributed to the tilted molecules).

The height distributions shown in Fig. 6.8, also indicates the presence of two adsorption sites. The peak at 2.82 Å is due to horizontal molecules (parallel site) whereas the peak at 3.1 Å corresponds to the tilted molecules. The size of the two peaks reflects the number of molecules associated with each peak; in keeping with the 3:2 ratio of parallel to tilted molecules. An increase in

temperature causes both peaks in Fig. 6.8 to broaden and shift to higher values as one would expect. At 8 K the parallel molecules have moved to a height of 2.9 Å but remain localized above the cationic sites, retaining a high degree of order. On the other hand, the tilted molecules reach heights of 3.8 Å or more. These increased exclusions in the z direction may be indicative of the tilted molecules undergoing external vibrational excitations with respect to the surface normal, which in turn leads to positional disorder.

The binding energy of H_2 molecules in the $p(8\times2)$ layer was found to be –0.784 kcal/mol with the molecules in the parallel sites more strongly bound (-0.808 kcal/mol) than the tilted molecules (–0.748 kcal/mol). The parallel molecules have a stronger binding energy due to their closer proximity to the surface.

Our MC simulations results show (see Fig. 6.5) that the $p(8\times2)$ monolayer may be thought of consisting of two sub-regions: one with $p(2\times2)$ symmetry and the other with $p(4\times2)$ symmetry. This means that upon adding more molecules to a $p(2\times2)$ monolayer, the local response is to form a $p(4\times2)$ structure (discussed in the next section). The $p(8\times2)$ monolayer might represent a transition state or stable island between the $p(2\times2)$ and $p(4\times2)$ structures.

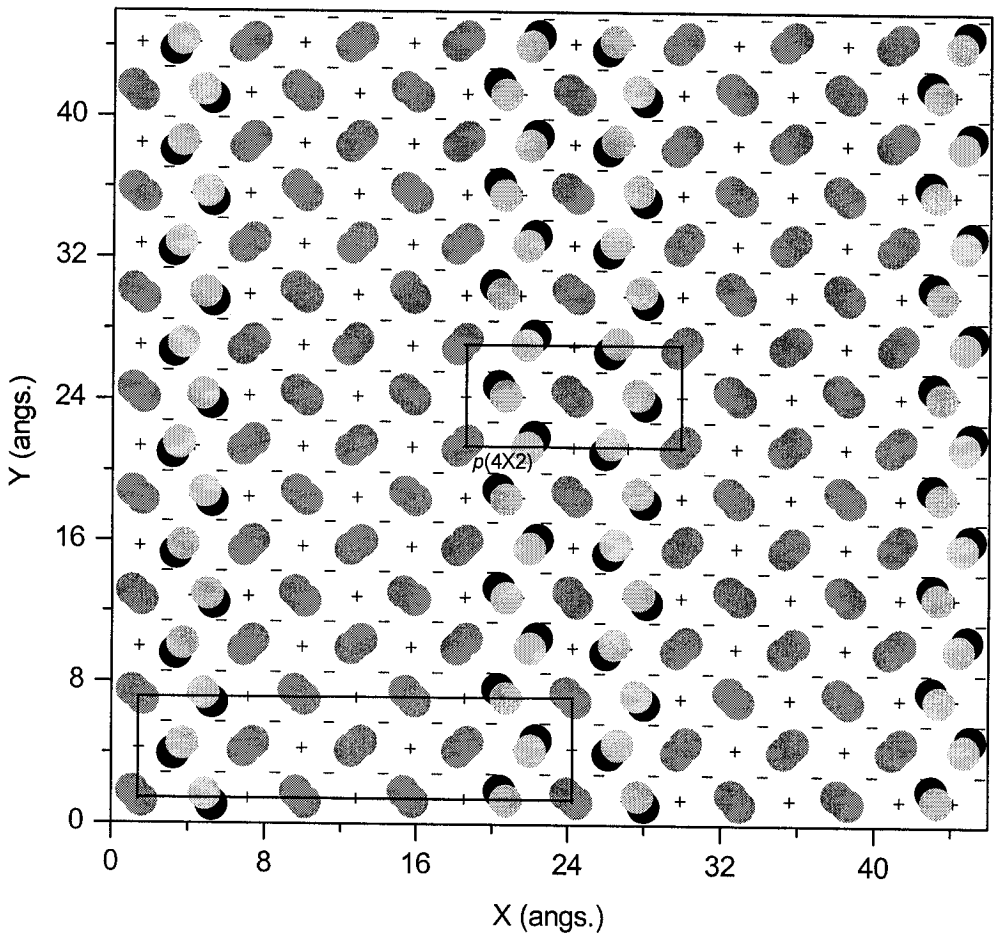

FIG. 6.5: The LiF(001) surface covered with 160 H_2 molecules at 1 K. The (+) symbol represents a Li^+ ion and the (-) symbol represents a F^- ion. The hydrogen atoms of molecules that lie flat over Li^+ sites are shown as gray circles; while for tilted H_2 molecules the lower H atoms are represented by solid black circles and the upper H atoms are represented by light gray circles. The $p(8\times2)$ unit cell is shown in solid lines.

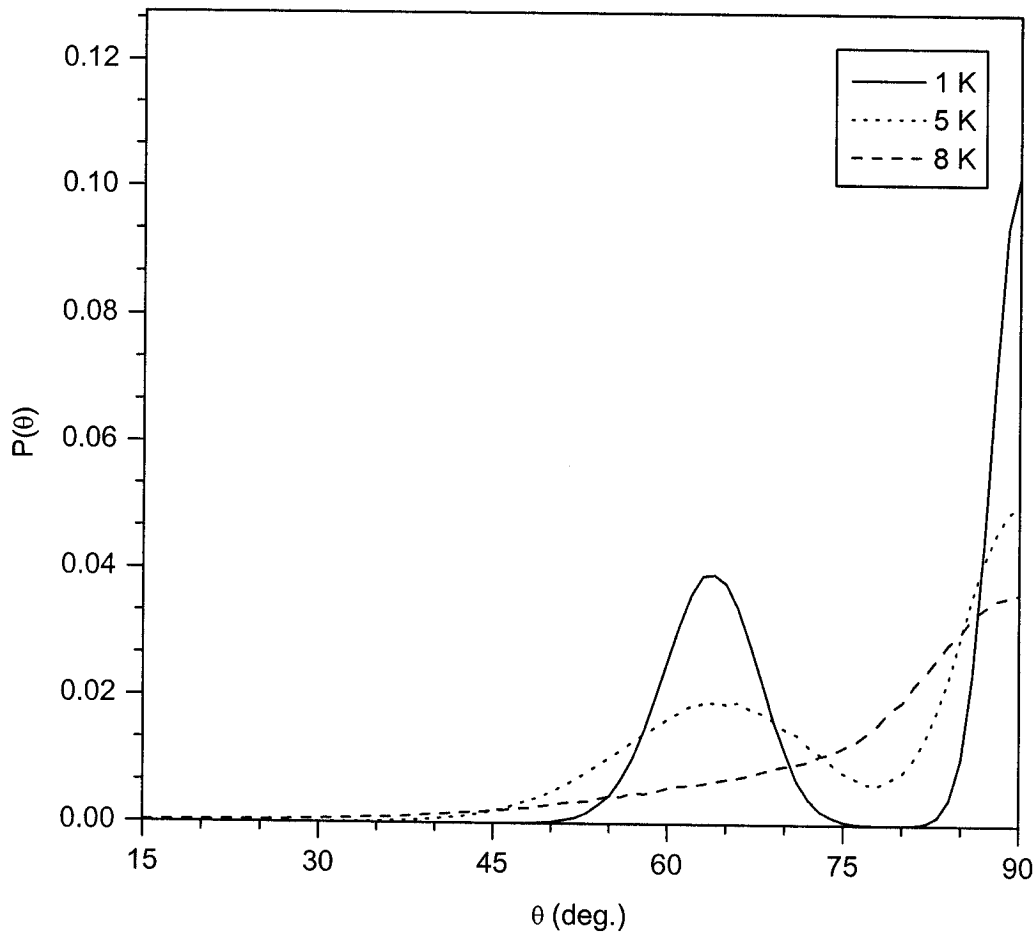

FIG. 6.6: The polar angle distribution of the $p(8\times2)$ layer plotted for temperatures T=1, 5, and 8 K. At 1 K, the distributions are symmetric and centred on $\theta \sim 63°$, 90°.

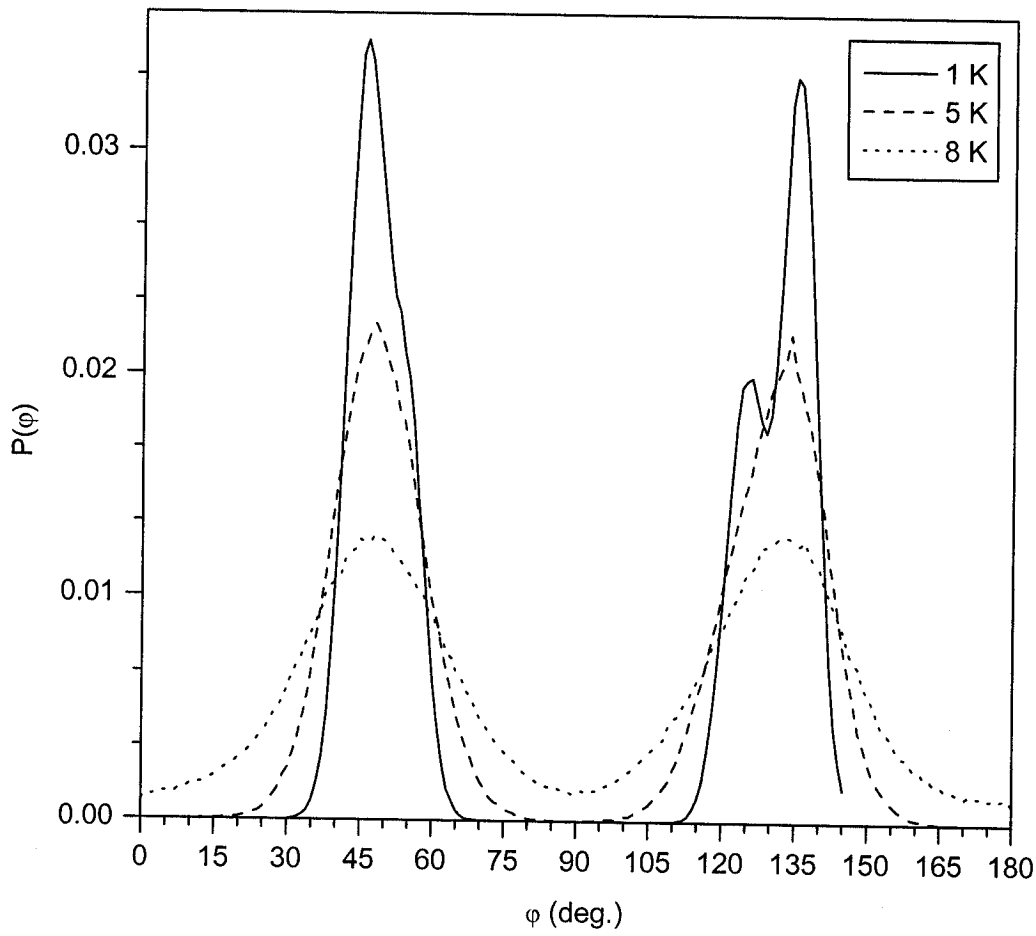

FIG. 6.7: The azimuthal angle (φ) distribution of the $p(8\times2)$ phase is plotted for temperatures T=1, 5, and 8 K. At T=1 K, the two sharp peaks at $\varphi = 45^{\circ}$ and 135° are due to flat molecules, while the smaller peaks at $\varphi = 55^{\circ}$ and 125° are attributed to the tilted molecules. As the temperature increases, the peaks merge into two broad peaks at $\varphi = 50^{\circ}$ and 130°.

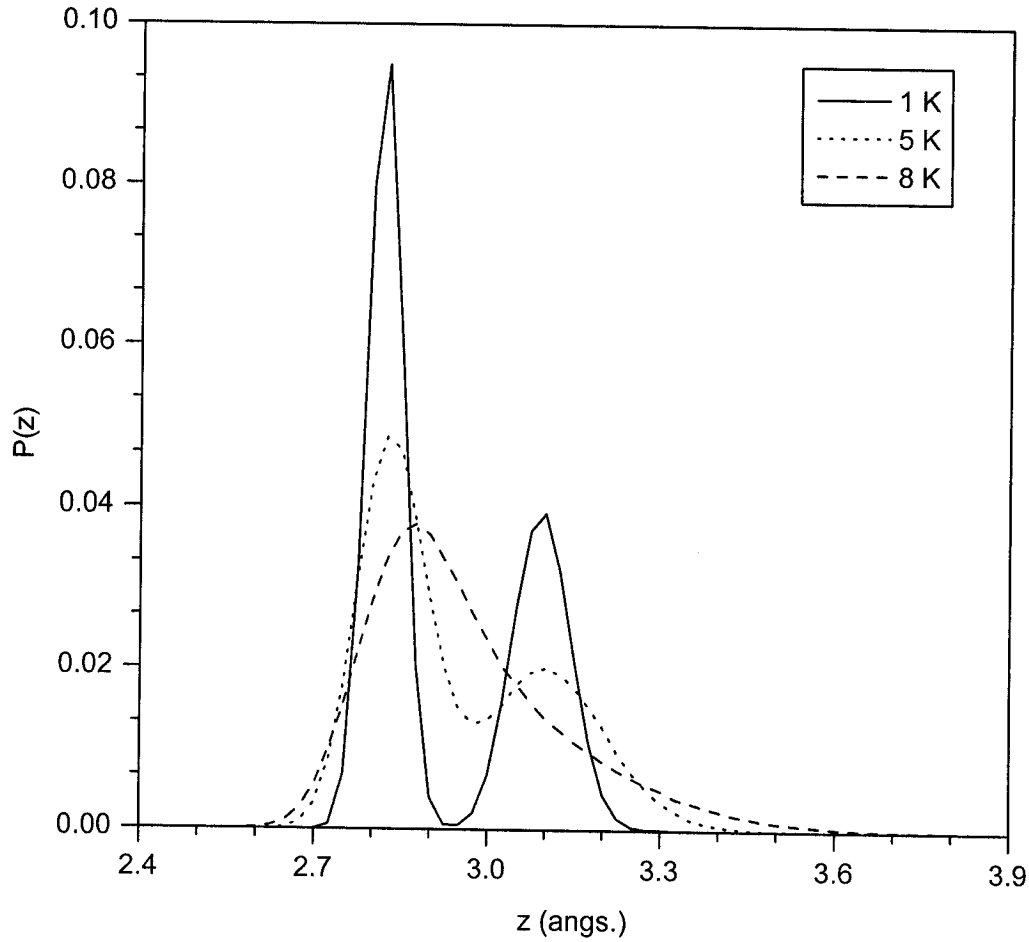

FIG. 6.8: The height (z) distributions of the centre of mass of H_2 molecules of the *p*(8×2) layer is plotted for temperatures T=1, 5, and 8 K. At T=1 K, the peak at 2.82 Å represents the flat molecules adsorbed over Li^+ sites, while the peak at 3.1 Å represents the tilted H_2 molecules.

.

6.1.4. H_2 adlayers: *p*(4×2) structure

According to our MC simulation findings of the *p*(8×2) monolayer, it appears that the *p*(8×2) structure consists of a patch that locally has a *p*(2×2) structure (coverage 0.5) and another patch with a coverage of 0.75. This structure is a likely candidate for a stable structure with long range order. To examine this possibility using the Metropolis MC method simulations using a (12×12) patch of surface and 108 H_2 molecules (coverage of 0.75) were run. Regardless of the initial configurations examined, the MC simulations yielded a single unique final configuration with a *p*(4×2) symmetry as shown in Fig. 6.9. The unit cell consists of two kinds of adsorption sites: a parallel site, where the H_2 molecules lie flat (θ = 90°) on the surface with its center of mass directly over the top of Li^+ sites; and a tilted site, where the H_2 molecules lie between the cation and anion sites with their molecular axes oriented towards the nearest F^- sites with a polar angle of θ = 65°. In Fig. 6.9, the parallel molecules are shown as solid gray atoms while the tilted molecules are shown as a combination of black and light gray atoms with the lower H atoms shown as black circles. The lower atoms are closer to the anionic sites than the cationic sites and the molecular center of mass is shifted away from the underlying Li^+ sites by 0.88 Å and 0.15 Å in the x and y directions respectively, where the long axis of the unit cell lies along the x direction.

The thermal stability of the $p(4\times2)$ layer can be partially monitored through an examination of the temperature dependence of the polar (θ) and azimuthal (φ) angle distributions. As shown in Fig. 6.10, the θ distributions have two sharp peaks at 1 K. The peak at θ = 65° represents the tilted molecules whereas the peak at 90° represents molecules that lie flat on the surface (parallel site). Increasing the temperature a few degrees Kelvin, the two peaks broaden, but still maintain the preferred orientations. It is obvious that the polar angle distributions show two kinds of adsorption sites. The φ distributions as shown in Fig. 6.11 also indicate the presence of two kinds of adsorption sites. The two peaks centered at φ =55° and 125° are associated with the tilted molecules whereas the two peaks centered at φ =45° and 135° are associated with the molecules that lie flat over Li^+ sites. At T=5 K, these peaks merge to form two equivalent peaks centered at φ =50° and 130°, and persist up to 8 K. At temperatures above 8 K, the tilted molecules become disordered and some desorb from the surface (see the discussion of the height distribution below). The parallel molecules, however, remain localized above the cation sites with preferred polar and azimuthal orientations. The Metropolis Monte Carlo method in the canonical ensemble requires that the number of particles in the simulation remain constant. Once particles leave the simulation this condition is violated and deviations from Boltzmann's statistics occur. The various distributions (energy, angle, *etc.*) are no longer valid and are thus not shown. Although the azimuthal distribution cannot differentiate between the two-adsorption sites beyond 5 K, the polar

distribution can, at least up to 8 K. Thus the $p(4\times2)$ structure is thermally stable up to 8 K.

The height distributions, shown in Fig. 6.12, also indicate the presence of two adsorption sites. The peak at 2.82 Å is due to horizontal molecules (parallel site) whereas the peak at 3.1 Å corresponds to the tilted molecules. The size of the two peaks reflects the number of molecules associated with each peak; the area under the parallel site peak is half the area under the tilted site peak in keeping with the 1:2 ratio of parallel to tilted molecules An increase in temperature causes both peaks in Fig. 6.12 to broaden and shift to higher values as one would expect. At T= 11 K the parallel molecules have moved to a height of 2.9 Å but remain localized above the cationic sites retaining a high degree of order. On the other hand, the tilted molecules are less tightly bound, reach heights of 3.8 Å or more, and become disordered.

The binding energy of H_2 molecules in the $p(4\times2)$ layer was found to be –0.76 kcal/mol with the molecules in the parallel sites more strongly bound (-0.791 kcal/mol) than the tilted molecules (–0.744 kcal/mol). The parallel molecules have a stronger binding energy due to their closer proximity to the surface.

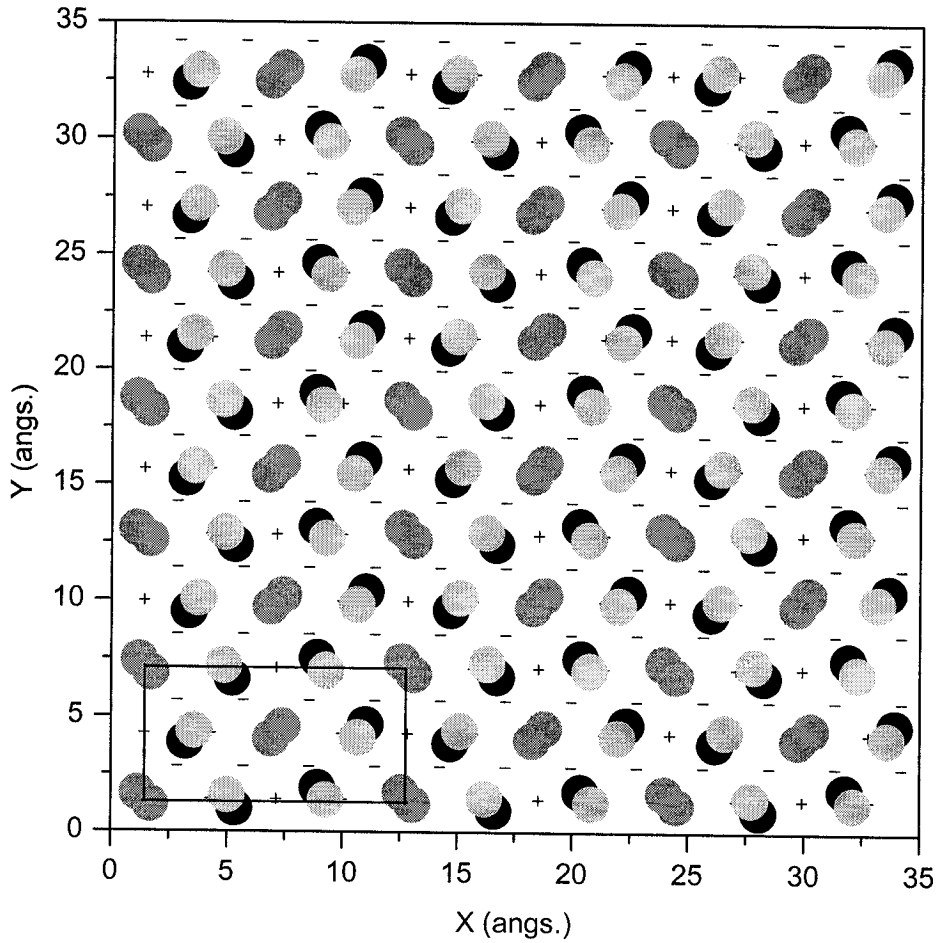

FIG. 6.9: The LiF(001) surface covered with 108 H_2 molecules at 1 K. The (+) symbol represents a Li^+ ion and the (-) symbol represents a F^- ion. The hydrogen atoms of molecules that lie flat over Li^+ sites are shown as gray circles; while for tilted H_2 molecules the lower H atoms are represented by solid black circles and the upper H atoms are represented by light gray circles. The $p(4\times2)$ unit cell is shown in solid lines.

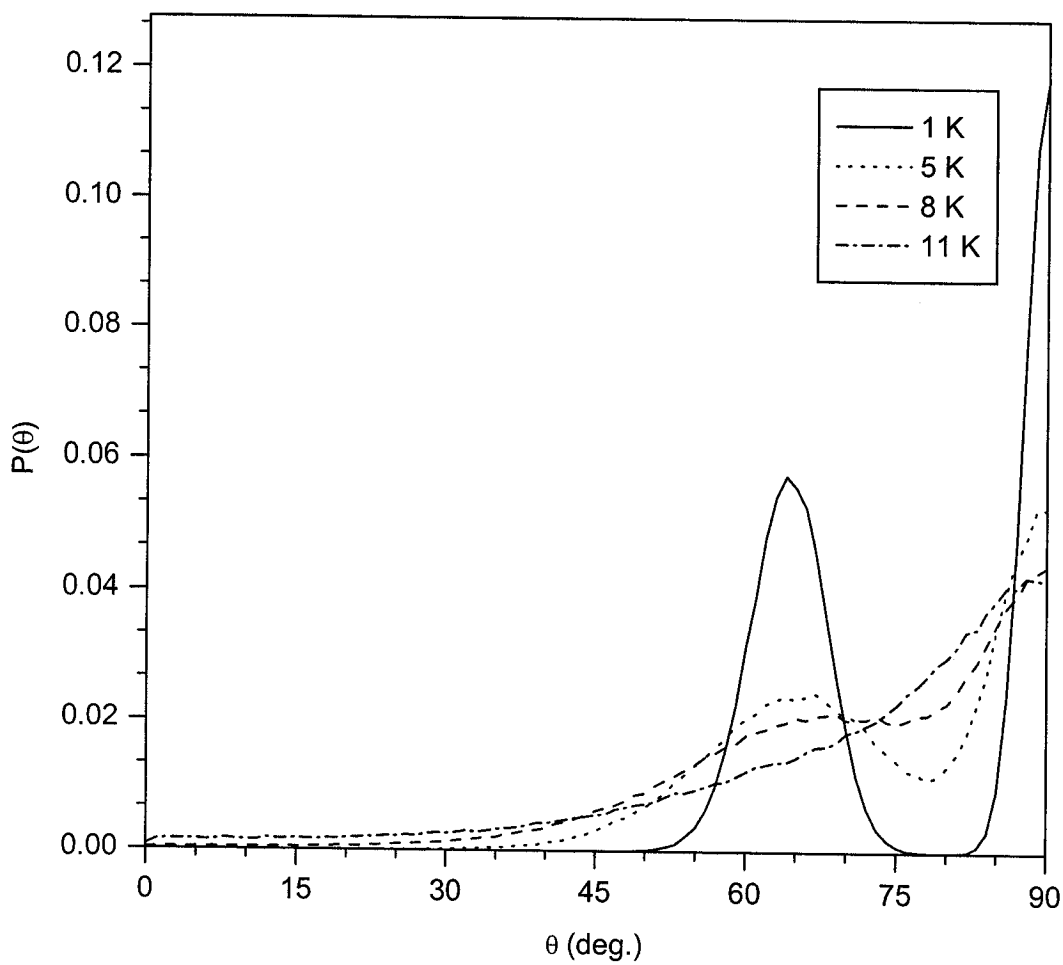

FIG. 6.10: The polar angle distribution of the $p(4\times2)$ layer plotted for temperatures T=1, 5, 8 and 11 K. At 1 K, the distributions are symmetric and centred on $\theta \sim 65°, 90°$. By increasing the temperature, the peaks decrease in height and broaden in width, which indicates the molecules still have the same orientation up to 8 K.

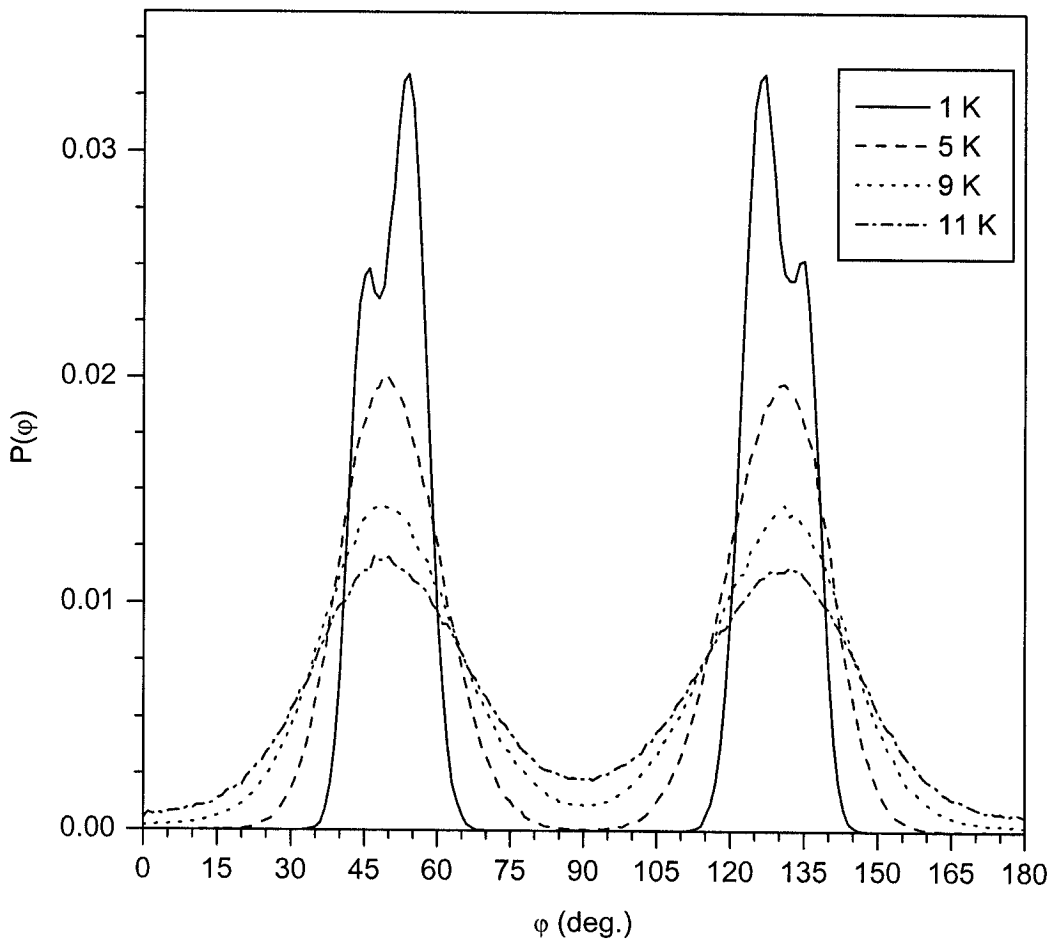

FIG. 6.11: The azimuthal angle (φ) distribution of the $p(4\times2)$ phase is plotted for temperatures T=1, 5, 8 and 11 K. At T=1 K, the two sharp peaks at $\varphi = 45^{\circ}$ and 135° are due to flat molecules, while the larger peaks at $\varphi = 55^{\circ}$ and 125° are attributed to the tilted molecules. As the temperature increases, the peaks merge into two broad peaks at $\varphi = 50^{\circ}$ and 130°.

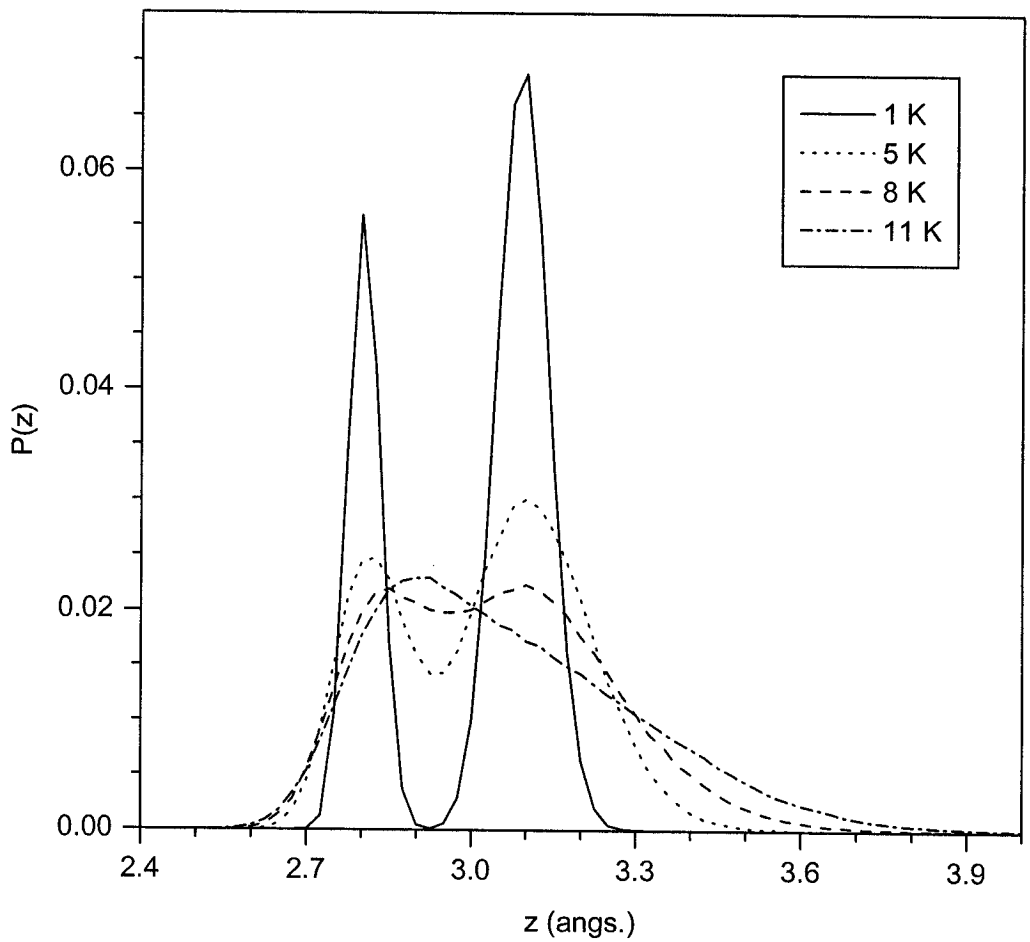

FIG. 6.12: The height (z) distributions of the centre of mass of H_2 molecules of the $p(4\times2)$ layer is plotted for temperatures T=1, 5, 8 and 11 K. At T=1 K, the peak at 2.82 Å represents the flat molecules adsorbed over Li^+ sites, while the peak at 3.1 Å represents the tilted H_2 molecules.

6.1.5. H_2 adlayers: *p*(6×2) structure

In order to determine if there is any further kinds of monolayer of H_2 molecules, the structure and thermal stability of a *p*(6×2) layer was examined. In these simulations, 120 hydrogen molecules were placed in the potential of a patch of surface containing 144 Li^+ sites to yield a coverage of 5/6. Many possible configurations were examined and in all cases the layer became highly disordered with molecules desorbing from the surface. As a result we conclude that *p*(6×2) layers are unstable along with any monolayer with coverage 5/6. This is in contrast with the observation by experiment finding [28] of a stable *p*(6×2) layer in the H_2/MgO(001) system. This difference is consistent with the smaller lattice constant of the LiF surface (4.03 Å) compared with the MgO surface (4.2 Å); where there is less area available for molecule adsorption on the LiF(001) surface making the *p*(6×2) layer unstable.

6.1.6. Summary and discussion of simulations

It is obvious that the Metropolis MC simulation results match the HAS results [46] in terms of coverage and thermal stability for the (2×2) structure, but disagree in terms of symmetry, *i.e.*: the HAS work found a "*c*" type structure whereas the MC simulations yield a "*p*" type structure due to the localization of the molecular axes in the φ = 45°, 135° directions. However, *c*-type structures can be obtained if the molecular axes of H_2 molecules are freely rotating or azimuthally delocalized. The freely rotating scenario might be realized at higher

temperatures but this would also lead to desorption. Azimuthal delocalization, however, is possible at low temperatures owing to the weak strength of the H_2 - LiF interaction and the light mass of the H_2 molecule. In particular, quantum mechanical tunnelling of the molecular axis might occur causing azimuthal delocalization and thus converting the *p*-type structures to *c*-type. This cannot be observed in our simulations because the MC method used employs classical statistics. Therefore, the rotational motion of the H_2 molecule in the adsorbed phase is examined using time-independent perturbation theory (PT) and presented in the following section.

6.2. Rotational State Calculations

Quantum mechanical delocalization of the hydrogen molecules' axes will change the symmetry of the adlayer structure from *p*(n×2) to *c*(n×2). Therefore, the nature of the rotational state of an adsorbed hydrogen molecule was investigated to see if delocalisation would occur. To obtain a complete understanding of the rotational states and determine which H_2 species (*ortho* and *para*) are preferentially adsorbed over the ions of the surface, fully 3-dimensional rotations must be examined.

In our calculations, an H_2 molecule is regarded as a rigid rotor rotating in the presence of the surface potential. The resulting rotational potential $V(\theta,\varphi)$ was treated as a perturbation, H', of the gas phase Hamiltonian, H°. Using a time-

independent Perturbation theory method, the Schrödinger equation has been solved to get the energies as well as wave functions of adsorbed hydrogen molecule in different rotational states. The procedure of calculations has been described in details in Chapter 3, and the results of these calculations will present in the following sections.

6.2.1. The rotational potential

The rotational potential of an H_2 molecule was constructed by fixing its center of mass directly on the top of Li^+ and F^- sites, at equilibrium heights of 2.82 Å and 3.1 Å respectively. The rotational potential of the molecule was calculated for a full range of polar (θ) and azimuthal (φ) angles in increments of 5°. The rotational potential has the general form:

$$V(\theta,\varphi) = A_o + A_1 \cdot \cos(4\cdot\varphi) + A_2 \cdot \cos^2\theta + A_3 \cdot \cos^2(2\cdot\theta) + A_4 \cdot \cos^2\theta \cdot \cos(4\cdot\varphi) + A_5 \cdot \cos^4\theta \cdot \cos(4\cdot\varphi) \quad (6.1a)$$

In terms of spherical harmonics function, the above formula (6.1a) can be written as follows:

$$V(\theta,\varphi) = A_o^{'} \cdot Y_{00} + A_1^{'} \cdot Y_{20} + A_2^{'} \cdot Y_{40} + A_3^{'} \cdot (Y_{44} + Y_{4-4}) \quad (6.1b)$$

The form of the potential reflects the four-fold azimuthal symmetry of the surface and the rotational symmetry of the homo-nuclear hydrogen molecule.

The values of these coefficients were determined by fitting the rotational potential function to the calculated potential energy of the hydrogen molecule using a least square method (Maple program version 7). The values of these parameters are presented in Tables 6.1 and 6.2.

Table 6.1: Rotational Potential Fitting parameters. These values are in the unit of kcal/mol.

Parameter	A_o	A_1	A_2	A_3	A_4	A_5
Above Li^+	-0.6634	0.0063	0.5482	-0.0353	-0.0144	0.0082
Above F^-	-0.1975	-0.0044	-0.3338	0.0678	0.0101	-0.0058

Table 6.2: Rotational Potential Fitting parameters. These values are in the unit of kcal/mol.

Parameter	A_o'	A_1'	A_2'	A_3'
Above Li^+	-1.7627	0.6008	-0.0381	2.947×10^{-3}
Above F^-	-0.2771	-0.3938	0.0732	-2.053×10^{-3}

The rotational potential above the Li^+ and F^- sites are plotted as a function of the polar and azimuthal angles as shown in Fig. 6.13 and Fig. 6.14 respectively. Above the Li^+ site, it is clear that the H_2 molecule has a minimum when the molecule lies flat (θ = 90°). As a function of azimuthal angle, the potential forms a sequence of four minima around φ = 45°, 135°, 225°, and 315° that reflect the four fold symmetry of the surface. The binding energy to the surface at each of these minima is –0.711 kcal/mol. The barrier to azimuthal rotation is approximately $\approx$ 0.025 kcal/mol. This relatively small value facilitates the occurrence of tunneling and azimuthal delocalization. In contrast, a barrier of about 0.6 kcal/mol forbids the rotation of H_2 molecule around the axis parallel to the surface plane (θ motion). Above the F^- site, the behaviour of the rotational potential is reversed (see Fig. 6.14), the energy is minimized when the molecular axis is perpendicular to the surface plane (θ = 0°), and maximized when the molecule locates flat (θ = 90°). Again at θ = 90°, the azimuthal rotational potential has four minima, at φ = 45°, 135°, 225°, and 315°, which reflect the presence of the four fold symmetry of the surface. These four minima no longer exist when the molecular axis becomes perpendicular to the surface plane (θ = 0°). The barrier energy for azimuthal rotation is found to be small (0.02 kcal/mol). The θ motion around the axis parallel to the surface plane is forbidden with a barrier energy of 0.4 kcal/mol. This value is less than that above the Li^+ site owing to the increased distance (3.1 Å *vs.* 2.82 Å) from the surface.

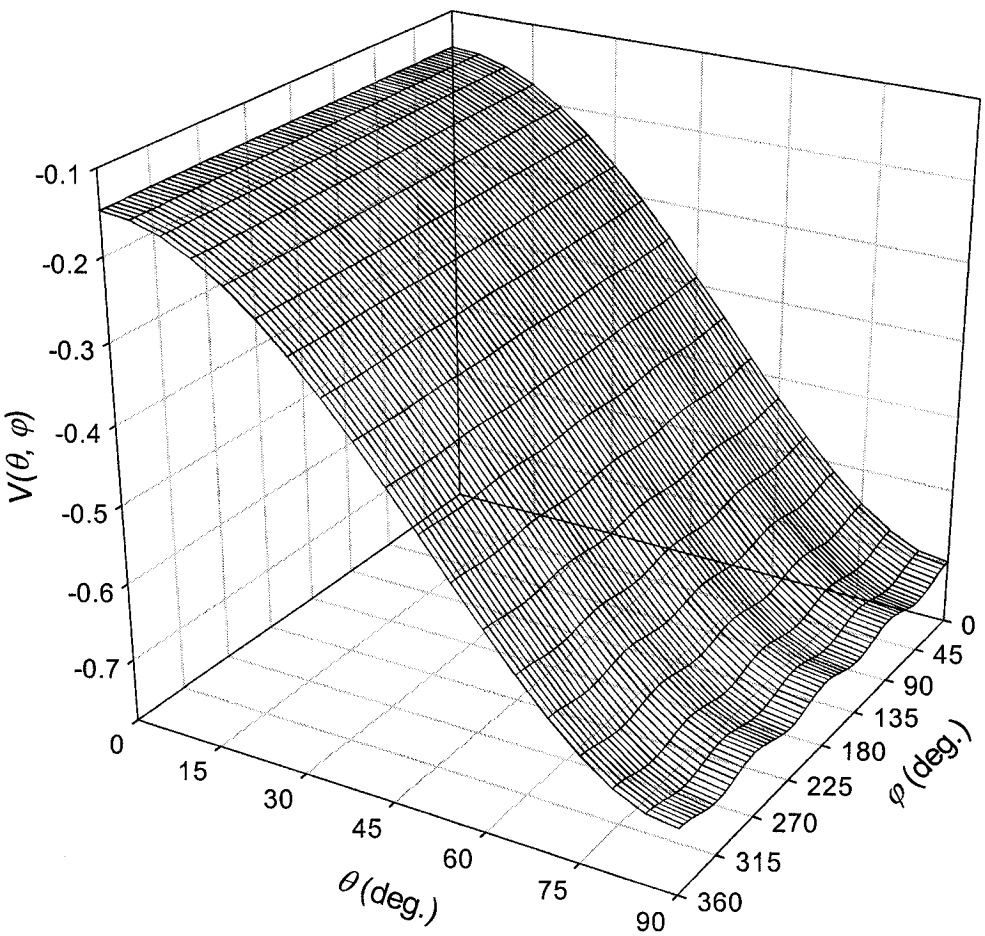

FIG. 6.13: The rotational potential $V(\theta,\varphi)$ for a H_2 molecule whose center of mass sits at a height of 2.82 Å above the Li^+ site.

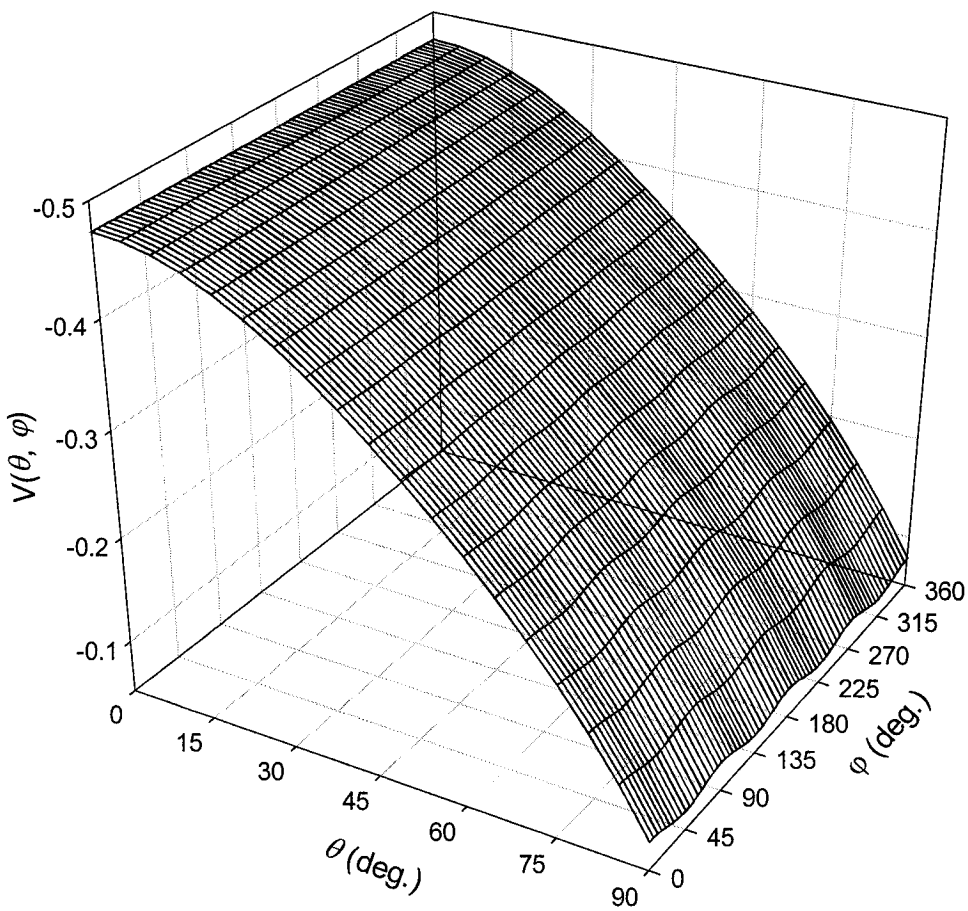

FIG. 6.14: The rotational potential $V(\theta,\varphi)$ for a H_2 molecule whose center of mass sits at a height of 3.05 Å above the F^- site.

6.2.2. The wave functions

Calculations of the quantum mechanical delocalization require determining the wave function of the H_2 species in adsorbed phase. Therefore these wave functions have been obtained using perturbation theory, including the first order correction, which can be written in the form:

$$\Psi_{Jm} \approx Y_{Jm} + \sum_{k \neq J} \frac{\langle Y_{Jm} | \hat{H}' | Y_{km} \rangle}{E_J - E_k} \cdot Y_{km} \tag{3.17}$$

where $\hat{H}' = V(\theta, \varphi)$.

By substituting the rotational potential obtained above Li^+ site in the above formula yields the following rotational wave functions for the lowest order *para* and *ortho* states.

1. For *para*-H_2 (J = 0, m = 0);

$$\Psi_{00}^{ads.} = Y_{00} - 0.162 * Y_{20} + 3.08 \times 10^{-3} * Y_{40} - 5.58 \times 10^{-4} * (Y_{44} + Y_{4-4})$$

2. For *ortho*-H_2 (J =1, m = ±1);

$$\Psi_{11}^{ads.} = Y_{11} - 0.073 * Y_{31} - 1.289 \times 10^{-3} * Y_{3-3} + 1.483 \times 10^{-3} * Y_{51} + 6.938 \times 10^{-5} * Y_{5-3} - 2.276 \times 10^{-3} * Y_{55}$$

3. For *ortho*-H_2 (J =1, m = 0);

$$\Psi_{10}^{ads.} = Y_{10} - 0.086 * Y_{30} - 1.914 \times 10^{-3} * Y_{50} - 2.137 \times 10^{-4} * (Y_{54} + Y_{5-4})$$

As shown in Fig. 6.15a, the wave function density of *para*-H_2 in its ground state is plotted as a function of θ and φ angles. A maximum in the angular distribution was found when the molecule locates flat over the surface (θ =90°), whereas the lowest value of the angular distribution is obtained when the H_2 molecular axis sits perpendicular to the surface normal (θ =0°). Consequently, *para*-H_2 is highly squashed over the Li^+ site, which is in sharp contrast to its angular distribution in the gas phase, where it has a spherical distribution with no dependence on either θ orφ. At θ =90°, the angular distribution as a function of azimuthal angle has been plotted and is shown in Fig. 6.15b. The distribution is almost uniform with a small ripple that reflects the four-fold symmetry of the surface. In other words, the molecular axis orientation is largely delocalised with a residual preference for orientation in the φ = ±45°, ±135° directions.

Similar behaviour has been observed for the angular distribution of helicoptering *ortho*-H_2 (J=1, m=±1) as can be seen in Figs. 6.16a and 6.16b. The angular distribution has a maximum value when the molecule lies flat over the surface (θ =90°) and a minimum value when it lies perpendicular to the surface plane (θ =0°). It is worth mentioning that the angular distribution of helicoptering *ortho*-H_2 (J=1, m=±1) relatively matches its angular distribution in gas phase. The

similarity of the angular distributions of the *para* and helicoptering *ortho* states may assist in the inter-conversion between *para*-H_2 and *ortho*-H_2 [95] by improving the overlap of their rotational wave functions. The angular distributions of the ground *para*-H_2 and helicoptering *ortho*-H_2 (J=1, m=±1) states are consistent with MC simulations findings that the molecule prefers to sit flat over the cationic site.

For cartwheeling *ortho*-H_2 (J=1, m=0) state, the wave function density is plotted as a function of θ, φ as shown in Fig. 6.17. The reverse behaviour is observed compared to that seen in the ground *para*-state and helicoptering *ortho*-state. The cartwheeling *ortho*-H_2 angular distribution has a maximum when the molecular axis adopts the surface normal orientation (θ =0°), and a minimum when its molecular axis makes a right angle with the surface normal (θ =90°). As can be seen from the rotational energy calculations, that will present in the next section, the cartwheeling *ortho*-H_2 is the least energetically favourable to adsorb over the cationic site.

Over the anionic F^- site, the wave functions of hydrogen molecule in their lowest levels of *para* and *ortho* states have been calculated by the same procedure applied to a single molecule located directly over Li^+ site. These calculations gave the following molecular hydrogen wave functions,

1. For *para*-H_2 (J = 0, m = 0);

$$\Psi_{00}^{ads.} = Y_{00} + 0.106 * Y_{20} - 5.912\times10^{-3} * Y_{40} + 3.908\times10^{-4} * (Y_{44} + Y_{4-4})$$

2. For *ortho*-H_2 (J =1, m = ±1);

$$\Psi_{11}^{ads.} = Y_{11} + 0.0519 * Y_{31} + 7.111\times10^{-4} * Y_{3-3} - 2.847\times10^{-3} * Y_{51} - 4.859\times10^{-5} * Y_{5-3} + 3.26\times10^{-4} * Y_{55}$$

3. For *ortho*-H_2 (J =1, m = 0);

$$\Psi_{10}^{ads.} = Y_{10} + 0.057 * Y_{30} - 3.676\times10^{-3} * Y_{50} + 1.458\times10^{-4} * (Y_{54} + Y_{5-4})$$

As shown in Fig. 6.18, the wave function density of the ground state *para*-H_2 molecule is plotted as a function of θ, and φ. The angular distribution has a minimum value when the molecule locates flat over the surface (θ =90°), and a maximum value when its axis lies parallel to the surface normal (θ =0°). Comparing to the results obtained above the Li^+ site, the angular distribution of the ground *para*-H_2 is completely reversed and at the same time is in sharp contrast to its spherical distribution in gas phase. Our findings show also that *para*-H_2 is highly elongated over the F^- site. In terms of azimuthal angle, the angular distribution seems to be uniform with a small ripple that reflects the four-fold symmetry of the surface, and is most prominent at θ = 90°. This uniform distribution represents an ideal condition for having azimuthal delocalization.

In the case of helicoptering *ortho*-H_2 (J=1, m=±1), the angular distributions also resemble their gas phase counterparts as may be seen in Fig. 6.19. The distribution is peaked around θ=90° indicating a preference for this molecules to sit parallel to the surface plane. As we will see from the rotational energy calculations, the helicoptering *ortho*-H_2 is energetically the least favourable state for sitting over the anionic site.

As shown in Fig. 6.20, the angular distribution of the cartwheeling *ortho*-H_2 (J=1, m=0) state is similar to that obtained for the ground state of *para*-H_2 in the adsorbed phase and also resembles their gas phase counterparts. As in the case of the ground state of *para*-H_2, a maximum in the angular distribution was found when the molecular axis sits perpendicular to the surface normal (θ=0°), and has a minimum when the molecule lies flat over the F^- site. Consequently, an inter-conversion between *para*- and cartwheeling *ortho*- states might be possible via the favourable overlap of their rotational wave functions. Our calculations of the rotational energies, presented in the next section, show that cartwheeling *ortho*-H_2 is the most energetically favoured state for the hydrogen when it sits over the anionic site. This is consistent with classical energy minimization calculations that show the most energetically favoured orientation of the hydrogen molecule above F^- site is one where the molecular axis sits perpendicular to the surface. Therefore, the most likely to adsorb over the anionic sites will be the cartwheeling *ortho*-H_2, followed by *para*-H_2 state with less probability.

a)

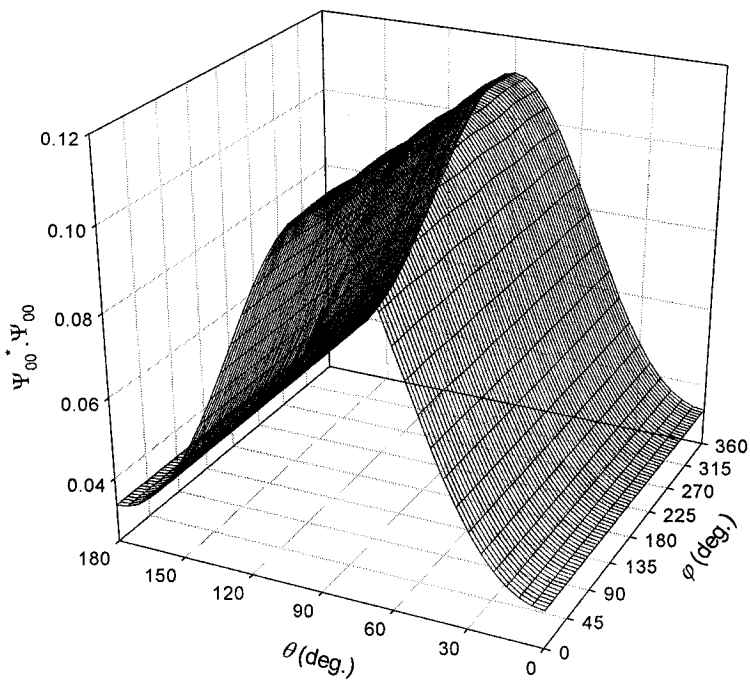

b)

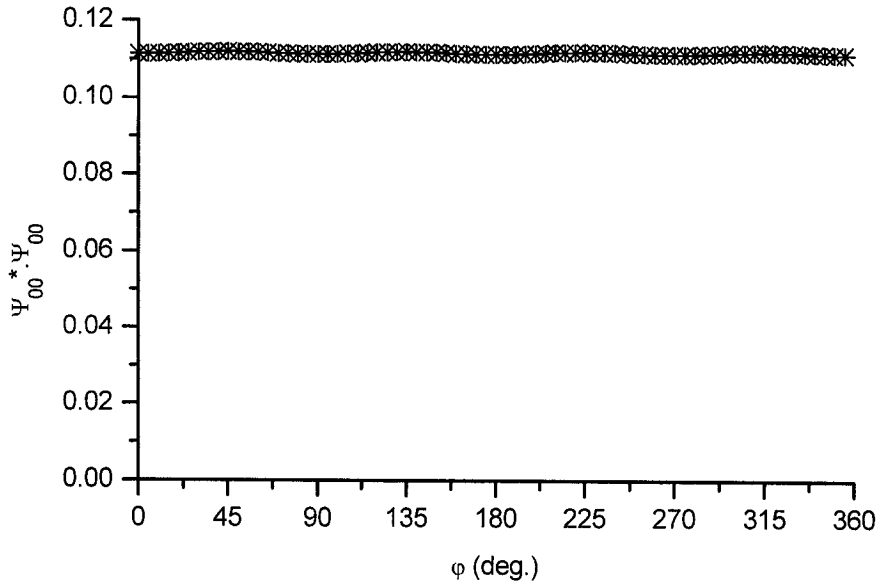

FIG. 6.15: (a) The angular distribution of a *para*-H_2 molecule above a Li^+ site. (b) The azimuthal distribution for θ =90° (the most probable polar orientation).

a)

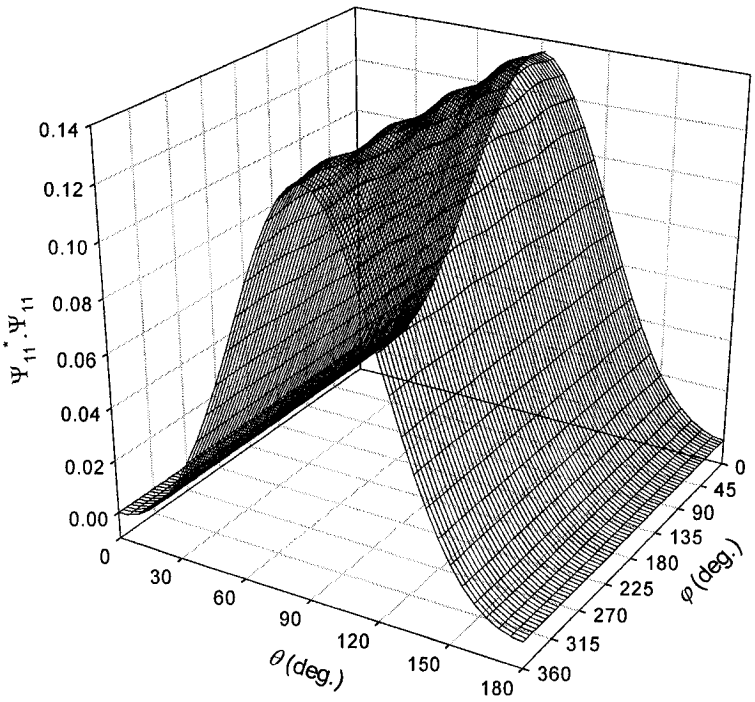

b)

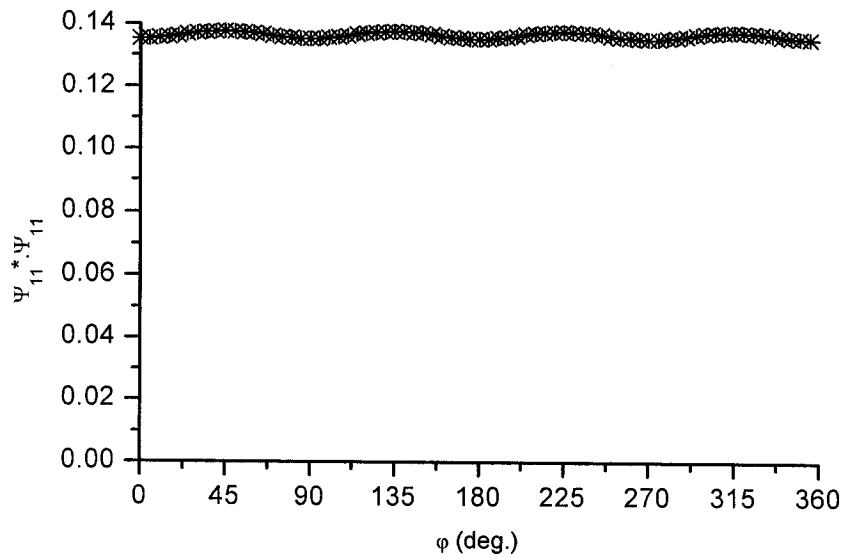

FIG. 6.16: (a) The angular distribution of a helicoptering *ortho*-H_2 molecule above a Li^+ site. (b) The azimuthal distribution for θ =90° (the most probable polar orientation).

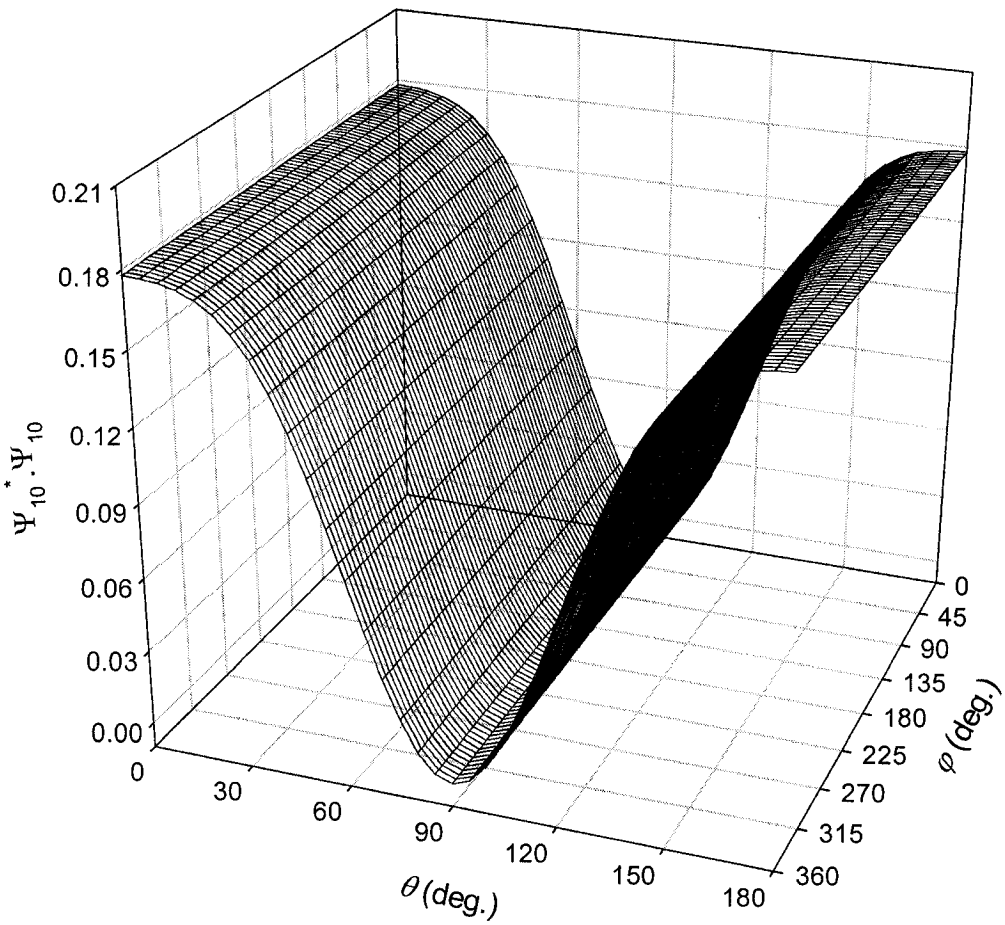

FIG. 6.17: The angular distribution of a cartwheeling *ortho*-H_2 molecule above a Li^+ site.

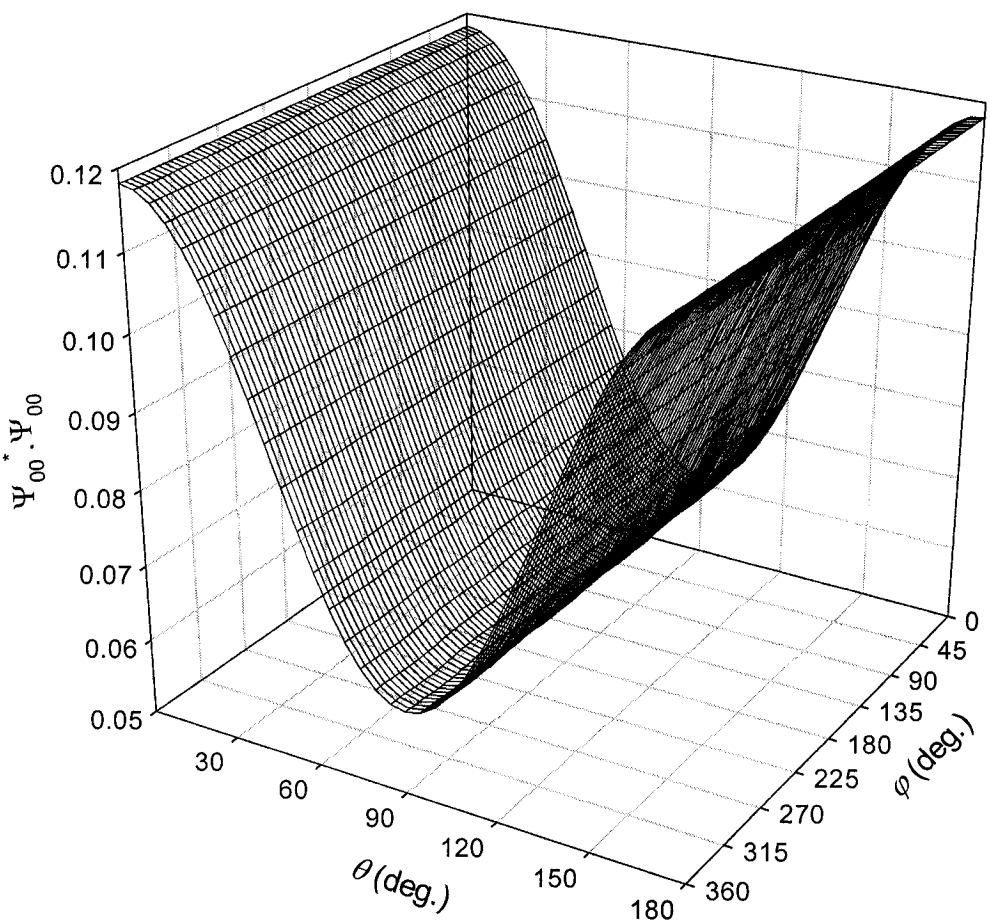

FIG. 6.18: The angular distribution of *para*-H_2 molecule locates over the F^- site.

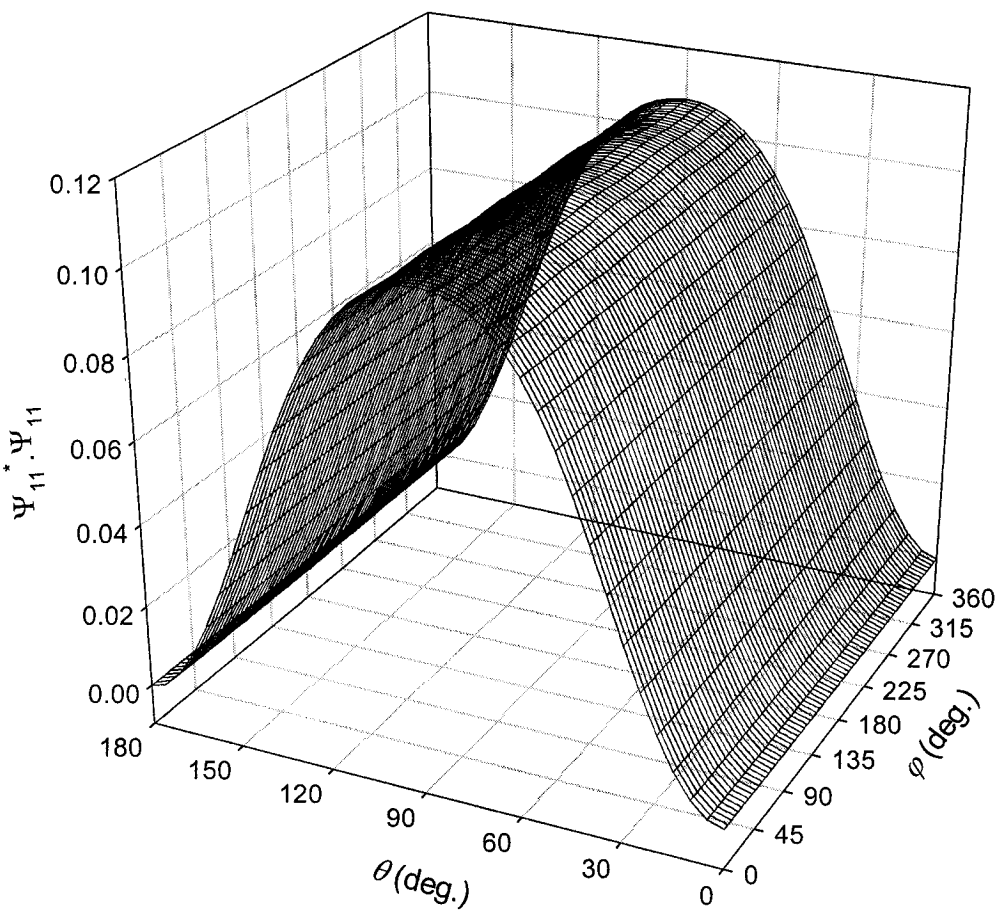

FIG. 6.19: The angular distribution of helicoptering *ortho*-H_2 molecule locates over the F^- site.

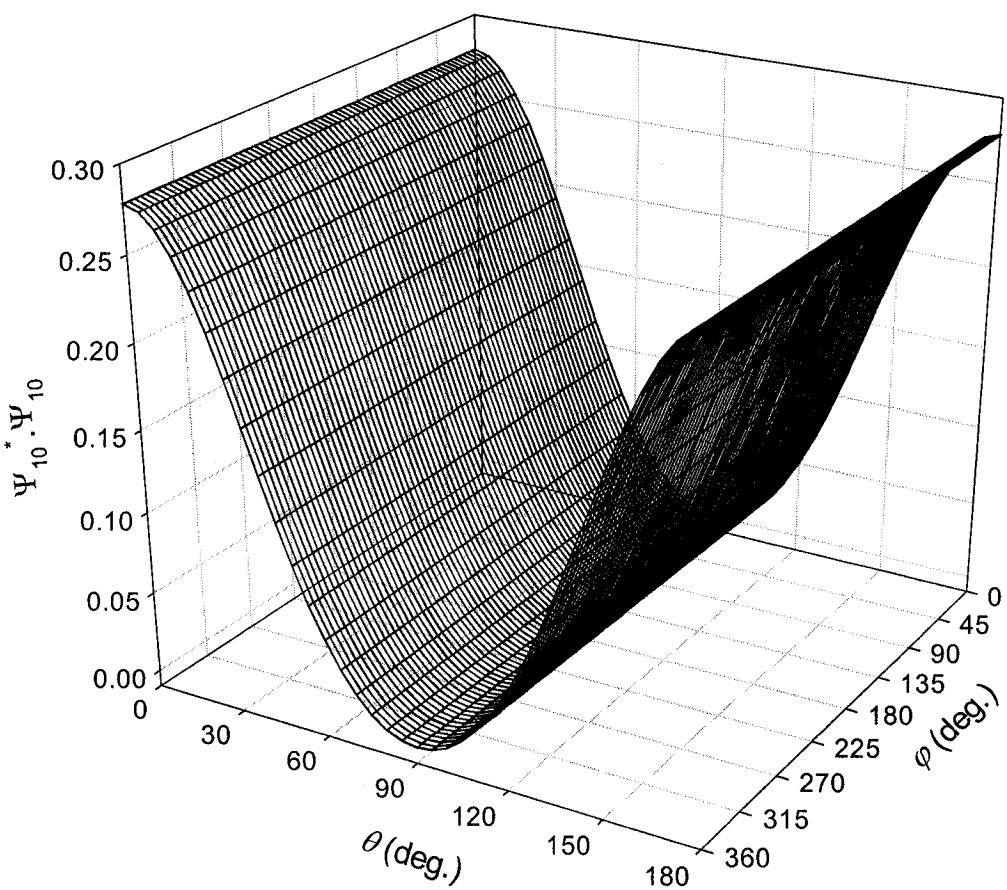

FIG. 6.20: The angular distribution of cartwheeling *ortho*-H_2 molecule locates over the F^- site.

6.2.3. The rotational energies

The energy of the adsorbed hydrogen molecule in its different rotational levels has been calculated using the time-independent PT method through the following formula, (for more details see Chapter 3),

$$E_{Jm} = \frac{J\cdot(J+1)\cdot\hbar^2}{2\cdot I} + A_o + A_2\cdot\left\langle\Theta_J^m\middle|\cos^2\theta\middle|\Theta_J^m\right\rangle + A_3\cdot\left\langle\Theta_J^m\middle|\cos^2(2\cdot\theta)\middle|\Theta_J^m\right\rangle - \frac{I\cdot\left|A_2\cdot\left\langle\Theta_J^m\middle|\cos^2\theta\middle|\Theta_{J+2}^m\right\rangle + A_3\cdot\left\langle\Theta_J^m\middle|\cos^2(2\cdot\theta)\middle|\Theta_{J+2}^m\right\rangle\right|^2}{\hbar^2\cdot(2\cdot J+3)} \qquad (3.16)$$

This formula can be used to calculate the rotational energy level for any values of quantum numbers J, and m over either the Li^+ or F^- sites. The rotational energies of different H_2 species above the cationic and anionic sites have been calculated and are presented in Table 6.3. It is clear that each energy level in adsorbed phase splits onto an ordered sequence of levels. Above a Li^+ site we found that, within a set of splittings, the $|m| = J$ states always have the lowest energy in the set, while the m = 0 state always has the highest energy when $J \neq 0$. These observations indicate that the $|m| = J$ states will adsorb preferentially on the Li^+ site (as well as the *para* J = 0 state) compared with the $J \neq 0$, m = 0 states. This situation is completely reversed over the F^- site, where each energy level splits also into an ordered sequence of levels. The lowest energy is always

the m = 0 states, while the $|m|$ = J states always have the highest energy in the set. Consequently, the m = 0 states are energetically more favoured than the $|m|$ = J states for adsorption over the anionic site. The reversal of the ordering of the energy levels for H_2 species adsorbed over different surface ions may be understood in terms of the interaction between the surface electric field and the charge distribution of the H_2 molecule. In the case of the *ortho*-states, where the charge distribution is anisotropic and a permanent molecular quadrupole moment exists, the energy will be sensitive to the sign of the electric field (and its divergence) at the cationic and anionic sites.

Due to the nature of the physical adsorption, in which the H_2 molecule has a small binding energy with LiF surface (-0.702 kcal/mol), the binding energy of each rotational state of H_2 molecule can be calculated as the difference in the rotational energy between the gas and adsorbed phases as presented in Table 6.4. Above the Li^+ cationic site, it was found that the binding energy increases in the order cartwheeling *ortho*-H_2 < *para*-H_2 < helicoptering *ortho*-H_2 whereas above the F^- anionic site, the binding energy behavior is completely reversed where it increases in the order helicoptering *ortho*-H_2 < *para*-H_2 < cartwheeling *ortho*-H_2. In order to understand those trends, it is necessary bring to mind that helicoptering state prefers the parallel site where the H_2 locates flat whereas the cartwheeling state prefers the perpendicular site where H_2 molecular axis parallels the surface normal. This orientation dependant of interaction creates large differences in electrostatic forces between H_2 and the ions of the surface

and leads to the above trends. Our calculations show that the *ortho*-H_2 state is more strongly bound to the surface than the *para*-H_2 state, which is in consistent with previous theoretical calculations of the adsorption potential of molecular H_2 with LiF surface [44].

Table 6.3: Rotational energies of different H_2 states over the ions of LiF surface using time-independent PT to the second order correction. The units are in kcal/mol.

Rotational state (J, m)	above Li^+ site	above F^- site
	E_{Jm} (kcal/mol)	E_{Jm} (kcal/mol)
(0,0)	-0.525	-0.289
(2,0)	0.642	0.715
(2,±1)	0.604	0.721
(2,±2)	0.437	0.843
(4,0)	3.084	3.16
(4,±1)	3.072	3.165
(4,±2)	3.035	3.183
(4,±3)	2.965	3.226
(4,±4)	2.853	3.313
(1,0)	-0.0074	-0.031
(1,±1)	-0.233	0.117
(3,0)	1.688	1.762
(3,±1)	1.668	1.769
(3,±2)	1.601	1.804
(3,±3)	1.467	1.906

Table 6.4: The binding energy of the H_2 species adsorbed over LiF(001) surface using a time-independent Perturbation theory method.

Adsorption site	Binding energy (kcal/mol)		
	para-H_2 (J = 0, m = 0)	Helicoptering *ortho*-H_2 (J =1, m = ±1)	Cartwheeling *ortho*-H_2 (J = 1, m = 0)
Li^+	-0.5245	-0.5822	-0.3567
F^-	-0.2888	-0.2321	-0.3801

6.3. Relation between Simulations and Calculations

Regardless of the rotational state of the adsorbed H_2 molecule, perturbation theory calculations have shown that the quantum effects will azimuthally delocalize the orientation of the molecular axis of H_2 with a residual amount of anisotropy that reflects the four-fold symmetry of the underlying surface potential. Therefore, molecules that reside in the plane of the layer with preferred but unequal azimuthal orientations, as obtained from the Monte Carlo simulations, will be orientationally delocalized and hence indistinguishable from site to site. This can be applied for the molecules lie at the vortices and the center of the *p*-type unit cell. Therefore, the *p*-type structures are indeed *c*-type structures and

the Monte Carlo simulation results are thus consistent with the experimental observation of a sequence of *c*-type structures.

It is worthwhile to mention here that PT calculations do not include the influence of the molecule-molecule interactions since these kinds of interactions are found to be relatively very weak (around 0.5 meV) and hence does not affect the PT calculation results. For $c(2\times2)$ structure, the neighbouring molecule positions will create additional four-fold symmetric anisotropy that leaves the molecules azimuthally delocalized and hence orientationally indistinguishable. In the (4×2) structure the molecules at the vertices and the center of the unit cell will see the same kind of hexagonal local environment, which create an additional six-fold symmetric anisotropy that leaves the molecules azimuthally delocalized. Thus, the inclusion of molecular interactions will not destroy the symmetry required by the *c*-type structures.

CHAPTER 7: RESULTS FOR H_2 MONO- and MULTI-LAYERS ON NaCl(001)

The structures of the mono- and bi-layers of H_2 molecules physisorbed on the (001) face of a NaCl surface have been studied using the Metropolis Monte Carlo simulations and are reported in this chapter. As before, the surface was constructed as an array of closed shell ions of periodic arrangement in the *x-y* plane and regular in the *z* direction. The H_2 molecule was described as two point dipoles, located on the hydrogen atoms, interact individually with the ions of the surface as well as with the atomic point dipoles of other H_2 molecules. It is worthwhile to mention here that our simulations are performed using classical statistics, which may seem at odds with the quantum nature of the H_2 molecules, but it is considerably simpler than attempting to perform a full blown quantum mechanical treatment on a many-particle system at finite (non-zero) temperatures. The Monte Carlo results are then used as the starting point for estimating how quantum mechanics will affect the adsorbate structures. In particular, the rotational motion of the H_2 molecule in the presence of the surface electric field has been fully studied using time-independent Perturbation Theory (PT). In the following sections, the results of the MC simulations as well as the PT theoretical calculations are reported in detail.

7.1. Simulation Results: H_2/NaCl(001)

7.1.1. Single molecule adsorbed on NaCl(001)

The adsorption of a single hydrogen molecule on the (001) face of the NaCl surface was examined using Monte Carlo simulation methods. The surface interaction potential and the parameters of the atom-ion pair interactions are presented in chapter 4. The simulations were run for 20 kcycles at T=1 K, in which the molecule is allowed to vary its position and orientation freely. On average it is found that the molecule prefers to sit flat (θ =90°) on the top of the Na^+ site at a height of 2.8 Å *i.e.*, the distance from the H_2 bond center to the ion directly below. Gaussian-like distributions were obtained for the angular orientations of the molecule, where the polar and azimuthal angles have symmetric peaks at θ =90°, and φ =45° respectively.

For the flat configuration, the molecular axis of H_2 was found to be directed towards the closest neighbouring Cl^- anionic sites (φ = ±45°), with a binding energy of –0.866 kcal/mol. This binding energy was found to be in good agreement with the experimental values of –0.812 ± 0.2 kcal/mol [37,38] and –0.922 ± 0.12 kcal/mol [40]. The zero point energy of the external vibration of the molecule with respect to the surface was estimated to be 0.1771 kcal/mol (7.68 meV). This was done by fitting the surface potential to a harmonic oscillator plus anharmonic terms and then employing perturbation theory. This then yields a binding energy of -0.69 kcal/mol, which matches the estimate value of Vidali [30,

31] but lies at the lower end of the experimental range of values (-0.646 to -1.038 kcal/mol).

The MC simulations result shows that a single H_2 molecule prefers to sit on the cationic Na^+ site is consistent with previous MD calculations [38]. Consequently, our model seems to reasonably describe the interaction potential of the hydrogen molecules with the NaCl(001) surface.

7.1.2. H_2 adlayers: *c*(2×2) structure

As mentioned earlier in the introduction, the physical adsorption of H_2 layers on NaCl(001) surface has been extensively studied experimentally using different techniques [37, 39, and 40]. They proposed that the adsorbed hydrogen molecules form an interesting commensurate structure of (1×1) unit cell symmetry. However, these experimental works are quite different in terms of layer coverage and adsorption site preference of the various H_2 species.

The proposed (1×1) commensurate structure, where the hydrogen molecules occupy cationic sites and are orientationally symmetric, and other possible configurations have been examined using the MC simulations. In our model a patch of surface consisting of 144 Na^+ ions was used, and the number of H_2 molecules was set to be 144. These simulations were run for 60 kcycles, with the results of the first 10 kcycles discarded at T=1 K. In spite of the

difference in the initial configurations used, a unique final structure was obtained where all the molecules adsorb over the cationic Na^+ sites, with a unit cell of $c(2\times2)$ symmetry. The $c(2\times2)$ configuration consists of four molecules per unit cell where each H_2 molecule locates flat over the surface and its axis oriented towards the bond center of the nearest neighbouring hydrogen molecules. This situation maximizes the quadrupole-quadrupole inter-molecules interaction, *i.e.* every pair of nearest neighbour molecules forms a "T" configuration in the layer plane as shown in Fig. 7.1.

The thermal stability of the $c(2\times2)$ structure has also been tested by studying its molecular positions and orientations at various temperatures (1—21 K) using the Metropolis MC simulations. The θ distributions as shown in Fig. 7.2, have one symmetric peak at θ =90° for all the temperatures tested (1—21 K) which suggests the existence of one kind of adsorption site. The peak at θ =90° shows that all the molecules prefer to lie flat in the plane parallel to the surface. As the temperature increases, the peak decreases in height and broadens in width. The φ distributions as presented in Fig. 7.3, show that at T= 1 K, there are two sharp peaks centered at φ =0°, and 90°. The relative peak sizes are equivalent in height and width, due to molecules adopting each orientation equally (see Fig. 7.3). These peaks still exist up to 11 K even they have been thermally broadened. At T ≥ 16 K, the $c(2\times2)$ symmetry no longer exists since these molecules are azimuthally freely rotating as shown in Fig. 7.3, while the molecules still lie flat above the cationic sites, and hence form a unit cell of (1×1)

symmetry. The angular distributions indicate that the $c(2\times2)$ layer persists up to 11 K after which the symmetry changes to (1×1).

The height distributions of the center of mass of H_2 molecules, as shown in Fig. 7.4, also predict the existence of one type of adsorption site. The molecular centre of mass sits at a height of 2.8 Å at T=1 K, and shift up to 2.92 Å at 26 K. At T=21 K, the molecules start to migrate from their adsorption sites, *i.e.* they are no longer localized at the cationic sites, causing disorder in the surface layer. At T=26 K, H_2 molecules would desorb completely from the surface.

The binding energy per molecule of the $c(2\times2)$ monolayer was also calculated and found to be –0.958 kcal/mol at T=1 K. This binding energy consists of a molecule-surface contribution of -0.849 kcal/mol and a small contribution of –0.11 kcal/mol comes from molecule-molecule interaction. Therefore, the overall binding energy per molecule is slightly stronger than that of a single isolated molecule due to intermolecule interactions, which provide extra energy to stabilize the $c(2\times2)$ adlayer. As the temperature increases, the molecular binding energy drops down to –0.868 kcal/mol at T=16 K as presented in Table 7.1. At $T \geq 16$ K, the molecules migrate from their adsorption site which causes disorder within the layer and some molecules desorb from the layer plane. This is consistent with Traeger and Toennies observation that hydrogen molecules start desorbing around 18 K [40].

Table 7.1: Break down of the adsorption energy of the hydrogen molecule in a c(2×2) adlayer on NaCl(001) at different temperatures.

	E (1 K) (kcal/mol)	E (6 K) (kcal/mol)	E (11 K) (kcal/mol)	E (16 K) (kcal/mol)
H_2-H_2 (Dispersion-repulsion)	-0.0752	-0.0743	-0.0731	-0.0718
H_2-H_2 (Electrostatic)	-0.0343	-0.0265	-0.0158	-0.0058
H_2-NaCl (Dispersion-repulsion)	-0.0896	-0.0885	-0.0873	-0.0859
H_2-NaCl (Electrostatic)	-0.7589	-0.7428	-0.7253	-.7048
H_2-H_2 total energy	-0.1095	-0.1008	-0.0889	-0.0776
H_2-NaCl total energy	-0.8485	-0.8313	-0.8126	-0.7907
Total Energy	-0.958	-0.9321	-0.9015	-0.8683

Based on the results of their FTIR-ATR experiments, Ewing's group [37], proposed that the H_2 molecules are adsorbed and distributed over both the Na^+ and Cl^- sites, whereas Heidberg's group, using the same technique [39] and Toennies' group, using HAS technique [40], conclude that only one type of adsorption site is present and propose that the H_2 molecules adsorb only over the Na^+ sites. However, the fact that the experiments were performed at different temperatures may be responsible for that discrepancy in their conclusions. Our MC simulations results seem to be consistent with Heidberg's and Toennies' findings, but at the same time we still need to study the Ewing's model further by adding more H_2 molecules and see where these molecules are likely to adsorb.

In the following section, the results of the MC simulations of the second layer are reported in detail.

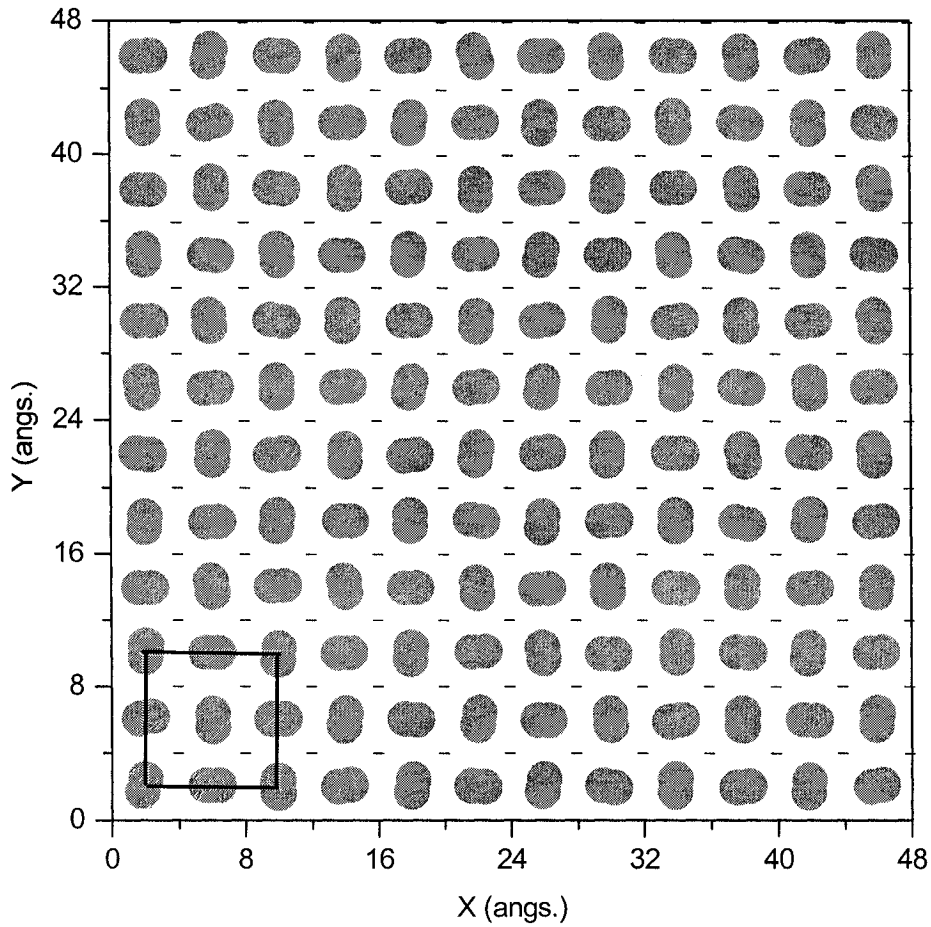

FIG. 7.1: The NaCl(001) surface covered with 144 H_2 molecules at 1 K. The (+) symbol represents a Na^+ ion and the (-) symbol represents a Cl^- ion. The hydrogen atoms are shown as gray circles and are occupied all the cationic Na^+ sites. The $c(2\times2)$ unit cell is shown in solid lines.

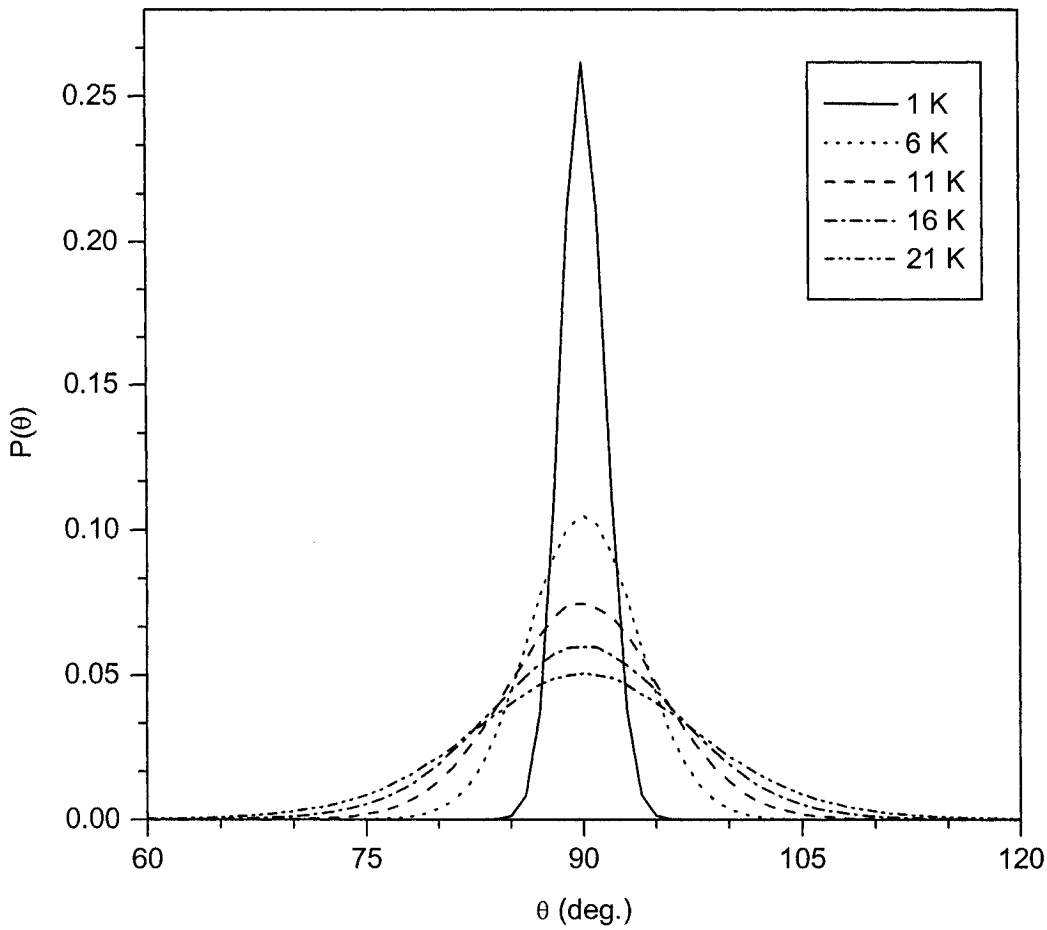

FIG. 7.2: The polar angle distribution of the $c(2\times2)$ layer is plotted for temperatures T=1, 6, 11, 16, and 21 K.

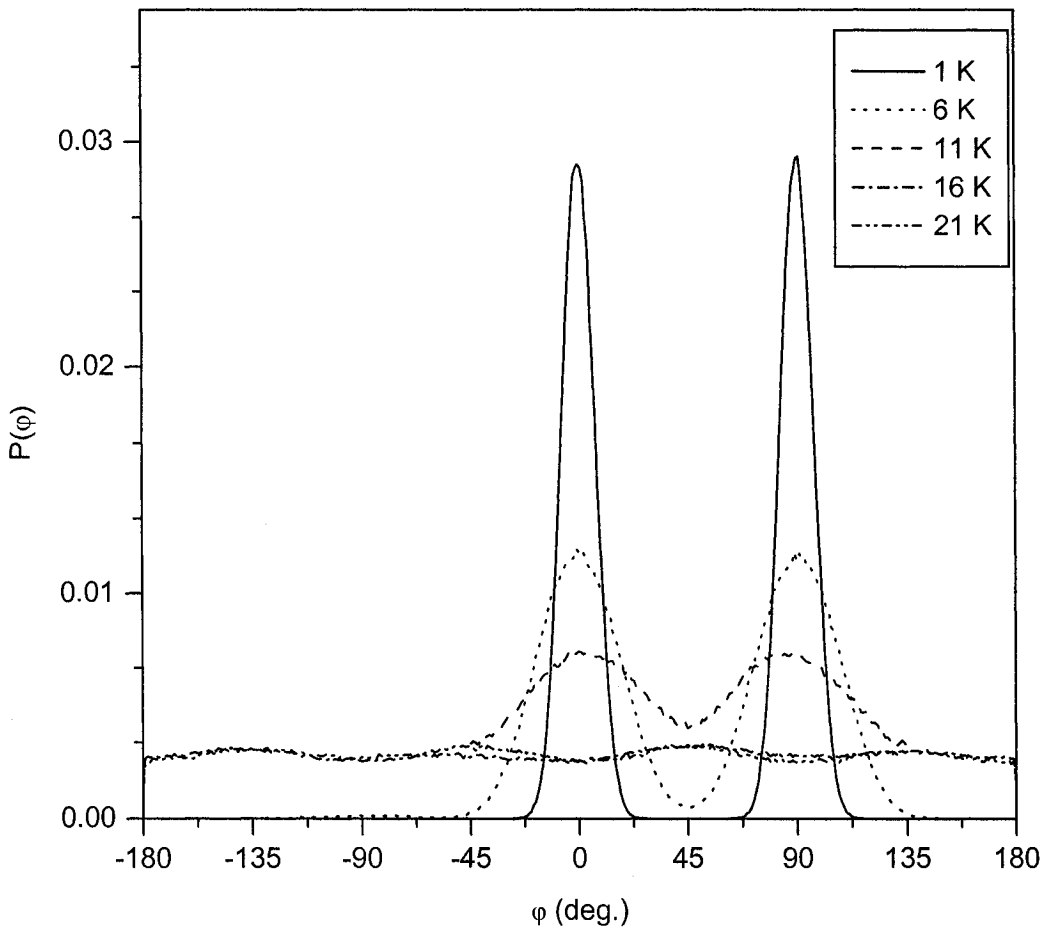

FIG. 7.3: The azimuthal angle (φ) distributions of the $p(2\times2)$ phase plotted for temperatures T=1, 6, 11, 16, and 21 K.

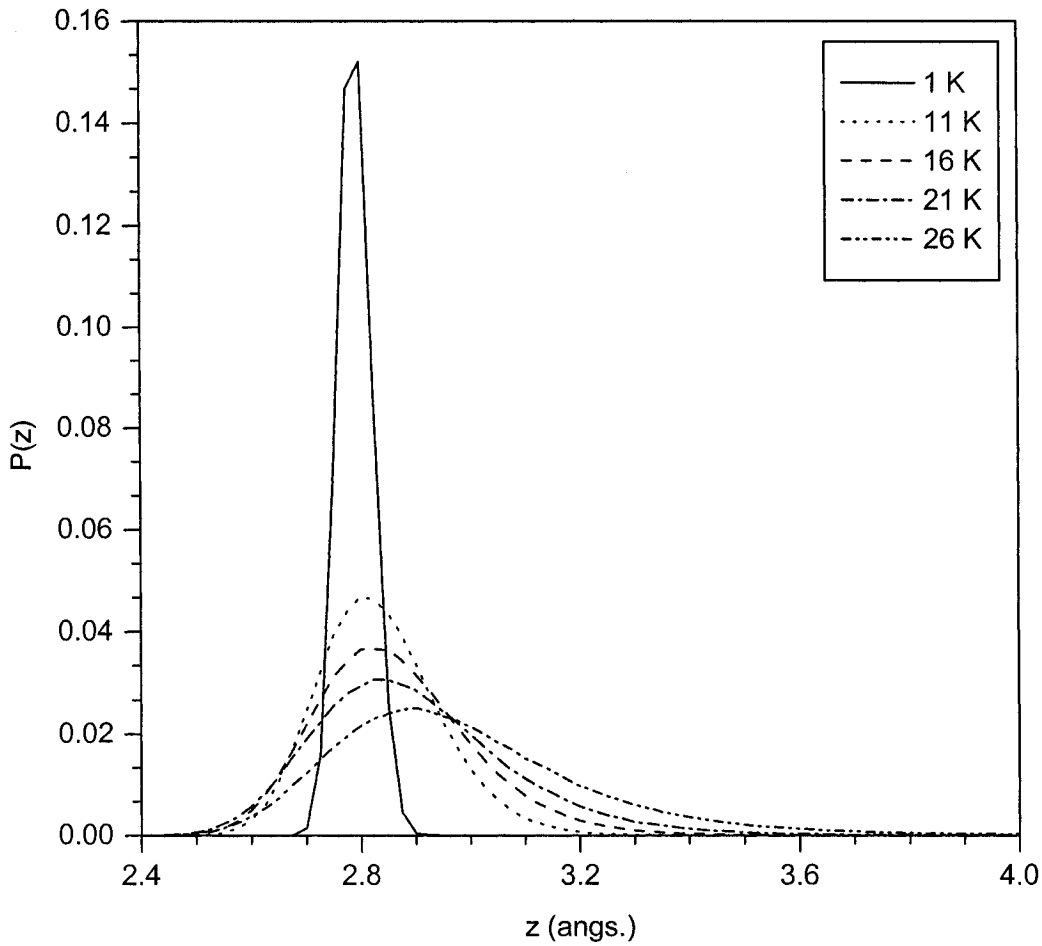

FIG. 7.4: The height (z) distribution of the H_2 molecules center of mass for the $c(2\times2)$ layer plotted for temperatures T=1, 11, 16, 21 and 26 K.

7.1.3. A single molecule adsorbed over the *c*(2×2) H_2 adlayer

In order to examine the presence of another adsorption site, a single molecule was placed arbitrarily over the *c*(2×2) ad-layer of H_2 molecules on NaCl(001). This initial configuration was tested using the Metropolis MC simulations, where all the molecules are allowed to vary their positions as well as orientations randomly. These simulations were run for 60 kcycles with the results of the first 10 kcycles discarded at T=1 K. On average, it is found that the bottom layer still has the same structure as shown in Fig. 7.5; and a single molecule locates over the anionic Cl^- site at a higher height of Z_{cm} = 4.6 Å (the distance from the center of mass to the ion below directly), but tilts away from the surface normal. In terms of angular distributions, a bell shaped peak was obtained for polar and azimuthal angles at $\theta \sim 23^\circ$ and $\varphi \sim 5^\circ$ respectively. The molecule is weakly bound to the surface with an energy of –0.315 kcal/mol. This binding energy is a third of the value for molecules adsorbed on the sodium sites and so it is expected that a molecule adsorbed on a chlorine site will desorb at a lower temperature than that a molecule in the *c*(2×2) monolayer. Thus, Ewing's proposed structure may indeed only be observable the lower temperature (T=5.2 K) at which his experiments were conducted.

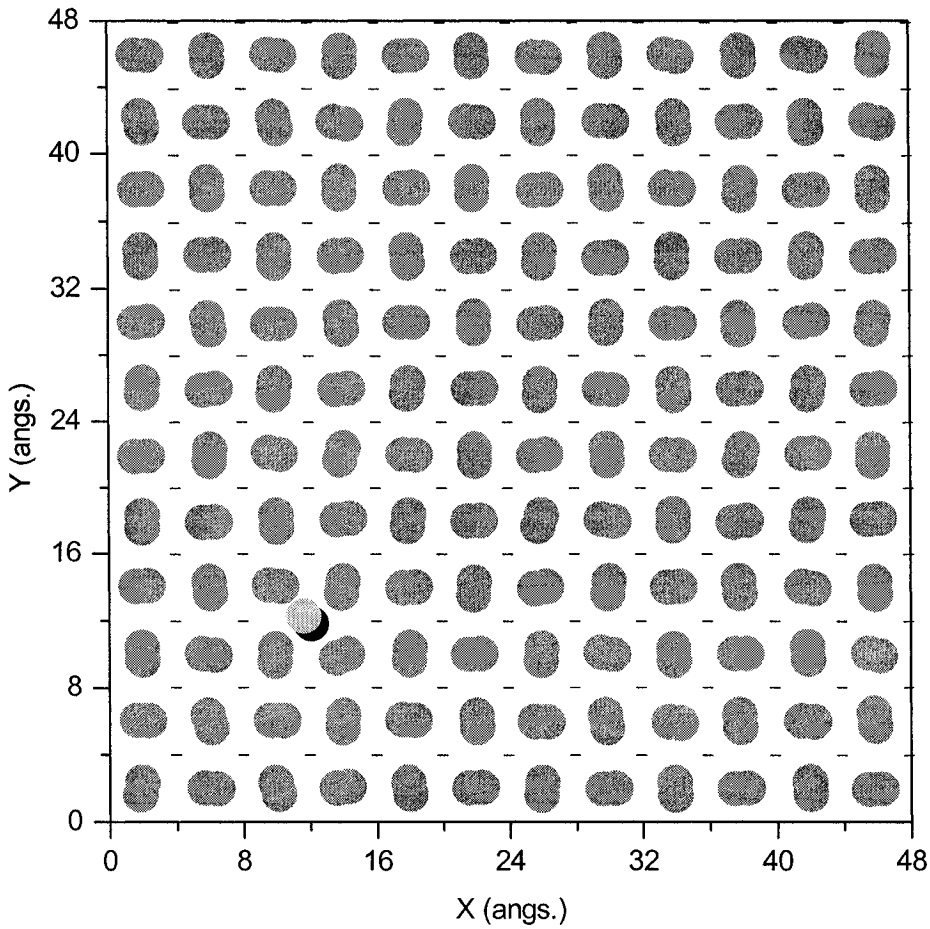

FIG.7.5: The NaCl(001) surface covered with 145 H_2 molecules at T=1 K. The hydrogen atoms are shown as gray circles and sit flat over the cationic Na^+ sites, whereas the tilted H_2 molecule locates over the anionic Cl^- site (-) is shown as solid black circle for the lower H atom and light gray circle for the upper H atom.

7.1.4. Bi-layer system of H_2/NaCl(001)

In order to study the structures of multilayer of the hydrogen molecules on NaCl(001) surface and resolve the discrepancies in the experimental findings, a bi-layer system was constructed with an initial structure in which the bottom layer has the *c*(2×2) symmetry, as described in section 7.1.2, and the upper layer has H_2 molecules located on top of each of the Cl^- sites. This structure but with many different starting orientations was tested on a 10×10 patch of surface (100 Na^+ sites and an equivalent number of Cl^- sites). These simulations were run for 100 kcycles at T=1 K with the results of the first 10 kcycles discarded. Regardless of the initial configuration chosen, the simulations all evolved to a single final configuration for both layers. In the bottom layer, MC simulation results show that the H_2 molecules sit flat (θ=90°) on the top of the Na^+ sites in a unit cell of *p*(2×1) type symmetry (see Fig. 7.6) with two possible azimuthal orientations. Next nearest neighbour molecules along diagonals adopt a tee configuration while molecules along a row have the same orientation. The orientation of molecules alternates across rows with an approximate difference of 90° between their azimuthal angles.

In the upper layer, the H_2 molecules were found to be sit tilted (θ=45°) at the top of Cl^- sites with two molecules in a unit cell of *p*(2×1) symmetry as shown in Fig. 7.6. Along a row the azimuthal orientation is the same with the orientation alternating by 180° from row to row. It is clear that the cationic and anionic sites

are entirely occupied by H_2 molecules in the bi-layer system, and the existence of the two kinds of the adsorption sites is obtained, which is in agreement with Ewing's proposed structure [37].

The thermal stability of the bi-layer system has been examined using the Metropolis MC simulations and may be determined by examining the structural details of the individual layers. The θ distribution, as shown in Fig. 7.7, indicates that at T=1 K, there are two peaks centered at θ = 45°, 90° and are associated with the molecules of the upper and bottom layers respectively. Upon increasing the temperature the upper layer peak at θ=45° is broadened but still exist up to 5 K. At T > 5 K, this peak has no longer existing and exhibits a flat distribution; the H_2 molecules in the upper layer are freely rotating and the symmetry of the top layer becomes (1×1). The peak at θ = 90°, which corresponds to the lower layer, is also thermally broadened but still persists up to 12 K as shown in Fig. 7.7.

The φ distribution of the bottom layer is shown in Fig. 7.8. At T=1 K, there are two peaks centered at φ =40° and 140°. Upon increasing the temperature those peaks are broadened but are still the preferred orientations up to 12 K. At T ≥ 16 K, the distribution becomes flat due to the molecules freely rotating azimuthally on the surface. Consequently, the angular distribution of the bottom layer show that the *p*(2×1) layer persists up to 12 K after which it shows (1×1) symmetry.

The φ distribution of the upper layer shows that at T=1 K, the molecules orientations in xy plane are localized at φ = 2°, and 178° as shown in Fig. 7.9. The two peaks are sharp and symmetric in height and width due to number of H_2 molecules associated with each peak are the same (see Fig. 7.6). Thermally those peaks exist up to 5 K even though they are broadened in width and decrease in height. At T=8 K, the distribution are almost flat as a result of molecules azimuthally rotating freely. The angular distribution shows that the upper layer of the $p(2\times1)$ unit cell symmetry is stable up to 5 K but at T= 8 K, the H_2 molecules of the upper layer are freely rotating.

The height distributions of the center of mass of the molecules have been plotted as a function of temperature as shown in Fig. 7.10. At T=1 K, the peak at 2.75 Å is associated with the molecules adsorbed over the Na^+ sites (the bottom layer), whereas the peak at 4.6 Å corresponds to the molecules located over the Cl^- sites (the upper layer). As the temperature increases, the first peak for the molecules in the bottom layer is shifted upward to 2.92 Å at T=12 K, whereas the second peak, for the molecules in the upper layer, is shifted upward to 4.9 Å at T=12 K. At T $\geq$ 10 K, molecules in the upper layer start to desorb and the layer becomes disordered.

The molecular binding energy was also calculated by energy minimization using the MC procedure. A binding energy of –1.023 kcal/mol was found for the molecules locate in the bottom layer, whereas the molecules in the upper layer

was found to be weakly bound to the surface with a binding energy of –0.389 kcal/mol at T=1 K.

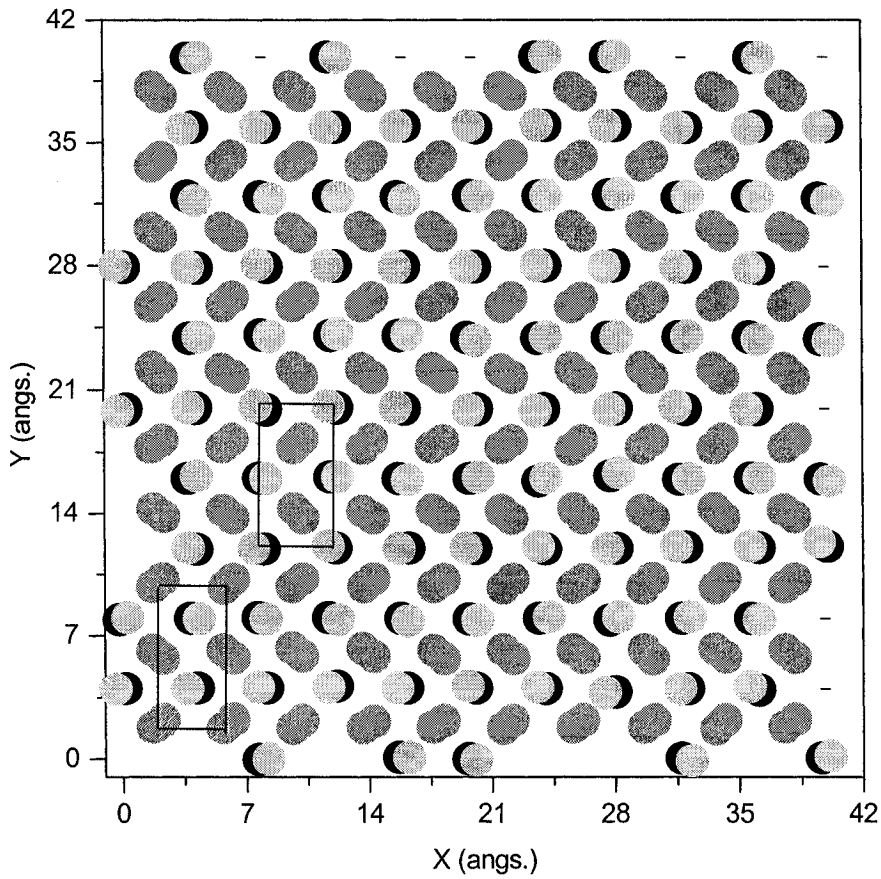

FIG. 7.6: NaCl(001) surface covered with 200 H_2 molecules at T=1 K. The (+) symbol represents a Na^+ ion and the (-) symbol represents a Cl^- ion. The hydrogen atoms of molecules that lie flat over Na^+ sites are shown as gray circles; while for tilted H_2 molecules sit on the top Cl^- sites are as the lower H atoms are represented by solid black circles and the upper H atoms are represented by light gray circles. The $p(2\times1)$ unit cell is shown in solid lines.

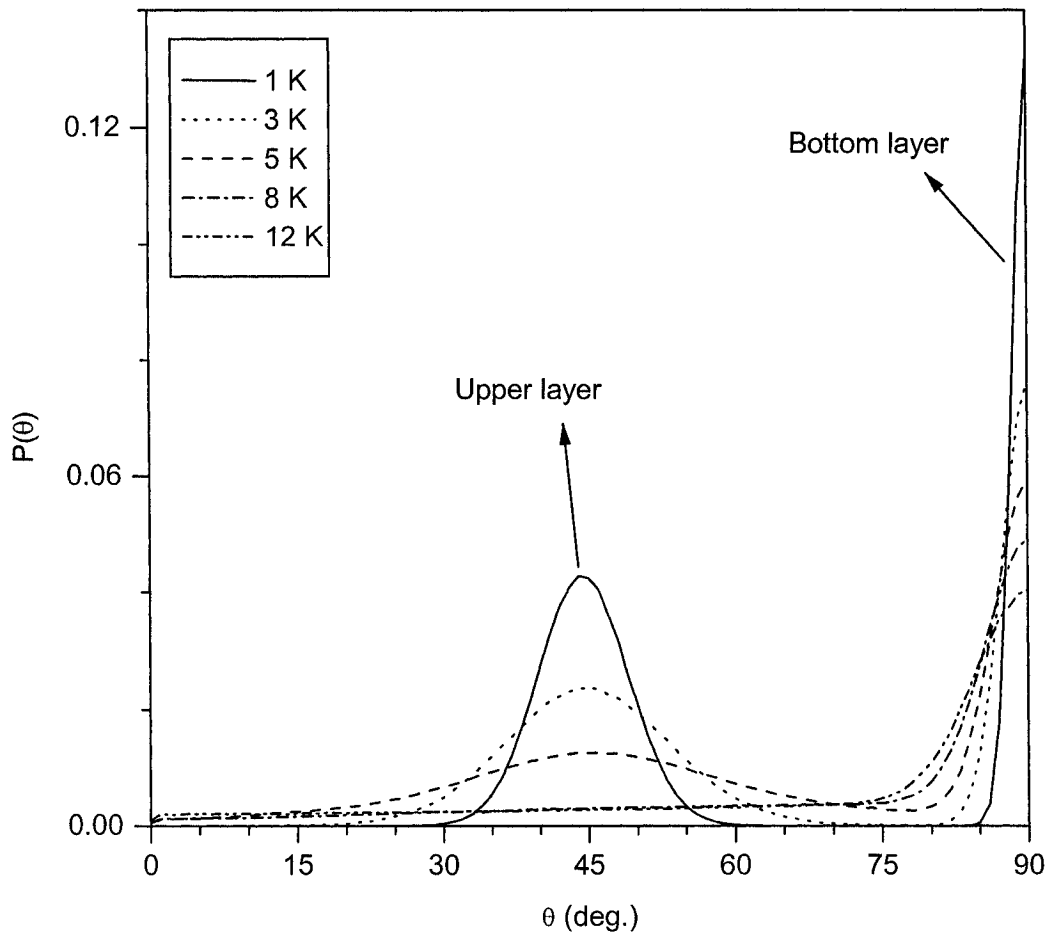

FIG.7.7: The polar angle distributions of $p(2\times1)$ phases of the bi-layer system plotted for temperatures T=1, 3, 5, 8 and 12 K.

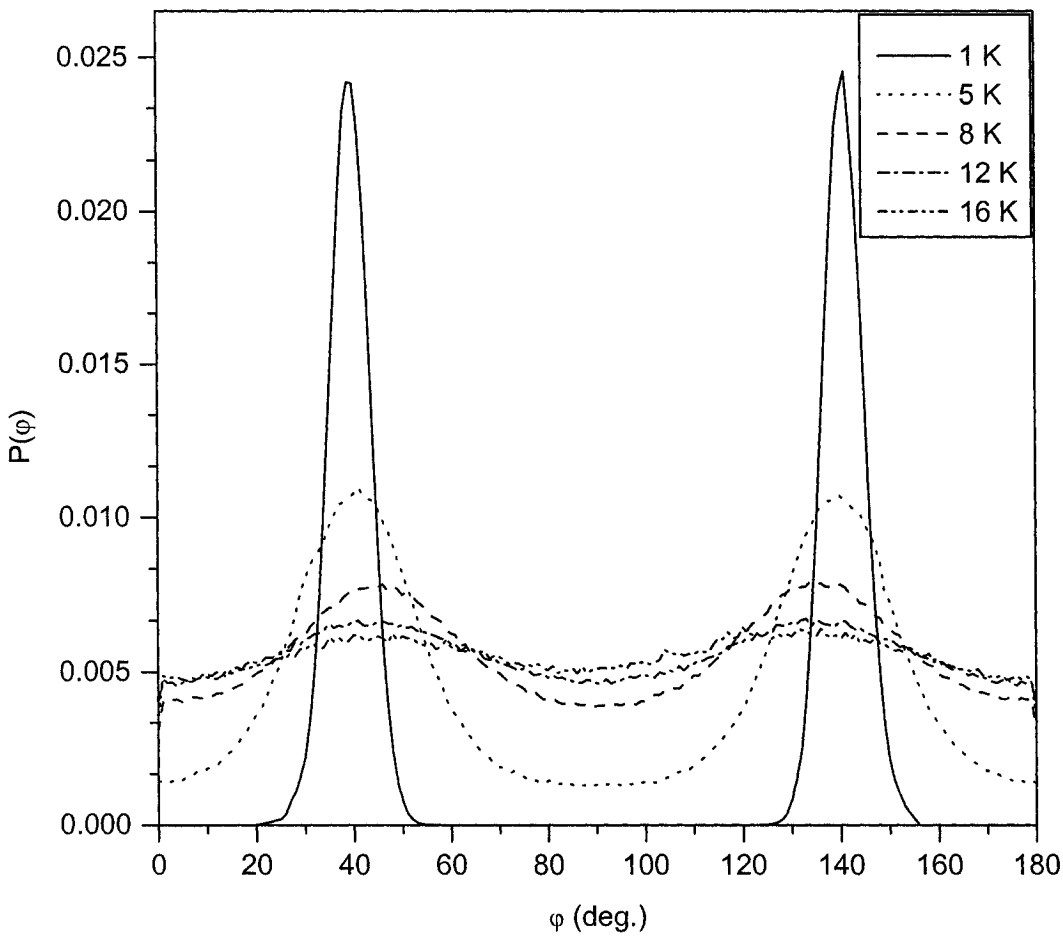

FIG. 7.8: The azimuthal angle (φ) distributions of the $p(2\times1)$ bottom layer plotted for temperatures T=1, 5, 8, 12, and 16 K.

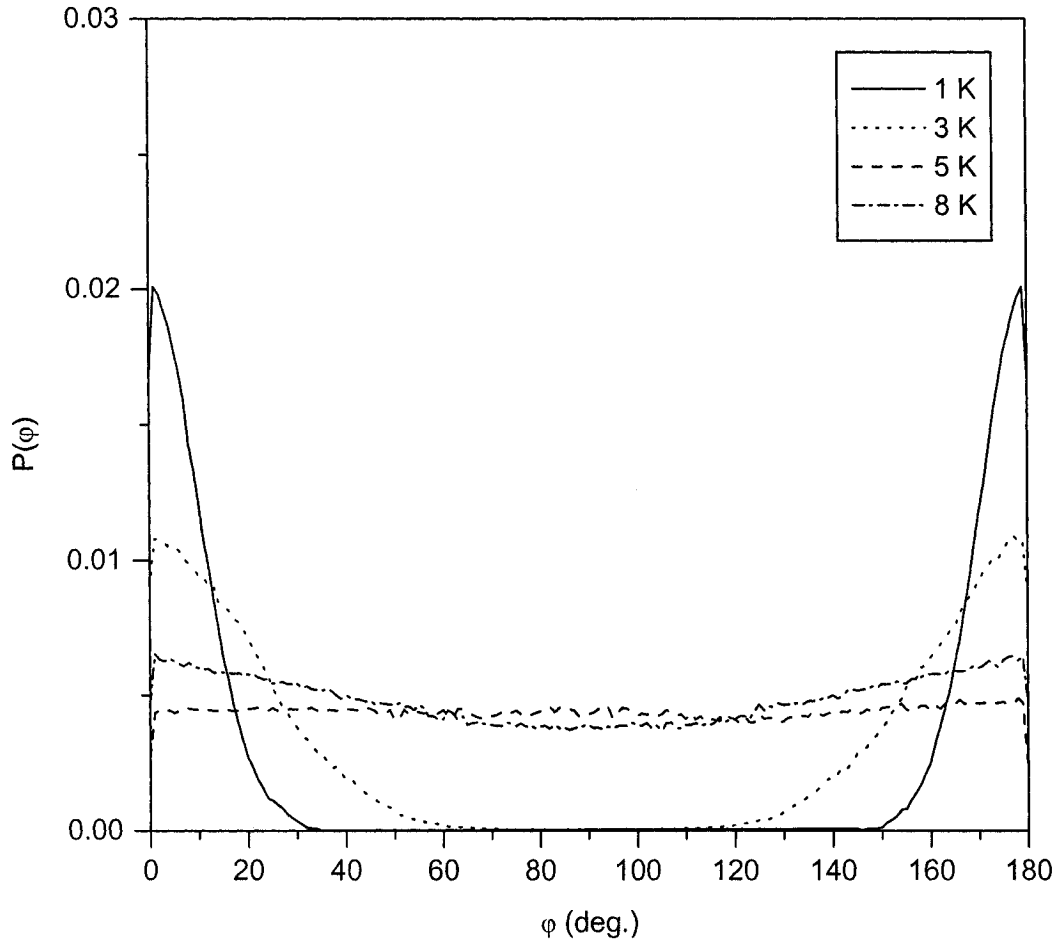

FIG. 7.9: The azimuthal angle (φ) distributions of the $p(2\times1)$ upper layer plotted for temperatures T=1, 3, 5, and 8 K.

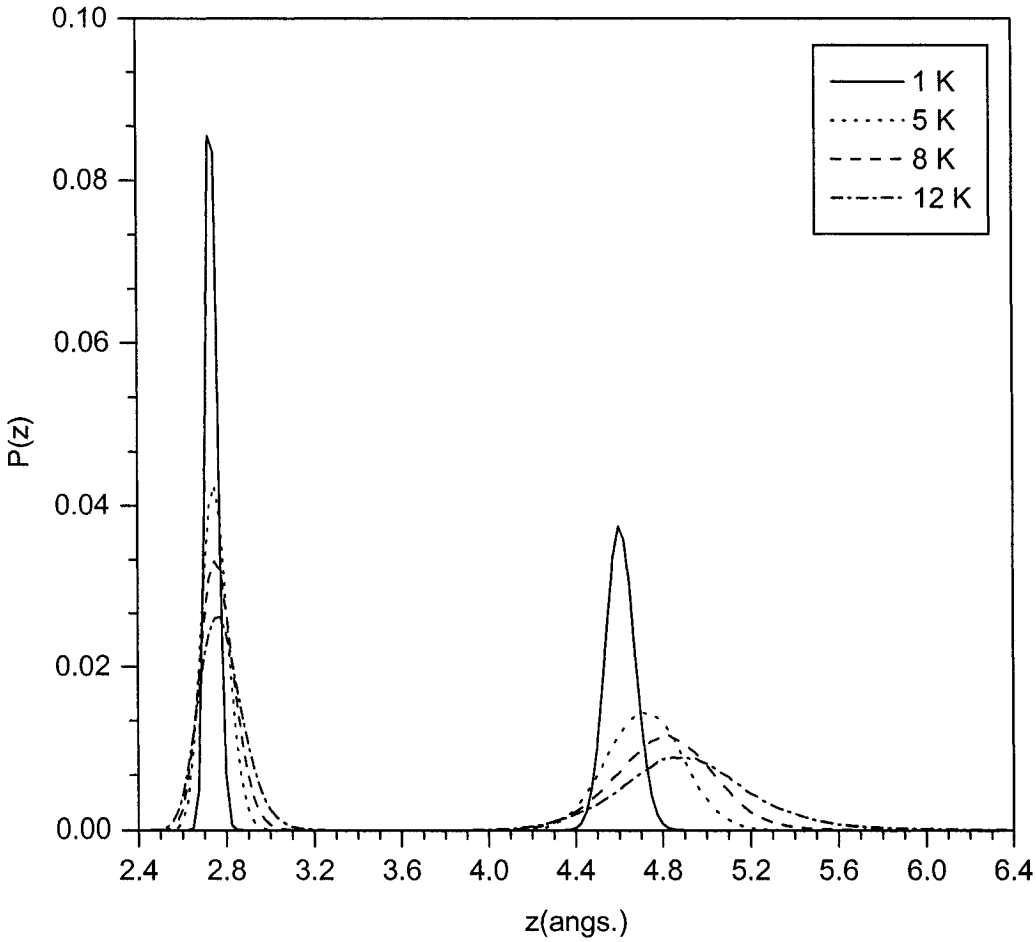

FIG. 7.10: The height (z) distribution of the center of mass of H_2 molecules in the bi-layer system where the peak at 2.75 Å associated with the molecules in the bottom layer, whereas the peak at 4.6 Å represents the molecules in the upper layer.

7.1.5. Summary and discussion of simulations

Our simulation results of the H_2 monolayer as presented in section 7.1.2 match the experiment findings [37, 39 and 40] in terms of coverage and stability but disagree in terms of structure symmetry for temperatures lower than 10 K. This point has been also observed in the bi-layer system since our results do not include the quantum nature of the H_2 molecules in the solid phase. However, in order to reconcile the experimental results, azimuthal quantum delocalization has been examined for H_2 molecules in the $c(2\times2)$ layer, where the molecules are flat and localized at $\varphi = 0^\circ$, and 90°. If these molecules are freely rotating in the layer plane or azimuthally delocalized, then these molecules, from a quantum view point, become symmetric on the surface and form a structure with a unit cell of (1×1) symmetry. In the next sections these possibilities are explored in detail.

The MC simulations results of the bi-layer system as described above show that the ions of the surface are entirely occupied by H_2 molecules and form two layers with a unit cell of $p(2\times1)$ symmetry. The upper layer is rotationally stable up to 5 K and stable with respect to desorption up to 10 K, whereas the bottom layer structure persists up to 12 K. At $T \geq 16$ K, the molecules in the bottom layer still lie flat ($\theta = 90^\circ$), but freely rotate azimuthally, yielding a unit cell with (1×1) symmetry. For the upper layer, the polar and azimuthal distribution almost becomes flat at T= 8 K, due to the molecules rotating freely at the surface. Desorption is seen to occur around 10 K.

Our MC simulation results for the bi-layer system holds a means for resolving the discrepancies between the sets of experimental results. In particular, the MC simulations show that occupation of the Cl^- sites are possible for temperatures below 10 K so that Ewing's claim that these sites are occupied in his experiments, done at T = 5.2 K, is indeed possible. But the simulations also indicate that above 10 K the upper layer of the bilayer system is unstable with respect to desorption, leaving only the bottom layer, which is stable. This scenario is consistent with the observations of the Heidberg and Toennies groups where only the bottom layer is observed in their experimental temperature range of 10 – 12 K. It is therefore possible for both sets of experimental findings to be correct and non-contradictory. The simulations differ from experiment in the assignment of the unit cell symmetry. At higher temperatures, azimuthal delocalization occurs in the simulation yielding a (1×1) symmetry in agreement with the experiments. But at temperatures lower than 8 K the bilayer structure is predicted to have a $p(2\times1)$ structure.

To resolve this discrepancy in symmetry and test other available theoretical calculations [38], the rotational motion of a single H_2 molecule in the presence of the surface electric field has been studied using perturbation theory. If it can be shown that rotational delocalization is always present, then only the (1×1) structure will be observed. Such a study will also address the plausibility of H_2 adsorption in the *para* and *ortho* states over the different ions of the surface.

These theoretical calculations in three dimensions are reported in the next sections.

7.2. Rotational State Calculations

In our calculations, the energies and wave functions of the H_2 molecules in different rotational levels are calculated. This has been done by applying time independent perturbation theory to the isotropic rigid rotator model, where the surface electric field is regarded as a perturbation. The procedure for conducting these calculations has been described in detail in chapter 3 and will be used in the next sections.

7.2.1. The rotational potential: one dimension

As mentioned earlier and can also be observed from the unit cell of $c(2\times2)$ symmetry, all H_2 molecules are lie flat over the Na^+ sites, where these molecules are localized, with either φ = 0° or 90° as shown in Fig. 7.3. Compared to the binding energy of the molecules with the surface, the inter-molecular binding energy is very weak (≈ –0.1 kcal/mol) and hence only a small energy barrier for rotations in the plane of the surface is expected. Consequently, quantum mechanical delocalization of the molecular axis within the surface plane seems likely. This would change the symmetry of the unit cell from $c(2\times2)$ to (1×1) and bring the simulations and experiments [37, 39 and 40] into agreement.

To study the rotational state of H_2 molecule in the c(2×2) adlayer, the rotational potential of the H_2 molecule in the center of the unit cell (shown in Fig. 7.1) was calculated in two ways as follows:

In the first kind of rotation (***Case a***), the molecules at the corners and the center of the unit cell (φ = 90°) were rotated counter clockwise, while the remaining molecules (φ = 0°) rotate clockwise, whereas in the second kind (***Case b***), all the molecules are rotated clockwise in the layer plane. Those rotational potentials were found to be periodic and have four-fold symmetry with minima at φ =0°, 90°, 180°, and 270°. This reflects the four-fold azimuthal symmetry of the surface and the rotational symmetry of the homo-nuclear hydrogen molecule as shown in Fig. 7.11. Those rotational potentials were constructed using the procedure described in detail in section 3.1.1 (see chapter 3) and are represented exactly by the following formula; $V(\varphi) = A_o + A_1 \cdot \cos(4 \cdot \varphi)$, where the fitting parameters are listed in Table 7.2.

Table 7.2: Rotational potential fitting parameters in unit of kcal/mol.

Parameter	A_o	A_1
Case a	-0.9582	-2.356×10^{-3}
Case b	-0.9244	-3.615×10^{-2}

7.2.1.1. Wave functions and energy levels

The rotational energy and wave functions of H_2 molecules adsorbed on NaCl(001) surface have been calculated using a time-independent perturbation theory to solve the Schrödinger equation of a rigid H_2 molecule rotating in the layer plane. Before going to more details, it is worthwhile to note that at low temperature (T<20 K), the n=0 and n=1 rotational levels are, practically speaking; the only ones populated according to the equilibrium Boltzmann distribution. We are therefore only interested in calculating the energy for these two levels. By using Eq. (3.5), these energy levels are calculated and listed in Table 7.3.

By comparing these values of the energy levels with the rotational potential curves shown in Fig. 7.11, we found that the n=1 state in both kinds of rotation has an energy greater than the rotational barrier height and can therefore rotate freely (i.e. the azimuthally quantum delocalization is most prevalent for n=1 state). From the classical viewpoint, the H_2 in its ground state (see Fig. 7.11) is azimuthally localized since its rotational energy is less than the rotational barrier height. The question now is whether the H_2 molecule in its ground state can tunnel through the rotational potential curve? In other words, can H_2 in state n=0 have a nonzero probability of being in the classically forbidden region? To answer this question, the probability density $\psi_{n=o}^{2}$ was calculated using Eq. (3.7), and was found to have the following form:

Case a: $$\psi_{n=0} = \frac{1}{\sqrt{2\cdot\pi}}\cdot\left(1+5.538\times10^{-4}\cdot\cos(4\cdot\varphi)+8.884\times10^{-8}\cdot\cos(8\cdot\varphi)\right)$$

Case b: $\psi_{n=0} = \frac{1}{\sqrt{2\cdot\pi}} \cdot \left(1 + 8.613\times10^{-3} \cdot \cos(4\cdot\varphi) + 2.091\times10^{-5} \cdot \cos(8\cdot\varphi)\right)$

The quantum probability density of a rotating H_2 molecule in its ground state, $\psi_o^* \cdot \psi_o$, was plotted as a function of φ and shown in Fig. 7.12. The probability distribution is almost flat with a small four-fold ripples in the probability density. On average, the probability of being out side the classical turning points given by the rotational potential is 0.159 at all angles, which indicates that H_2 in its ground state is azimuthally delocalised. By using Eq. (3.8), a similar probability density was found for the H_2 in state n=1 as shown in Fig. 7.13, where its wave function has the following form:

Case a: $\psi_{n=1} = \frac{e^{i\varphi}}{\sqrt{2\pi}} \begin{pmatrix} 1 + 2.167\times10^{-4} \cdot e^{4i\varphi} + 2.646\times10^{-4} \cdot e^{-4i\varphi} + 2.369\times10^{-8} \cdot e^{8i\varphi} \\ + 1.185\times10^{-7} \cdot e^{-8i\varphi} \end{pmatrix}$

Case b: $\psi_{n=1} = \frac{e^{i\varphi}}{\sqrt{2\pi}} \begin{pmatrix} 1 + 3.351\times10^{-3} \cdot e^{4i\varphi} + 4.293\times10^{-3} \cdot e^{-4i\varphi} + 5.576\times10^{-6} \cdot e^{8i\varphi} \\ + 2.788\times10^{-5} \cdot e^{-8i\varphi} \end{pmatrix}$

Consequently, It is obvious that the hydrogen molecules in the *c*(2×2) adlayer are azimuthally delocalized on surface, which means those molecules are symmetric and arranged in a unit cell of (1×1) symmetry. This results reconcile and agree with the experimental predictions of the H_2 adlayer on NaCl(001).

Table 7.3: Rotational energy levels of a single adsorbed H_2 molecule calculated by using PT second order correction level. The values are in the unit of kcal/mol.

Quantum number	E_n (*case a*)	E_n (*case b*)
n=0	-0.9582	-0.9243
n=1	-0.7836	-0.7497

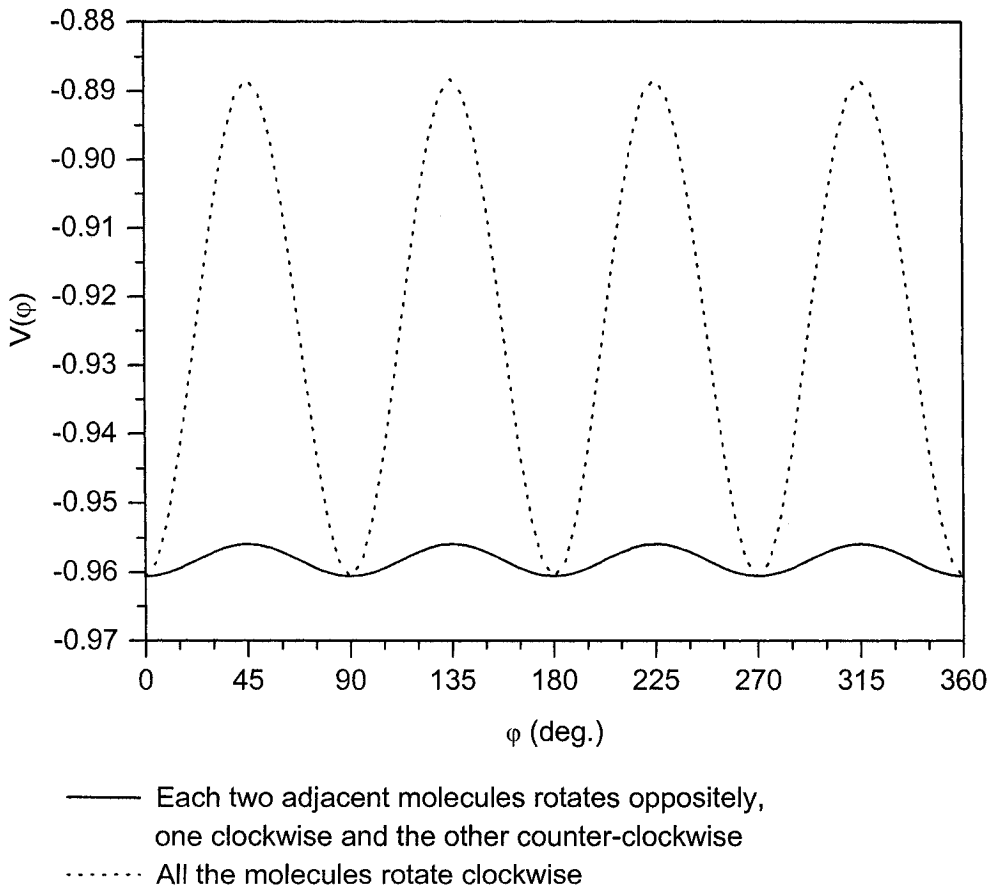

FIG. 7.11: The rotational potential of the H_2 molecule in the $c(2\times2)$ adlayer on NaCl(001).

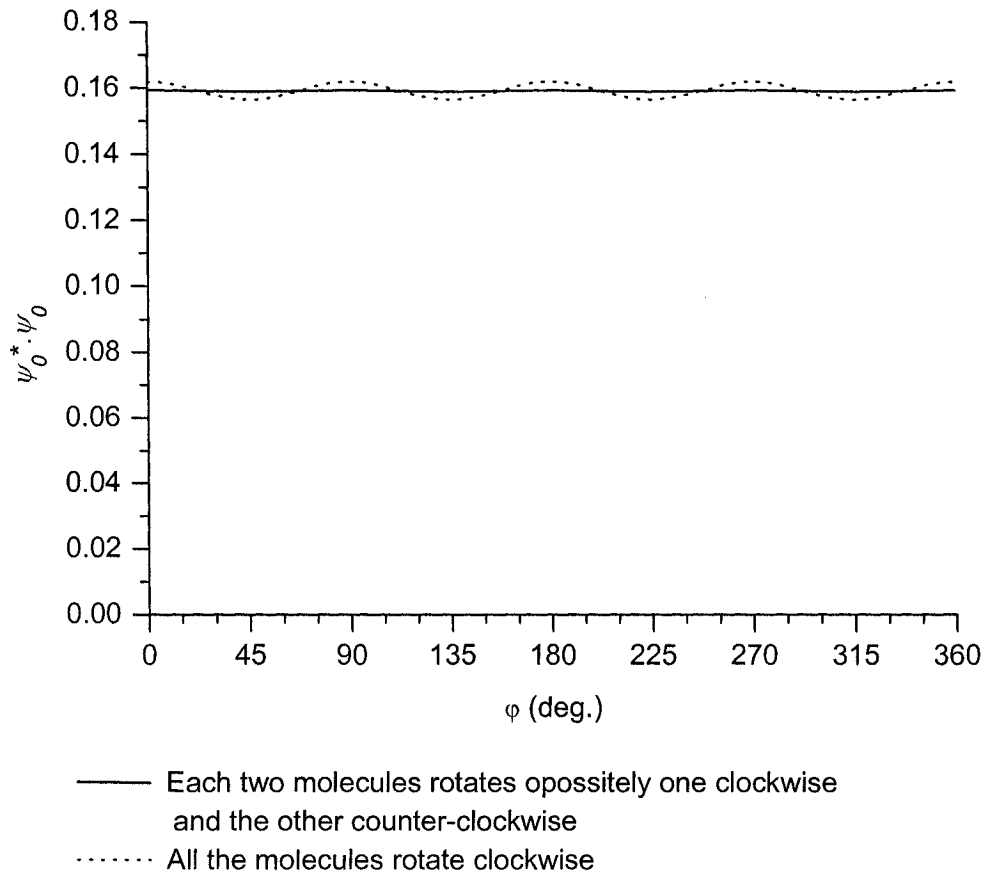

FIG.7.12: The probability density of the azimuthal rotation of H_2 molecule in its ground state (n=0) of the $c(2\times2)$ layer on NaCl(001).

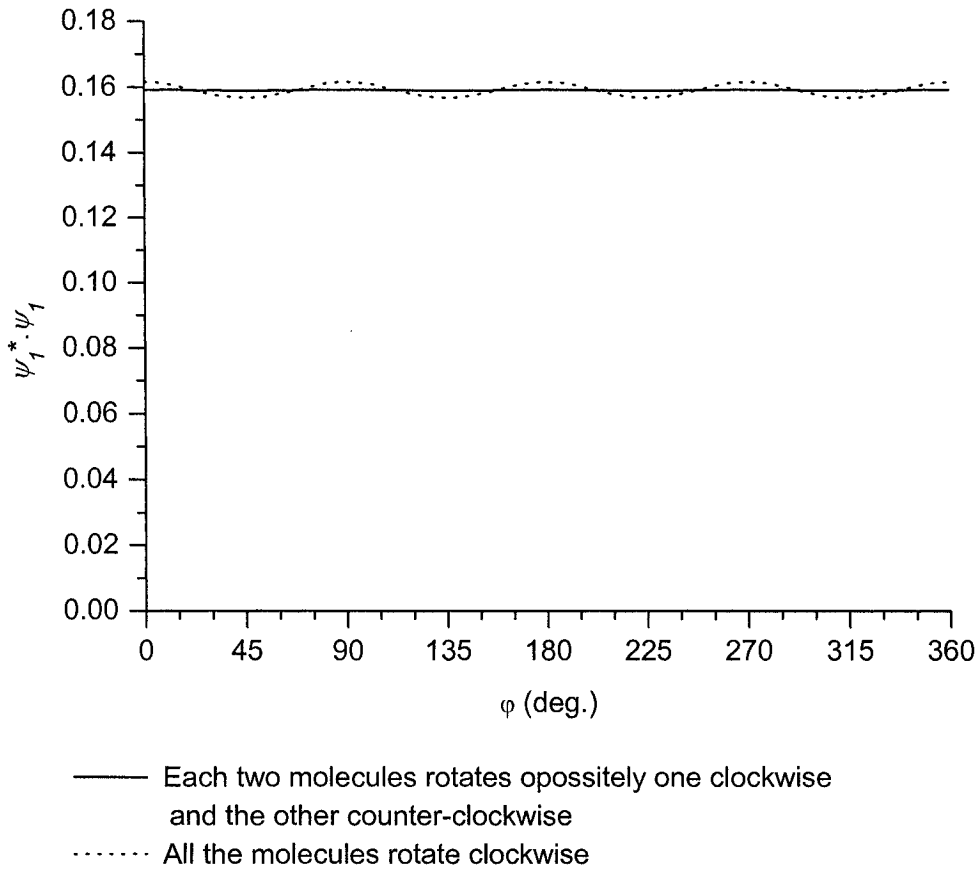

FIG. 7.13: The probability density of the azimuthal rotation of H_2 molecule in its first excited state (n=1) of the *c*(2×2) layer on NaCl(001).

7.2.2. The rotational potential: three dimensions

In order to determine the adsorption site preference of different H_2 species on the ions of NaCl(001) surface, the rotational motion of H_2 molecule in the presence of the surface electric field must fully examined in three dimensions. By applying the procedure that described in details in Chapter 3, the rotational potential for a single H_2 molecule sitting at an equilibrium height of 2.8 Å (3.65 Å) on Na^+ site (Cl^- site), was constructed by varying the angular orientations (θ, and φ) of the molecular axis of H_2 with respect to the surface coordination system as described before. These rotational potential was found to be fit to the following formula:

$$V(\theta,\varphi) = A_o + A_1 \cdot \cos(4\cdot\varphi) + A_2 \cdot \cos^2\theta + A_3 \cdot \cos^2(2\cdot\theta) + A_4 \cdot \cos^2\theta \cdot \cos(4\cdot\varphi) + A_5 \cdot \cos^4\theta \cdot \cos(4\cdot\varphi)$$

Note that the mathematical formula of the rotational potential can be simplified and written in terms of spherical harmonic functions of the following form:

$$V(\theta,\varphi) = A_o^{'} \cdot Y_{00} + A_1^{'} * Y_{20} + A_2^{'} \cdot Y_{40} + A_3^{'} \cdot (Y_{44} + Y_{4-4})$$

where the values of these coefficients are presented in Tables 7.4 and 7.5.

The rotational potential of the hydrogen molecule above Na^+ and Cl^- ions are plotted as a function of θ, and φ as shown in Figs. 7.14 and 7.15 respectively.

On the cationic Na^+ site, the rotational potential has a minimum when the molecule locates flat (θ = 90°) on the surface, with a binding energy of –0.866 kcal/mol, and has a maximum when the molecules sit along the surface normal with a binding energy of 0.432 kcal/mol. This large difference in binding energy can be attributed to the difference in the electrostatic interaction between the molecule and the surface electric field. In terms of azimuthal orientation, the potential has four minima at φ = 45°, 135°, 225°, and 315° as a result of surface four-fold symmetry. The barrier energy, for azimuthal rotation, has a height of only 0.014 kcal/mol, which makes tunneling likely to occur. Regardless of the azimuthal orientation, the energy barrier to rotating the molecule to the upright position ($\theta = 0°$) is a prohibitive of 1.3 kcal/mol.

On the anionic Cl^- site, the opposite behaviour is obtained where the rotational potential shows the lowest energy (-0.352 kcal/mol) when the molecular axis is parallel to the surface normal (θ = 0°) and highest (0.084 kcal/mol) when the molecular axis is parallel to the surface plane (θ = 90°). The energy barrier for rotation in the plane perpendicular to the surface (θ rotation) is 0.44 kcal/mol. This value is less than that above the Na^+ site owing to the increased distance (3.65 Å *vs.* 2.8 Å) from the surface. Evidence of the four-fold symmetry of the surface potential appears on the top of the potential ridge where $\theta = 90°$ but is not present when the molecule sits perpendicular to the surface ($\theta = 0°$).

Table 7.4: Rotational potential fitting parameters in units of kcal/mol.

Parameter	A_o	A_1	A_2	A_3	A_4	A_5
Above Na^+	-0.7679	0.0072	1.2777	-0.0799	-0.0163	0.0092
Above Cl^-	0.0131	-0.0023	-0.4188	0.0705	0.0052	-0.003

Table 7.5: Rotational potential fitting parameters in units of kcal/mol.

Parameter	A_o'	A_1'	A_2'	A_3'
Above Na^+	-1.0615	1.3989	-0.0863	3.357×10^{-3}
Above Cl^-	-0.3318	-0.4852	0.0761	-2.573×10^{-3}

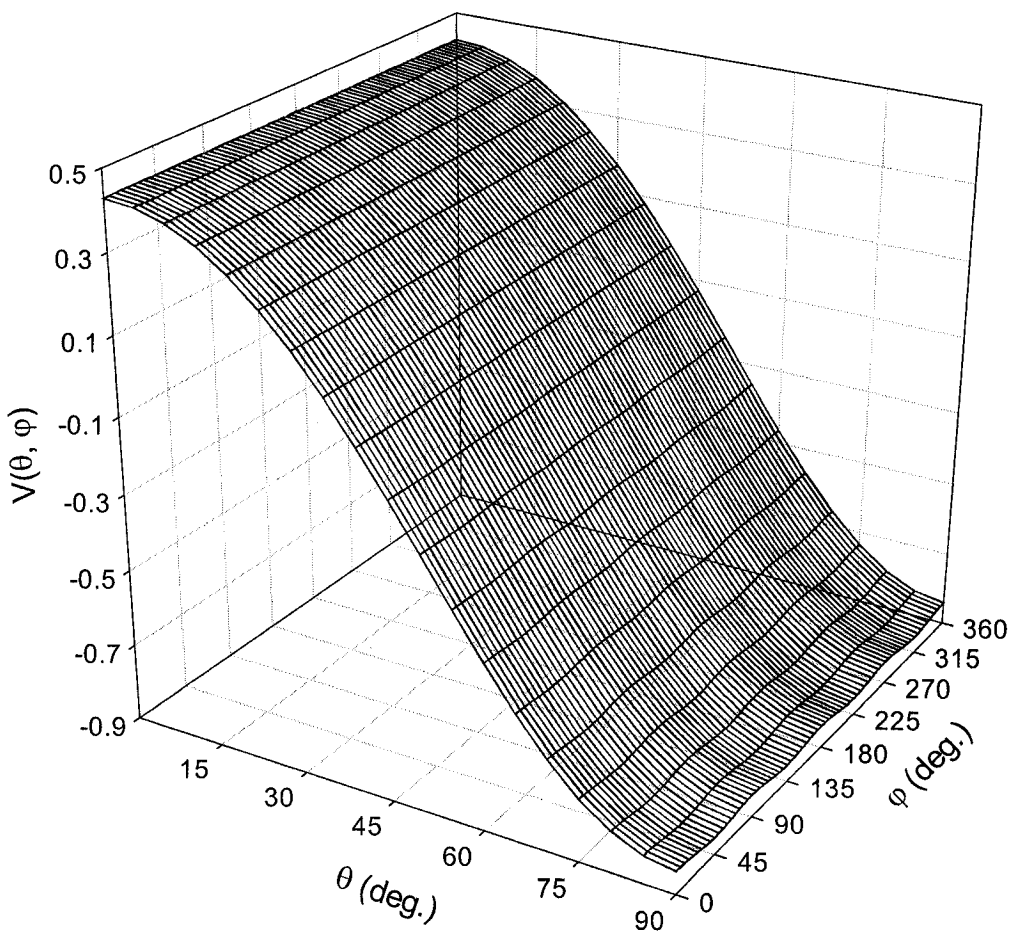

FIG. 7.14: The rotational potential $V(\theta, \varphi)$ for a H_2 molecule whose center of mass sits at a height of 2.8 Å above the Na^+ site.

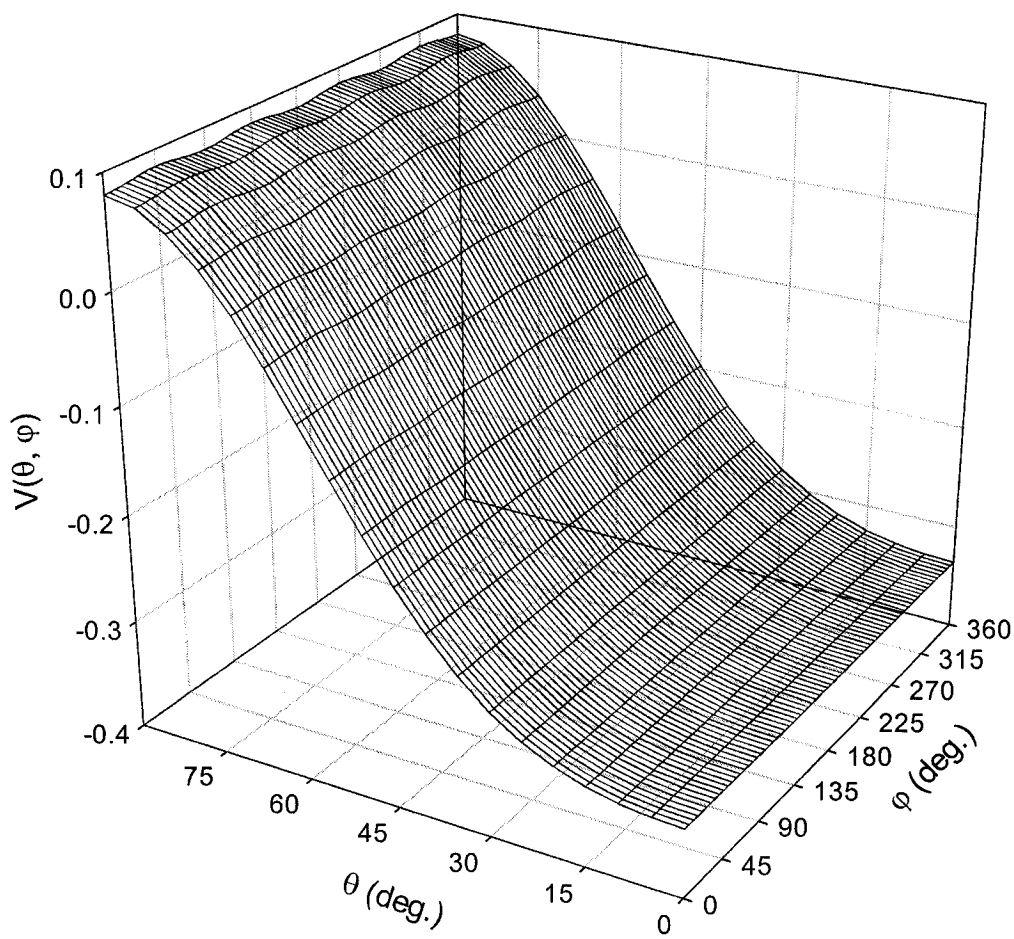

FIG. 7.15: The rotational potential $V(\theta, \varphi)$ for a H_2 molecule whose center of mass sits at a height of 3.65 Å above the Cl^- site.

7.2.2.1. Wave Functions

The goal of calculating the wave functions of H_2 molecule in different rotational states is to determine whether the molecular axis is delocalized or not. Using perturbation theory, to the first order correction level, the wave functions of H_2 in the adsorbed phase were calculated, and written as a linear combination of spherical harmonic functions using Eq. (3.17).

For a H_2 molecule sits at the top of Na^+ site, our PT calculations yielded the following rotational wave functions of the lowest order of *para*- and *ortho*-states:

1. For *para*-H_2 (J = 0, m = 0);

$$\Psi_{00}^{ads.} = Y_{00} - 0.376 * Y_{20} + 6.968 \times 10^{-3} * Y_{40} - 2.71 \times 10^{-4} * (Y_{44} + Y_{4-4})$$

2. For *ortho*-H_2 (J =1, m = ±1);

$$\Psi_{11}^{ads.} = Y_{11} - 0.169 * Y_{31} - 6.259 \times 10^{-4} * Y_{3-3} + 3.355 \times 10^{-3} * Y_{51} + 3.37 \times 10^{-5} * Y_{5-3} - 2.261 \times 10^{-4} * Y_{55}$$

3. For *ortho*-H_2 (J =1, m = 0);

$$\Psi_{10}^{ads.} = Y_{10} - 0.186 * Y_{30} + 4.332 \times 10^{-3} * Y_{50} - 1.011 \times 10^{-4} * (Y_{54} + Y_{5-4})$$

The wave function density of *para*-H_2 in its ground state ($\Psi_{00}^{*} \cdot \Psi_{00}$) is plotted as a function of θ, and φ as shown in Fig. 7.18. The angular distribution of *para*-

H_2 has a maximum at θ =90° where the molecular axis spends most of the time flat on the top of the cationic site. As the molecule turns up from the flat configuration (θ = 90°) to the tilted configuration, 90° >θ > 0°, the distribution decreases to zero when the molecular axis is oriented along the surface normal at θ =0°. The behaviour of the angular distribution shows that the *para*-H_2 is squashed on surface, in sharp contrast to its gas phase angular distribution, which has no dependence on either θ, or φ. The azimuthal distribution, with (θ =90°) is shown in Fig. 7.17. It is almost uniform with small ripples that reflect the four-fold symmetry of the surface. This situation indicates that the molecular axis of *para*-H_2 is azimuthally delocalized with a residual preference for orientations in the φ = ±45°, ±135° directions.

Similar behaviour is observed in the angular distribution of the helicoptering *ortho*-H_2 state (J =1, m= ±1) on the top of Na^+ site. As shown in Fig. 7.18, the angular distribution shows that the most probable orientation occurs when the molecular axis locates flat on surface. From Fig. 7.19, it may be observed that the molecule is azimuthally delocalized with only a faint hint of the underlying four-fold symmetry imparted by the surface. The angular distribution of the helicoptering *ortho* state strongly resembles that of its gas phase counterpart.

The angular distribution of the cartwheeling *ortho*-H_2 state (J = 1, m= 0) located on the top of Na^+ site is plotted as a function of θ, and φ as shown in Fig. 7.20. Its angular distribution is affected by the surface and has a peak around θ =

35°. This is a significant shift from the gas phase where the maximum occurs at θ = 0°. This distribution has been squashed in the vertical direction leading to a suppression of the vertical orientation and a shift in the distribution to favour a tilted orientation. Together our PT calculations and MC simulations show that *para*-H_2 (J=0, m=0) and helicoptering *ortho*-H_2 (J =1, m= ±1) prefers to sit flat on the top of the cationic Na^+ site.

Comparing the azimuthal distribution of a hydrogen molecule rotating in the *c*(2×2) layer, as discussed in section 7.2.1.1, to the azimuthal distribution of a single molecule sitting on a Na^+ site (Figs. 7.17 and 7.19), it is apparent that the distributions are almost the same, with small ripples that reflects the four fold surface symmetry. This means that the molecule-molecule interaction on surface does not perturb the azimuthal distribution, and hence all the molecules in the ad-layer are azimuthally delocalized in a unit cell of (1×1) symmetry as observed experimentally.

Directly over the anionic Cl^- site, the PT calculations of the rotational wave functions of H_2 molecule in its lowest order of *para*- and *ortho*- states yielded the following:

1. For *para*-H_2 (J = 0, m = 0);

$$\Psi_{00}^{ads.} = Y_{00} + 0.1306 * Y_{20} - 6.147 \times 10^{-3} * Y_{40} - 2.077 \times 10^{-4} * (Y_{44} + Y_{4-4})$$

2. For *ortho*-H_2 (J =1, m = ±1);

$$\Psi_{11}^{ads.} = Y_{11} + 0.063 * Y_{31} + 4.797 \times 10^{-4} * Y_{3-3} - 2.96 \times 10^{-3} * Y_{51} - 2.583 \times 10^{-5} * Y_{5-3} + 1.733 \times 10^{-4} * Y_{55}$$

3. For *ortho*-H_2 (J =1, m = 0);

$$\Psi_{10}^{ads.} = Y_{10} + 0.0581 * Y_{30} - 5.404 \times 10^{-3} * Y_{50} + 7.749 \times 10^{-5} * (Y_{54} + Y_{5-4})$$

For H_2 molecule located above the anionic Cl^- site, the wave function density of *para*-H_2 ($\Psi_{00}^* \cdot \Psi_{00}$) in its ground state is plotted as shown in Fig. 7.21. It has a maximum when the molecular axis perpendicular to the surface at θ =0°, and a minimum value when the molecular axis lies flat on the surface at θ =90°. This behaviour is quite different from its counterpart gas phase distribution; *para*-H_2 adsorbed over the anionic Cl^- site is elongated in the vertical direction compared with the uniform gas phase distribution.

Similar behaviour is also observed for the cartwheeling *ortho*-H_2 state (J =1, m= 0) as shown in Fig. 7.22. Although its angular distribution ($\Psi_{10}^* \cdot \Psi_{10}$) resembles the gas phase counterpart, this angular distribution is also elongated in the vertical direction. As in the gas phase, the highest value of the angular distribution is obtained when the molecule locates perpendicular to the surface plane at θ =0°, and decrease as the molecular axis tilts (0° < θ < 90° or 90° < θ < 180°) and become zero when the molecular axis lies flat on the surface (θ =90°).

The MC simulations show that above the anionic sites the H_2 molecular axis is most likely to sit perpendicular on the surface plane, which is consistent with the maxima of the angular distributions of the cartwheeling *ortho-* and *para-* states. Consequently, we anticipate that these will be the preferred orientation for molecules on top of the Cl^- site. This will be confirmed later in the energy level calculations.

For helicoptering *ortho*-H_2 (J =1, m= ±1) above the anionic site, the angular distribution is somewhat affected by the surface electric field but it still resembles their angular distribution in gas phase. As shown in Fig. 7.23 the highest probability density obtained when the molecule lies flat on the surface. However, this orientation was not observed in our MC simulation results. This observation is consistent with our PT calculations of the rotational energy levels, where the helicoptering *ortho-* state is not a preferred state above the anionic site.

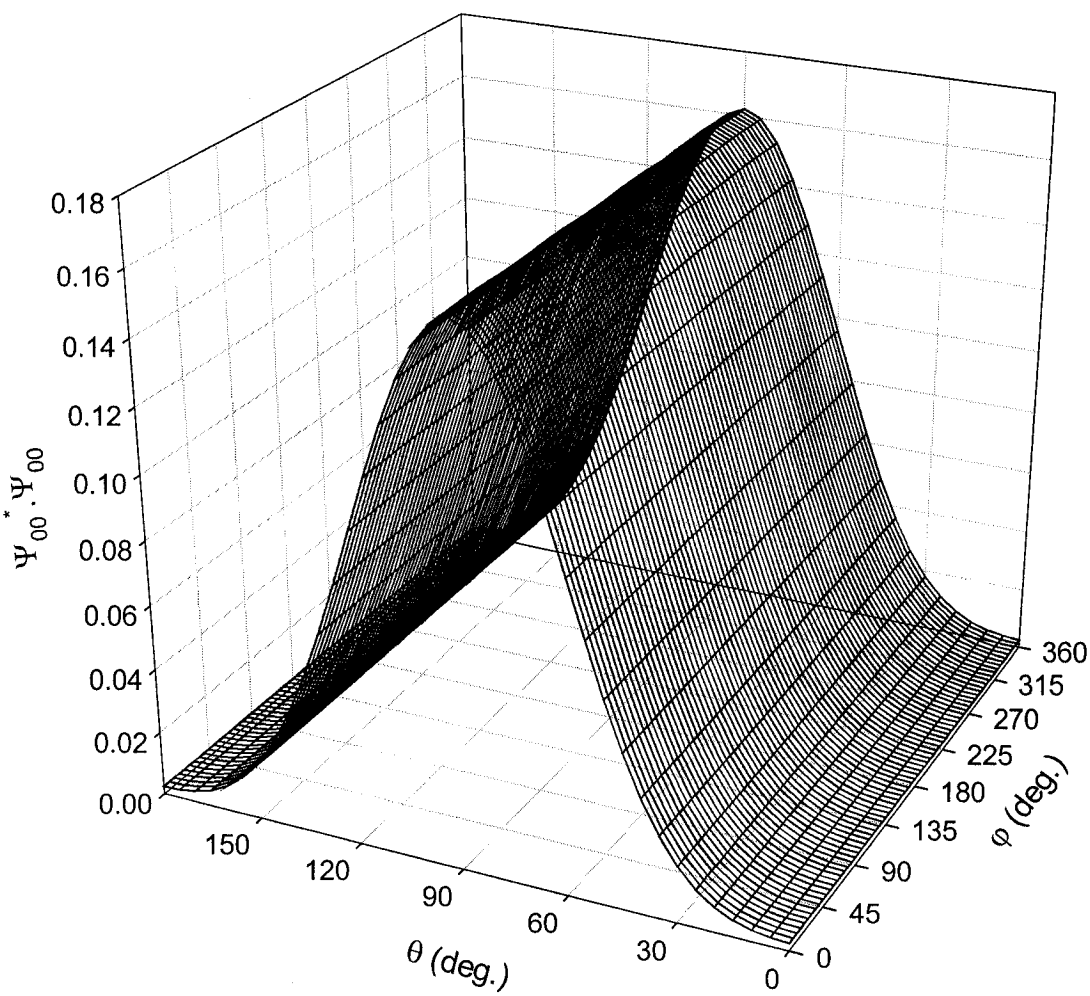

FIG. 7.16: The angular distribution of a *para*-H_2 molecule above a Na^+ site.

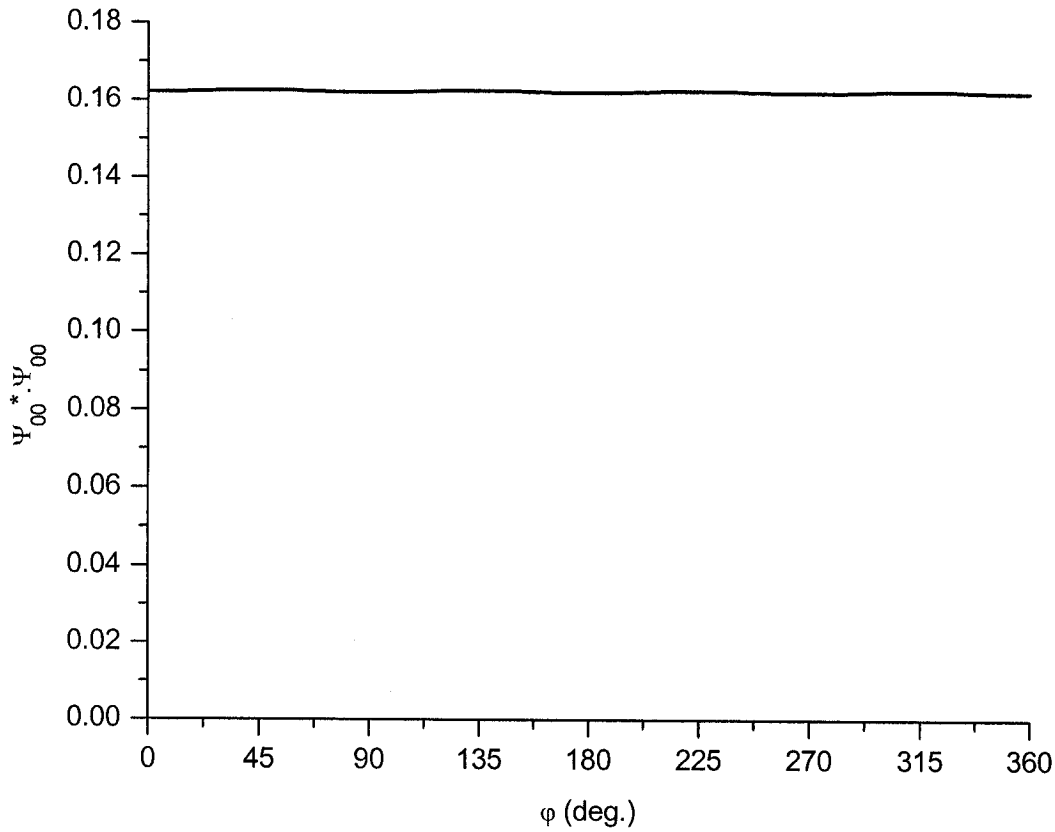

FIG. 7.17: The azimuthal distribution of a *para*-H_2 molecule above a Na^+ site, at the most probable polar orientation (θ=90°).

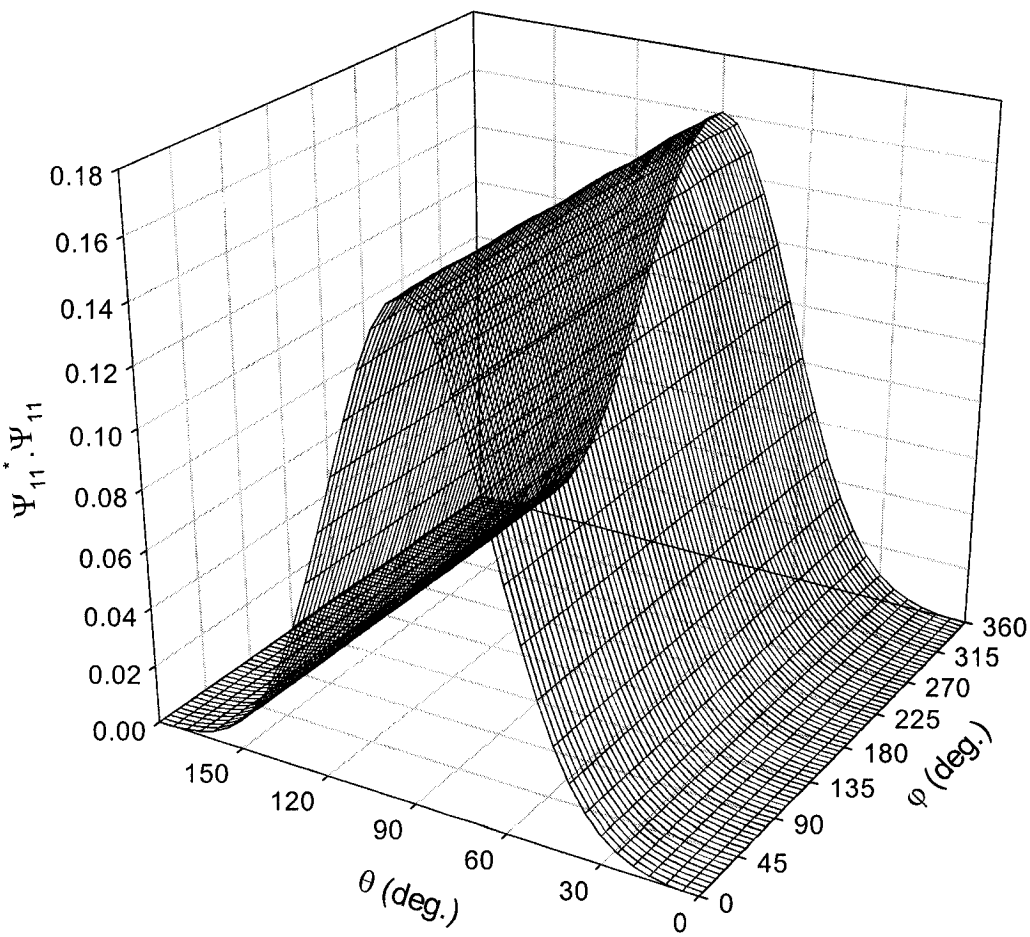

FIG. 7.18: The angular distribution of a helicoptering *ortho*-H_2 molecule above a Na^+ site.

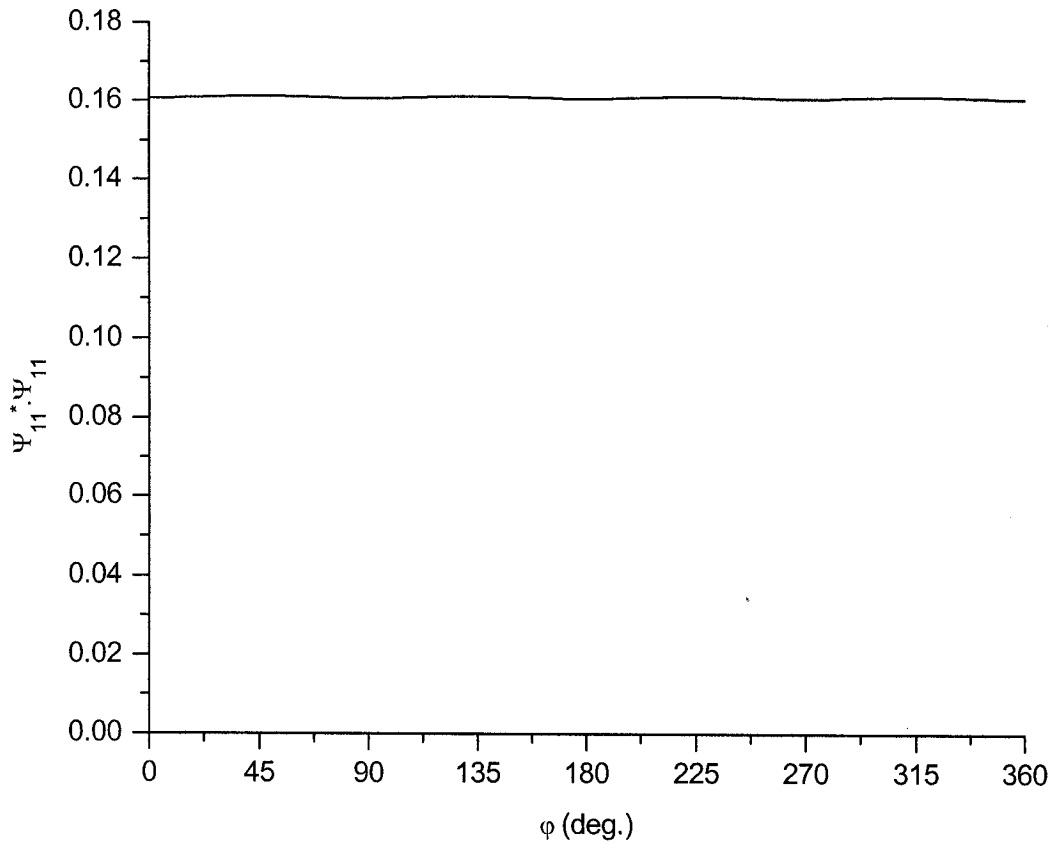

FIG. 7.19: The azimuthal distribution of a helicoptering *ortho*-H_2 molecule above a Na^+ site, at the most probable polar orientation (θ=90°).

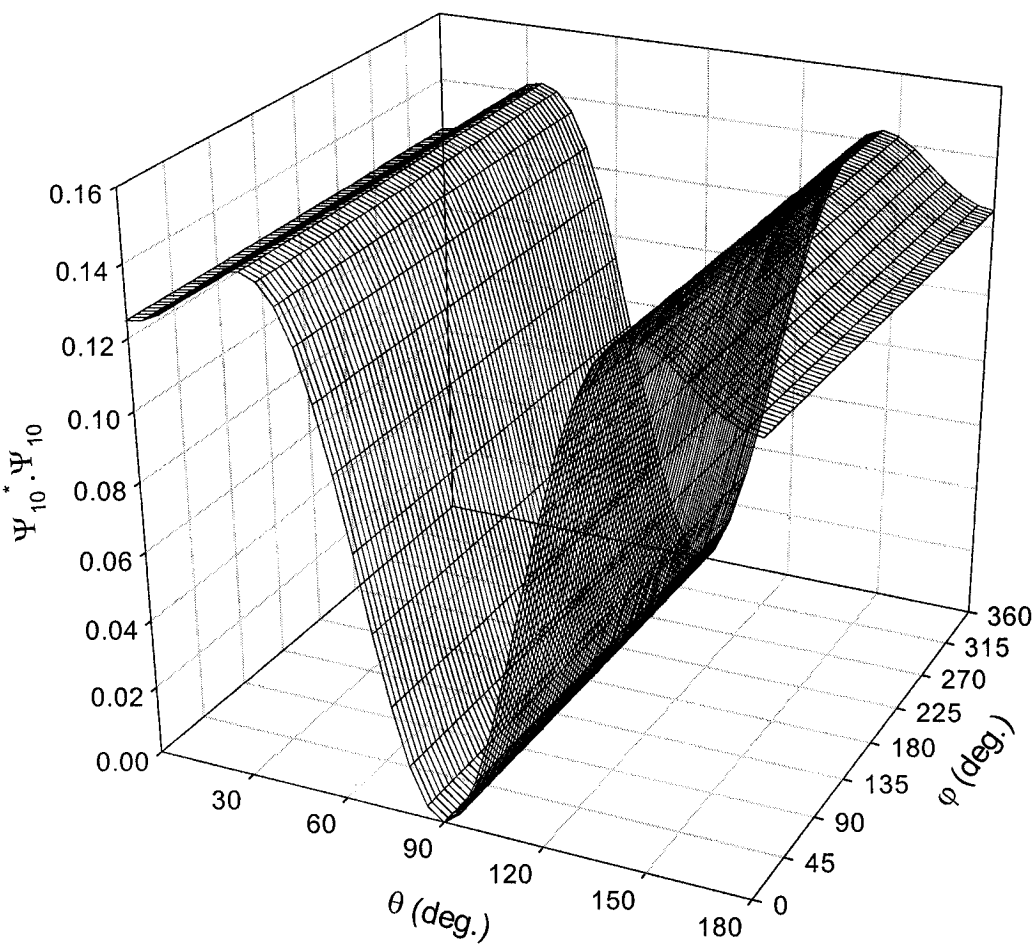

FIG. 7.20: The angular distribution of a cartwheeling *ortho*-H_2 molecule above a Na^+ site.

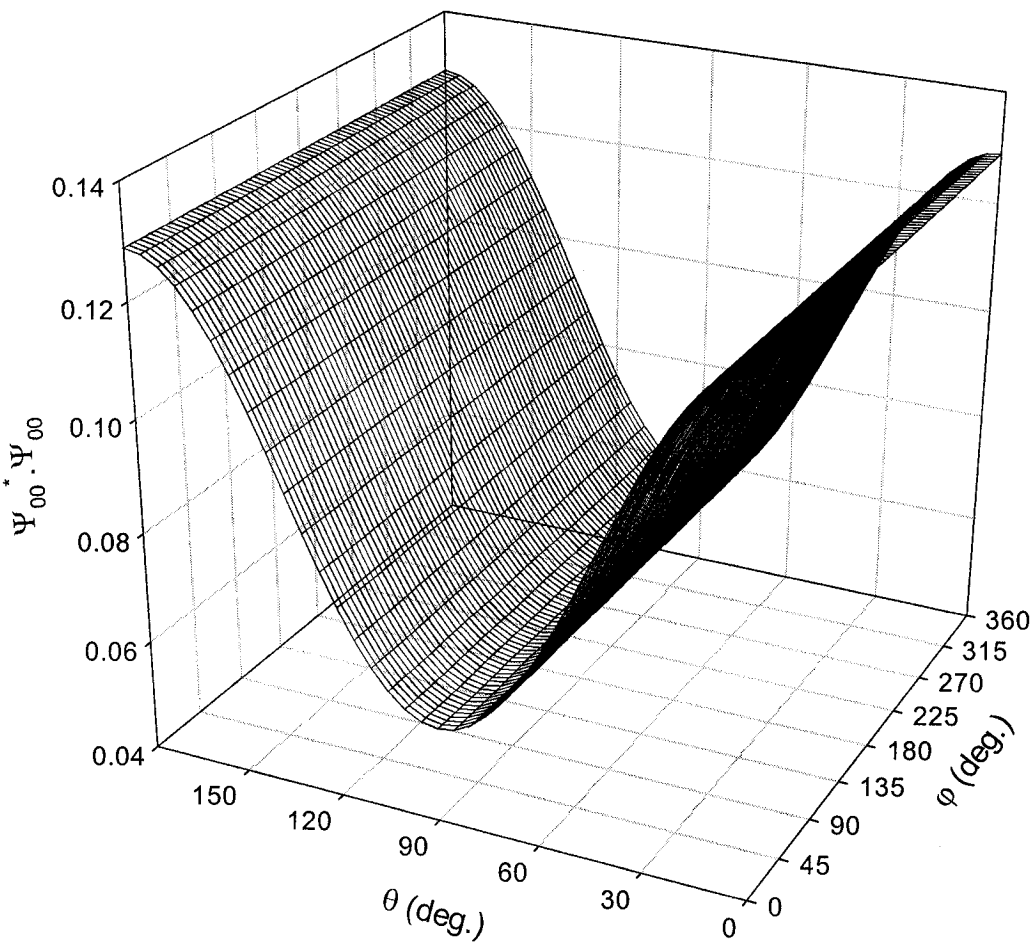

FIG. 7.21: The angular distribution of the ground state *para*-H_2 molecule above a Cl^- site.

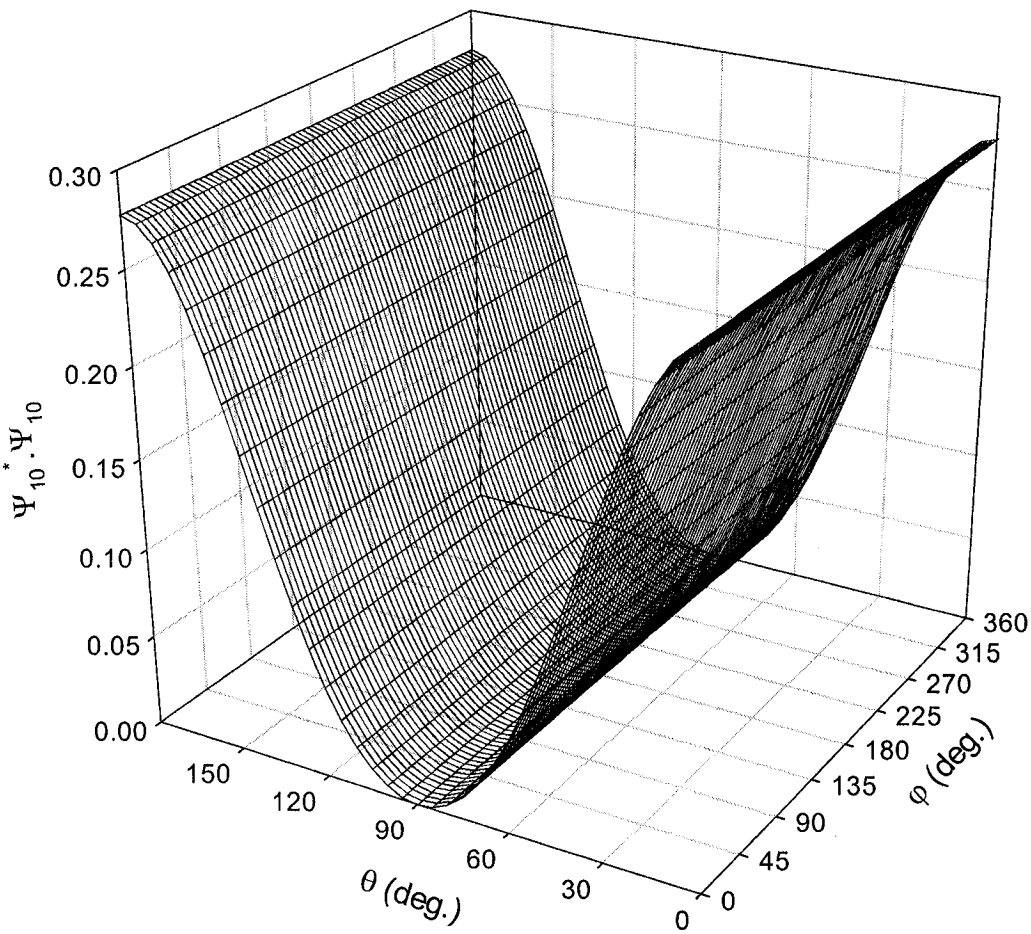

FIG. 7.22: The angular distribution of a cartwheeling *ortho*-H_2 molecule above a Cl^- site.

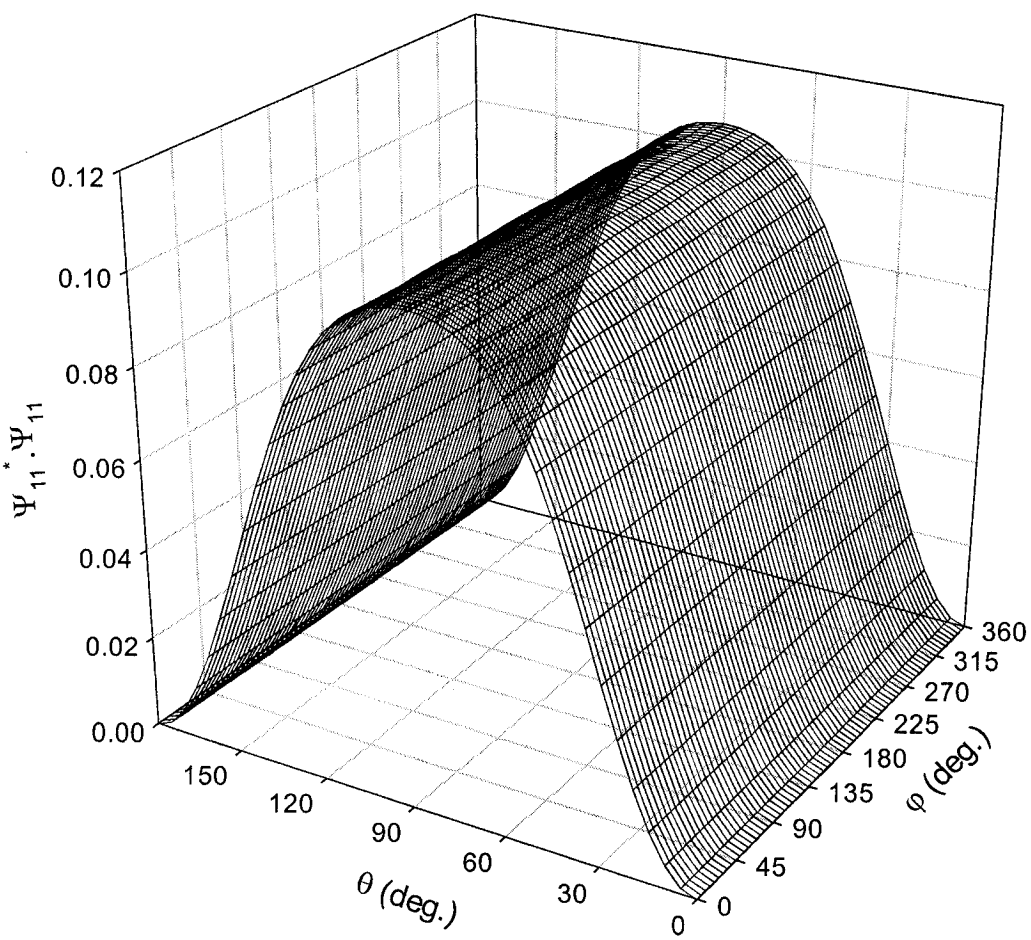

FIG. 7.23: The angular distribution of a helicoptering *ortho*-H_2 molecule above a Cl^- site.

7.2.2.2. Rotational levels energies

The rotational energy of a hydrogen molecule was calculated, using Eq. (3.16), for the different states listed in Table 7.6. It is clear that our calculations do not mix eigenstates with different m values (see equation 3.16) and, as a consequence m is still a good quantum number. Actually these calculations represent the energy of the orientational levels of a hydrogen molecule (i.e. the rotational motion actually is restricted to the azimuthal rotation type). On the Na^+ site, each rotational level splits into a set of states with respect to their azimuthal orientations, in which the state of (J, m=±J) has the lowest value of the rotational energy level, whereas the state of (J, m=0) has the highest rotational energy level. In the case of a hydrogen molecule located over the anionic Cl^- site, the different rotational levels of *ortho*- and *para*- states again split into a set of sub-levels of the same rotational state (ΔJ = 0) but are different in the rotational magnetic quantum number m value. As shown in Table 7.6, the lowest rotational energy level was found for cartwheeling state of (J, m=0), while the highest rotational energy level was found for helicoptering state of (J, m=±J). Consequently, the most preferred state to adsorb on the top of the cationic site is the helicoptering state, while the cartwheeling state prefers to sit on the anionic site.

The physical adsorption of hydrogen molecules on NaCl(001) surface involves only weak interaction between the molecules. Consequently, it is expected that the rotational states are only affected by the surface electric field.

Therefore, we can approximately estimate the adsorption binding energy of H_2 molecule as the difference in the rotational energy level value between the gas and adsorbed phases. These results are calculated and listed in Table 7.7. Directly over the Na^+ site, the adsorption energy increases in the order of cartwheeling *ortho*-H_2 < *para*-H_2 < helicoptering *ortho*-H_2. So the helicoptering *ortho*-H_2 ($J = 1, m = \pm 1$) state is the most strongly bound to the surface with a binding energy of –0.606 kcal/mol. Above the anionic Cl^- site, the adsorption energy decreases in the order of cartwheeling *ortho*-H_2 > *para*-H_2 > helicoptering *ortho*-H_2, where the cartwheeling *ortho*-H_2 ($J = 1$, $m = 0$) has the highest binding energy. This opposite behaviour of the *ortho*-H_2 species (helicoptering *vs.* cartwheeling) in terms of adsorption binding energy and site preference is due to the strong dependence of the electrostatic energy on the orientation of H_2 molecular axis. In particular, H_2 in the helicoptering state the molecular axis orients parallel to the surface plane whereas in the cartwheeling state, the molecular axis orients perpendicular to the surface plane (along the surface normal).

In case of *para*-H_2 ground state, we found that its adsorption energy falls between that of the two *ortho*-H_2 species. This actually agrees with the nature of the spherical ground state *para*-H_2 where there is no electrostatic interaction with the surface. Compared with the available experimental and theoretical results for the binding energy of H_2 in different rotational levels, our PT calculations yielded lower values of the binding energy for *para*- and *ortho*- ground states but as can

be seen from Table 7.8, the experimental results still suffer from large uncertainty in their values. On the other hand, our results match the general trend of the experimental and theoretical results in which *ortho*-H_2 is more bound to the surface than *para*-H_2.

Table 7.6: Rotational energies of different H_2 states over the ions of NaCl surface using time-independent PT to the second order correction. The units are in kcal/mol.

Rotational state (J, m)	above Na^+ site	above Cl^- site
	E_{Jm} (kcal/mol)	E_{Jm} (kcal/mol)
(0,0)	-0.546	-0.111
(2,0)	0.857	0.881
(2,±1)	0.771	0.895
(2,±2)	0.391	1.042
(4,0)	3.304	3.328
(4,±1)	3.277	3.335
(4,±2)	3.191	3.359
(4,±3)	3.032	3.392
(4,±4)	2.777	3.518
(1,0)	0.262	0.149
(1,±1)	-0.257	0.311
(3,0)	1.906	1.929
(3,±1)	1.86	1.94
(3,±2)	1.709	1.986
(3,±3)	1.404	2.108

Table 7.7: The binding energy of the H_2 species adsorbed over NaCl(001) surface using a time-independent Perturbation theory method.

Adsorption site	Binding energy (kcal/mol)		
	para-H_2 ($J = 0, m = 0$)	helicoptering *ortho*-H_2 ($J = 1, m = \pm 1$)	cartwheeling *ortho*-H_2 ($J = 1, m = 0$)
Na^+	-0.5462	-0.6059	-0.0869
Cl^-	-0.1115	-0.0392	-0.2008

Table 7.8: Adsorption energies of the different H_2 species on NaCl(001) surface.

	Theory	IR results	HAS results	This work
		-0.717±0.2[a]		
para-H_2	-0.796	-0.715±0.23[b]	-0.853±0.12[c]	-0.546
ortho-H_2	-0.98	-0.876±0.23[b]	-	-0.606

a) Taken from ref. [37]
b) Taken from ref. [38]
c) Taken from ref. [40]

7.2.2.3. Rotational level energies of H_2 molecule in the second layer

Our MC simulations show the existence of a second layer where the molecules are located tilted on the top of Cl^- sites. In order to determine which kind of H_2 species prefers to locate in the second layer, the rotational motion of H_2 molecule must fully be examined. Therefore, in the presence of the bottom layer of *c*(2×2) unit cell, the rotational potential of a single H_2 molecule, whose center of mass is fixed directly over Cl^- site at an equilibrium height of 4.6 Å, was calculated by systematically varying the angle of its molecular axis. This potential was generated and fitted to the following mathematical formula using a least squares fit program from MAPLE V.7:

$$V(\theta,\varphi) = A_o + A_1 \cdot \cos(4\cdot\varphi) + A_2 \cdot \cos^2\theta + A_3 \cdot \cos^2(2\cdot\theta) + A_4 \cdot \cos^2\theta \cdot \cos(4\cdot\varphi) + A_5 \cdot \cos^4\theta \cdot \cos(4\cdot\varphi)$$

where the fitting parameters are found to be (in the unit of kcal/mol): A_o= -0.125. A_1= -2.71×10^{-3}, A_2= -0.197, A_3= 0.0384, A_4= 6.74×10^{-3}, and A_5= -4.12×10^{-3}.

The rotational potential of the molecule in the second layer was plotted as a function of θ, and φ as shown in Fig. 7.24, where the lowest energy when the molecular axis locates perpendicular to surface plane (θ=0°), and the highest energy when its molecular axis parallels the surface plane (θ=90°). The azimuthal distribution shows the existence of four minima at φ = 0°, 90°, 180°, and 270°, which reflects the four-fold symmetry of the surface of the underlying *c*(2×2)

layer. Regardless of the azimuthal rotation, the barrier energy to rotating the molecule to upright position ($\theta = 0°$) is only 0.2 kcal/mol (8.5 meV), whereas the barrier energy for the molecule to rotate in the plane parallel to the surface (azimuthal rotation) is only 0.02 kcal/mol. Consequently, in the second layer, where the molecules are farther from the NaCl(001) surface, the interaction between the molecules and the surface becomes weaker. This condition allows the molecules to rotate in three dimensions with more preference towards azimuthal rotation.

Using Eq. (3.16), the rotational energy of the H_2 molecule in the second layer has been calculated in the lowest order of *para*- and *ortho*- states, along with the adsorption energy. These results are listed in Table 7.9. It is clear that the results match those performed for a single molecule sits above the Cl^- site, where the cartwheeling *ortho*-H_2 (J=1, m=0) is still the most strongly bound to the surface with a binding energy of –0.233 kcal/mol. The other two species show lower binding energy to the surface in the range of –0.16 kcal/mol. So we expect the second layer consists of cartwheeling *ortho*-H_2 molecules that are freely rotating (azimuthally delocalized) on surface in a unit cell of (1×1) symmetry.

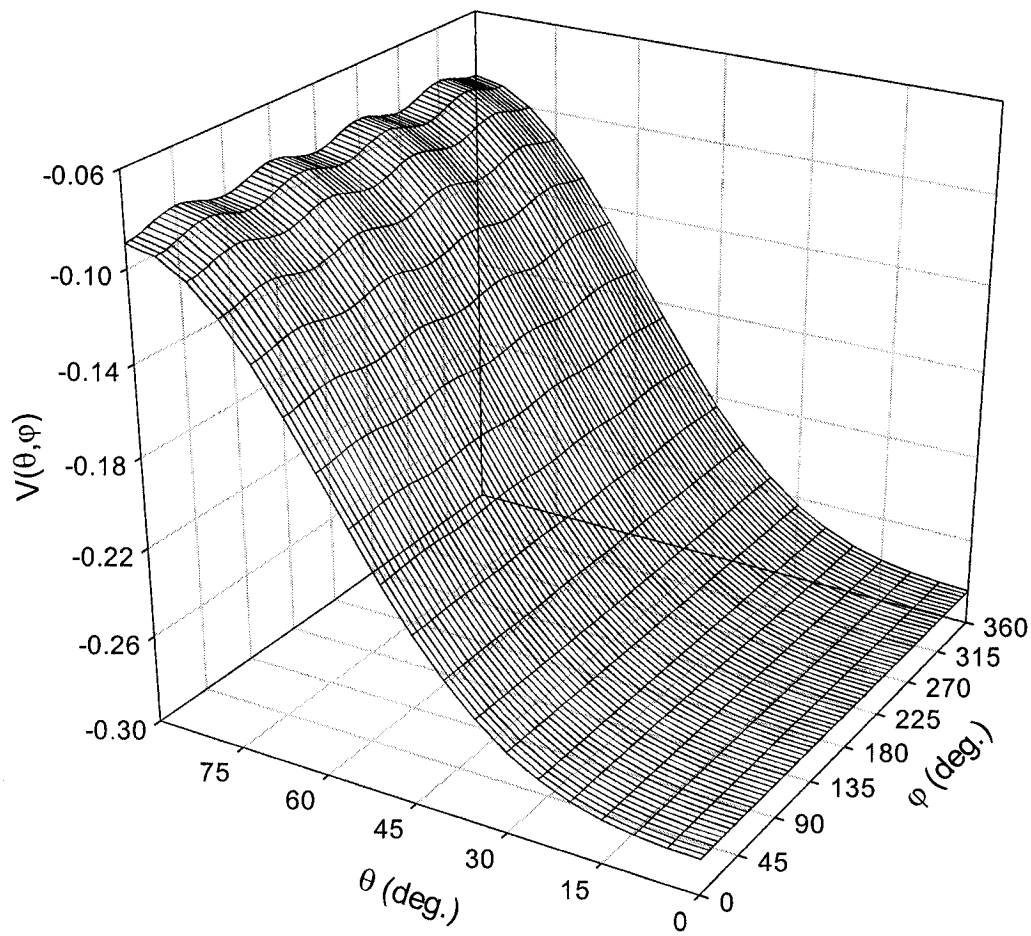

FIG. 7.24: The rotational potential for a single molecule rotates in the second layer, whose center of mass fixed directly over the anionic Cl^- site at an equilibrium height of 4.6 Å.

Table 7.9: Rotational and adsorption energy of H_2 molecule in its lowest states for a molecule in the second layer at an equilibrium height of 4.6 Å from the Cl^- ion directly below.

	E_{Jm} (kcal/mol)	E_b (kcal/mol)
para-H_2(J = 0, m = 0)	-0.177	-0.177
ortho-H_2(J = 1, m = ±1)	0.204	-0.145
ortho-H_2(J = 1, m = 0)	0.1167	-0.233

7.3. Relation between simulations and calculations

Using perturbation theory, the energies and angular distributions of the lowest order *ortho*- or *para*- states of adsorbed H_2 molecule were calculated. In all cases these states were found to be azimuthally delocalized. This finding has an important impact on the interpretation of the MC simulation results. In the case of the *c*(2×2) structure obtained from the MC simulations each molecule may be in one of two distinct azimuthal orientations. The PT result indicates that all molecules are orientationally equivalent so that all cation sites are occupied with equivalent molecules. The *c*-type structure thus converts into a (1×1) structure and so the MC simulations coupled with the PT results yield a picture that is consistent with the experimental findings.

The same considerations hold for the *p*(2×1) structure where the bottom layer molecules lie flat directly over the cationic Na^+ sites with each molecule possessing one of two distinct orientations. The quantum calculations indicate

that the rotational states may be interpreted as either a helicoptering *ortho*-state or a squashed *para*-state, both of which are azimuthally delocalized. And so the lower layer symmetry will be (1×1) instead of *p*(2×1). The MC simulations indicated that the upper layer had tilted molecules around the Cl^- sites in a *p*(2×1) structure; the *p*(2×1) structure arising because the tilted molecules have two possible azimuthal orientations as shown in Fig. 7.6. The quantum calculations indicate that these molecules will be in a cartwheeling *ortho*- state or possibly an elongated *para*- state. In either case, the molecular axis is azimuthally delocalized and the symmetry of the layer will be converted to (1×1). Thus, the combination of the MC simulations and the quantum calculations leads to the conclusion that the adlayer will have a (1×1) structure, as observed in experiment.

The quantum calculations also indicate that there will be peferential adsorption on the surface. In particular, the cation sites will be occupied by adsorb helicoptering *ortho*-H_2 molecules. It is possible to adsorb *para*-H_2 molecules on these sites but they will not be bound as strongly. These calculations also indicate that the adsorption on an anion site is possible and that cartwheeling *ortho*-H_2 molecules will preferentially adsorb there, although the adsorption of *para*-H_2 molecules is also possible. However, the binding at these sites is considerably less than at the cation sites and they will only be occupied after the cation sites are filled. This is consistent with the observation from the MC simulations of the formation of a second layer above the anion sites after the

cation sites are filled. The second layer is not as thermally stable as the first layer and will desorb at temperatures of 10 K whereas the bottom layer (cation sites) is thermally stable up to 16 K. This finding reconciles the apparently contradictory experimental observations of the Ewing group and Heidberg –Toennies groups; Ewing *et al.* observed a bilayer structure at 5.2 K whereas the other groups observed only monolayers at 10 – 12 K. In conclusion, the use of MC simulations coupled with quantum calculations yields a description of the adlayer structure that is consistent with all of the experimental observations.

CHAPTER 8: CONCLUSION

In this thesis, I have presented the MC simulation results of hydrogen mono-layers on ionic crystal surfaces, *viz.* MgO(001), LiF(001) and NaCl(001), along with perturbation theory calculations of the rotational energies and wave functions of a hydrogen molecule in the adsorbed phase. These simulations and calculations are based on a detailed potential model that assumes the interaction energy between H_2 molecules and with the ionic crystal surface may be expressed as a sum of atom-atom and atom-ion interaction.

The structures and thermal stabilities of hydrogen adlayers are explored using the Metropolis MC simulations. These simulations are conducted in the canonical ensemble using the detailed potential model and classical statistics. Consequently, our MC simulations did not consider the quantum behaviour of hydrogen molecules in the adsorbed phase (2-dimension solid phase). The MC simulations yielded structures that match the experimental findings [H_2/MgO(001), H_2/LiF(001) and H_2/NaCl(001)] in terms of surface coverage, and thermal stability but disagree in terms of monolayer structure symmetry. For example, the MC simulations of hydrogen mono-layers on MgO(001) show a series of structures with *p*-type symmetry *i.e.* $p(2\times2)\rightarrow p(4\times2)\rightarrow p(6\times2)$, whereas the HAS work found these monolayers are of *c*-type symmetry. In order to estimate the quantum effects of hydrogen molecules in the adsorbed phase and reconcile the experimental results, time-independent perturbation theory was applied to study the rotational motions of H_2 in different rotational levels, and to

get a clear picture how these molecules sit on the crystal surface from a quantum view point

The PT calculations of the energy and wave function of molecular H_2 in its different rotational levels have been performed by solving the Schrödinger equation of a rigid rotor rotating on the top of the adsorption site in the presence of the surface electric field. The PT calculations of H_2 in the adsorbed phase show that the choice of adsorption sites depends on the rotational states of hydrogen molecule. It is found that *ortho*-H_2 in state ($J, |m| = \pm J$) (helicoptering) prefers to locate above the cationic site, whereas *ortho*-H_2 in state ($J, |m| = 0$) (cartwheeling) prefers to reside at the top of the anionic site. The difference in the adsorption site preference can be attributed to the difference in the interaction of the hydrogen molecules in those different states with the surface electric field. In terms of azimuthal rotational motion, the PT calculations show that an adsorbed hydrogen molecule, in either of these *ortho* states, is azimuthally delocalized and free to rotate (φ motion) in the plane of the surface.

The PT calculations also show that it is possible for ground state *para*-H_2 to adsorb on both cationic and anionic sites. The angular distribution of *para*-H_2 was found to differ significantly from its uniform gas phase distribution. Over the cationic site, its angular distribution shows *para*-H_2 is squashed on the surface (flattered in the *xy* plane) and its distribution resembles the helicoptering *ortho*-H_2 distribution. On the top of the anionic site, the angular distribution of *para*-H_2

resembles the cartwheeling *ortho*-H_2 distribution, where *para*-H_2 is elongated along the surface perpendicular. The adsorption energy of *para*-H_2 is intermediate between the helicoptering and cartwheeling *ortho*-states, regardless of whether the molecule is adsorbed over the cation or anion site. In the adsorbed phase, the ground state ($J = 0$) *para*-H_2 maintains a cylindrical symmetry and hence is azimuthally delocalised.

Since the molecules are azimuthally delocalized regardless of their rotational state, the *p*-type structures observed in the MC simulations become *c*-type. Thus the experimentally observed sequence of $c(n\times 2)$ structures of hydrogen adlayers on an MgO(001) surface, is indeed possible. Furthermore, the MC simulations provide details of these structures. The $c(2\times 2)$ structure consists of an array of molecules covering every other Mg^{2+} site of the surface in a checkerboard pattern, with quantum mechanical delocalisation of the molecular axes eliminating azimuthal differences between molecules. Specifically, the *para* and helicoptering *ortho* states are allowed to adsorb here. The $c(4\times 2)$ structure consists of two kinds of adsorption sites. One third of the molecules adsorb directly over Mg^{2+} ions with a preference for a horizontal orientation for the molecular axes (*para* or helicoptering *ortho*-states), while the remaining two thirds adsorb near, but are offset from, the O^{2-} ions with orientations that prefer a tilt from the surface normal. In terms of rotational states these are thought to be a mix of cartwheeling and helicoptering *ortho*-states or possibly skewed *para*-states. The tilted molecules sit 0.5 Å further from the surface than the horizontal

molecules. The $c(6\times2)$ structure is an extension of the $c(4\times2)$ structure with only $1/5^{th}$ of the molecules adopting a horizontal orientation; the rest are tilted near O^{2-} ions. Besides confirming the symmetry of the experimentally observed structures, our simulations and calculations provide detailed information about these structures that are not directly accessible by experiment. This knowledge may be used in subsequent calculations of the phonon dispersion modes that have been measured experimentally.

Similar results have been observed for hydrogen monolayers formed on LiF(001) surface, where the existence of $c(n\times2)$ structure (n=2, 8, and 4) has been shown and details of these structures obtained using the combined theoretical calculations results and MC simulation findings. The $c(2\times2)$ structure is the same as the one formed on MgO(001) where the molecules arranged in a checkerboard pattern. The molecules locate flat over the Li^+ sites. This layer was found to be thermally stable up to 14 K. For the $c(4\times2)$ structure, there are two kinds of adsorption sites where the molecules located flat as in case of $c(2\times2)$ structure, and a tilted site where the molecular hydrogen center of mass lies between the cationic Li^+ and anionic F^- sites, with a polar angle of 65°. The coverage is 0.75. A structure with intermediate coverage was also observed. The $c(8\times2)$ monolayer with a coverage of 0.625 was found to be stable up to 5 K and consists of two adsorption sites as in case of $c(4\times2)$. Our MC simulations show that the $c(8\times2)$ structure is a transition state since it consists of two sub-region of $c(2\times2)$ symmetry and $c(4\times2)$ symmetry. Consequently, the $c(8\times2)$ layer can be

visualized as one row of $c(4\times2)$ unit cell followed by two rows of $c(2\times2)$ unit cells. Our results does not fully match the HAS results since the $c(4\times2)$ layer is not observed experimentally.

For H_2 adlayers formed on the (001) face of NaCl surface, together the MC simulation findings and PT calculations of the bi-layer system show that the existence of two layers is possible. In the bottom layer, the H_2 molecules lies flat on each cationic site in a unit cell of (1×1) symmetry. This layer is thermally stable up to 12 K. For the upper layer, the molecules locate tilted over the anionic Cl^- sites with a polar angle of 45°, in a unit cell of (1×1) symmetry. This layer was found to be orientationally disordered at T > 5K, and molecules subsequently desorb at T= 10 K. This finding of a stable bi-layer system only at temperatures below 10 K resolves the discrepancy between the experimental observations of the Ewing group and the Toennies-Heidberg groups. It is clear that the adsorption of H_2 on NaCl(001) surface is highly sensitive to the temperature condition applied since these physisorbed layers are weakly bound to the surface, and is consistent with Ewing's results that show the formation of another H_2 adlayer over the Cl^- sites at T= 5.2 K whereas the HAS [40] and IR [39] experiments performed at temperatures range 8—12 K have not observed H_2 adsorption over the anionic sites.

In terms of the energy and wave function calculations of the adsorbed H_2 molecule, the same results have been obtained as in case of H_2 molecules over

MgO(001) and LiF(001) surfaces. Above Na^+ site, the amount of binding energy decreases in the order: helicoptering *ortho*-H_2 < *para*- H_2 < cartwheeling *ortho*-H_2, whereas above the Cl^- site, the trend was completely reversed in which the cartwheeling *ortho*-H_2 is the most bound to the surface and the helicoptering *ortho*-H_2 is the lowest bound to the surface.

One of the conclusions that can be seen from the MC simulations, and agrees with the experimental findings, is that the variance in the lattice constants of the ionic surfaces is the major reason behind the differences in monolayer coverage. The maximum monolayer coverage increases in order of LiF (Θ =0.75 for the $c(4\times2)$ structure) < MgO (Θ =0.83 in case of $c(6\times2)$) < NaCl (Θ =1 in case of (1×1)). This mainly occurs in order to avoid sterical hindrance by reducing the repulsive portion of the lateral interactions between molecules in the layer. In other words, increasing the lattice constants of the surface leads to more area space available for molecules to adsorb in an energetically favourable situation and hence increase the monolayer coverage.

According to our PT calculations, the hydrogen molecules in the adsorbed phase are azimuthally delocalized and hence all the *p*-type structures, observed by MC simulations, are actually *c*-type structures. Therefore one of the idea that might be useful to apply as a further work is to change the model of constructing the H_2 molecules from two point dipoles located on the atoms of H_2 molecule to a single point quadrupole that interacts individually with the point quadrupole of

other H_2 molecules within the layer plane as well as with different ions of the surface. It is expected that this model will enhance the MC simulation results to be able to match completely the experimental observations in terms of coverage, thermal stability and structure symmetry.

REFERENCES

[1]: A.W. Adamson, *"Physical Chemistry of Surfaces"*, 4th edition, New York: Wiley- Interscience, (1982).

[2]: K.J. Laidler and J.H. Meiser, *"Physical Chemistry"*, 3rd edition, Houghton Mifflin company, New York, pages 844-846, (1999).

[3]: D. Schmicker, J.P. Toennies, R. Vollmer, and H. Weiss, *J. Chem. Phys.* ***95***, 9412 (1991) .

[4]: J. Heidberg, E. Kampshoff, R. Kühnemuth, M. Suhren, and H. Weiss, *Surf. Sci.* ***128***, 269 (1992).

[5]: A. Zangwill, *"Physics at Surfaces"*, Oxford University Press, Oxford, (1988).

[6]: D. White, and E.N. Lassettre, *J. Chem. Phys.* ***32***, 72 (1960).

[7]: M.W. Cole, F. Toigo, and E. Tosatti, Eds., Statistical Mechanics of Adsorption *Surf. Sci.* ***125***, 1 (1983).

[8]: A. Patrykiejew, S. Sokolowski, and K. Binder, *Surf. Sci. Rep.* ***37***, 207 (2000).

[9]: N-T. Vu, A. Jakalian, and D.B. Jack, *J. Chem. Phys.* ***106***, 2551 (1997).

[10]: A.K. Sallabi and D.B. Jack, *J. Chem. Phys.* ***112***, 5133 (2000).

[11]: J. Heidberg, N. Gushanskaya, O. Schönekäs, and R. Schwarte, *Surf. Sci.,* ***331-333***, 1473 (1995).

[12]: I.F. Silvera, *Rev. Mod. Phys.* ***52***, 393 (1980).

[13]: O.E. Vilches, *J. Low Temp. Phys.* ***89***, 267 (1992).

[14]: D.J. Hollenbach and A.G.G.M. Tielens, *Rev. Mod. Phys.* ***71***, 173 (1999).

[15]: I. Estermann and O. Stern, *Z. Phys.* ***61***, 95 (1930); R. Frisch, *Z. Phys.* ***84***, 443 (1933).

[16]: R. Frisch and O. Stern, *Z. Phys.* ***84***, 430 (1933).

[17]: J. Heidberg, E. Kampshoff and M. Suhren, *J. Chem. Phys.* ***95***, 9408 (1991).

[18]: K. Jug, G. Geudtner, *J. Mol. Catal. A.* ***119***, 143 (1997).

[19]:A. Lakhlifi and C. Girardet, *Surf. Sci.* ***241***, 400-415 (1991).

[20]: G.A. Somorjai, *"Surface Chemistry and Catalysis"*, A Wiley-Interscience Publaction, John Wiley & Sons, Inc. (1994).

[21]: L.W. Bruch, M.W. Cole, and E. Zaremba, *"Physical Adsorption: Forces and Phenomena"*, Oxford University Press, Oxford (1997).

[22]: J. Cui, S.C. Fain, Jr., H. Freimuth, H. Wiechert, H. P. Schildberg and H. J. Lauter, *Phys. Rev. Lett.* ***10***, 1848 (1988).

[23]: J. Van Kranendonk, Solid Hydrogen, Plenum, New York, (1983).

[24]: A.L. Gelbov, V. Panella, J.P. Toennies, F. Traeger, E. Pijper, H. Weiss, S. Picaud, P.N.M. Hoang and C. Girardt, *Phys. Rev. B* ***61,*** 14028 (2000).

[25]: O. E. Vilches, *J. Low Temp. Phys.* ***89***, 267 (1992).

[26]: J. Ma, D.L. Kingsbury, F. Liu, and O.E. Vilches, *Phys. Rev. Lett.* ***61***, 2348 (1988).

[27]: G. Vidali, G. Ihm, H. Kim, and M.W. Cole, *Surf. Sci. Rep.* ***12***, 133 (1991).

[28]: J.G. Skofronick, J.P. Toennies, F. Traeger, and H. Weiss, *Phys. Rev. B.* ***67***, 035413 (2003).

[29]: F. Traeger, Ph.D. Thesis, Max-Planck-Institut für Strömungsforschung and Universität Göttingen, Göttingen, Germany, (2001).

[30]: G. Vidali, and M. Karimi, *Langmuir* ***5***, 612 (1989).

[31]: M. Karimi, and G. Vidali, *Phys. Rev. B* ***39***, 3854 (1989).

[32]: C. Schwartz, M. Karimi, J. Zhang and G. Vidali, *Surf. Sci.* ***247***, 51 (1991).

[33]: L. W. Bruch, *Phys. Rev. B* ***68***, 235420 (2003).

[34]: M. Folman, and Y. Kozirovski, *J. Colloid. Interface Sci.* ***38***, 51 (1972).

[35]: A.B. Ephraim and M. Folman, *J. Chem. Soc., Faraday Trans. 2.* ***72***, 671 (1976).

[36]: D.J. Dai and G.E. Ewing, *J. chem.. Phys.* ***100***, 8432 (1994).

[37]: M. Grunwald and G.E. Ewing, *J. Chem. Phys.* ***109***, 4990 (1998).

[38]: S. Briquez, S. Picuad, and C. Girardet, P.N.M. Hoang, J. Heidberg and A. Voβberg, *J. Chem. Phys.* ***109***, 6435 (1998).

[39]: J. Heidberg, A. Voβberg, M. Hustedt, M. Thomas, S. Briquez, S. Picuad, and C. Girardet, *J. Chem. Phys.* ***110***, 2566 (1999).

[40]: F. Traeger, and J.P. Toennies, *J. Phys. Chem. B* ***108***, 14710 (2004).

[41]: M.F. Bertino, A.L. Glebov, J.P. Toennies, F. Traeger, E. Pijper, G.J. Kroes, and R.C. Mowrey, *Phys. Rev. Lett.* ***81***, 5608 (1998).

[42]: D.R. O'Keefe, J.N. Smith, Jr, R.L. Palmer and H. Saltsburg, *J. Chem. Phys.* ***52***, 4447 (1970).

[43]: A. Tsuchida, *Surf. Sci.* ***14***, 375 (1969); revised analysis by Tsuchida (1976), in private communication to R.J. Le Roy.

[44]: G.J. Kroes, and R.C. Mowrey, *J. Chem. Phys.* ***103***, 2186 (1995).

[45]: G.J. Kroes, *J. Phys. Chem. B* ***103***, 9397 (1999).

[46]: Private communication with J.P. Toennies and F. Traeger.

[47]: F. Jensen, Introduction to Computational Chemistry, John Wiley & Sons Ltd. (1999).

[48]: G.H. Grant, and W. Graham Richards, *"Computational Chemistry"*, Oxford Science Publications, 33 (1995).

[49]: N. Metropolis, A.W. Rosenbluth, M.N. Rosenbluth. A.H. Teller and E. Teller, *J. Chem. Phys.* ***21***,1087 (1953).

[50]: M.P. Allen and D.J. Tildesley, *"Computer Simulation of Liquids"*, 1st edition, Oxford University Press, Oxford (1987).

[51]: K. Binder, *"Applications of the Monte Carlo Method in Statistical Physics"*, 2nd edition, Springer-Verlag (1987).

[52]: D.S. McQuarrie, *"Statistical Mechanics"*, New York: Harper & Row (1976).

[53]: I.N. Levine, *"Quantum Chemistry"*, 4th edition, Prentice-Hall International, Inc., (1991); D.A. McQuarrie, *"Quantum Chemistry"*, 1st edition, Oxford University Press, Oxford (1983).

[54]: Tang, K.T., Toennies, J.P., *J. Chem. Phys.* ***66***, 1496 (1977).

[55]: J.D. Dash. *"Films on Solid Surfaces"*, A cademic, New York, (1975).

[56]: C. Schwartz, M. Karimi and G. Vidali, *Surf. Sci.* ***216***, L342 (1989).

[57]: B. Deprick and A. Julg, *Chem. Phys. Lett.* ***110***, 150 (1984).

[58]: R. Dovesi, R. Orlando, F. Ricca and C. Roetti, *Surf. Sci.* ***186***, 267 (1987).

[59]: V. Celli, D. Eichenauer, A. Kaufhold, and J.P. Toennies, *J. Chem. Phys.* ***83***, 2504 (1985).

[60]: D. Eichenauer, and J.P. Toennies, *Surf. Sci.* ***197***, 267 (1988)

[61]: W.A. Steele, *"The Interaction of Gases with Solid Surfaces"*, Pergamon, Oxford (1974).

[62]: V.J. Barclay, D.B. Jack, J.C. Polanyi, and Y. Zeiri, *J. Chem. Phys.* ***97***, 9458 (1992).

[63]: J.C. Polanyi and R.J. Williams, *J. Chem. Phys.* ***94***, 978 (1991).

[64]: D.B. Lawson and J.F. Harrison, *J. Phys. Chem. A.* ***101***, 4781 (1997).

[65]: D.A. Davies, *"Waves, Atoms and Solids"*, 1st edition, Longman Group Limited London, P. 128 (1978).

[66]: K.T. Tang, and J.P. Toennies, *J. Chem. Phys.* ***74***, 1148 (1981).

[67]: F. Visser, P.E.S. Wormer, and P. Stam, *J. Chem. Phys.* ***79***, 4973 (1983).

[68]: M. Causa, R. Dovesi, C. Pisani, C. Roetti, *Surf. Sci.* ***175***, 551 (1986).

[69]: M. Causa, R. Dovesi, E. Kotomin, C. Pisani, *J. Phys. C: Solid State Phys.* ***20***, 4983 (1987).

[70]: M. Baudin, M. Wojcik, and K. Hermansson, *Surf. Sci.* ***375***, 374 (1997).

[71]: K. Hermansson, M. Baudin, B. Ensing, M. Alfredsson, and M. Wojcik, *J. Chem. Phys.* ***109***, 7515 (1998).

[72]: C.R. Henry, C. Chapon, and C. Duriez, *J. Chem. Phys.* ***95***, 700 (1991).

[73]: M. Rigby, E.B. Smith and W.A. Wakeham, *"The Forces Between Molecules"*, Oxford Science Publications (1986).

[74]: G.Y. Liu, G.N. Robinson, and G. Scoles, *Surf. Sci.* ***262***, 409 (1992).

[75]: K.T. Tang and J.P. Toennies, *J. Chem. Phys.* ***80***, 3726 (1984).

[76]: T.L. Gilbert, *J. Chem. Phys.* ***49***, 2640 (1968).

[77]: F.T. Smith, *Phys. Rev. A.* ***5***, 1708 (1972).

[78]: M. Matsui, *J. Chem. Phys.* ***91***, 489 (1989).

[79]: T.L. Gilbert, O.C. Simpson, and M.A. Williamson, *J. Chem. Phys.* ***63***, 4061 (1975).

[80]: K.T. Tang and J.P. Toennies, *Z. Phys. D* ***1***, 91 (1986).

[81]: P. Habitz, K.T. Tang, J.P. Toennies, *Chem. Phys. Lett.* ***85***, 461 (1982).

[82]: C. Douketis, G. Scoles, S. Marchetti, M. Zen, and A. Thakkar, *J. Chem. Phys.* ***76***, 3057 (1982).

[83]: P.W. Fowler, P.J. Knowles, and N.C. Pyper, *Mol. Phys.* ***56***, 83 (1985).

[84]: N. C. Pyper, and P. Popelier, *J. Phys.: Condens. Matter* ***7***, 5013 (1995).

[85]: U. Opik, *Proc. Phys. Soc. London* ***92***, 566 (1967); R. R. Freedman and D. Kleppner, *Phys. Rev. A* ***14***, 1614 (1976).

[86]: A. D. McEachran, A. D. Stauffer, and S. Greita, *J. Phys. B* ***12***, 3119 (1979).

[87]: E. Escalona-Platero, D. Scarano, G. Spoto, and A. Zecchina, *Faraday Discuss. Chem. Soc.* ***80***, 183 (1985).

[88]: N. C. Pyper and P. Popelier, *Proc. R. Soc. London, Ser.* ***A 398***, 377 (1985).

[89]: H. M. Kelly and P.W. Fowler, *Mol. Phys.* ***80***, 135 (1993).

[90]: R. William, WMIN, A Computer Program to Model Molecules and Crystal in Terms of Potential Energy Functions, 1981, Oak Ridge National Laboratory Oak Ridge, Tennessee 37830.

[91]: P. W. Fowler, and P. A. Madden, *Phys. Rev. B.* ***29***, 1035 (1984).

[92]: P.W. Fowler, and N. C. Pyper, *Mol. Phys.* ***59***, 317 (1986).

[93]: R. Ahlrich, H. J. Bohm, S. Brode, K. T. Tang, and J. P. Toennies, *J. Chem. Phys.* ***88***, 6290 (1988).

[94]: D. Degenhardt, H.J. Lauter, and R. Haensel, *Jpn. J. Appl. Phys., Part 1* ***26***, 341 (1987).

[95]: R. Muhida, W.A. Dino, Y. Miura, H. Kasai, H. Nakanishi, A. Okiji, K. Fukutani, and T. Okano, *Surf. Sci.* ***514,*** 273 (2002).